WARD-D-0210, REV. 1

Clinch River Breeder Reactor Plant Nuclear Island

PREDICTED STEADY STATE THERMAL-HYDRAULIC PERFORMANCE OF THE FUEL AND BLANKET ASSEMBLIES IN THE CRBRP HETEROGENEOUS CORE

M. D. CARELLI

C. W. BACH

JANUARY 1979

Prepared for the Project Management Corporation as part of the U.S. Energy Research and Development Administration Liquid Metal Fast Breeder Reactor Demonstration Program

Westinghouse Electric Corporation
ADVANCED REACTORS DIVISION
BOX 158
MADISON, PENNSYLVANIA 15663

6279-2

PREDICTED STEADY STATE THERMAL-HYDRAULIC PERFORMANCE OF THE FUEL AND BLANKET ASSEMBLIES IN THE CRBRP HETEROGENEOUS CORE

January 1979

PREPARED BY: M.D. Carelli,
Core T&H Analysis

C. W. Bach,
Core T&H Analysis

APPROVED BY: R. A. Markley,
Manager, Core T&H Analysis

LIST OF CONTRIBUTORS

A. Biancheria
C. W. Bach
M. D. Carelli
K. D. Daschke
D. R. Forsyth
A. J. Friedland
K. B. Kittredge
T. S. Roth
E. C. Schwegler
D. R. Sundquist
D. R. Spencer
D. O. Tomlin
M. L. Travis
J. M. Willis

ACKNOWLEDGEMENTS

The authors gratefully appreciate the assistance throughout the entire work of J. L. Robertson, W. R. Rymer and R. A. Zebley in the endless computer runs, data elaboration and display. Also, many thanks are due to S. J. Hoover for her skill and patience in translating our "chicken scratch" into this report.

TABLE OF CONTENTS

TABLE OF CONTENTS (Continued)

SUMMARY

The steady state thermal-hydraulic performance of the fuel and blanket assemblies in the heterogeneous configuration of the CRBRP core is reported here.

Analyses were conducted for the projected first and second core, i.e., a total of four cycles of CRBRP operation; additionally, since radial blanket assemblies in the outermost row have a five year continuous residence prior to refueling, they were analyzed for their entire lifetime.

Relevant thermal-hydraulic parameters calculated for each fuel and blanket assembly throughout their lifetime were: maximum cladding temperature and fission gas pressure in the hot rod, mixed mean exit temperature, linear power rating. Three-dimensional duct temperatures on a core-wide basis were calculated at beginning of the first cycle and end of the fourth cycle, thus bracketing the entire behavior. Detailed pressure drops were calculated throughout the core, utilizing the most recently available experimental data and sophisticated analytical tools. The effect of engineering uncertainties (hot channel/hot spot factors) at various levels of confidence were accounted for in the analyses. Power-to-melt analyses were conducted for the highest power rod in the fuel and blanket assemblies to verify that the criterion of no-incipient melting, considering uncertainty factors at the 3σ level of confidence and a reactor power equal to 115% of the nominal rated power, was actually satisfied. A programmed startup was identified to assure compliance with the above criterion in the fuel assemblies at beginning-of-life.

Two novel concepts and analytical methods were introduced and implemented for the first time in the thermofluids design of LMFBR cores. The first was a comprehensive, integrated method of orificing the fuel and blanket assemblies. Coolant flow was allocated to simultaneously satisfy performance, design and safety constraints such as attainment of burnup/lifetime objectives, compliance with transient limitations, minimization of temperature level and radial gradient in the coolant flow impinging on the upper internals, limitation on the total number of discriminators, and consistency with cooling requirements of other reactor components.

The second was the determination of duct temperatures accounting for uncertainties directly in the temperature calculations, rather than by superposition over nominal temperatures. Additionally, both positive and negative uncertainties were considered, i.e., hot channel factors greater and lower than unity, since under particular combinations they will yield the worst cross-duct gradients.

During the course of these studies, room for significant improvement of the thermal-hydraulic performance was identified in the reduction of the orificing resistance with consequent reactor flow increase in excess of 5%. Even though the analytical procedure and techniques have been developed, the results here reported only partially reflect this improvement. Chiefly for schedular reasons it was decided not to redo all the thermal performance analyses, since the predicted performance will be enveloping the actual conditions once the aforementioned improvements are put into effect, e.g., assembly temperatures will be lower than predicted here. Advantage of the possibility of increasing the total reactor flow will be taken in the final, as-built design analyses. However, even neglecting this improvement, the thermal-hydraulic performance of the CRBRP heterogeneous core, as reported here, is indeed adequate and satisfactory.

1. INTRODUCTION

The design of the Clinch River Breeder Reactor Plant (CRBRP) core has evolved over the years and a very brief discussion is necessary to put into proper perspective how the core thermal-hydraulic design and analysis has played a key role in such evolution.

The original core layout was of the homogeneous type with fuel assemblies (in two different enrichment zones) surrounded by radial blanket assemblies. The steady state core thermal-hydraulic performance analyses were reported in References 1 and 2. Subsequently, a modified core layout (see Figure 1 and Table I) was proposed to satisfy, with margin, the original objective of a breeding ratio equal to or larger than 1.2. Various other performance and safety improvements resulted from adoption of this core, which was of the heterogeneous type, where fuel and blanket (called inner blanket) assemblies are inter-mixed in the inner region of the core and are surrounded by two rows of outer (also called radial) blanket assemblies. Fuel and inner blanket assemblies were alternating at each yearly refueling in six core positions. The fuel assemblies consisted of only one enrichment. In parallel to the thermal-hydraulic performance predictions documented in this report, an extensive effort was conducted in totally reviewing and updating the CRBR hot channel factors values as well as providing their rationale and methodology of application[3]. Only part of the hot channel factors recommendations from Reference 3 were actually factored into the T&H performance predictions because the two efforts were being conducted in parallel. Nuclear uncertainties were, however, specifically derived for the heterogeneous core. Full consideration of the new hot channel factors will be factored into the final, as-built design analyses.

It is obvious that the thermal-hydraulic performance predictions will differ for different core layouts. For example, the heterogeneous cores have higher linear power rating in the fuel assemblies than the homogeneous configuration due to the reduced number of fuel assemblies utilized. Two fuel enrichment zones (which affect the orificing) were adopted in the homogeneous and only

one in the heterogeneous configuration. Radial blanket assemblies were shuffled in the former, while no shuffling of either inner or radial blanket is performed in the heterogeneous core. The projected lifetime in the homogeneous core was three years for the fuel and six years for the radial blanket assemblies, while in the heterogeneous scheme, the fuel and inner blanket assemblies have a two year lifetime, the first row radial blanket assemblies have four years, and the second row radial blanket five years (obviously the alternating fuel/inner blanket assemblies have only one year). Equilibrium core conditions were predominantly considered in the homogeneous core analyses, while first and second cores are analyzed for the heterogeneous.

The aforementioned differences are, of course, fundamental. However, an additional reason exists in making the predicted T&H performance of the two cores different, a reason which is just as important as the different core configuration. Over the years, the knowledge of the core T&H design has obviously increased by the automatic "hands on" learning process, where new approaches, constraints, potential problems as well as areas of improvement have been discovered. This continuous learning process has led to shifts in design philosophy, improvement of analytical tools, development of new computer codes, and above all, elaboration and implementation of new concepts, all towards the goal of optimizing the CRBRP core thermal-hydraulic design. Therefore, it has to be kept in mind that if, for example, the homogeneous core would be analyzed today, much different results than previously reported would be obtained. To visualize the impact of the continuous improvement of the core T&H analytical approach, following is a brief summary of the key differences in performing the two designs.

The most striking difference between the homogeneous and heterogeneous core thermofluids design was the adoption of a new philosophy in core orificing. For the homogeneous, the criterion in orificing fuel and blanket assemblies was essentially to equalize the end-of-life (EOL) maximum cladding temperature, somewhat tempered by a zoning arrangement assigning relatively more flow to the high burnup fuel assemblies[2].

The idea, which germinated in the homogeneous core study, that not only cladding temperature, but also burnup, had to be taken into account in orificing, was fully exploited in the heterogeneous core analyses. By this time, it was realized that, by far, the most important step in the core thermofluids design was the core orificing. Thus, flow allocation to the core assemblies simultaneously satisfied not only lifetime/burnup goals, but also transient limitations and limitations (as much as practical) posed by the upper internals structure on the assemblies exit temperature and temperature gradient. Simultaneous consideration of these different constraints and optimization of the core flow allocation was possible through use of the newly developed ØCTØPUS code[4]. Limiting temperatures (see Section 2) were calculated for all core assemblies and fuel, inner blanket and radial blanket assemblies were orificed simultaneously. Limiting temperatures were also calculated for both first and second core and a combination of the most restrictive ones was selected for orificing.

Analyses were conducted in greater depth in the areas of characterization of plant operating conditions and uncertainties evaluation. Expected plant operating conditions were calculated for various times in the plant life (rather than at 30 years only as for the homogeneous core), and associated uncertainties were calculated more rigorously. Nuclear uncertainties were evaluated in more detail for the heterogeneous core, accounting for local effects due to the presence of control rods and for lifetime effects. Some of the engineering uncertainties were also further evaluated as previously discussed.

Power-to-melt analyses conducted for the heterogeneous core introduced, for the first time in the core design, the concept of a programmed startup to increase the power-to-melt capability of the fuel assemblies, due to the fuel restructuring effect occurring very early in life. An elaborated power-to-melt analysis for the inner blanket assemblies was performed following realization that the cladding temperature has a very significant effect on cladding swelling, hence on fuel/cladding gap size, hence gap conductance, fuel temperature and finally on power-to-melt. This prompted examination of the hot (maximum cladding temperature) rod in addition to the peak (maximum power) rod, which was the only one analyzed in previous studies.

One of the codes developed during the heterogeneous core thermal-hydraulic design was the TRITØN code[5] which evaluates duct temperatures by rigorously accounting for the effect of inter-assembly heat transfer. Additionally, for the first time duct temperatures were calculated accounting for the effect of uncertainties. TRITØN uncertainty calculations are performed such that assembly and duct temperatures are evaluated accounting simultaneously for the effect of uncertainties and inter-assembly heat transfer. This represents a marked improvement over the usual method of calculating nominal temperature first and then superimposing the effect of uncertainties, as discussed in Section 3.2.1 of this report. The concept of abandoning the superposition approach is by no means limited to duct temperature calculations and, in principle, it can be extended to all other temperature calculations, thus opening a new area of improvement.

The concept of positive and negative uncertainties in duct temperature calculations was also first introduced in the heterogeneous core analyses reported here. The worst cross-duct gradient in a given assembly would occur when the adjacent assembly towards the core centerline (thus, next to the hot side of the considered assembly) is at higher temperature than nominal (positive uncertainties), while the assembly away from the core center and next to the cold side is at lower temperatures (negative uncertainties).

Mixed mean temperatures were calculated as for the homogeneous core assuming adiabatic boundaries; however, in the present analysis, these calculations were paralleled by other calculations performed with the TRITØN code, where the effect of inter-assembly heat transfer is duly taken into account.

In future analyses the designer will consider, even though not necessarily adopt, such concepts as: a) factoring of uncertainties in all temperature calculations through the integral rather than the superposition approach; b) extension of the positive/negative uncertainties approach to other than duct temperature calculations; c) full consideration of the interassembly heat transfer effect in all of those analyses (e.g., cladding temperature calculations) presently conducted under the assumption of adiabatic assembly

boundaries; d) extension of power-to-melt analyses to other rods than hot and peak which could conceivably be slightly worse due to a particular combination of the various factors; and e) complete implementation of the hot channel factors and methodology recommended in Reference 3. These are just examples, since new avenues are continuously discovered as the design proceeds. One of these new avenues, which proved to be quite fruitful, became evident when during the present studies a critical look at how to distribute the orificing resistance in radial blanket assemblies between the assembly itself and the lower inlet module (LIM) prompted an overall review of the required orificing, which eventually led to modified flow conditions. Since no system temperatures, specifically reactor inlet temperature, corresponding to the modified reactor flow (and ΔT) conditions had yet been calculated, most of the studies reported here, and expecially the thermal performance predictions in Section 4, were conducted for the plant conditions evaluated at the inception of the heterogeneous core analyses. Pressure drop calculations (Section 6) were, however, partially performed for the new, modified conditions. For this reason, plus the very significant effect on the entire core T&H design, and the fact that these conditions will be the basis of the next round of design analyses, they will be briefly discussed here.

As previously mentioned, shuffling of radial blanket assemblies was contemplated in the homogeneous design, thus their orificing was located in the LIM; since shuffling was not considered for the heterogeneous core, all the orificing was located in the assembly. Even though shuffling is not the reference approach, there is no reason why this design option should be precluded for the entire life of the CRBRP (the LIM is a permanent, 30-year component). Therefore, the radial blanket orificing was apportioned between assembly and LIM to allow shuffling, if so desired at a later time. More importantly, during the homogeneous design, it was decided to size the orificing resistance in zone 1 (highest flow zone) to give a pressure drop of the order of 30 psi. Since, in principle, the zone 1 pressure drop is zero or more realistically, a few psi to allow for final flow trimming, the allowance of 30 psi parasitic pressure drop was designed to accommodate future cores with higher rod bundle pressure drop, e.g., gridded and/or carbide cores. Analyses of the heterogeneous core showed that the flow requirements were

quite similar to those of the homogeneous configuration, while on the other hand, emphasis on the CRBRP was shifted from providing for insertion of future, hypothetical cores to improving the performance and design margins of the cores actually analyzed and designed. From these premises, it followed that the parasitic pressure drop in zone 1 orifice (and in the entire reactor, since zone 1 is the highest pressure drop flow path) was actually hindering the overall core performance. In fact, once the overall core hydraulic resistance is lowered, the pump operating point will shift to the right along the characteristic head/flow curve with the end result that the pump will deliver more flow at a lower head. Obviously, this will improve the core performance, since higher flows mean lower temperatures, thus, either longer lifetime and higher burnup (lower fuel cycle cost) or increased margins to limiting conditions (enhanced safety). A computer code, named CATFISH[6], was developed and is now operational. CATFISH is a hydraulic code which models the entire primary system; it considers all the hydraulic resistances in the core plus inlet and outlet plenum, primary system piping, check valve, IHX, etc. It also models all the various reactor flow paths (fuel and blanket orificing zones, primary and secondary control assemblies, radial shield assemblies, vessel, leakage), and ties this entire, complex hydraulic network with the pump head/flow characteristic curve. Thus, for any specified set of resistances CATFISH calculates the pump head, the total reactor flow, the flow in each assembly and the pressure drop across each subcomponent. CATFISH also has the capability of calculating the above parameters under nominal conditions or accounting for uncertainties, either positive (increased resistances, which will yield the minimum reactor flow) or negative (decreased resistances, yielding the maximum reactor flow). It was found that by reducing the parasitic orificing pressure drop, and still remaining within the presently specified "window" of pump operating characteristics, the total reactor flow could be significantly increased, with flow through the fuel and blanket assemblies increasing in the 5-10% range. A 1% increase in flow corresponds to $\sim 5^{o}$F decrease in maximum cladding temperature, which corresponds to an allowable burnup increase of ~2500 MWd/ton and fuel cycle cost savings of ~$12.5M. Consequently, a 5% flow increase will yield an increased lifetime in each core of approximately 86 full power days or 4 calendar months and cost savings of ~$60M over the CRBRP lifetime.

Due to schedular requirements, predictions of the heterogeneous core thermal performance could not include conclusions of the CATFISH code development and of related analyses, which had been conducted in parallel. Additionally, new plant system temperatures were not yet available, as previously mentioned. Thus, the performance predictions reported in Sections 2 through 5 still reflect the presence of parasitic core orificing resistance and the core assemblies feature lower flows and higher temperatures than otherwise achievable. These predictions envelope the actual operating conditions, once the core hydraulic resistance is reduced and "CATFISH predicted" flows are factored into the design. The fact that the CRBRP core assemblies still exhibit excellent performance, satisfying all design constraints and limitations as will be shown in this report, points out the soundness of the CRBRP core thermofluids design. Since, however, room exists for significant performance improvement and considerable cost savings, reduction of parasitic resistance and related analyses will be an integral part of the core thermofluids analyses to be conducted for final, as-built conditions. A quantitative comparison of the reactor hydraulics for the "old" and "new" plant flow conditions will be found in Section 6.

2. CORE ORIFICING

2.1 Introduction

Core orificing, i.e., flow allocation to the various fuel and blanket assemblies is the single most important step in the core thermal-hydraulic design. Since the assembly temperatures are directly dependent on the amount of flow and since the flow allocation is the only design parameter which can be varied at will, within certain limits, by the designer, it logically follows that the core T&H design and performance is only as "good" as the core orificing. Therefore, more and more attention in the CRBRP core T&H design has been placed on core orificing, which for the heterogeneous core was the item receiving primary emphasis.

Previous experience has indicated that a successful orificing should account "a priori" for all the various aspects to be considered through the design, in order to avoid time consuming and costly iterations. Thus, going from the homogeneous to the heterogeneous design, a systematic orificing approach was developed, which accounted for lifetime/burnup, transient, upper internals temperature constraints. This new approach represented a drastic change in philosophy and quite a significant improvement over the previous and commonly accepted maximum temperature equalization method.

Limiting temperatures were determined (see Section 2.3) for all fuel and blanket assemblies, which were subsequently orificed simultaneously, thus providing the best flow allocation and utilization. Finally, both first and second core conditions were investigated in determining the orificing constraints and the most restrictive in either core was used in deriving the orificing configuration. This guaranteed, a priori, that the thermal-hydraulic performance would have satisified the considered constraints in both cores. The following sections, discussing in detail the orificing philosophy, procedure and results, will clarify and enlighten what briefly was discussed above.

2.2 Orificing Philosophy and Approach

The following constraints[7] must be satisfied in selecting the flow orificing for the CRBRP fuel, inner blanket and radial blanket assemblies:

- Maximum cladding temperature must be compatible with lifetime and burnup objectives, which can be expressed in terms of maximum allowable inelastic cladding strain and cladding cumulative damage function (CDF).
- Maximum coolant temperature conditions must be such as to assure, with adequate margin, that no sodium boiling occurs during the worst emergency transient (e.g., the three-loop natural circulation event), accounting for uncertainties at the 3σ level of confidence.
- Maximum assemblies mixed mean outlet temperature and radial temperature gradient at the assemblies exit must be compatible with upper internals structure (UIS) limitations.
- Maximum of eight discrimination zones (fuel plus inner blanket) are allowed.
- Flow allocation to fuel, inner blanket and radial blanket assemblies must not exceed 94.0% of the total reactor flow to account for cooling requirements of other reactor components.

Since the heterogeneous core contains a single fuel enrichment and because the number of required discriminators depends on the unique combinations of flow orificing and fuel enrichment zones, the maximum number of fuel plus inner blanket assembly orificing zones is equal to the total allowable number of discriminators (i.e., 8). Inner blanket and fuel assemblies employ identical inlet nozzles. Therefore, both must be considered in determining the total number of discriminator zones. The outer blanket assemblies, due to the high pressure drop requirement across the inlet nozzle, employ a unique inlet nozzle and, therefore, are not considered in determining the total number of discriminators. The row 6 corner positions which alternate between inner blanket and fuel assemblies during successive cycles, form a separate discriminator zone which is included among the eight.

To put the lifetime/burnup and transient temperature constraints on the same quantitative basis, the concept of equivalent limiting temperature is

employed. The equivalent limiting temperature is defined as that cladding temperature at a specified radial position (cladding ID in these analyses) and time in life (end-of-life) which must not be exceeded in order to satisfy the considered constraint. Three equivalent limiting temperatures were defined to represent the lifetime/burnup and transient constraints, i.e., SELT, DELT and TELT. They are defined as the end-of-life maximum cladding ID temperatures for Plant Expected Operating conditions, considering uncertainty factors at the 2σ level of confidence, such that accounting for the assembly temperature/pressure lifetime history, the limiting value of the inelastic cladding strain (SELT), or cumulative damage function (DELT), or worst time-in-life transient coolant temperature (TELT) is not exceeded. As it appears from the above definition, the equivalent limiting temperatures are calculated for each assembly. In fact, all the various assemblies have individually different lifetime histories of cladding temperature and fission gas pressure, and therefore, the limiting equivalent temperatures are necessarily different from assembly-to-assembly to stay within a constraint common to all assemblies. Calculations are performed for plant expected operating conditions, which are the conditions where the CRBRP is expected to operate on a probabilistic basis and the conditions used in the design of replaceable components such as the core assemblies. The other set of plant conditions used in thermofluids analyses are plant thermal-hydraulic design values (THDV), which are the plant rated conditions and, being more conservative than plant expected conditions, are used in the design of permanent components and in transient and safety analyses. Orificing of core assemblies is performed on the basis of plant expected conditions.

As mentioned in Section 2.1, both first and second core conditions have been considered in defining the core orificing, therefore, the SELT, DELT and TELT have been calculated for both cores. In the case of the radial blanket assemblies, where the lifetime spans both cores, obviously only one set of limiting temperatures was calculated. Using the ØCTØPUS code[4], the assemblies minimum flow in the first and second core necessary to satisfy the most restrictive of the limiting conditions was calculated for each assembly. Subsequently, the various assemblies were grouped in zones and the orificing arrangement was selected such that the flow allocated to each assembly was at

least equal to the larger of the flow requirements in first and second core. This assured meeting of all constraints for both cores. Finally, the excess flow, if any, is supposed to be allocated among the fuel assemblies to minimize and equalize the assemblies exit temperature and temperature gradients.

2.3 Calculation of Equivalent Limiting Temperatures

Assemblies lifetime/burnup goals are achieved when both the cladding inelastic strain and cladding CDF are within the established limits during steady state operation. The ductility strain limit was set at 0.2% and the CDF limit was set at 0.7 in the fuel assemblies and 0.5 in the blanket assemblies. Since the CDF limit for steady state plus transient operation is by definition 1.0, the margin for CDF transient accumulation was 0.3 in the fuel assemblies and 0.5 in the blanket. Both cumulative cladding strain and CDF depend on the rod cladding temperature/pressure history. Thus, using a preliminary estimate of the assembly flow (but using the proper physics data), the hot rod(*) in each assembly at end-of-life was identified using the subchannel analysis code CØTEC[8]. Subsequently, the hot rod so identified was followed throughout lifetime and the lifetime temperature/pressure history was calculated with the NICER code[9]. Uncertainty factors (see Section 3) at the 2σ level of confidence were used in the cladding temperature/pressure calculations. Based on the above lifetime histories, a strain equivalent limiting temperature (SELT) and a strain equivalent temperature (SET) were calculated for each assembly. A typical example of these calculations is reported in Table II. The SET is defined as the end-of-life temperature which, if maintained constant throughout lifetime, would cause the same end-of-life strain as the actual temperature/pressure history. The SELT can thus be defined as that SET which would cause, for the particular assembly relative behavior of cladding temperature and pressure through lifetime, and end-of-life cumulative strain of 0.2%. Thus, while the SET depends on the actual temperature/pressure

(*) Each assembly is characterized by its hot rod at end-of-life, which is obviously the one with the highest strain and CDF.

values, therefore, on the guessed value of assembly flow, the SELT does not depend on the assembly flow, but rather on the relative behavior through lifetime, which is only a function of the power generation changes during life.

Since the DELT is the equivalent end-of-life temperature corresponding to a CDF of 0.7 or 0.5, the method employed in its determination was to extract it from a curve correlating the cladding ID temperature at EOL with the corresponding CDF. Thus, at least three (in some instances more were necessary) lifetime temperature/pressure histories were generated for each assembly varying the flow and the corresponding CDF was calculated. Typical curves are reported in Figures 2 through 6 for the fuel and inner blanket assemblies (first and second cores) and radial blanket assemblies. By interpolation, the DELT corresponding to the CDF constraint was then determined.

Regarding the transient constraint, the general guideline is to provide adequate margin-to-sodium boiling throughout the assembly lifetime during the worst transient. This was quantitatively translated into a value of 1550^{o}F which was conservatively defined as the maximum coolant temperature allowable during a natural circulation transient in any assembly at any time in life accounting for uncertainty factors at the 3σ level of confidence. This limit also assumes plant THDV conditions and a 750^{o}F reactor inlet temperature. The determination of the TELT for each core assembly then proceeded as follows.

From preliminary transient calculations performed using the FØRE-2M code[10], the maximum coolant transient temperature at the worst time in life and the corresponding steady state coolant temperature were obtained for the worst fuel, inner blanket and radial blanket assembly. As previously mentioned the transient considered was the natural circulation event which had proved to be the most severe. Then, the temperature T_M was calculated, which is defined as the maximum steady state coolant temperature at plant expected operating conditions and 2σ hot channel factors corresponding to a 1550^{o}F transient maximum coolant temperature at plant THDV conditions, 3σ

hot channel factors and 750°F inlet. Calculation of T_M was quite straightforward from ratioing the transient temperature rise calculated by FØRE-2M, fixing the maximum transient temperature at 1550°F for all three types of assemblies and accounting for the differences in plant conditions and hot channel factors. Table III summarizes the FØRE-2M and T_M temperatures.

Rigorously speaking, the T_M thus calculated are only valid for the three assemblies whose transient behavior was actually investigated; it was conservatively assumed that they apply to all other assemblies of the same ty Since: a) the value of T_M essentially depends on the magnitude of the temperature swing from steady state to transient; b) higher swing implies higher T_M; and c) other assemblies will have lower steady state-transient swings than the worst representatives investigated through FØRE-2M, it follows that adoption of the values of T_M from Table III in calculation of the TELT's for assemblies of the same type is conservative.

Finally, using the lifetime temperature profile for each individual assembly, the TELT in each core assembly is calculated by the equation:

$$TELT = T_{in} + \frac{(T_M - T_{in})}{(T_{cool} - T_{in})_{t',x'}} (T_{cool} - T_{in})_{t",x"} + (T_{ID} - T_{cool})_{t",x"}$$

where

T_{in} = reactor inlet temperature in first or second core;
T_{cool} = hot subchannel coolant temperature;
T_{ID} = hot spot cladding ID temperture
t' = time in life when maximum transient temperature occurs;
t" = EOL (i.e., EOC2, EOC4 or EOC5);
x' = axial position where maximum transient coolant temperature occurs;
x" = axial position where maximum T_{ID} occurs at EOL.

Again, it should be noted that since the TELT's depend on temperature differences rather than absolute values, lifetime temperature profiles corresponding to first guestimates of assembly flows are perfectly adequate for an accurate evaluation of the TELT's.

The SELT, DELT and TELT thus calculated for each assembly are reported in Figure 7 (first core) and Figure 8 (second core). Since the radial blanket assemblies are refueled only once, their values are reported only in Figure 8. No SELT's are reported for the blanket assemblies, nor for the fuel assemblies in the first core since very little cladding strain occurs, and therefore, their value was very high, thus being not limiting at all. Actually, an inspection of Figure 8 shows that even in the second core no fuel assembly is strain limited. The limiting constraint in each assembly is given by the ELT with the minimum value. Fuel assemblies are generally CDF limited with the exception of the ones farther from the core center which are transient limited; inner blanket assemblies are transient limited; radial blanket assemblies are CDF limited if flanked by at least two fuel assemblies, otherwise, they are transient limited.

2.4 Results

The ØCTØPUS code was used to calculate the flow rate needed in each assembly to produce an end-of-life cladding ID temperature equal to the most limiting of the ELT's, as discussed in the previous section. Figure 9 reports such flow rates for the first and second cores (cycles 2 and 4, respectively). Obviously the minimum flow in each assembly necessary to satisfy all considered constraints in both cores is equal to the most restrictive of the two flow requirements. The higher of the two values reported in Figure 9 is not necessarily the most restrictive. In fact, due to the alternating of fuel and inner blanket assemblies in the six row 6 positions, the total core flow varies slightly from cycle-to-cycle. The replacement of three inner blanket assemblies by fuel assemblies at the beginning-of-cycle 2 results in 0.8% flow reduction(*) in each of the remaining assemblies. At the beginning-of-cycle 4, six inner blanket assemblies are replaced by six fuel assemblies with a 1.6% resultant flow reduction(*) in the remaining assemblies. Thus, when comparing the flow requirements for the first and second cores, minimum flows

(*)This preliminary estimate was subsequently proved to be conservative by CATFISH analyses.

must be put on the same basis. Cycle 4 was chosen as the standard basis since it will require the higher core flow fraction (fuel assemblies are in alternating row 6 positions). When flow requirements for cycle 2 are translated to their cycle 4 values, second core requirements are found to be slightly more restrictive in some outer fuel assemblies, as shown in Figure 9. Cycle 5 flows are reported for the transient limited second row radial blanket assemblies, since their TELT's are maximum at EOL.

Using the required minimum flows are guidelines, the ØZØNE code (which is now incorporated in ØCTØPUS as a subroutine) selected, for a given number of orificing zones, that combination of assemblies grouping into orificing zones which among all the various possible combinations, yielded the minimum value of total core flow and was therefore the most effective. As mentioned in Section 2.2, a maximum number of eight discriminators (and orificing zones) is allowed for the fuel and inner blanket assemblies. The number of orificing zones in the radial blanket assemblies was selected as 4 for a total number of core orificing zones equal to 12. The selected arrangement is reported in Figure 10, where the starred assemblies are the ones which determine the amount of flow allocated to the orificing zones (they are actually called zone driver assemblies, or drivers). Also indicated are the limiting assemblies in each orifice zone for first and second core; obviously the driver is the one with the more restrictive flow requirement (compare with Figure 9).

As shown in Figure 10, the orificing arrangement does not present a 30^{o} symmetry, a direct consequence of the fact that the control rod location and insertion pattern, hence the power generation, does not have a 30^{o} symmetry. For example, considering the assemblies around the row 7 corner control assemblies (see Figure 8), first core conditions are limiting for the fuel assemblies around the control assembly at the right of the figure, while second core conditions are prevalently limiting for the fuel assemblies surrounding the control assembly at the left.

The minimum amount of core flow necessary to satisfy the various constraints and the grouping of the core assemblies into 12 orificing zones was equal to 93.07% of the total reactor flow at cycle 4 conditions. Since 94% of the

total reactor flow is allocated to the fuel and blanket assemblies and since 93.07% is the minimum required, it follows that slightly less than 1% of the total reactor flow is available to be allocated as deemed necessary by the designer. The ØCTØPUS code is programmed to distribute the excess flow among the fuel assemblies to minimize/equalize the assemblies mixed mean temperature and temperature gradient. This option, however, was not fully exercised in these studies since the amount of available excess flow is not enough to significantly influence the value of the outlet temperatures. Rather, the excess flow was distributed roughly evenly among the various core orificing zones to provide a little margin above what flow is strictly necessary. The final core flow allocation is reported in Table IV, which shows the cycle-by-cycle variation of flow in the various orificing zones. Both THDV and PEOC flows are reported in Table IV.

3.0 UNCERTAINTY ANALYSIS

This section is divided into two main subsections: Section 3.1 dealing with the uncertainties traditionally adopted in calculation of rod cladding temperature, assembly mixed mean temperature and gas plenum pressure; and Section 3.2 dealing with uncertainties for duct temperature calculations which are introduced here for the first time. A discussion of the uncertainties used in thermal-hydraulic calculations does not, rigorously speaking, belong to a report devoted to describing the thermofluids design and performance predictions, but rather should be the subject of a separate report like Reference 3. However, the uncertainties are reported in detail here since in one case (duct temperature) they are derived and used for the first time, in the other (calculation of other parameters) it was necessary to clearly spell out which uncertainties are actually used in the calculations.

Uncertainties for power-to-melt calculations are reported in Section 5.2.

3.1 Rod and Mixed Mean Temperature Uncertainties

3.1.1 Introduction

During the previous thermal-hydraulic analyses conducted for the homogeneous core[2], a preliminary study was performed to assess the impact of theoretical and experimental analyses uncertainties, instrumentation accuracy, manufacturing tolerances, and physical properties and correlation uncertainties on the core thermal-hydraulic performance predictions. Hot channel/hot spot factors for fuel and radial blanket assemblies were determined to account quantitatively for the above uncertainties and semi-statistically combined. Separate groups of uncertainty factors were established for calculation of: a) local rod temperatures (coolant, cladding, fuel); b) assembly coolant mixed mean exit temperature; and c) rod fission gas plenum temperature and rod burnup (which together with uncertainties on fission gas yield, fission gas release and plenum volume, determine the overall uncertainty on plenum pressure).

A set of uncertainty factors for prediction of the heterogeneous core thermal-hydraulic performance was established along the same lines and is presented in Tables V through X. For convenience, the factors have been tabulated by assembly type (fuel, inner/radial blanket), intended application (rod temperatures, mixed mean temperatures, plenum pressure calculations), and type (engineering - table numbers with the "A" suffix; nuclear - table numbers with the "B" suffix). Note that 3σ statistical values are presented which are the basis for transient and safety analyses. Uncertainties at 2σ level are used in calculation of steady state thermal-hydraulic parameters, such as cladding temperature and pressure, which are input to replaceable core assembly lifetime analyses.

As previously mentioned, these factors represent an adaptation to the heterogeneous core configuration of the hot channel factors adopted in the thermal-hydraulic design of the homogeneous core. Of course, nuclear uncertainty factors were, however, properly determined for the power and burnup histories characteristics of the heterogeneous core[11]. The significant features in the application of the nuclear uncertainty factors to the thermal-hydraulic analyses are reported in Section 3.1.3.

In parallel with the studies reported here, a thorough reevaluation of uncertainties analyses, their numerical values and methodology of application was performed. This reevaluation led to a revised set[3], which was approved by the CRBRP Project Office in December 1978. It must, therefore, be emphasized that the performance predictions herein contained are not consistent with the uncertainty factors documented in Reference 3, but are actually more conservative. In fact, temperatures calculated using the factors and method of Reference 3 are lower(*) than the values reported in Section 4, which were predicted utilizing the hot channel factors from Tables V through X.

(*) Calculations for a typical fuel, inner blanket and radial blanket assembly hot rod, 2σ, plant expected conditions at end-of-life showed the present analysis yielding a maximum cladding ID temperature approximately 54°F, 25°F and 8°F, respectively, higher than obtained using Reference 3 uncertainty factors and analytical procedures.

The major differences between the engineering uncertainty factors adopted here for rod temperature calculations and those recommended in Reference 3 are briefly summarized in Section 3.1.2. Uncertainties applied in power-to-melt analyses are consistent with Reference 3 and are discussed in Section 5. A discussion of how uncertainties are conservatively accounted for in plenum pressure calculations is reported in Section 3.1.4.

3.1.2 Rod Temperature Engineering Uncertainty Factors

The hot channel/hot spot factors representing engineering uncertainties in rod temperature calculations and adopted in these analyses differ from those recommended in Reference 3 as follows:

- pellet-cladding eccentricity hot channel factor. Both a direct and statistical component were evaluated in Reference 3 as well as a lifetime dependency, while only a statistical component unchanged throughout life was considered here. Note that the latter is conservative when calculating end-of-life temperatures, which are the ones of utmost importance in steady state analyses, since Reference 3 recommends to consider no end-of-life uncertainty factor, neither direct nor statistical, due to pellet-cladding eccentricity;

- assembly inlet flow maldistribution factor. Detailed analyses conducted in Reference 3 recommended a split of this factor into a direct and a statistical component, in lieu of the entirely direct factor adopted here; and again, the latter approach is more conservative;

- subchannel flow area. A reevaluation of the analyses performed to establish this factor led to a reduction in its value;

- cladding circumferential temperature variation. Recent modifications to the FATHØM-360 code[12] allowed calculation in Reference 3 of individual hot spot factors representing separately the effect of the wire wrap on the film and cladding temperature drop. Previous practice was to consider only one factor to be applied to the temperature difference between the bulk coolant and the radial cladding position considered. Of the two factors reported in Reference 3, the cladding hot spot is less than unity, as it physically should be, since it represents the beneficial effect of circumferential heat transfer through the cladding. The film hot spot, on the other hand, accounts for the presence of the

wire wrap in the channel. The approach recommended in Reference 3 is, therefore, more adherent to reality than used here, however, the two methods yield the same overall effect on cladding temperature. In fact, the overall factor reported in Tables V-A and VIII-A applies to the total temperature drop through the cladding and film; the Reference 3 approach features a higher hot spot factor to be applied to the film ΔT alone, which is balanced by a less than unity hot spot factor to be applied to the cladding ΔT;

- cladding thickness and conductivity. A critical reevaluation conducted in Reference 3 of the correlation adopted in design, its deviation from experimental data and the effect of irradiation led to the conclusion that the 5% under-estimation directly built in the correlation is more than adequate to account for irradiation swelling and cladding thickness effects on temperatures and, therefore, no hot channel factor is recommended in Reference 3. Again, the present analysis is conservative by adopting a 1.12 hot spot factor;

- fissile fuel maldistribution. The value recommended in Reference 3 (1.052) is higher than the value used here (1.03), by a factor of $\sqrt{3}$; this is due to the use of a rectangular distribution, rather than normal as adopted in the preliminary hot channel factors assessment;

- reactor ΔT and inlet temperature variation. This is discussed in Section 4.1;

- flow distribution calculational uncertainty. There are several differences between the values adopted in this study and those recommended in Reference 3. In the fuel and inner blanket assemblies case, the values used for rod temperature calculations are similar, while the values for plenum temperature calculation adopted in these studies were conservatively assumed to be higher. In the radial blanket case, the values both for rod and plenum temperature calculations, adopted in these studies are lower than recommended in Reference 3. These discrepancies are attributable to the fact that comparison/calibration/verification of the CØTEC code is an on-going task as more data become available. For example, since issuance of Reference 3 and inception of these studies, data have been obtained from the ARD full scale 61-rod blanket heat transfer test in sodium for flow and skewed power conditions prototypic of the radial blanket assemblies.[13] Comparison of experimental data with CØTEC predictions indicated that CØTEC consistently predicts higher temperatures, both at the hot rod maximum cladding temperature axial position and in the unheated plenum region, than obtained in the tests. Preliminary evaluation of this data justify reducing the maldistribution calculation uncertainty factor for the radial

blankets from 1.2 (rod temperature) and 1.3 (plenum temperature) to 1.1 for both. A conservative approach was also taken for the inner blanket; since experimental data for flatter power distributions typical of inner blanket assemblies were not yet available, the higher uncertainty factors were retained in this study, even though every indication exists that they can be reduced.

As mentioned, elaboration of data from the blanket heat transfer test was concurrent with this analysis; thus, determination of limiting temperatures and flows as discussed in Section 2 was based on the higher value (1.2) of the maldistribution calculational factor. Since such a procedure is conservative, resulting in lower limiting temperatures, a reevaluation of the orificing calculations was not warranted, but rather the updated value was adopted in the performance predictions reported in Section 4.

Neither in Reference 3 nor here have results been incorporated from the recently obtained fuel bundle test data from the MIT 61-rod salt injection in water[14], the KFK 61-rod heating in sodium[15] and the JOYO 91-rod heating in sodium[16]. Additionally, the 5:1 air flow tests on a blanket assembly conducted at the Westinghouse Research Laboratory[17] have just been completed, the ARD 61-rod bundle blanket heat transfer test is in progress and the ORNL 61-rod fuel assembly bundle sodium heat transfer test is planned in CY 1979. As these additional test data are factored into the code calibration, the basis for the statistical component of the flow distribution calculational uncertainty will be improved as well as the direct component (simulation bias) will be reduced or eliminated altogether since the forthcoming data are from larger bundle, more prototypic heated rod experiments in sodium.

In conclusion, as previously mentioned, the overall effect of using the hot channel factors in Tables V through X rather than those recommended in Reference 3, is a more conservative evaluation of the core steady state thermal performance reported in Section 4.

3.1.3 Nuclear Uncertainties

The total power or burnup uncertainty is composed of nuclear design methods uncertainties and/or biases (based on comparisons of calculations and measurements of isotopic fission and capture rates and gamma-heating in ZPPR criticals), plus CRBR design uncertainties relating primarily to absolute power normalization and fissile content variations, and a general class of

modeling uncertainties. In the fuel, the power uncertainty is broken down into a statistical part which can be combined in quadrature (root-mean square) with other statistical uncertainties, and a non-statistical bias and uncertainty which is applied directly to envelope the upper limits of the peak power density. Due to the limited scope of the available blanket data, only a non-statistical uncertainty is developed. Uncertainties are provided for the fuel, inner and radial blanket assemblies. Where a basis exists, a spatial distribution of the uncertainty is provided (e.g., adjacent to, and removed from the influence of inserted control rods, and by assembly row in the outer blanket). Otherwise, the uncertainty is developed for the peak power locations and should be assumed to be applicable throughout the region for the stated time-in-life. For a detailed discussion, and definition of all the nuclear power uncertainties and individual factors, see Reference 11.

Of particular interest to the thermal-hydraulic design is the spatial dependence of the uncertainties:

a. Radial (i.e., adjacent to, and removed from the influence of an inserted control rod; locally dependent bias due to ZPPR-7 flux tilt; and by assembly row in the outer blanket).

b. Axial (i.e., at the peak power density near the core midplane, and at the core/upper axial blanket interface).

In the case of the radially distributed uncertainties, how and where the uncertainties are to be applied is shown in Tables V through X with the B suffix. The axial uncertainties are a result of the nuclear design calculations and modeling techniques. In particular, the peak and integrated power densities in the fuel are well predicted with the standard two-dimensional synthesis nuclear design techniques, while the "power density at the top of the core" is relatively poorly predicted due to difficulties in simultaneously modeling the behavior in the region while preserving the integral and peak (core midplane) power in two dimensions. In addition, the accuracy of few group diffusion theory is poorer in the presence of the steep

flux gradient and in the region of the fuel/upper axial blanket material discontinuity. These factors are reflected in the larger "power density at top of core" uncertainty.

The temperature distribution along the entire fuel rod is necessary for the evaluation of relevant thermal-hydraulic parameters (i.e., fuel temperature, cladding temperature, fission gas generation and release, etc.). As noted above, only two values of the spatially-dependent (in the axial direction) factors are provided. Therefore, it was necessary to make several assumptions and approximations. First, it was assumed that the value of uncertainties at the fuel/upper axial blanket (UAB) interface also apply at the fuel/lower axial blanket (LAB) interface. The actual shape of the axial variation of the heat flux uncertainty from the peak power position to the fuel/UAB and fuel/LAB interfaces is generally not a very critical item since: a) it does not affect the channel enthalpy rise (an uncertainty integrated over the rod length is provided); b) the heat flux is specified at those positions of most interest (i.e., top of the core for cladding temperature calculations, peak power position for fuel temperatures). Thus, the most immediate assumption, i.e., a linear variation in both directions, was adopted. This was also a conservative assumption for plenum pressure calculations, as discussed in Section 3.1.4. In power-to-melt calculations it was, however, discovered (see Section 5.3) that due to the effect of cladding swelling, which is extremely sensitive to the cladding temperature value, the fuel was closest to melting not at a location corresponding to the peak power position. A more realistic definition of the heat flux uncertainty axial shape was therefore necessary. An inverted chopped cosine curve fitting the heat flux uncertainties at the peak power and interfaces positions was therefore adopted in predicting the axial profiles of rod temperatures necessary as input to power-to-melt evaluations. For both assumed distributions, linear and inverted chopped cosine, the local values of the heat flux factor are routinely calculated by NICER.

Finally, the uncertainties at the fuel/UAB and fuel/LAB interfaces were assumed constant over the respective axial blankets.

3.1.4 Plenum Pressure Uncertainties

The fission gas plenum pressure in CRBR fuel and blanket rods is calculated from the perfect gas law:

$$p = \frac{nRT}{V}$$

The physical parameters affecting the pressure value are, therefore(*):

- fission gas generation, which depends on the rod burnup;
- fission gas yield, which depends on the type of atom fissioned;
- fission gas release to the plenum, which depends on the rod burnup, linear power rating and temperature;
- plenum temperature; and
- plenum volume

Uncertainties on the above parameters are accounted for as follows:

- uncertainties on burnup (see Tables VII and X; 2σ level of confidence is adopted for performance calculations reported in Section 4);
- the adopted value for the fission gas yield, regardless of the fissioned atom, is 0.266. Recommended[18] values are: 0.2554 for U^{235}, 0.2385 for U^{238}, and 0.2506 for Pu^{239};
- a comparison between fission gas release predictions and experimental data from EBR-II irradiation experiments was performed for the fuel assemblies; the +2σ release correlation was adopted in the analyses. In the radial blanket case, since no pertinent experimental data are available, nominal fission gas release predictions from the fuel assemblies calibrated model were increased by 15%.
- uncertainties on plenum temperature (2σ level of confidence is adopted - see Tables VII and X); and

(*)Discussed here is only the component due to fission gases, which is by far overwhelming, especially at EOL. The pressure component due to initial gases is computed separately and added to the fission gas component to yield the total plenum pressure.

- minimum plenum volume was adopted in the calculations.

It is evident from the above that while the resulting fission gas pressure is labeled as "2σ", in reality the level of confidence is much higher. In fact, 2σ uncertainties on the various parameters are superimposed on each other; the uncertainty on the plenum volume is a bounding value rather than a 2σ; and, the adopted uncertainty on fission gas yield is much higher for U^{238} and Pu^{239} than for U^{235} (which is only a small fraction of the fuel, even more so at EOL when the plenum pressure value is most important and critical). Predictions of fission gas plenum pressure have additional conservatism in the blanket assemblies case since: a) the same release model as for the fuel assemblies is assumed, which is by preliminary indications conservative; b) the release so calculated is multiplied by a 1.15 factor, thus very closely approaching 100% release. Assumption of a linear, rather than inverted chopped cosine heat flux uncertainty distribution (which affects the fuel temperature, hence the gas release) as discussed in Section 3.1.3 is also conservative, since it tends to increase the fuel temperature and gas release in the central region of the rod where most of the gases are released.

A more proper and realistic way of calculating the 2σ plenum pressure would be to individually vary each of the affecting parameters by the corresponding 2σ level of uncertainty and calculate the induced change in plenum pressure. Adding the root-mean square of the various changes in plenum pressure to the 0σ value will yield the true 2σ value of the fission gas pressure. This calculation was performed for the hot pin in inner blanket assembly #99 and radial blanket assembly #201 at end-of-life (EOC4) to quantify the margin of conservatism implicit in the current evaluation of plenum pressure. Factored in this analysis were also the very recently obtained fission gas release data from WBA-20 (the first fission gas release data for blanket assemblies) which indicated a very substantial over-estimation of fission gas release by the present high burnup fuel calibrated LIFE-III code model. It was found that for the inner blanket rod using the r.m.s. method, the calculated 2σ total plenum pressure was 175 psi, while the value used in design by accounting simultaneously for all uncertainties was 249 psi. For the radial blanket pin, the calculated 2σ pressure was 188 psi versus a design adopted value of 273

psi. For comparison, the total plenum pressure assuming 100% fission gas release and simultaneously accounting for all the other uncertainties was 264 psi for the inner blanket and 310 psi for the radial blanket. Thus, the design adopted value is quite comparable with the 100% release value, a direct consequence of the over-prediction of the fission gas release model and the additional 15% increase. The above examples therefore show quite clearly the large amount of conservatism implicit in the plenum pressure values used throughout these analyses.

3.2 Duct Temperature Uncertainties

3.2.1 Introduction

As mentioned, the core thermofluids analysis of the heterogeneous core represented the first instance where a significant effort was attempted to systematically define duct temperature uncertainties. They closely resemble and are consistent with the uncertainties discussed in Section 3.1 rather than the much more elaborate set and procedure developed in Reference 3. In addition to the fact that the latter was not yet available for design use when these analyses were being conducted, past history has taught that a fair amount of design experience is necessary before attempting a very elaborate and much more complicated approach. Before future analyses are undertaken, the uncertainties proposed here should, therefore, be critically reviewed and eventually updated along the same lines as for rod temperature calculations for final as-built analyses. Since characterization of the thermal-hydraulic behavior of the control assemblies is necessary when calculating duct temperatures in surrounding assemblies (inter-assembly heat transfer is very pronounced at the control assemblies interfaces), uncertainties are reported here for all three types of core assemblies; i.e., fuel, inner and radial blanket and primary control assemblies. Due to the lack of data for the secondary control assemblies it was assumed that the same uncertainties as for the primary control assemblies apply.

Uncertainties are broken down in factors affecting the nominal values of assembly heat generation, assembly flow, coolant enthalpy rise, film heat transfer coefficient, duct and interstitial gap thermal conductivities, duct

thickness and interstitial gap geometrical variations. In the control assembly, separate enthalpy rise uncertainties are calculated for the bundle and the bypass and additionally an uncertainty on the bundle/bypass flow split is considered.

The most recent version of the TRITON code is capable of calculating duct temperatures throughout the core under nominal and "with uncertainties" conditions.

A major difference in accounting for uncertainties between duct temperature calculations and all the other calculations reported in Section 3.1 should be pointed out. In the latter, the nominal temperature differences (ΔT) across each component are multiplied by the hot channel/hot spot factors (superposition approach). In duct temperature calculations, a new and more realistic approach is adopted: the various uncertainties are input to TRITØN and energy equations are solved accounting simultaneously for the effect of uncertainties and inter-assembly heat transfer (integral approach). The superiority of the integral approach in duct temperature calculations, where inter-assembly heat transfer is of paramount importance, is evident. Since TRITØN also has the capability to calculate cladding temperatures, in future analyses the conservatism implicit in the superposition approach adopted for rod temperature calculations can be quantitatively evaluated by comparing temperatures calculated by TRITØN and current temperatures calculated via CØTEC/NICER without accounting for inter-assembly heat transfer.

Another major feature of this analysis is that both positive and negative uncertainties are considered, i.e., uncertainties either increasing or decreasing the nominal ΔT's. In fact, cross duct gradients are magnified when the considered assembly is flanked on the hot side (towards the core centerline) by an assembly with positive uncertainties, i.e., running at higher temperature than nominal, and on the cold side by an assembly with negative uncertainties and running colder than under nominal conditions. Caution must be exercised in calculating the values of the uncertainties when both positive and negative uncertainties in the same core are considered (e.g., fuel assemblies positive, blanket negative). In fact, once a certain uncertainty is selected, its value might remain frozen; for example, if the

uncertainty on stainless steel conductivity is selected as positive in fuel assemblies calculations, it is obviously illogical to take a negative value in blanket assemblies calculations. In this analysis, it was decided that positive uncertainties have first priority, which is equivalent to say that absolute level of temperature is of more concern than relative gradients. Consequently, while the positive uncertainties are all positive indeed, the negative set is a mixture of negative and positive values. Again, the concept of negative uncertainties is a novel one, with the potential for significantly impacting the overall core design, of which duct temperature is only an example.

Following are the values for the various uncertainties and their rationale and justification; they are grouped by assembly type (refer for a summary to Tables XI through XV).

3.2.2 Fuel Assemblies

3.2.2.1 Heat Generation

Calculations in TRITØN are performed using individual assembly powers directly multiplied by the heat generation uncertainty. Thus, each assembly in the core can have a different uncertainty, but within the assembly all the rods are assumed to have the same heat generation uncertainty. Therefore, uncertainties recommended[11] for assembly power are adopted. There are five different groups of assemblies in respect to the uncertainty associated with their power evaluation:

- Group I - Assemblies adjacent to inserted Row 7 corner control rod with a 3% bias at BOC due to ZPPR-7 flux tilt;
- Group II - Assemblies adjacent to inserted Row 7 corner control rod with a 1% down bias at BOC due to ZPPR-7 flux tilt;
- Group III - Assemblies not affected by control rod but with a 3% ZPPR-7 bias;
- Group IV - Assemblies not affected by control rod but with a 1% ZPPR-7 bias; and
- Group V - Assemblies neither affected by control rod nor by ZPPR-7 bias.

Going from positive to negative uncertainties, the following subfactors maintain their initially chosen (positive)(*) value:

- Control Rod Banking - Since this factor affects the whole core, obviously it can have only one sign, either positive or negative;
- ZPPR-7 Flux Tilt - This is a systematic bias obtained by comparing calculated values with ZPPR-7 data. By its very own nature, the same positive/negative consideration above applies;
- Criticality - This uncertainty characterizes the prediction of the hot critical state of the reactor, thus the control rod insertion, thus the power distribution. Since it is related to the whole reactor, it cannot have locally variable values.

The various subfactors comprising the heat generation nuclear uncertainty are reported in Table XII. Except for the negative uncertainties and a different format, they are the same as in Table VI-B.

In addition to the nuclear uncertainties discussed above, a direct factor must be considered to account for variations in power level measurement and control system dead band. A value of 1.03 was used, as per Table V-A. This reactor-dependent factor remains at the same value for both positive and negative uncertainties.

3.2.2.2 Assembly Flow

The individual assembly flow is divided in TRITØN by this uncertainty. Among the various subfactors which affect the coolant enthalpy rise, the only one physically related to the amount of coolant actually flowing in the assembly is the inlet flow maldistribution. The value (1.05) from Table V-A is also adopted here. The negative uncertainty is the reciprocal, i.e., 0.95. This factor is treated as direct.

(*)The reason why positive uncertainties are the primary choice is detailed in Section 4.5.

3.2.2.3 Coolant Enthalpy Rise (ΔH)

This uncertainty comprises all the subfactors which affect the coolant enthalpy rise, but are not directly attributable to assembly power or flow. The ΔH uncertainty factor is applied in TRITØN to the temperature change over each axial calculation increment to provide immediate feedback and avoid calculational instabilities. Subfactors included in the ΔH uncertainties are discussed below.

Flow Distribution Calculational Uncertainty (Simulation Bias)

The same value as recommended in Section 3.1.2 is adopted. Being a simulation bias, the negative uncertainty has to be the same as the positive.

Reactor ΔT Variation

The same values as in Table V-A are adopted. Since this is a reactor-dependent uncertainty, there is no distinction between positive and negative value.

Wire Wrap Orientation

This subfactor accounts for the fact that due to the swirl flow induced by the wire wrap in peripheral channels, the flow and temperature distribution in the assembly depends slightly on the relative orientation of the wire wrap and the power skew. Since there is no rotational discriminator in CRBR assemblies, six TRITØN runs were conducted for a typical fuel assembly varying in steps of 60^{o} the position of the wire wrap from the reference position (0^{o}) used in all TRITØN analyses. The average coolant ΔT (at several axial positions) in the side channels of the hottest and coldest face for the five rotated wire wrap cases were ratioed to the corresponding ΔT for the reference case. This dimensionless factor ranged from 0.981 to 1.022 for the hottest face and from 0.978 to 1.017 for the coldest face, with an average of 1.01 and 0.99, respectively. These were the values adopted as positive and negative uncertainty.

Subchannel Flow Area

This subfactor accounts for variations in side channels temperature due to geometrical tolerances and bundle displacement. An analysis was conducted, using a CØBRA-IV across assembly strip model for a typical fuel assembly, under nominal conditions as well as the following perturbed condition: assembly of minimum diameter rods, compacted to the minimum pitch in a duct of maximum across flats dimensions, with the bundle moved to contact the duct at the flat side towards the core centerline. A ratio of the side average coolant ΔT under perturbed conditions to the nominal case will yield the positive uncertainty when the face towards the core centerline is considered (flow channels area reduced to a minimum on the hot side) and the negative uncertainty when the 180^{0} opposite face is considered (flow channels area increased to the maximum on the cold side). As in the case of the wire wrap orientation factor, several axial locations were examined and the dimensionless factors varied slightly with axial position. Values adopted were average in the top of the core region which is the area of most interest for the core restraint design.

Flow Distribution Calculational Uncertainty (Calibration)

This subfactor accounts for deviations observed between experimental data and the corresponding predictions by the subchannel analysis code CØTEC, which is the basic building block of TRITØN. As mentioned in Section 3.1.2, calibration and comparison of CØTEC against experimental data has been an ongoing task in the past few years, as more data became available. The value (1.08) selected for duct temperature calculations is somewhat larger than the one used in rod temperature calculations (1.054 - Table V-A). In fact, most of the data available (and all the theoretical elaborations of data), are for inboard channels, while side channels are of primary importance in duct temperature calculations, and therefore, the statistical uncertainty would be higher for side than for inboard channels due to the paucity of pertinent data and absence of analyses. As more detailed analyses, as

discussed in Section 3.1.2, are performed, the flow distribution calculational uncertainty (both the direct simulation bias and the statistical calibration components) will be reassessed.

When going from positive to negative uncertainties, this being a statistical calibration factor, it is quite legitimate to assume that the negative uncertainty is symmetric to the positive value, i.e., 0.92. However, caution should be exercised regarding how the negative uncertainty is used; once a poisitive or negative uncertainty is selected, that value applies to all the fuel assemblies. On the other hand, nothing in principle would preclude to having, e.g., a positive uncertainty in the fuel assemblies and a negative uncertainty in the blanket or vice versa. The point is that if it is decided to maximize differential gradients, then opposite uncertainty signs can be taken when different types of assemblies are involved, but such a procedure is illogic when considering the same type of assembly.

Coolant Properties

This factor accounts for uncertainties in sodium coolant properties (density, enthalpy, conductivity). The value recommended in Reference 3 is adopted.

3.2.2.4 Film

This uncertainty comprises the various subfactors which affect the value of the film heat transfer coefficient between side channels and duct wall. These factors are: a) variations in the channel coolant flow rate due to pertinent uncertainties (inlet flow maldistribution, flow distribution calculation uncertainties) cause a variation in the Reynolds number, hence in the Nusselt number, hence in the convection heat transfer coefficient; and b) discrepancy between the film heat transfer coefficient correlation adopted in TRITØN and experimental data.

The film coefficient correlation adopted in TRITØN is:

$$Nu = 5.8 + 0.02\ Pe^{0.8}$$

which applies to sodium flow between parallel plates. The side channels geometry is not exactly representable by parallel plates; additionally, experiments are conducted for either constant temperature or constant heat flux, neither of which represents the side channels. Finally, no sodium heat transfer data exist yet for side channels. Since the contribution of the film resistance to the overall resistance between the side channels of two adjacent assemblies is negligible when compared with the ducts and gap resistance, during the TRITØN development it was concluded that an extensive effort in securing a more accurate representation of the film heat transfer was not warranted. From the above premises, it follows that a sophisticated analysis of the film heat transfer coefficient uncertainty is completely meaningless.

It was, therefore, decided that in TRITØN uncertainty analyses the value of the film coefficient will be bracketed by the two extremes: for positive uncertainties (maximum duct temperature) $h = k/\delta$ where k is the sodium conductivity and δ is the distance between the side channel centroid and the duct wall; for negative uncertainties (minimum duct temperature) $h = \infty$, i.e., the duct ID temperature is taken equal to the side channel bulk coolant temperature.

3.2.2.5 Duct

Two subfactors directly affect the temperature drop through the duct: geometrical deviations and thermal conductivity of the duct. They are treated differently in TRITØN as discussed in the following.

Geometrical Deviations

Variations in the assembly pitch and duct thickness are accounted for in TRITØN by physically changing the value of these dimensions during the calculations. This approach is conservative, since it actually treats these uncertainties as direct, rather than statistical. TRITØN has the capability of varying pitch and duct thickness independently for each pair of interfacing assemblies (i.e., in a cluster of seven assemblies, the user can specify seven different duct thicknesses and six different assembly-to-assembly pitches).

When considering positive uncertainties, dimensions leading to the highest duct temperature are considered, i.e., maximum duct thickness and inter-assembly pitch; for negative uncertainties, minimum duct thickness and pitch will yield the lowest duct temperature.

Duct Thermal Conductivity

The nominal duct (316SS) thermal conductivity is divided in TRITØN by the corresponding uncertainty factor. This factor accounts for deviations in experimental data and irradiation effects. A 10% value was adopted, consistently with the value reported in Table V-A, where out of the 1.12 factor for cladding thickness and conductivity, variations in cladding thickness account for the balance.

3.2.2.6 Interstitial Gap

Subfactors affecting the temperature drop through the interstitial gap between adjacent assemblies are geometrical variations and either uncertainties on the film heat transfer coefficient (if flowing interstitial sodium is considered) or uncertainties on the sodium thermal conductivity (if stagnant sodium is assumed). They are discussed in the following.

Geometrical Deviations

Variations in the interstitial gap due to tolerances are treated in TRITØN similarly to variations in duct dimensions (see Section 3.2.2.5). Once the assembly pitch and the ducts thickness are specified, the gap thickness is also necessarily fixed; thus, the previous discussion applies.

Film Heat Transfer Coefficient

TRITØN has the option of considering either flowing or stagnant sodium in the gap. However, a numerical instability developed for sodium flows of the order of 200 lb/hr, an instability which has not yet been corrected. All TRITØN analyses are therefore currently performed under the conservative assumption

of stagnant sodium. Thus, this uncertainty does not apply at present. When the option of flowing sodium is fully operational in TRITØN, the uncertainty factor affecting the heat transfer coefficient in the gap will be evaluated.

Coolant Properties

This uncertainty applies only when the sodium in the gap is assumed as stagnant. TRITØN divides the sodium conductivity by the corresponding uncertainty factor. A value of 1.017 was assumed as discussed in Section 3.2.2.3.

3.2.3 Inner and Radial Blanket Assemblies

The same philosophy as discussed in detail in Section 3.2.2 for the fuel assemblies applies to the blanket assemblies. Therefore, only the areas in which the blanket assemblies differ from the fuel assemblies evaluation will be discussed.

3.2.3.1 Heat Generation

The major difference in nuclear uncertainties evaluation with respect to the fuel assemblies is that rod power rather than assembly power uncertainties are adopted. The reason is that modeling uncertainties in power predictions of blanket assemblies show a much more pronounced local dependence, and therefore, adoption of assembly power uncertainties would not have been sufficiently conservative.

Different nuclear related uncertainties are calculated for inner blanket, radial blanket first row, radial blanket second row at beginning and end-of-life. All uncertainty factors are treated as direct. Positive and negative uncertainties are calculated directly from Reference 11. The "control rod banking" and "criticality" uncertainties do not change from positive to negative, as discussed in Section 3.2.2.1. The various subfactors comprising the heat generation nuclear uncertainties are reported in Table XIV. In addition, the power level measurement and control system dead band factor must be considered as discussed in Section 3.2.2.1.

3.2.3.2 Assembly Flow

A 7% variation in assembly flow due to inlet flow maldistribution is adopted, as per Table VIII-A.

3.2.3.3 Coolant Enthalpy Rise (ΔH)

The same discussion as in Section 3.2.2.3 applies for the flow distribution calculational uncertainty (simulation bias), reactor ΔT variation, and coolant properties subfactors.

Wire Wrap Orientation

The same analysis as for the fuel assemblies was performed for the blanket assemblies. Slight deviations between the reference and the rotated cases were found at an elevation of 50", with a positive and negative uncertainty factor of 0.98 and 0.96, respectively. However, at elevations of 64" and 112" there was no difference in the side temperatures predicted for different rotation of the assemblies. Thus, it was concluded that this effect is negligible in blanket assemblies and no uncertainty factor was considered.

Subchannel Flow Area

An analysis similar to the one performed for the fuel assemblies resulted in a positive factor of 1.15 and a negative factor of 0.75. The negative factor is somewhat conservative since it is slightly lower than values calculated at 50" and 64".

Flow Distribution Calculational Uncertainty (Calibration)

For added conservatism, the same value (rounded to 1.2) as for rod temperature calculations in inner blanket assemblies is adopted here for both inner and radial blanket assemblies. Regarding the negative value, the same precautions as previously discussed apply, i.e., once a positive or negative uncertainty is chosen, it applies to all blanket assemblies.

3.2.3.4 Film

See corresponding Section 3.2.2.4.

3.2.3.5 Duct

See corresponding Section 3.2.2.5.

3.2.3.6 Interstitial Gap

See corresponding Section 3.2.2.6.

3.2.4 Primary Control Assemblies

Uncertainty analyses for primary control assemblies rod temperatures calculations have not been conducted to the same level of depth and detail as for the fuel and blanket assemblies (in fact, control assembly uncertainty factors reported in Reference 3 were obtained in the only analysis performed so far, which referred to the homogeneous core). Thus, treatment of the control assemblies uncertainties is generally less detailed and sophisticated than for the fuel and blanket assemblies; see, for example, nuclear and flow distribution calculational uncertainties. The same situation of course applies to the duct temperature uncertainties analysis, since it relies on analyses previously conducted for rod temperature uncertainties.

As was the case for the blanket assemblies, only those uncertainties where a significant difference exists in respect to fuel assemblies analysis will be discussed in the following. The most significant feature characteristic only of the control assemblies is the need for additional uncertainties on the bundle/bypass flow split and on the bypass enthalpy rise. Regarding the latter, it is obvious that both inner and outer duct temperatures depend on the amount of flow and enthalpy rise in the bypass; on the other hand, the enthalpy rise in the bundle and the bypass are affected by different types of uncertainties, thus, the need to handle them separately.

3.2.4.1 Heat Generation

Nuclear uncertainties are as recommended in Reference 3. The uncertainty on power level measurement and control system dead band is obviously the same as for the fuel and blanket assemblies.

3.2.4.2 Assembly Flow

The inlet flow maldistribution uncertainty is from Reference 3.

3.2.4.3 Bundle/Bypass Flow Split

An additional uncertainty has to be considered for the control assemblies, i.e., the one affecting the flow split between absorber bundle and bypass. The flow split predicted by the CRAB code[19] is input to TRITØN; a comparison between CRAB predictions and HEDL experimental data for the FFTF 61-pin absorber assembly showed a maximum over-prediction of the bundle flow fraction by CRAB of 6%. To account for additional uncertainties for a 37-pin bundle, a 10% positive uncertainty is considered. Since the CRAB code over-estimates the amount of flow through the bundle, the negative uncertainty is taken as unity.

TRITØN calculates the nominal bundle flow as the total assembly flow multiplied by the nominal flow split. If uncertainties are accounted for, then the following calculations are performed: a) the nominal flow split is divided by the flow split uncertainty; b) the total assembly flow is divided by the assembly flow uncertainty; c) the bundle flow is equal to the total flow (with uncertainties) from (b) multiplied by the flow fraction (with uncertainties) from (a); and d) the bypass flow is equal to the total assembly flow from (b) multiplied by the difference to unity of the flow fraction from (a).

3.2.4.4. Bundle Enthalpy Rise

Since no calibration/verification of subchannel analysis codes against experimental data has yet been done, a direct factor of 8% is estimated[3] for the flow distribution calculational uncertainty. The reactor ΔT variation and coolant properties uncertainties are obviously the same as for the fuel and blanket assemblies. Analyses were performed to assess the effect of wire wrap variations and it was found that the average side channel temperatures were insensitive to such variations, thus yielding a hot channel factor of unity. Finally, an analysis similar to the fuel assemblies, to assess the effect of subchannel flow area variations, showed on the average a positive uncertainty of 1.16 and a negative uncertainty of 0.87.

3.2.4.5 Bypass Enthalpy Rise

The subfactors affecting the bypass enthalpy rise uncertainty, which still need to be considered, are: reactor ΔT variation, subchannel flow area and coolant properties. In fact, the effect on the bypass flow due to the uncertainty on the bundle/bypass flow split has already been accounted for as discussed in Section 3.2.4.3. While the reactor ΔT variation and the coolant properties uncertainties are necessarily the same as discussed for the other components, ad hoc analysis was needed to assess the effect of subchannel flow area variations since the same rod bundle displacement affects differently the temperature in the bundle side channels and in the bypass. In fact, positive and negative uncertainties of 1.23 and 0.89, respectively, were calculated for the bypass, which are different from the corresponding values for the rod bundle.

3.2.4.6 Film

See corresponding Section 3.2.2.4.

3.2.4.7 Duct

See corresponding Section 3.2.2.5.

3.2.4.8 Interstitial Gap

See corresponding Section 3.2.2.6.

4. STEADY STATE THERMAL PERFORMANCE

4.1 Plant Conditions

Following the practice established during previous analyses[1], two sets of plant conditions are used in the thermal-hydraulic design, i.e., plant thermal-hydraulic design value (THDV) conditions and plant expected operating conditions (PEOC). The THDV conditions (730°F inlet/995°F outlet temperature; total reactor flow 41.446 x 10^6 lb/hr) are the Clinch River rated plant conditions and are used in: a) analyzing permanent components which have the same 30-year lifetime as the plant; b) transient and safety analyses, since they are more conservative than the plant expected conditions and represent the "worst bound" of plant conditions. The plant expected operating conditions represent the plant conditions at which the CRBR is expected to operate accounting for the operating conditions of the heat transport systems, such as pump characteristics, reactor and primary loop pressure drop uncertainties, fouling and plugging of heat exchangers, etc. Expected operating values for the primary heat transport system principal parameters (inlet, outlet temperature and ΔT) are thus evaluated, together with the associated uncertainties. The results of this study for the heterogeneous core, which comprised a Monte Carlo type analysis, are reported in Table XVI. The major differences in respect to an analogous study previously performed for the homogeneous core are: 1) the consideration of the progressive fouling of the heat exchangers during the plant 30-year lifetime, which affects the predicted values of the plant operating conditions (in the previous studies, end-of-life fouling, i.e., after thirty years operation, was conservatively assumed in evaluating plant expected operating conditions); and 2) a more comprehensive accounting of all uncertainties affecting plant operation. Plant expected operating conditions are adopted in core thermofluids analyses of replaceable components, such as the core assemblies, chiefly in determining the fuel rod parameters (cladding temperature, fission gas pressure) which are the basis for evaluating the structural behavior and for assessing whether lifetime/burnup objectives are actually met.

As mentioned in Section 1, a critical reevaluation of the flow impedance in the entire primary system led to a significant increase in the value of the expected reactor flow. A new consistent set of plant expected operating conditions to be used in thermal calculations has not yet been developed, thus, the decision of utilizing in the interim the more conservative conditions already determined, which will yield higher temperatures in the core. Updated values of expected reactor flow were used for pressure drop calculations, as reported in Section 6.3.

Plant expected operating conditions and associated uncertainties adopted in the thermal performance analyses are reported in Table XVII. Following is a brief discussion of the rationale in determining the values reported in Table XVII from the ones in Table XVI.

First, the mean values of Table XVI are chosen as the nominal values of Table XVII, thus, conservatively including the bias factor directly into the nominal values. Since the most critical time for core assemblies is at the end-of-life, when the cladding strain and damage function are maximum, second core values have been selected as corresponding to four-year fouling conditions. Due to the fact that four-year fouling conditions were not evaluated, it was assumed that the same difference in plant parameters between year two and year zero repeats between year four and year two. Again, the selected approach is conservative for two reasons: 1) plant conditions have been considered constant over the two-year span and equal to the worst end-of-span conditions, thus neglecting the more favorable conditions which exist throughout the core lifetime; and 2) the effect of fouling is not linear with time, but it is rather pronounced at the beginning and then tapers off during the plant lifetime, as can be seen by comparing plant parameters in Table XVI for 0, 2 and 30 years. Thus, the assumption that the same deterioration of plant conditions which occurs in the first two years (first core) also occurs during the third and fourth year (second core) is conservative.

While the mean values of plant parameters are consistent (i.e., outlet temperature equals inlet temperature plus ΔT), the same is not true when uncertainties are included. In fact, uncertainties quoted in Table XVI are

for each parameter independently; thus, if the inlet temperature and the ΔT at the 97.7 confidence level (e.g., for the two year fouling) are added, the outlet temperature is equal to $999^{o}F$, significantly higher than the $976^{o}F$ reported. Actually, $976^{o}F$ represents the 2σ outlet temperature, while $999^{o}F$ is, roughly, a 4σ value.

Because the inlet temperature and ΔT are defined, while the outlet temperature is derived, the following procedure is used:

- The uncertainty on the ΔT is calculated as a dimensionless factor and is combined statistically with other engineering and nuclear uncertainties.
- The uncertainty on the inlet temperature is combined statistically with the loop-to-loop imbalance effect and the combined uncertainty is directly added to the nominal value.

This approach is conservative. The loop-to-loop imbalance effect is much smaller than the inlet temperature uncertainty. If there were no other uncertainties, the outlet temperature would be at approximately the 4σ level, as previously mentioned. However, other uncertainties, engineering and nuclear, do affect the reactor ΔT, and therefore, when combined statistically with the plant conditions uncertainty on ΔT, will actually decrease its value.

Finally, with regard to the uncertainties on plant operating conditions reported in Table XVII, the following must be noted:

- Uncertainties on reactor ΔT are calculated and applied as in previous analyses[1];
- Uncertainties on inlet temperature are treated differently than for the homogeneous core studies. Previously, an uncertainty on reactor inlet temperature, as evaluated through Monte Carlo type analyses, was translated into a reactor ΔT uncertainty and combined statistically with other subfactors affecting the reactor ΔT. In addition, a $16^{o}F$ uncertainty was superimposed directly on the nominal inlet temperature value to account for loop-to-loop imbalance and primary loop temperature control uncertainties. The improved procedure adopted in these analyses was, as previously

mentioned, to combine statistically the loop-to-loop temperature imbalance effect with the uncertainty on inlet temperature (which is due to all effects related to plant operating conditions) and to add the combined uncertainty to the inlet temperature. The loop-to-loop imbalance effect was evaluated from experimental data obtained in the CRBR inlet plenum feature test conducted at HEDL where different values were obtained for each inlet module ranging from practically zero near the reactor center to a maximum value of 4.6°F at the core periphery. Because such variation was minimal, compared with the much greater plant uncertainty with which the imbalance effect is combined, for simplicity the maximum value is conservatively used for all assemblies.

- In previous analyses[1], the power level measurement/control dead band uncertainty was considered separately in the hot spot/channel tables as a direct factor. However, in the present analyses, it is already included in the Monte Carlo evaluation of plant operating conditions uncertainties. Therefore, the power level measurement/control dead band uncertainties are not considered separately in thermal-hydraulic analyses conducted for plant expected operating conditions, but are still considered separately in those analyses performed for plant thermal-hydraulic design conditions.

- Even though the plant operating conditions uncertainties adopted in these studies represent a sensible improvement over the analogous analyses performed for the homogeneous core, they are still quite conservative, as previously mentioned. In fact, a statistical analysis performed in Reference 3 showed that the value assigned here to the uncertainty factor on ΔT is actually inclusive of the inlet temperature variation effect as well. The loop-to-loop imbalance uncertainty recommended in Reference 3 is 7.4°F, higher than the 4.6°F used here, but this is more than offset by the fact that a 2σ inlet temperature uncertainty of 33°F (first core) or 36°F (second core) is adopted here (see Table XVII), while in Reference 3, the inlet temperature uncertainty is included in the ΔT factor (1.14), as mentioned above.

4.2 Linear Power

Linear power ratings over a 60° core sector (fuel, inner and outer blanket assemblies) are reported in Figures 11 through 20.

Average, peak, 3σ and 3σ plus overpower linear ratings are reported. To clarify the adopted nomenclature, "average" represents an arithmetic average over the 217 (61) rods of the fuel (inner/outer blanket) assembly. Therefore,

it generally represents a fictitious rod not exactly corresponding to any physical rod in the assembly. "Peak" refers to the rod in the assembly having the highest power; i.e., no uncertainty factors are applied in the evaluation of the peak power rating. "3σ" power rating refers to the value resulting from applying to the peak rod both the uncertainties on the nuclear peaking factors (radial and axial) and the engineering uncertainty factors, both at the 3σ level of confidence. The "3σ plus overpower" values are derived from the 3σ linear power ratings by applying an additional 15% over the CRBR rated nominal full (975 MWt) power.

The maximum (at 3σ plus 15% overpower conditions) fuel assembly total linear power rating occurs in assemblies 101 and 68 (15.8 kw/ft at beginning-of-cycle 1; 15.1 kw/ft at beginning-of-cycle 3, Figures 11 and 15, respectively). The maximum inner blanket assembly linear power rating occurs in assembly 99 at end-of-cycle 4 (20.6 kw/ft, see Figure 18). During the first core, the highest inner blanket power rating is in assembly 67 at end-of-cycle 2 (19.2 kw/ft, Figure 14). Finally, the maximum linear power rating in radial blanket assemblies occurs in assembly 201, and the symmetrical 301, at end-of-cycle 3 (16.4 kw/ft, Figure 18), in spite of the fact that the assembly power is highest at end-of-cycle 4 (compare peak power ratings at EOC3, 12.2 kw/ft, Figure 16 and at EOC4, 12.4 kw/ft, Figure 18). This is due to the time-dependence of the nuclear uncertainties (see Table VIII-B) which are maximum at BOL and decrease to a minimum value at EOL.

4.3 Assemblies Mixed Mean Temperatures

Assemblies mixed mean temperatures are presented in Figures 21 through 30 for beginning and end of each of the first four (five for second row radial blanket assemblies) cycles. Since calculated values of the mixed mean temperatures, specifically maximum temperatures and temperature gradients between adjacent assemblies, are a critical input to the upper internals structure design, plant THDV conditions were adopted in these calculations. In fact, the UIS is a permanent, 30 year lifetime, component.

Nominal (no uncertainty factors applied), 0σ (only direct uncertainty factors are applied), 2σ and 3σ (direct plus statistical uncertainty factors at the 2σ and 3σ level of confidence are applied) are reported in the figures.

First core conditions are the worst for the UIS from the point of view of both maximum temperatures and temperature gradients. The maximum temperature(*) is 1123°F in assembly 45 at BOC1, with a maximum gradient (273°F) between assembly 52 and 302 (see Figure 21). Mixed mean temperatures follow the same lifetime pattern as the power generation, thus inner blanket assemblies which start very cold at beginning-of-life (≈850°F at BOC1) attain temperatures comparable with those of the fuel assemblies at EOC2. The same pattern repeats in the second core, cycles 3 and 4. The radial blanket assemblies start at approximately the same temperature as the inner blanket at BOC1, but it is not until cycle 4 or 5, which is the end of their life, that their temperatures are comparable with those of the other assemblies. The maximum mixed mean temperature for the second core occurs at BOC3 in assembly 45 (1115°F). While first and second cores are quite similar in terms of maximum mixed mean temperature, they show a markedly different behavior as far as maximum gradients are concerned. During the first core, the maximum temperature difference between adjacent assemblies occurs at the fuel/radial blanket interface: in cycle 1 between assemblies 52 and 302 (273°F at BOC1, 225°F at EOC1), in cycle 2 between assemblies 24 and 202 (227°F at BOC2, 163°F at EOC2). In the second core, the maximum gradient position moves at the fuel/inner blanket interface: between assemblies 37 and 99 at BOC3 (239°F), assemblies 2 and 128 at EOC3 (136°F), assemblies 4 and 62 at BOC4 (149°F). At the end of cycle 4, the mixed mean temperatures of fuel and inner blanket assemblies are quite close, so that the maximum gradient occurs between two radial blanket assemblies, i.e., assemblies 206 and 213 (96°F).

Mixed mean temperatures reported in this section are calculated assuming adiabatic boundaries at the assemblies interface. Thus, the beneficial effect of inter-assembly heat transfer in flattening the high temperature gradients is not taken into account.

(*)All temperature values reported in this discussion are nominal.

Mixed mean temperatures accounting for inter-assembly heat transfer are calculated by TRITØN. Core-wide TRITØN calculations were performed for BOC1 and EOC4, as reported in Section 4.5. A comparison of mixed mean temperatures under adiabatic conditions and more realistically accounting for inter-assembly heat transfer (Figures 66 and 67) is discussed in that section.

4.4 Rod Lifetime Cladding Temperature/Pressure Histories

All fuel, inner blanket and outer blanket assemblies in a 60^{o} core symmetry sector were followed during their lifetime (i.e., first and second core for fuel and inner blanket assemblies; row 1 outer blanket assemblies over cycles 1 through 4 and row 2 radial blanket assemblies over cycles 1 through 5). The maximum cladding temperature and fission gas pressure in the hot rod at the 2σ level of confidence for plant expected operating conditions were predicted for each assembly. Lifetime profiles are reported here (see Figures 31 through 51) only for selected assemblies, due to obvious space limitations. The limiting, for both first and second core, fuel and inner blanket assembly in each orificing zone, are provided. The limiting assembly is the one requiring, in a given zone and for a given core, the highest amount of flow (see Figures 9 and 10). Note that the driver assembly of each orificing zone as defined in Section 2.4, is the assembly requiring the highest amount of flow in either core. Thus, the limiting assemblies in zone 1 (#10) and zone 4 (#52) in the first core are the drivers of the respective zones, while the limiting assemblies in the second core for zones 2 (#37), zone 3 (#2) zone 7 (#99) and zone 8 (#46) are the drivers of the respective zones. The same assembly (#49) in zone 5 is limiting for both the first and second core and is obviously the driver. The radial blanket assemblies remain in the reactor through the first and second core, thus, no distinction is necessary: the drivers of zones 9 (#201), 10 (#203) and 11 (#206) are first row assemblies and have a 4 cycle lifetime; the driver of zone 12 (#212), a second row assembly, has a 5 cycle lifetime. Regarding orificing zone 6, where fuel and inner blanket assemblies are alternating, typical examples of the various combinations are shown here: inner blanket assembly remaining in the same location in the first two cycles (#98, Figure 41), inner blanket assembly in the odd cycle followed by a fuel assembly in the even cycle (#62, cycles 1 and 2, Figure 42; #62, cycles 3 and 4, Figure 43). As a general

trend, fuel assemblies in the inner region of the core (see, e.g., Figure 36), experience a cladding temperature jump from the odd to the even cycle, while the fuel assemblies in the outer region (see, e.g., Figure 37), experience a drop. The cladding temperature generally decreases during a given cycle. The cladding temperature, however, increases during the even cycle (see Figures 31, 33, 34) in those assemblies adjacent to the Row 7 corner control assemblies. Blanket assemblies have obviously a continuously increasing temperature during their lifetime, a direct consequence of the increase in power. The lifetime behavior of a given assembly during first and second core is quite similar, both qualitatively and quantitatively. The only major difference is that a higher fission gas pressure is attained in the second core, due to the longer residence time and burnup.

As an overall summary, the highest cladding ID temperature attained in each assembly in the first and second core is reported in Figures 52 and 53, respectively, together with the time of occurence. As shown in the figures, the maximum cladding temperatures vary significantly from assembly to assembly, a direct consequence of the orificing philosophy, where assemblies were orificed to satisfy burnup/lifetime goals and transient limitations, rather than equalizing cladding temperature. It can be noted for example that fuel assemblies in the inner core region, which are CDF limited, require lower temperatures than assemblies in the outer region, which are transient limited. Blanket assemblies, when starting from the same steady state temperature, attain a higher transient temperature than fuel assemblies. Thus, the steady state maximum cladding temperature in blanket assemblies is lower than for the transient limited fuel assemblies, a direct reflection of the adoption of the same transient limit for all core assemblies.

Structural analyses performed utilizing the core assemblies thermal performance data reported here verified that indeed the burnup/lifetime goals are satisfied in all assemblies during the first and second cores. Similarly, transient analyses were performed for some worst assemblies, starting from the steady state conditions reported here, and it was verified that the transient limitations are indeed met.

4.5 Duct Temperature and Related Analyses

Detailed three-dimensional duct temperature distributions (axially, radially and circumferentially) were predicted in support of the core restraint design and related (duct bowing, dilation, reactivity coefficient) analyses. A 60^{o} core symmetry sector was analyzed at plant THDV conditions at BOC 1 and EOC4, thus bracketing the entire lifetime considered.

The current version of the TRITØN code which models a cluster of seven adjacent assemblies was used. The outer boundaries of the cluster are assumed to be adiabatic, while heat is transferred across the internal interfaces (i.e., ducts and interstitial sodium flow gap). The CRBRP core 60^{o} symmetry sector, plus one row of assemblies at each of the boundaries to provide the necessary boundary conditions to the assemblies within the sector, was analyzed in groups of seven assemblies at one time and changing each time to a different central assembly, which is "dumped" to output. The TRITØN model, based on the subchannel analysis code CØTEC, explicitly solves the thermal-hydraulics of wire wrapped assemblies (by considering turbulent mixing, sweeping, pumping and swirl flow). In addition, it accounts for the exchange of heat between adjacent assemblies. The code is able to model all types of core assemblies, including the radial shield, which were in fact analyzed to provide the proper boundary to the second row radial blanket assemblies.

Gamma-heating in the ducts is considered in TRITØN by including it in the total assembly power. For the control assemblies case, the gamma-heating is split between the absorber bundle and the bypass. Therefore, gamma-heating is accounted for in a global fashion when calculating duct temperatures, rather than as a localized effect.

Duct temperatures were calculated under nominal conditions and accounting for uncertainties (at the 2σ level of confidence). The uncertainties runs were as follows:

- BOC1 - Fuel assemblies have positive uncertainties, blanket and control assemblies have negative uncertainties, uncertainties on power and flow in the radial shield were such to minimize their temperature;

- EOC4 - All fuel, blanket and control assemblies have positive uncertainties, radial shield power and flow uncertainties are such to maximize their temperature.

The rationale behind the choice of these combinations of uncertainties was that at BOC1 fuel assemblies have their maximum power, thus temperature, while blanket assemblies are at the coldest time in their life. Therefore, choosing the uncertainties in order to increase the fuel assemblies temperature and at the same time to decrease even further the blanket and control assemblies temperature, i.e., "make the hot hotter and the cold colder", will yield the worst possible cross-duct gradients in the CRBRP first two cores. At end-of-cycle 4, blanket assemblies are at their maximum temperature, thus adoption of positive uncertainties in all core assemblies will yield the highest level of duct temperature across the core. It is apparent that the selected combination of uncertainties and time in life is the one giving the highest temperatures when it is considered that selection of positive uncertainties will tend to increase the temperature in the affected and neighboring assemblies, while EOC4 is the only time when all the blanket assemblies (except the radial blanket second row) are at end-of-life (maximum power) conditions.

Uncertainty values used in these analyses were reported in Section 3.2. Geometrical variations were selected to minimize inter-assembly heat transfer (thus maximize thermal gradients) at BOC1, hence the maximum values of assembly pitch and duct thickness were used for all assemblies. At EOC4, where the purpose is to maximize temperatures, the duct thickness and assembly pitch was maximum for the fuel assemblies, but was minimum for the other assemblies and at the interfaces of different types of assemblies. In fact, increasing the heat transfer between fuel and blanket assemblies has a noticeable impact on increasing the blanket temperature, but it is not very significant in decreasing the fuel assembly temperatures.

It should also be noted that even though no formal uncertainties were discussed in Section 3.2 for the radial shield assemblies, their power and flow were adjusted in the TRITØN runs, in order to provide a "cold" and "hot" boundary to the radial blanket at BOC1 and EOC4, respectively.

Typical results of duct temperatures calculated by TRITØN are reported in Figures 54 through 65. Midwall duct temperatures reported for each face are the average over the face of the detailed temperature profile calculated by TRITØN (TRITØN calculates local duct temperatures circumferentially along the face at each peripheral subchannel). In addition, the direction (with arrow) and magnitude of the maximum cross-duct (midwall) temperature gradient in each assembly is shown. Generally, the largest gradients occur at the fuel/radial blanket interface, which is therefore a very critical region for the core restraint design. The typical mappings shown here are for three axial elevations; i.e., 32" (middle of the core), 60" (approximately the above-core-load-pad location) and 112" (top of the rod bundle). TRITØN calculates core-wide duct temperatures at 0.5" intervals and all these data were transmitted, via computer tapes, to the core restraint designers.

In examining the results reported in Figures 54 through 65 it is evident that the worst gradients, by far, are at BOC1 when positive uncertainties in the fuel and negative uncertainties in the blanket are considered. While this result was anticipated, some interesting observations can be made. Blanket assemblies temperatures accounting for uncertainties are generally lower than the corresponding nominal values, which means that the effect of negative uncertainties is greater than that of inter-assembly heat transfer, even though the latter was enhanced by considering opposite uncertainties. Cross-duct gradients in individual assemblies increase significantly, in some instances they almost double. Even more importantly from the core restraint standpoint, is the increase in the temperature difference between adjacent faces of fuel and blanket assemblies. For example, at the top of the core (see Figures 56 and 57) the adjacent faces temperature difference is of the order of 50-80^{o}F under nominal conditions, but of the order of 100-140^{o}F if the effect of uncertainties is considered. At EOC4, the duct temperatures increase quite uniformly throughout the core if the uncertainties are

considered, with increases in excess of 100°F. The cross-duct gradients and temperature differences between adjacent faces also increase, but not nearly as much as for the BOC1 case, the increase being of the order of 20°F.

It is obvious that many combinations of uncertainties exist; the two combinations adopted in these analyses are to be considered only as representatives of typical extreme conditions. Calculations of duct temperatures provide the input necessary to structural analyses. Only after these are completed and the designers examine both the thermal and structural behavior, will it be possible to define more precisely which distribution of uncertainties throughout the core should be used in the design. Such distribution must be tailored to the particular analysis being conducted, since a certain combination of uncertainties could be the critical one for the core restraint design, a different one for duct dilation analyses, and so on.

Calculations of assemblies mixed mean temperatures have also been performed by TRITØN; the results are reported in Figures 66 and 67 for BOC1 and EOC4, respectively, which compare TRITØN calculated temperatures with the corresponding temperatures obtained for adiabatic conditions in Section 4.3 (and reported in Figures 21 and 28), thus showing the effect of inter-assembly heat transfer. As expected, at BOC1 where the fuel assemblies have the maximum power in life and the blanket assemblies the minimum, heat is transferred from the fuel to the blanket assemblies and mixed mean temperatures are higher in the blanket and lower in the fuel than otherwise calculated under adiabatic conditions. The maximum temperature difference between adjacent assemblies, which occured between assemblies 52 and 302 was 273°F under adiabatic conditions and is reduced to 261°F when considering inter-assembly heat transfer, a reduction of ~4%. Reductions in adjacent assemblies gradients are greatest at the core center (where the power production in the fuel is maximum); for example, between assemblies 34 and 59, the gradient of 227°F calculated under adiabatic conditions, is reduced by 10% to 205°F when accounting for inter-assembly heat transfer. It should be also pointed out that the coolant does not exit from the assembly with a uniform temperature equal to the mixed mean, but a radial temperature gradients exists within the assembly exit. TRITØN divides the assembly exit

area into 6 sectors and calculates the local temperature in each of these sectors; thus, this detailed information is available to the structural designers for refined analyses.

Finally, as input to duct dilation and bundle/duct interaction, selected assemblies (see Figure 68) were followed through their entire lifetime with TRITØN. Parameters calculated and transmitted to the assembly structural designers were duct midwall temperatures over each assembly face and rod cladding midwall temperatures averaged over the rod circumference for two transverses; i.e., from corner to corner and flat to flat of the assembly (see Figure 69). All temperatures were calculated as a function of axial position.

The capability to calculate rod cladding temperature was therefore added to TRITØN to perform these calculations. Obviously, calculating both duct and cladding temperatures in the same TRITØN runs was much more efficient than calculating duct temperatures with TRITØN and rod cladding temperatures via CØTEC and NICER. More importantly, the CØTEC/NICER route considers adiabatic assembly boundaries, thus duct temperatures would have been calculated accounting for inter-assembly heat transfer, while calculated cladding temperatures would have neglected this effect, which is significant in the blanket assemblies. Thus, the temperatures calculated here and provided to the mechanical designers are correctly self-consistent. Typical examples of these calculations are reported in Figures 70 and 71.

It should be pointed out that TRITØN now has the capability of calculating not only average cladding temperatures as in this case, but also local cladding temperatures accounting for hot channel/hot spot factors and in the same detail as presently calculated by CØTEC and NICER. As mentioned in Section 1, this significant upgrading of analytical methods capability now opens the possibility of predicting fuel and blanket rods thermal performance rigorously accounting for the effect of inter-assembly heat transfer.

5. POWER-TO-MELT ANALYSES

5.1 Introduction

Analyses for the worst fuel and inner blanket assemblies were performed to investigate whether the criterion of no incipient melting at 115% rated power and accounting for uncertainties at the 3σ level of confidence is actually met. The fuel assemblies analyses focused on the peak power pins at beginning-of-life, which are the most critical from the point of view of power-to-melt, and showed that adoption of a programmed startup will guarantee satisfaction of the no-melting criterion. Analyses of the inner blanket assemblies (which envelope the radial blanket assemblies, since the latter attain much lower powers at EOL) investigated both the hot(maximum cladding temperature) pin and the peak (maximum power) pin. In fact, the cladding temperature has a very marked effect on cladding swelling and ultimately, through gap size, gap conductance and fuel centerline temperatures, on the power-to-melt. Analyses indicated that the no fuel melting criterion in the inner blanket is satisfied, in spite of the adopted conservatism, which is believed to be excessive.

5.2 Fuel Assemblies Power-to-Melt Analyses

A detailed power-to-melt of the peak power pins in fuel assemblies 101 and 14 were performed, using the LIFE-3 code[20]. Geometry and operating conditions of these pins (calculated by NICER for plant THDV conditions and 0σ hot spot factors) are reported in Table XVIII. Assembly 101 was selected as the one with the maximum power rating at 3σ overpower conditions, while assembly #14 has the highest peak power pin (see Figure 11). LIFE-3 input was obtained from appropriate NICER runs. The startup ramp used in this study is shown in Figure 72. No effort was devoted in this study to the optimization of the startup procedure, which will be performed for final, as-built design. An experimental program to investigate the startup procedure and to guide in its optimization has been proposed. Since BOL is the time when the power is maximum and the power decreases with life due to the depletion effect, power-to-melt analyses for the fuel assembies were not conducted beyond the programmed startup.

The cladding swelling used in this study was Revision 5 of the first core steel swelling[18]. Note, however, that since early-in-life cladding swelling is negligible, the choice of cladding swelling equations is actually unimportant.

The nominal powers-to-melt computed using LIFE-3 are tabulated in Table XIX. The axial location (X/L) values of Table XVIII were chosen since they are the positions of maximum power. Due to the axially increasing temperature in the cladding, melting will first occur slightly above the position of maximum power, but this effect is neglected here, since it can be easily accommodated in the optimization of the programmed startup. Note that the programmed startup can not affect the power-to-melt in blanket, which occurs at end-of-life, thus, the actual temperature gradient was taken into account for the analyses reported in Section 5.3.

To determine whether the pin designs and power histories are able to withstand a 15% overpower transient without melting within a 3σ level of confidence, relative statistical power-to-melt uncertainties must be applied. The same uncertainty values and procedure reported in Reference 3 were adopted in this analysis and are briefly summarized in the following and in Section 5.2.1.

The primary data used for this work were the results of the short time (low burnup) HEDL P-19[21] and P-20[22] tests which were designed to provide thermal performance information.

The LIFE-3 code used in this study is a detailed model for describing the thermal and mechanical behavior of fast reactor oxide fuel pins and has been calibrated and verified with the HEDL P-19 and P-20 tests in addition to a number of intermediate and high burnup pins. Figure 73 and Table XX show how well the code represents the P-19 and P-20 data. The code was used to calculate the power-to-melt of the CRBRP fuel and blanket rods, and the sensitivities to variations in fuel pin parameters used for uncertainty analysis.

For fuel applications, the uncertainties in the code predictions of the power-to-melt arising from data scatter and the overall accuracy of measurements in the EBR-II reactor are first analyzed. The uncertainties which occur when applying the code to the CRBRP conditions are then evaluated. The factors considered here include the tolerances on fabrication parameters and reactor instrumentation, nuclear, thermal-hydraulic and systematic uncertainties. The individual uncertainties were determined by calculating the effect of a variation in each parameter on the nominal power-to-melt.

All the individual uncertainties are then statistically combined and the probability distribution for the reactor power-to-melt determined. The design criterion can then be measured by determining if the 115% of nominal power is at least three standard deviations below the power-to-melt.

5.2.1 EBR-II Uncertainties

The factors associated with EBR-II experiments which contribute to uncertainties in power-to-melt measurements are listed and defined below (where σ is the standard deviation):

1. σ_{time} is due to uncertainty on overall power level due to variations in EBR-II instrumentation and the uncertainty in the neutronics calculation for a given core loading. This uncertainty causes random fluctuations in quoted power level that vary with time.

2. σ_{sys} is due to a difference between actual and quoted overall EBR-II power that doesn't change with time. It is known that a systematic shift in EBR-II power level exists and a correction is made by experimenters. An estimate is required of the uncertainty on this correction for this analysis which is identified here as σ_{sys}. This uncertainty does not show up as scatter in the data. Such a systematic uncertainty would show up in the scatter of data comparing different reactors.

3. σ_{space} is due to uncertainties in the spatial dependence of neutronics calculations and local inhomogeneities in the EBR-II core.

4. σ_{fab} is due to variation in fuel pin fabrication parameters from their nominal values.

5. σ_{PIE} is due to uncertainty in post-irradiation examination measurements.

The evaluation of each of these uncertainties will now be discussed.

σ_{time}

The major contribution to this uncertainty results from fluctuations in the primary and secondary EBR-II coolant loop heat balance. This yields a 2% standard deviation[23]. Neutronic calculations of γ precursors in the P-19 test introduce a further uncertainty of less than 1%[24] and a value of 0.8% was used. Accordingly, this factor was evaluated as

$$\sigma_{time} \leq \sqrt{2\%^2 + 0.8\%^2} = 2.2\%$$

This uncertainty would not show up as fluctuations in results from a single subassembly since all pins would have been subjected to the same errors in overall power determination during the same time.

σ_{sys}

A detailed analysis of the P-19 test indicated that a correction factor of 0.94 must be applied to the calculated EBR-II power level[24]. This factor has been used in all reported analyses of these results and those of the P-20 test and was used for the LIFE-3 calibration. Subsequent work suggested a factor of 0.91[23], while a recent analysis by the EBR-II Project indicates a value of 0.96[25]. As an interim position, the 0.94 factor is being retained. An evaluation of the recent analysis

by the EBR-II Project will be performed when an official documentation is issued. In addition, burnup analysis data will be evaluated with respect to this factor. The EBR-II Project also estimated that further systematic bias should be not more than $\pm 2\%$[25]. An uncertainty, σ_{sys}, of 3% is used here which covers both the .91 and .96 power factors and is more conservative than the 2% estimate by EBR-II.

σ_{space}

The spatial uncertainties in pin powers arise from uncertainties in neutron transport calculations. Calculations have been checked by comparison of measurements of control rod worth[24]. Table XXI and Figure 74 show the resulting percentage difference between measured and calculated flux, which has a standard deviation, σ''_{space}, of 1.7%. In addition, local flux peaks produce an estimated uncertainty, σ'_{space}, of about 0.5%. Finally in the highly enriched fuel of P-19, differences in the γ absorption can produce a +0.7% to -0.7% variation in pin power going from the center to the outside of the assembly. This introduces a standard deviation of $0.7/\sqrt{3} \overset{\sim}{=} 0.4\%$. Combining:

$$\sigma_{space} \overset{\sim}{=} \sqrt{1.7^2 + 0.5^2 + 0.4^2} = 1.8\%$$

σ_{fab}

The scatter in burnup measurements as compared to values calculated from EBR-II powers has been analyzed and found to be $\sigma_{BU} \overset{\sim}{=} 1.1\%$. This analysis is from individual subassemblies, and since pins in a subassembly are in the reactor for the same time, they would not reflect the uncertainties σ_{time} and σ_{sys}. The scatter in the burnup data includes a combination of EBR-II power uncertainties and uncertainty in the burnup measurement technique. Thus:

$$\sigma_{BU} \overset{\sim}{=} 1.1\% \overset{\sim}{=} \sqrt{\sigma'^2_{space} + \sigma_{fab}^2 + (0.5\%)^2} \qquad (i)$$

where the 0.5% is the estimated burnup measurement accuracy of the mass spectrometry. The spatial uncertainty $\sigma'_{space} \sim 0.5\%$ is that for an individual subassembly and not the entire core.

The burnup uncertainty has also been independently calculated by HEDL to be 3% (1σ). In this work, a single power factor for all subassemblies was used. The data scatter due to power fluctuation with time, σ_{time}, and core-wide spatial uncertainty, σ_{space}, would therefore apply and the 3% standard deviation obtained can be attributed to

$$3\% \simeq \sqrt{\sigma_{time}^2 + \sigma_{space}^2 + \sigma_{fab}^2 + (0.5\%)^2} \qquad \text{(ii)}$$

Using the previously determined values for σ_{time}, σ_{space} and σ'_{space} in equations (i) and (ii) two values for σ_{fab} are obtained, 0.85% and 0.82%, which are therefore in excellent agreement. For simplicity, a rounded-off value of 0.8 was used in these studies.

$\underline{\sigma_{PIE}}$

The scatter of the P-19 and P-20 experiments relative to the LIFE calibration has been calculated (see Table XX and Figure 73). The standard deviation is about 1.3%. It is interesting to note that only one pin in this group, P-19-30, was significantly outside this standard deviation. If P-19-30 had been excluded, the standard deviation would have been 0.8%.

It might be more reasonable to use 0.8%, but to be conservative, 1.3% will be used. The scatter in P-19 and P-20 data reflect uncertainties in fabrication, local spatial fluctuations and post-irradiation examination measurement uncertainty. Since P-20 powers were normalized to P-19 results, P-20 is not an independent experiment at a separate time and σ_{time} does not apply. So

$$\sigma_{P\text{-}19/P\text{-}20} \approx 1.3\% = \sqrt{\sigma_{fab}^2 + \sigma'^2_{space} + \sigma_{PIE}^2}$$

and

$$\sigma_{PIE} = 0.9\%$$

Values of the above uncertainties are summarized in Table XXII.

Total Uncertainty

The total uncertainty is a combination of all the components

$$\sigma_{tot} = \sqrt{\sigma_{fab}^2 + \sigma_{PIE}^2 + \sigma_{space}^2 + \sigma_{time}^2 + \sigma_{sys}^2} = 4.3\%$$

Resolution of the EBR-II power factor is expected to reduce the systematic uncertainty to 2%, and σ_{tot} will drop to 3.7%.

σ_{tot} represents the scatter and uncertainty in the power-to-melt data. The uncertainty in the average of these data is given by the standard deviation of the mean. The standard deviation of the mean takes into account the number of data points N, and is given by $\sigma/\sqrt{N}$. In the various components of σ_{tot}, a separate measurement toward determining σ_{sys} would require use of a different reactor; a separate measurement for σ_{time} would require an experiment done at a different time and a separate measurement for σ''_{space} would require another experiment done in a different position in EBR-II. As explained above, P-19 and P-20 cannot be counted as being done at different times or different positions. So for σ_{sys}, σ''_{space} and σ_{time} it is N = 1. For the other components N is equal to 10, the number of rods used. Thus,

$$\sigma_{mean} = \sqrt{\sigma_{sys}^2 + \sigma_{time}^2 + \sigma''^2_{space} + (\sigma_{fab}^2 + \sigma_{PIE}^2 + \sigma'^2_{space})/10} = 4.1\%$$

σ_{mean} is dominated by σ_{sys} and σ_{time} with the other components making a small contribution. The mean of the power-to-melt data is represented by the LIFE-3 calibration and the uncertainty on this mean is given by σ_{mean}.

5.2.2 Results

To evaluate the probability of melting in CRBRP, the LIFE-3 calibration will be extrapolated from P-19/P-20 to CRBRP conditions. Since only fresh and very low burnup fuel is considered and since this is the burnup range covered by P-19/P-20, the extrapolation is small and it is assumed that no biases are introduced. An additional uncertainty comes from the use of fuel with 33% Pu enrichment instead of 25% enrichment used in the calibration. An estimate of the values and uncertainties of power-to-melt in CRBR with reference fuel can be made. Then the uncertainties in the CRBR power-to-melt are statistically added to the P-19/P-20 σ_{mean} uncertainty and to the extrapolation uncertainty to define a probability of melting.

The uncertainties in a CRBRP power-to-melt analysis due to the factors listed in Table XXIII are considered. Fabrication and irradiation uncertainties arise from design tolerances and uncertainties in neutron physics and thermal-hydraulic calculations. These uncertainties can be estimated from the design tolerances by computing their effect on power-to-melt using LIFE-3. The design tolerances will be for pellet density, cladding ID, enrichment, instrumentation and pellet diameter. There is also a tolerance on fuel weight per length which prevents certain combinations of density and diameter. To simplify analysis and add the conservatism of not taking credit for the weight per length restriction, this effect will be neglected. Tolerances lead to fabrication of parts whose means may lie with approximately uniform probability anywhere within the fabrication tolerance bounds. The bounds of such a rectangular distribution correspond to $\pm \sqrt{3}\sigma$. The tolerances are listed in Table XXIII. Actual distributions of dimensions and fuel density are expected to be available for use in the FSAR hot channel factor analyses.

LIFE-3 runs were made to analyze the effect of variations in the parameters of Table XXIII on the melting of the pins investigated. A programmed reactor startup is specified by giving the steady state reactor power as a function of time, REPOW (t). This is the total reactor power as determined by the reactor control settings, while Q(t) is the corresponding linear power, including direct factors, of the peak pin near its axial midplane at the location of peak centerline fuel temperature. The reactor power units are normalized to a value of 1.0 at nominal full power, i.e., REPOW(t) is 1.0 when the nominal power of the highest peak power pin (assembly #14) at X/L = 0.45, Q(t), is 12.73 kw/ft, which is the nominal power used for the uncertainty analyses. The power-to-melt is defined in LIFE-3 by ramping the reactor power up until melting starts. This is done at various times during the program startup. The programmed startup assumed for this study is illustrated in Figure 72.

Using the nominal conditions of Table XXIII and the power history of Figure 72, the mean reactor power-to-melt for the nominal peak pin is defined as:

$$\overline{REPOW}_M \text{ (nominal, t)} = \frac{1}{CP_o} \bar{Q}_M \text{ (nominal, t)}$$

where $\bar{Q}_M$ is the peak pin linear power at X/L = .45 when the LIFE-3 centerline temperature reaches the fuel melting point and $\overline{REPOW}_M$ is the reactor power at that time. CP_o = 12.73 kw/ft because of the normalization of units chosen for reactor power. $\overline{REPOW}_M$ is defined as the mean reactor power-to-melt (signified by the bar) since the mean of P-19/P-20 has been used to calibrate LIFE-3 and the P-19/P-20 power uncertainty will be subsequently added.

The effect of small perturbations of the design parameters was analyzed to determine the sensitivity of power-to-melt to variations in each parameter. The sensitivities are shown in Table XXIV and the corresponding standard deviations in power-to-melt obtained from the standard deviations in the parameters from Table XXIII are shown in Table XXV.

It is assumed that reactor power-to-melt can be approximated by a linear function of each parameter about the nominal point. This assumption was checked for pellet diameter variations for which the greatest non-linearities would be expected. Figure 75 shows the actual variations of power-to-melt with pellet diameter and the assumed linearizations which were selected to give a close fit over the range where power-to-melt was below nominal.

The melting temperature of $(U,25\%Pu)O_2$ is $2760^{o}C$ ($5000^{o}F$) with a 3σ uncertainty of $\pm 60^{o}C$ ($108^{o}F$). This value was based on an extensive review of all published data and a thorough analysis of the techniques and data can be found in the Nuclear Systems Material Handbook.[18] It is not necessary to use an uncertainty on melting temperature when the LIFE-3 code is employed to analyze $(U,25\%Pu)O_2$ since the code was calibrated with fuel with this plutonium content. The nominal melting point value was used for calibration. Since the current CRBRP fuel contains 33% PuO_2, additional uncertainties due to increased Pu content must be considered. Based on the calibrated melting point of $2760^{o}C$ for 25% PuO_2 fuel, and considering the $\pm 3\sigma$ uncertainty of $\pm 60^{o}C$ for the entire range of $(U,Pu)O_2$ solid solutions, the uncertainty in extrapolating from 25% to 33% PuO_2 was determined by estimating the uncertainty of the slopes. The 3σ uncertainty in extrapolation is $1.2^{o}C$ per wt% PuO_2 or $9.6^{o}C$ for the 33% PuO_2 fuel (i.e., melting point uncertainty $\sigma_{TM} = 5.8^{o}F$). The sensitivity of power-to-melt changes in melting point

$$\partial \overline{REPOW}_M / \partial T_{MP}$$

is calculated from the nominal LIFE-3 run, and this is used to convert the uncertainty on melting temperature to uncertainty on power-to-melt, i.e.,

$$\sigma_{extrap} = \partial \overline{REPOW}_M / \partial T_{MP} \; \sigma_{TM}$$

To obtain the probability distribution for the reactor power-to-melt, the uncertainty in the P-19/P-20 experiments and the extrapolation uncertainties are added to the CRBRP design uncertainties, resulting in the probability distribution for reactor power-to-melt with standard deviation

$$\sigma_{REPOW}(t) = \sqrt{\sigma_{\overline{R}}(t)^2 + \sigma_{mean}^2 + \sigma_{extrap}^2}$$

and a mean of $\overline{REPOW}_M$ (nominal,t).

The design criterion is that, throughout life, the fuel linear power rating is at least three standard deviations below melting power, when the reactor power is 15% above nominal conditions, i.e.:

$$K * REPOW(t) \leq \overline{REPOW}_M \text{ (nominal,t)} - 3\sigma_{REPOW_M}(t)$$

Note that the uncertainty (1.03) on power level (see Table V-A) is already accounted for in the 0σ operating conditions (Table XVIII) of the pins, which represented the starting point for this analysis. Thus, it must be extracted from the 15% overpower factor, to avoid being considered twice. Consequently, the value of K in the present study is 1.15/1.03; obviously, if nominal conditions were used as the operating conditions for power-to-melt analyses, K would have been equal to 1.15.

The results of the analyses outlined above are summarized in Tables XXIV through XXVII. In Table XXIV, the derivatives of the power-to-melt with respect to the different parameters are calculated. In Table XXV, these are used to convert design uncertainties into uncertainties on power-to-melt which are then statistically combined.

The uncertainty on melting point due to extrapolation to a Pu enrichment different from P-19/P-20 is given in Table XXVI. The nominal LIFE-3 run is used to find the effect of a change in melting point on power-to-melt. This is used to convert the uncertainty on melting point into an uncertainty on power-to-melt.

In Table XXVII, the uncertainties from the measured power-to-melt (converted to reactor power units), the extrapolation to CRBRP conditions, and the CRBRP design uncertainties are statistically combined, and the design criterion for melting is examined to see if it is fulfilled for the programmed reactor startup chosen.

Table XXVIII gives a comparison of the 3σ minimum powers-to-melt with the power at 15% overpower for the two pins examined in this study. The 3σ uncertainties in power-to-melt ($3\sigma_{REPOW_M}$) from Table XXVII are tabulated in column 5 of Table XXVIII (expressed as a fraction of nominal full power). It can be seen in the last column of Table XXVIII that there exists an adequate margin against melting for both pins when the present calibration of LIFE-3 is used; i.e., the no-melting criterion is satisfied at the 3σ level of confidence with additional margin in power remaining.

The results clearly demonstrate that a programmed startup for the fuel rods can be identified which ensures that the no-melting criterion can be satisfied. The programmed startup used was not an optimum one and further work will be performed in this area. As previously mentioned, an experimental program has been identified to characterize the startup procedure, namely duration of initial period during which power is held below the rated level and magnitude of the hold power as percentage of the rated full power, as well as to determine the corresponding power-to-melt. This program will help in defining the optimum startup procedure to be recommended for CRBRP.

5.3 Inter Blanket Assemblies Power-to-Melt Analyses

Inner blanket assembly #99 was investigated in these analyses, as the blanket assembly having the highest power in the first five years of CRBRP operation. Assembly #99 reaches its maximum power in the second core, at end-of-cycle 4 (see Figure 18). Inner blanket assemblies are enveloping as regards power-to-melt conditions, since their much higher power rating overshadows, by far, the additional decrease in fuel melting temperature occurring in the longer residence time radial blanket assemblies. As in the fuel assemblies case, thermal parameters (circumferentially averaged cladding and surface

temperatures, rod linear power and burnup) predicted by NICER at THDV conditions and 0σ level of confidence were used as input to LIFE-3 analyses. Additionally, thermal parameters at the 3σ level were calculated by NICER for use, together with the 0σ values, in the uncertainties calculations. Cladding properties were those for first core steel with Rev. 5 swelling[18] and cladding swelling uncertainties (τ = 5.0, R * 1.30) were from the same source. Table XXIX summarizes the LIFE-3 runs.

For the first seven LIFE-3 runs, the neutron flux uncertainty was assumed to be the same as the power uncertainty; for the final run in which the axial variation of power-to-melt was investigated at two-inch intervals, the neutron flux uncertainty was conservatively estimated as 1.15 throughout life, and the power uncertainty was fitted to an inverted chopped cosine distribution between the values given at core midplane and fuel/blanket interfaces (see discussion in Section 3.1.4). The power-to-melt uncertainties other than those for cladding swelling and surface temperature are not expected to be significantly different from those given in Reference 3, thus the Reference 3 values were used.

The power-to-melt in reactor power units (nominal full power = 1.0) is shown in Table XXIX for each run.

The margin-to-melt analyses were performed as in Reference 3. Two cases were considered:

1. Reactor operating at 0σ power including the 1.03 hot channel factor for power level measurement and control system dead band, with an overpower margin of 1.15/1.03 required at EOL.

2. Reactor operating at 0σ power not including the 1.03 hot channel factor, with an overpower margin of 1.15 required at EOL.

Re-evaluated values for the uncertainty analysis are shown in Table XXX, with the remaining uncertainties the same as those in Tables 4.4 through 4.7 of Reference 3. From Table XXX, it is seen that case (2) has 0.004 less margin-to-melt than case (1), and that the peak pin has 0.004 less margin-to-melt than the hot pin.

From Run 8, the elevation with the minimum margin-to-melt was found to be 2 inches above the core midplane. Applying the margin-to-melt analysis at this elevation to the peak pin, case (2) resulted in zero margin-to-melt. Thus, the design goal of no incipient center melting at 3σ 115% power conditions in satisfied, although with no margin.

It should be noted, however, that in reality additional margin exists, because of the conservative manner in which power uncertainty factors have been applied. Each blanket power uncertainty (see Section 3) is expressed as a $\pm$ uncertainty, plus (in some cases) a bias. For the analyses to-date, all of these factors have been combined directly with the other uncertainties in the blanket assemblies, which is a conservative approach. However, the overall $\pm$ power uncertainty could be combined statistically with the remaining uncertainties, since they are independent. Adopting this approach would substantially improve the power-to-melt margin.

Future analyses could also investigate other pins, located between the peak and hot pin. In fact, their behavior in terms of margin-to-melt is so similar that it cannot be excluded "a priori" that an intermediate pin could become limiting, due to a worst combination of linear power rating and cladding temperature/swelling.

6. CORE ASSEMBLIES PRESSURE DROPS

6.1 Introduction

The area of pressure drop calculations has gone through many improvements and reevaluations throughout the CRBRP core design. Following is a brief discussion of the reasons for this continuous reassessment:

- More experimental data from prototypic hydraulic experiments of various reactor and assembly components have become available, thus replacing analytical/engineering estimates with experimentally derived correlations.

- Uncertainties on predicted pressure drops of several components have changed from engineering estimates (a typical example being a 20% uncertainty on form losses) adopted in previous analyses to actual calculations based on regression analysis of experimental data.

- Removal of unnecessary, parasitic pressure drops in the assemblies orificing has led to an increase in available actual reactor flow, by moving to the right along the pump head/flow characteristics curve.

- Several modifications have been factored into the lower inlet modules (LIM) design. The requirement of a constant pressure drop across the various LIMs, and consequent orificing, has been removed. Thus, assemblies belonging to the same orificing zone but to different LIMs will have slightly different flows, depending on the total pressure drop across the respective LIMs. As mentioned in Section 1, the capability for radial blanket assemblies shuffling has been retained in the heterogeneous design. All the radial blanket assemblies are therefore identical and the radial blanket orificing is apportioned between the assembly and the LIM. Thus, in zone 9 (highest flow orificing zone in the radial blanket) all the orificing is in the assembly, while in zones 10, 11 and 12, a progressively increasing pressure drop is incorporated in the LIM orificing to balance the decrease in assembly pressure drop going to lower flow orificing zones. The amount of orificing in the LIMs is thus designed to permit shuffling of zone 9 assemblies in zones 10, 11 and 12, zone 10 assemblies in zones 11 and 12 and zone 11 assemblies in zone 12.

- A new computer code, CATFISH, whose features have been briefly summarized in Section 1, has been developed to conventiently handle all the modifications and improvements discussed above. Specifically, CATFISH is necessary to calculate the reactor flow conditions corresponding to the given pump head and reactor hydraulic impedance and to evaluate the coolant flow in each individual core assembly following removal of the pressure drop equalization in the LIMs.

- Finally, development of CATFISH and correlating the reactor impedance with the pump characteristic curve has very clearly pointed out a rather ovbious fact which was however overlooked in previous analyses. Reactor pressure drops had been previously calculated for a given reactor flow under nominal conditions and accounting for uncertainties (either positive-maximum ΔP or negative-minimum ΔP); thus, more than one pressure drop was calculated as corresponding to the same flow. It is clear that this is physically impossible, since if, e.g., the reactor impedance is greater than predicted, the reactor flow has to be less than the nominal flow corresponding to the predicted hydraulic resistances, in order not to violate the pump characteristics. Therefore, in this study only mutual pairs of reactor flow/ΔP are reported. For example, Section 6.3 reports calculations performed by CATFISH for two such pairs: a) when the reactor flow is at its THDV value and the hydraulic resistance is maximum (which are the worst possible conditions for the thermal performance of the core assemblies) and b) when the reactor hydraulic resistance is nominal with a corresponding reactor flow equal to the maximum flow compatable with the pump operating range and flow measurement/controller uncertainties.

The following sections discuss the correlations used in calculating the pressure drops across the assemblies, their bases and some typical results.

6.2 Pressure Drop Correlations

Preliminary hydraulic characteristics of the CRBRP fuel and blanket assemblies are reported here. Since several test programs are still in progress, the best available information has been included in this analysis which will be reviewed as new test data are obtained.

Correlations reported here are valid over the entire range of operation, either turbulent, transition or laminar. However, in this study only full

flow conditions are of interest, therefore, the flow in all components is in the turbulent regime. This distinction is important when considering the uncertainties associated with the proposed correlations, as discussed later.

The rod bundle frictional pressure drop is defined by:

$$\Delta P = (fL/D)\ \rho V^2/2$$

where

f is the friction factor;

L is the rod length;

D is the rod bundle hydraulic diameter calculated from the rod bundle total flow area, A, and wetted perimeter, P_w: $D = 4A/P_w$;

V is the rod bundle average velocity; and

ρ is the fluid density.

The component hydraulic characteristic, K, is defined for all other components by the form losses equation:

$$K = 2\Delta P/\rho V_r^2$$

Wherever possible, the irreversible pressure loss, ΔP, was determined from test data

$$\Delta P = P_{s1} - P_{s2} + \rho V_1^2/2 - \rho V_2^2/2$$

where

$P_{s1} - P_{s2}$ is the differential pressure measured between upstream (1) and downstream (2) static pressure taps;

V_1 and V_2 are the average velocities over cross-sections 1 and 2;

ρ is the test fluid density.

Thus K has the form

$$K = 2\,(P_{s1} - P_{s2})/\rho V_r^2 + (A_r^2/A_1^2 - A_r^2/A_2^2)$$

where

V_r is the reference velocity, i.e., the average velocity through some convenient reference cross-section A_r;

A_1 and A_2 are the areas at cross-sections 1 and 2;

A_r is the reference cross-section area.

The first component of the form loss equation represents the measured static pressure difference between points 1 and 2 and the second component represents the fluid acceleration between cross-sectional areas 1 and 2 and has a constant value. The form loss coefficient, K, represents the non-recoverable pressure drop between points 1 and 2 and can generally be correlated with the Reynolds number by a function of the form CRe^{-n}. The hydraulic characteristics thus defined combine both the form and friction losses of the component into one expression.

The data included in the characterizations developed herein are from tests of FFTF assemblies and components [26-28], and tests of CRBRP components [29-31].

Linear regression analyses were performed on the fuel assembly component pressure drop data. The coefficients of the regression functions were calculated for the fuel assembly components and are presented in Table XXXI along with the relevant statistical parameters. Rigorous statistical analyses were not performed for the blanket assemblies, due to the incompleteness of data.

The data in Table XXXI may be used to calculate the confidence band on K at any values of the independent variables from the equation [32]:

$$\Delta Y = t\sigma_y \left(1+1/N + \sum_{i=1}^{M} (\bar{X}_i - X_i)^2/N\sigma_{xi}^2\right)^{1/2}$$

where

t is Student's T statistic;

σ_y is the "standard error of estimate" from Table XXXI;

N is the number of data points;

M is the number of independent variables;

$\bar{X}_i$ is the experimental mean of the i-th independent variable from Table XXXI;

X_i is the value of the i-th independent variable at which σ is being calculated; and

σ_{xi} is the standard deviation about $\bar{X}_i$ from Table XXXI.

Note that t is evaluated at some desired confidence level and hence, the resulting value of ΔY has associated the same confidence limit.

The rod bundle is the only assembly component which can operate in all flow regimes. Since, however, only full turbulent flow is of interest in these studies, the uncertainty on the pressure drop correlation at 100% flow is lower than over the entire flow range, as indicated in Table XXXI. In fact, the data scatter in three separate flow tests [26-28] was greater in the transition region than at higher Reynolds numbers.

The recommended hydraulic correlations for fuel assembly components are presented in Table XXXII. All fuel assemblies are hydraulically identical except for the orifice stack which is unique to each flow orificing zone. Selction of the proper orifice design from the five orifice correlations requires selection of both the number of plates and the hole diameter to achieve the zone flow rate. Selection should be done to minimize the number of orifice plates while avoiding cavitation which may damage hardware or affect pressure drop. While final selection must await the results of final

cavitation tests, in the present analyses a design criterion(*) of 40 ft/sec maximum coolant velocity in the orifice holes was selected as a first approximation and the maximum achievable pressure drop for each orifice configuration was determined and is presented in Figure 77 as a function of assembly flow rate. Given an assembly flow rate, the pressure drop resulting from all components except the inlet nozzle/orifice/shield can be determined from the correlations in Table XXXII. This result subtracted from the total assembly pressure drop is the required inlet nozzle/orifice/shield pressure drop. The number of orifice plates for this pressure drop and flow rate can be determined from Figure 77 and the corresponding Reynolds number-dependent hydraulic correlation determined by solving for the orifice hole diameter.

The correlation presented for the rod bundle outlet results from a calculation of expansion form losses [33], since no relevant data are available. Because the associated pressure drop is of the order of 1 psi or less, the inherently large uncertainty of such a calculation, is acceptable for preliminary calculations. Data from the CRBR fuel assembly flow and vibration test will be used when available.

The correlation presented for the rod bundle inlet results from a calculation of expansion and contraction form losses [33]. Although this component's pressure drop was measured [28], the data are ambiguous since the

---

(*) Analyses were in progress at the time of writing, to better define the cavitation margin criterion. It appears that the 40 ft/sec limit will be replaced by a maximum allowable cavitation number to be substantiated by testing. Figure 76 shows typical results being obtained in the cavitation tests of CRBRP fuel assembly orifice stacks. It should be noted, however, that the amount of pressure drop allocated in the orificing is practically independent of the particular no-cavitation criterion selected, which will only determine the geometry necessary to satisfy the no-cavitation limit. Therefore, all the data reported in Section 6.3 for the various components pressure drop will vary only marginally following redefinition of the no-cavitation criterion.

experimentally determined form loss was negative. This could be due to either poor data or to the fact that the pressure taps were located in regions of not fully developed flow distribution. While the data scatter was excessive, it is, however, suspected that the latter was primarily responsible. Jets were observed to issue from the top shield block and to impinge upon the support grid; the dynamic head ($\rho V^2/2$) of the jet was 2 to 3 times the estimated grid pressure drop. For best accuracy, the rod bundle inlet pressure drop should be combined with the upstream or downstream components to avoid applying the standard pressure drop definition to regions where fully developed flow does not exist.

The recommended hydraulic correlations for the inner blanket assembly components are presented in Table XXXIII. The inner blanket assemblies utilize a fuel assembly type inlet nozzle, radial blanket type shield, rod bundle and outlet nozzle, and a unique orifice stack within the assembly. The inlet nozzle geometry and hydraulic correlation are identical to the fuel assembly. The inlet nozzle-orifice-shield has not been tested, so the weak Reynolds number dependence shown in Table XXXIII is recommended, based on the Reynolds number dependence of the four and five plate fuel assembly orifices [29] and the dependence of sample cases of the radial blanket inlet module orificing [30]. The constant, C, represents the capability to design an orifice stack for any required pressure drop. The shield, rod bundle inlet and rod bundle outlet form losses were estimated based on Reference 33. The rod bundle friction was measured [31] over a sufficiently wide range of flow rates to cover the full range of inner blanket flow rates. The inner blanket assembly outlet nozzle form loss assumes sufficient similarity exists to apply the fuel assembly outlet nozzle test data [29] with the smaller blanket assembly reference area.

Except for the inlet nozzle and rod bundle friction, no data are available on the inner blanket assembly component pressure drops. However, because there is no a priori reason to anticipate worse uncertainties on inner blanket assembly components than were found on fuel assembly components once tests are completed, it is recommended to apply the same uncertainties as for the

corresponding fuel assembly components(*) (Table XXXI). In the case of the blanket rod friction, where data exist [31], the standard error on the recommended correlation is 5% over the entire flow range and 3.3% over the full flow design range.

The recommended hydraulic correlations for the radial blanket assembly components are presented in Table XXXIV. The radial blanket assemblies have low rod bundle pressure drops and are dominated by orificing located both within the assembly and in the lower inlet module. The orificing located in the lower inlet module was characterized [30] over a range of flow rates near design conditions. A preliminary examination of the test data shows the losses can be modeled proportional to $Re^{-0.05}$ as was typically found for the four and five plate fuel assembly orifices [29].

The remainder of the radial blanket assembly inlet hardware has not been tested, so it is recommended that the combined inlet nozzle-orifice-shield and lower inlet module orificing, identified as "inlet region" in Table XXXIV, be modeled proportional to $Re^{-0.05}$. The rod bundle inlet and outlet form losses were estimated based on the methods of Reference 33. The rod bundle friction factor was experimentally determined [31] over the full range of radial blanket flow rates and the inlet and outlet nozzle characteristics are based on a similarity extrapolation from the fuel assembly tests [29].

Following the previous logic, the inner blanket assembly component uncertainties are recommended for use in radial blanket analyses. Final characterization of all inner and radial blanket assembly components over the necessary range of Reynolds numbers will result from the CRBRP blanket assembly flow and vibration test.

(*) It should also be kept in mind that the limiting pressure drop is represented by orificing zone 1, thus the blanket orificing can be easily adjusted to accommodate possible discrepancies between predictions and actual test data.

6.3 Results

Pressure drops were calculated for all reactor components by the newly developed CATFISH code. As previously mentioned, CATFISH models all the primary system resistances including the fuel, inner and radial blanket, radial shield and control assemblies, vessel cooling path and leakage as parallel flows. Below and above this parallel flow network are the inlet and outlet plena plus the primary loop resistances (check valve, piping, IHX). The pump characteristics curve ties, and provides the boundary conditions to, the hydraulic network. The preceding Section 6.2 discussed modeling of the fuel and blanket assemblies resistances. Modeling of all the other resistances and of the pump characteristics are not discussed here for brevity since they are not, strictly speaking, directly related to the fuel and blanket assemblies. They will be discussed in detail in the CATFISH user's manual to be issued in the future. CATFISH also has the capability of accounting for the effect of uncertainties associated with prediction of the various resistances; thus, for each calculation it shall be clearly stated whether nominal resistances are considered or whether uncertainties are accounted for and at what level of confidence. In addition to the hydraulic resistance, an uncertainty also exists on the pump head/flow characteristics where a 5% spread was specified between minimum and maximum pump head capability for a given flow.

Before presenting some typical results obtained with CATFISH, it is necessary to discuss how orificing requirements are considered in the overall picture of the entire primary system hydraulics. A required flow allocation to the various orificing zones has been determined in Section 2 and has been used in calculating the thermal performance in Sections 4 and 5. The flow orificing can quantitatively be reduced to two requirements, i.e., fixed flow ratios between zone 1 and all the other flow orificing zones and amount of flow in zone 1.

Other defined constraints are: a) pump characteristics curve; b) whether uncertainties are considered; and c) resistances in all flow paths. The designer has one degree of freedom, i.e., the resistance in the core assemblies orifices, or, more precisely, the resistance in orificing zone 1, since, once this is defined, the orifice resistance in all the other zones is automatically set to provide the required flow ratio among orificing zones. It follows that, since all the other variables are defined by their geometry, operational characteristics (pump) or flow requirements, one-to-one correspondence between total reactor flow and zone 1 orificing resistance exists, which provides a unique solution to the primary system flow network. The designer can therefore specify the total reactor flow and obtain orificing resistances or specify an orificing resistance in zone 1 and obtain the total reactor flow. Examples will be shown in the following.

The first case considered was plant THDV conditions, where the flow is specified (41.446×10^6 lb/hr). Since these are the worst possible conditions from the thermal performance standpoint, i.e., minimum reactor flow, it is consistent to assume positive uncertainties for the various hydraulic resistances and the minimum pump head curve. As the most conservative assumption, uncertainties on all resistances were taken at their maximum value, either 3σ where a statistical basis existed, or at their boundary value (generally 1.2) where only an engineering estimate was available. It is rather obvious that assuming that all the resistances in all components are simultaneously at their maximum value, is extremely pessimistic, in fact, it is extremely improbable. Calculations were however performed for this set of conditions to provide an absolute minimum, worst case and the results are reported in Table XXXV. The zone flow reported in the table is an average for the zone (remember per previous discussion, that due to the fact that assemblies in the same orificing zone are in different LIMs, their flow will be slightly different). The components pressure drop correspond to the average assembly flow, thus again slightly different pressure drops are attained in the individual assemblies. Flow variations from assembly-to-assembly in the same orificing zone are generally less than $\pm 1\%$, with maximum variations not exceeding $\pm 2\%$. All pressure drops are reported for cycle 4 conditions, which were the ones used in determining the orificing (see Section 2). The only obvious exception is zone 6 inner

blanket, since only fuel assemblies are in zone 6 during cycle 4. Flow and pressure drops for zone 6 IB are at cycle 2, conditions adopted for orificing of assembly #98, the only inner blanket remaining for two years in zone 6. The distinction between zones 10C and 10P is due to the fact that zone 10 assemblies are the only assemblies which belong to the same orificing zone, but to two different types of modules. The modules at the core periphery (see Figure 78) have a dif ·ent geometry from the other modules (called central) and therefore, a different resistance and pressure drop. Assemblies 10C are the zone 10 assemblies located in the central modules, while assemblies 10P are located in the peripheral modules. The lower inlet modules have been orificed for zones 10, 11 and 12 to provide the capability of shuffling radial blanket assemblies if so desired, as discussed in Section 6.1. Thus, the pressure drop reported under "LIM upper portion and orifice" for zones 1 through 9 is due to the hardware of the upper portion of the LIM, i.e., the region where the orificing plates are inserted for zones 10 through 12; the plates pressure drops are added for zones 10, 11 and 12. Whether or not orificing plates are physically in the LIM is quite obvious from the relative magnitude of the reported pressure drops. The "LIM, lower portion" ΔP is attributable to the resistance in the remainder of the LIM. While the pressure drop in the upper portion depends on the individual assembly flow, the pressure drop in the remainder of the LIM depends on the total flow through the LIM, i.e., on the sum of the flows in the seven-assemblies fed by the LIM. It is not possible, therefore, to attribute the LIM, lower portion pressure drop to a given orificing zone, since the same orifice zone assemblies can be fed by different LIMs and the same LIM can feed different orifice zone assemblies. Pressure drops reported in Table XXXV under "LIM, lower portion" are therfore only indicative of the order of magnitude.

The average zone flows thus calculated for THDV conditions by CATFISH and reported in Table XXXV agree (within 0.05%) with the flows reported in Table IV, which is quite a strong indication of the soundness of the CATFISH model. The vessel nozzle-to-nozzle pressure drop was calculated as 126.4 psi, which is actually consistent with the 123 psi value commonly adopted, when one considers that 126.4 psi is the vessel nozzle-to-nozzle irreversible pressure loss, while 123 psi is the vessel nozzle-to-nozzle static pressure difference minus the nozzle-to-nozzle velocity head. The difference of 3.4 psi is

therefore the difference in velocity head between the reactor vessel inlet nozzle and outlet nozzle. Similarly, the value of the pump head, 163.5 psi, reported in Table XXXV, is the total developed head, while the commonly used value of 160.3 psi is the static pump head.

The most important point to be noted in examining the results in Table XXXV is the value of the orifice pressure drop in zone 1, i.e., 38.7 psi. As mentioned in Section 1, the zone 1 orifice pressure drop is by and large parasitic, since only a few psi are needed for final flow trimming; the pressure drop dissipated in the case just considered is a staggering 23.6% or nearly one-fourth of the entire pump head capability.

The next step is therefore rather obvious; i.e., decrease the parasitic pressure drop, thus increasing the total reactor flow and the flow through each assembly. The substantial payoff in thermal performance and economics has been outlined in Section 1. However, a limit exists on the present plant and pump specifications regarding the maximum amount of reactor flow, which was set at 115% of THDV conditions, or 47.663 x 10^6 lb/hr. It should be pointed out this is not a hard "no go" physical limit, but a design specification and its removal will require a lengthy reevaluation of the various impacts, which was deemed impractical at the present time. It was therefore decided that the orificing resistance will be reduced to the amount necessary to stay within the present pump "operating window", namely a flow range of 41.446 to 47.663 x 10^6 lb/hr. Uncertainties of 1% in flow controller and 2% in flow measurements (calorimetric) were taken into account and conservatively were used in summation rather than in r.m.s. statistical combination. Thus, the nominal plant expected flow for the CRBRP was set at 112% of THDV conditions or 46.420 x 10^6 lb/hr. Consistent with the definition of nominal flow, nominal flow resistances and nominal pump head curve were adopted in the CATFISH analyses. The results are reported in Table XXXVI. One additional difference exists between conditions considered in Tables XXXV and XXXVI. The LIM orificing pressure drop reported in Table XXXV for zones 10, 11 and 12 was the exact amount necessary to guarantee the same flow ratio among the various orificing zones as reported in Section 2. For a given orifice plate geometry, where the number of holes and hole diameters are defined and only the number of plates is variable, it is obvious that only a

fractional number of plates will yield the exact value specified for the orifice pressure drop. Thus, for the actual design case, which is the one reported in Table XXXVI, a finite number of LIM orifice plates had to be specified; the chosen number was the closest, by defect, integer to the fractional number which would have exactly satisfied the orificing requirements(*). It was decided to round the number of plates to the next lower rather than the next higher integer because by so doing, the blanket would have been overcooled rather than undercooled. Since the fuel assemblies flows are much higher than the blanket assemblies flows, the reduction in fuel assemblies flow corresponding to a blanket overcooling is quite minor; thus, the overall flow allocation among the core assemblies is comparatively better than if the other alternative were chosen.

The pressure drop in orificing zone 1 is reduced to 17.6 psi, which is still 11.2% of the total head. These new plant conditions are, by their very definition, plant expected operating conditions and they represent a significant improvement over the previous conditions used in the thermal performance analyses reported in Section 4, with an increase in assembly flows of the order 5-6%. An evaluation of system temperatures corresponding to these new flow conditions will soon be initiated. Analyses were conducted to evaluate $\pm 2\sigma$ limits on the nominal expected plant flow. The hydraulic resistance in each component, e.g., zone (i) orificing, fuel bundle frictional resistance, vessel, etc. was varied individually and the corresponding effect on the total reactor flow calculated. In total, the resistance in 83 components was varied. A root mean square of all the variations in reactor flow due to the individual variation in hydraulic resistance (as well as pump head curve) at the 2σ confidence level, resulted in a maximum 2σ expected plant flow of 47.159×10^6 lb/hr, i.e., 1.6% higher than the nominal expected flow. Thus, the total reactor flow was within the specified window

---

(*) Number of LIM orifice plates are as follows: 10 plates both in zone 10C and 10P (required fractional number is 9.8 in 10C and 10.3 in 10P); 7 plates in zone 11 (required number 7.6); 6 plates in zone 12 (required number 6.6). Note that different hole diameters and number of holes are used in the various zones, which explains the apparent discrepancy that a larger number of orificing plates are used in the higher flow zone and vice versa.

even at the +2σ level. Analyses will be updated as new evaluations of components pressure drop and relative uncertainties become available from ongoing and planned experimental tests.

The fact that over 10% of the pump head is still parasitic losses points out that ample room is left for improvement. To provide a quantitative evaluation, a CATFISH run was performed for nominal conditions and specifying no resistance in orificing zone 1. This resulted in a total reactor flow equal to 48.445 x 10^6 lb/hr or ~117% of THDV conditions, an additional 5% flow increase over the updated nominal plant expected operating conditions with ~18 psi parasitic ΔP. Whether this improvement can ever be utilized is speculative at present, however, it is important to know that it exists and is available.

7. CONCLUSIONS

Specific conclusions have been provided throughout this report. Rather than repeating previous statements, a very brief overview of the core T&H analytical process is given here. As indicated in Sections 2 and 4, the current core T&H design, which will provide the basis for fuel and blanket assembly final design, was successful since all the constraints were met. This occurred since the core was orificed and flows allocated a priori, to guarantee satisfaction of all criteria based on the adopted orificing philosophy which consisted of identifying all constraints, quantifying them in terms of comparable parameters and meeting these constraints. Obviously enough flow must be available to the core to utilize this orificing philosophy to its full advantage. This was the case for this analysis.

At the same time, a method to significantly increase, without associated penalty, the total plant flow was identified and pursued. Reduction (roughly halving) of parasitic pressure drops in the orifices would allow a flow increase of the order of 5%, with a comparable amount still available if the remaining parasitic pressure drop were eliminated altogether. The actual thermal performance of the CRBRP core would therefore be better than reported here and significant margin exists to accommodate more restrictive constraints and more severe flow requirements which may be incurred in the future by the core thermofluids designers.

Improvements to existing analytical tools, development of new computer codes, factoring of available experimental data in the analyses, implementation of new design approaches and concepts, extension of in-depth analyses, critical reevaluation and elaboration of design uncertainties have all contributed to a more realistic assessment of the core thermofluids design and predicted performance.

It could be stated therefore, and this is perhaps the most important conclusion of this work, that the T&H design has satisfactorily fulfilled its scope, i.e., to provide a smooth translation of the core power distribution and nuclear characteristics into the core structural and mechanical behavior.

This means more than a good thermal-hydraulic performance; it means that the T&H design, by integrating the nuclear design on one side and the structural design on the other, can highlight the strength and weaknesses implicit in both, point out potential problem areas and lead to an overall optimization of the integral core design.

Continuous improvements in core T&H design and analyses will contribute to minimize uncertainties germaine to the T&H functional link in the overall core design. To this end, several suggestions have been made throughout this report and they will be implemented to the maximum extent possible in the next design round for final, as-built conditions.

REFERENCES

1. M. D. Carelli, C. W. Bach, F. C. Engel and D. R. Spencer, "Clinch River Breeder Reactor Plant; Predicted Thermal-Hydraulic Performance of CRBRP Fuel and Blanket Assemblies", CRBRP-ARD-0054, August 1976 (Availability: US/DOE Technical Information Center).

2. M. D. Carelli and R. A. Markley, "Preliminary Thermal-Hydraulic Design and Predicted Performance of the Clinch River Breeder Reactor Core", ASME paper 75-HT-71.

3. A. J. Friedland, "CRBRP Assemblies Hot Channel Factors Preliminary Analysis", WARD-D-0050, Rev. 3, September 1979.

4. W. C. Chiang, "ØCTØPUS: A Flow Orificing Optimization Code for Fast Breeder Reactor Cores. Preliminary User's Manual", to be published as topical report.

5. M. D. Carelli and C. W. Bach, "LMFBR Core Thermal-Hydraulic Analysis Accounting for Inter-Assembly Heat Transfer", Trans. Amer. Nucl. Soc., 28, pp. 560-562 (1978).

6. M. D. Carelli and J. M. Willis, "An Analytical Method to Accurately Predict LMFBR Core Flow Distribution", Trans. Amer. Nucl. Soc., 32, pp. 575-576 (1979).

7. M. D. Carelli, A. J. Friedland, C. W. Bach and R. A. Markley, "An Optimized Method for Orificing LMFBR Cores", Trans. Amer. Nucl. Soc., 26, pp. 437-438 (1977).

8. E. H. Novendstern, "Mixing Model for Wire Wrap Fuel Assemblies", Trans. Amer. Nucl. Soc., 15, pp. 866-867 (1972).

9. M. D. Carelli, C. W. Bach and R. A. Markley, "Analytical Techniques for Thermal-Hydraulic Design of LMFBR Assemblies", Trans. Amer. Nucl. Soc., 17, pp. 423-424 (1973).

10. J. V. Miller and R. D. Coffield, "FØRE-2M: A modified Version of the FØRE-II Computer Program for the Analysis of LMFBR Transients", CRBRP-ARD-0142, May 1976. (Availability: US/DOE Technical Information Center).

11. R. A. Doncals, et al., "CRBR Nuclear Design Data", to be published as topical report.

12. M. C. Chuang, M. D. Carelli, C. W. Bach and J. S. Killimayer, "Three-Dimensional Thermal-Hydraulic Analysis of Wire Wrapped Rods in Liquid Metal Fast Breeder Reactor Core Assemblies", Nucl. Sci. Eng., 64, pp. 244-257 (1977).

13. F. C. Engel, R. A. Markley and B. Minushkin, "Heat Transfer Test Data of a 61-Rod Electrically Heated LMFBR Blanket Assembly Mockup and Their Use for Subchannel Code Calibration", in Fluid Flow and Heat Transfer Over Rod or Tube Bundles, pp. 223-229, ASME, December 1979.

14. A. S. Hanson and N. E. Todreas, "Fluid Mixing Studies in a Hexagonal 61-Pin Wire-Wrapped Rod Bundle", COO-2245-51TR, August 1977.

15. H. Hoffmann and E. Baumgartner, "Experimental Investigation of the Thermodynamic Behaviour of Fast Breeder Reactor Fuel Elements with Different Spacer Types", in Fuel and Fuel Element for Fast Reactors, Vol. 1, pp. 351-368, International Atomic Energy Agency, Vienna, 1974.

16. K. Takahashi, E. Ishibashi, "Experimental Study on Coolant Sodium Mixing Effect in JOYO Fuel Assembly with Spiral Wire Spacer. Experimental Results on Core Fuel Subassembly", SN 941-75-77, July 1975.

17. L. Patch, R. M. Roidt, M. D. Carelli and R. A. Markely, "Experimental Studies of Flow Distribution in a Wire Wrapped LMFBR Blanket Assembly", in Fluid Flow and Heat Transfer Over Rod or Tube Bundles, pp. 55-65, ASME, December 1979.

18. "Nuclear Systems Materials Handbook", TID-26666. (Availability: Hanford Engineering and Development Laboratory, Richland, WA).

19. M. D. Carelli, C. W. Bach and R. A. Markley, "Hydraulic and Scram Dynamics Analysis of LMFBR Control Rod Assemblies", Trans. Amer. Nucl. Soc., 16, pp. 218-219 (1973).

20. M. C. Billone, et al., "LIFE-III Fuel Element Performance Code", ERDA-77-56, July 1977. (Availability: US/DOE Technical Information Center).

21. R. D. Leggett, E. O. Ballard, R. B. Baker, G. R. Horn and D. S. Dutt, "Linear Heat Rating for Incipient Fuel Melting in UO_2 - PuO_2 Fuel", Trans. Amer. Nucl. Soc., 15, pp. 752-753 (1972).

22. R. D. Leggett, R. B. Baker, D. S. Dutt and S. A. Chastain, "Influence of Burnup on Heat Rating-to-Melting for UO_2 - PuO_2 Fuel", Trans. Amer. Nucl. Soc., 19, pp. 136-137 (1974).

23. G. H. Golden, A. Gopalakrishnan and R. A. Laskiewicz, "Correlation and Interpretation of Data Relative to EBR-II Power Level", in Irradiation Experimentation in Fast Reactors, pp. 314-332, American Nuclear Society, Hinsdale, Illinois.

24. L. B. Miller, G. H. Golden and R. E. Jabkac, "Characterization of the Power in an Experimental Irradiation Subassembly of Mixed-Oxide Fuel in EBR-II", ANL/EBR-047, September 1971.

25. G. H. Golden (EBR-II), private communication with A. Biancheria (ARD), 1977.

26. "Covered Pressure Drop Flow Test/Cross Flow Mixing Test", HEDL-TI-76049, November 1976. (Availability: US/DOE Technical Information Center).

27. W. L. Thorne, "Pressure Drop Measurements in FFTF Fuel Vibration Tests", HEDL-TC-812, April 1977. (Availability: US/DOE Technical Information Center).

28. W. L. Thorne, "Pressure Drop Measurements from Fuel Assembly Vibration Test II", HEDL-TC-824, April 1977. (Availability: US/DOE Technical Information Center).

29. P. M. McConnell, "Clinch River Breeder Reactor Fuel Assembly Inlet/Outlet Nozzle Flow Tests", HEDL-TME-77-8, February 1977. (Availability: US/DOE Technical Information Center).

30. H. M. Geiger, D. C. Meess and D. K. Schmidt, "Radial Blanket Flow Orificing Testing: Calibration Tests", WARD-RB-3045-18, April 1977. (Availability: US/DOE Technical Information Center).

31. F. C. Engel, R. A. Markley and A. A. Bishop, "Laminar, Transition and Turbulent Parallel Flow Pressure Drop Across Wire Wrap Spaced Rod Bundles", Nucl. Sci, Eng., 69, pp. 290-296 (1979).

32. M. R. Spiegel, Schaum's Outline of Theory and Problems of Statistics, p. 247, Schaum Publishing Co., New York, 1961.

33. I. E. Idel'chik, "Handbook of Hydraulic Resistance. Coefficients of Local Resistance and of Friction", AEC-TR-6630, 1960.

34. L. F. Moody, "Friction Factors for Pipe Flow", Trans. Amer. Soc. Mech. Eng., 66, pp. 671-684 (1944).

TABLE I

CRBRP CORE LOADING DURING CYCLES 1 THROUGH 5

CYCLE NUMBER	ASSEMBLY TYPE	TOTAL NUMBER OF ASSEMBLIES	REMARKS
1	Fuel	156	All Fresh Assemblies
	Inner Blanket	82	
	Radial Blanket	132	
2	Fuel	159	3 Fresh Fuel Assemblies
	Inner Blanket	79	
	Radial Blanket	132	
3	Fuel	156	All Fresh Fuel and Inner
	Inner Blanket	82	Blanket Assemblies
	Radial Blanket	132	
4	Fuel	162	6 Fresh Fuel Assemblies
	Inner Blanket	76	
	Radial Blanket	132	
5	Fuel	156	All Fresh fuel and Inner
	Inner Blanket	82	Blanket Assemblies plus 60
	Radial Blanket	132	Fresh Row 1 Radial Blanket Assemblies

TABLE II

SUMMARY OF STRAIN EQUIVALENT LIMITING TEMPERATURE CALCULATIONS FOR SECOND CORE FUEL ASSEMBLIES

ASSEMBLY	EOL STRAIN (%)	EOL PRESSURE (psi)	SELT (^{o}F)	SET (^{o}F)
2	.003	816	1264	1180
3	.007	845	1260	1192
13	.068	875	1258	1232
15	.031	891	1254	1211
24	.037	781	1270	1227
25	.039	861	1258	1220
26	.025	725	1281	1235
27	.057	748	1277	1247
28	.13	771	1272	1264
29	.003	815	1265	1181
30	.004	828	1262	1184
33	.001	855	1259	1194
34	.0086	862	1258	1193
37	.096	921	1249	1233
43	.015	892	1254	1197
44	.18	930	1248	1247
45	.034	876	1256	1217
47	.13	914	1251	1241
48	.12	773	1272	1261
49	.06	750	1276	1249
50	.023	726	1281	1232
51	.04	862	1258	1221
10	.19	920	1250	1250
11	.34	941	1247	1259
14	.36	928	1249	1263
36	.33	943	1247	1259
68	1.37	966	1243	$\leq$1295
101	1.43	970	1242	$\leq$1295
62	.029	529	not a limit	
98	.018	488	not a limit	

TABLE III

COOLANT LIMITING TEMPERATURES FOR TELT CALCULATIONS

(TEMPERATURES IN ^{O}F)

ASSEMBLY TYPE	AFMS MAXIMUM TRANSIENT TEMP. (FØRE-2M CALCULATED)	STEADY STATE TEMP. CORRESPONDING TO AFMS MAXIMUM TRANSIENT TEMP. (FØRE-2M)	STEADY STATE TEMP. CORRESPONDING TO 1550^{O}F MAXIMUM TRANSIENT TEMP.	T_M
Fuel Assembly	1571 (F/A #46 @ BOC1)	1331	1316	1252 First Core 1261 Second Core
Inner Blanket Assembly	1498 (IB/A #100 @ EOC4)	1247	1282	1198 First Core 1207 Second Core
Radial Blanket Assembly	1580 (RB/A #212 @ EOC5)	1331	1310	1232

Temperatures at THDV, 3σ, 750^{O}F Inlet

Temperatures for PEOV, 2σ

6001A-661A

TABLE IV

CORE ORIFICING ZONES FLOW ALLOCATION

ZONE	TYPE	NO. ASSYS/ ZONE	FLOW (lb/hr) CYCLES 1,3,5,...	CYCLE 2	CYCLES 4,6,8,...
1	Fuel	39	189,990 (201,900)	188,520 (200,340)	187,050 (198,780)
2	Fuel	54	176,790 (187,870)	175,420 (186,420)	174,060 (184,970)
3	Fuel	21	166,900 (177,360)	165,610 (175,990)	164,320 (174,620)
4	Fuel	18	153,400 (163,020)	152,220 (161,760)	151,030 (160,500)
5	Fuel	24	149,480 (158,850)	148,330 (157,630)	147,170 (156,400)
6	Fuel	0,3 or 6		178,590 (189,780)	177,190 (188,300)
	Inner Blanket	6,3 or 0	68,790 (73,100)	69,330 (73,680)	
7	Inner Blanket	57	88,790 (94,360)	88,110 (93,630)	87,420 (92,900)
8	Inner Blanket	19	78,030 (82,920)	77,420 (82,270)	76,810 (81,620)
9	Radial Blanket	12	62,300 (66,210)	61,820 (65,700)	61,340 (65,190)
10	Radial Blanket	36	48,300 (51,330)	47,930 (50,930)	47,550 (50,530)
11	Radial Blanket	48	35,090 (37,290)	34,820 (37,000)	34,540 (36,710)
12	Radial Blanket	36	25,740 (27,350)	25,540 (27,140)	25,330 (26,920)

NOTE: Flows are for THDV (PEOC) conditions.

92

CORE REGION FLOW FRACTIONS

REGION	CYCLES 1,3,5...	CYCLE 2	CYCLES 4,6,8...
Fuel	0.65	0.66	0.66
Inner Blanket	0.17	0.16	0.16
Radial Blanket	0.12	0.12	0.12
Total	0.94	0.94	0.94

6001A-661A

TABLE V-A

CRBR FUEL ASSEMBLIES ROD TEMPERATURE ENGINEERING UNCERTAINTY FACTORS

	COOLANT	FILM	CLADDING	GAP	FUEL	HEAT FLUX
DIRECT(o)						
Power Level Measurement and Control System Dead Band	1.03(1.0)					1.03
Inlet Flow Maldistribution	1.05					
Flow Distribution Calculational Uncertainty (Simulation Bias)	1.03	1.022				
Cladding Circumferential Temperature Variation		1.0(†) 1.7(*)	1.0(†)			
STATISTICAL (3σ)(o)						
Reactor ΔT Variation	1.0(1.144)					
Wire Wrap Orientation	1.01					
Subchannel Flow Area	1.028	1.0				
Film Heat Transfer Coefficient		1.12				
Pellet-Cladding Eccentricity		1.15	1.15			
Cladding Thickness and Conductivity			1.12			
Gap Conductance				1.48(ϕ)		
Fuel Conductivity					1.10	
Coolant Properties	1.01					
Flow Distribution Calculational Uncertainty (Calibration)	1.054	1.015				

(*) For cladding midwall temperature calculations. Applies to the nominal temperature drop between cladding midwall and bulk coolant.
(†) For fuel temperature calculations.
(ϕ) Applies to BOL conditions.
(o) Nuclear Uncertainty Factors are given on Table V-B.

NOTE: Same values of subfactors apply to both Plant T&H and Expected Operating conditions except when two values are given; in this case, the parenthesized values apply to Plant Expected Operating conditions while the non-parenthesized values apply to THDV conditions.

TABLE V-B

CRBR FUEL ASSEMBLIES ROD TEMPERATURE NUCLEAR UNCERTAINTY FACTORS
WITH AND WITHOUT CONTROL ASSEMBLY INFLUENCE

	Coolant	Heat Flux
Direct[a]		
Physics Modeling	1.02(1)	(*)1.02 (1.10)(1)
Control Rod Banking	1.02(2)	1.02(2)
ZPPR-7 Flux Tilt	1.0(4)	1.0(4)
Statistical (3σ)[a]		
Nuclear Data	1.07	1.07
Criticality	1.01(3)	1.01(3)
Fissile Fuel Maldistribution	1.03	1.03

If assembly is influenced by adjacent control rod, replace with:

		Coolant		Heat Flux			
				"Peak Power Position"		"Top of Core"	
		BOL	EOL	BOL	EOL	BOL	EOL
1) Physics Modeling	Adjacent	1.04	1.02	1.03	1.02	1.15	1.15
	Far Side	1.01	1.02	0.95	1.02	1.30	1.15
2) Control Rod Banking	Adjacent	1.04	1.02	1.04	1.02	1.01	1.02
	Far Side	1.02	1.02	1.02	1.02	1.01	1.02
3) Criticality	Adjacent	1.04	1.04	1.04	1.04	1.0	1.01
	Far Side	1.01	1.01	1.01	1.01	1.03	1.01

4) ZPPR-7 Flux Tilt - Assemblies 9, 10, 13, 14, 15, 16, 17, 23, 25, 37, 38, 41, 42, 43, 44, 45, 51, 53 (0.97 @ BOL, 1.0 @ EOL). Assemblies 8, 11, 19, 36, 39, 47, 65, 68, 101, 104 (0.99 @ BOL, 1.0 @ EOL). Assemblies 62, 98 (0.99 @ BOL, 1.0 @ EOL).

(*) Non-parenthesized value applies at the peak power position (i.e., core midplane). Parenthesized value applies at the core lower/upper axial blanket interface except as superseded by note (1).

(a) Engineering Uncertainty Factors are given on Table V-A

BOL = Beginning of life

EOL = End of life

TABLE VI-A

CRBR FUEL ASSEMBLIES MIXED MEAN EXIT TEMPERATURE
ENGINEERING UNCERTAINTY FACTORS

	ASSEMBLY EXIT
DIRECT(o)	
Power Level Measurement and Control System Dead Band	1.03(1.0)
Inlet Flow Maldistribution	1.05
STATISTICAL(3σ)(o)	
Reactor ΔT Variation	1.0(1.144)
Coolant Properties	1.01

(o) Nuclear Uncertainty Factors are given on Table VI-B.

NOTE: Same values of subfactors apply to both plant T&H and expected operating conditions except when two values are given; in this case, the parenthesized values apply to plant expected operating conditions while the non-parenthesized values apply to THDV conditions.

TABLE VI-B

CRBRP FUEL ASSEMBLIES MIXED MEAN EXIT
TEMPERATURE NUCLEAR UNCERTAINTY FACTORS

	ASSEMBLY EXIT
DIRECT[a]	
Physics Modeling	(*)1.01(1.02 @ BOL, 1.01 @ EOL)
Control Rod Banking	(*)1.02(1.03 @ BOL, 1.02 @ EOL)
ZPPR-7 Flux Tilt	1.0[4]
STATISTICAL (3σ)[a]	
Experimental (Nuclear)	1.07
Criticality	(*)1.01 (1.02)
Fissile Fuel Maldistribution	1.052

(4) ZPPR-7 Flux Tilt - Assy's. 9, 10, 13, 14, 15, 16, 17, 23, 25, 37, 38, 41, 42, 43, 44, 45, 51, 53 (0.97 @ BOL, 1.0 @ EOL). Assy's. 8, 11, 19, 36, 39, 47, 65, 68, 101, 104 (0.99 @ BOL, 1.0 @ EOL). Assy's 62, 98 (0.99 @ BOL, 1.0 @ EOL).

(*) Non-parenthesized values are applied for assemblies not adjacent to control assemblies. Parenthesized values are applied for the control assembly effect for assemblies adjacent to control assemblies.

(a) Engineering uncertainty factors are given on Table VI-A.

TABLE VII-A

CRBR FUEL ASSEMBLIES PLENUM PRESSURE
ENGINEERING UNCERTAINTY FACTORS

	PLENUM TEMPERATURE	BURNUP
DIRECT(o)		
Power Level Measurement and Control System Dead Band	1.03(1.0)	1.02
Inlet Flow Maldistribution	1.05	
Flow Distribution Calculational Uncertainty (Simulation Bias)	1.03	
STATISTICAL (3σ)(o)		
Reactor ΔT Variation	1.0(1.144)	
Wire Wrap Orientation	1.01	
Coolant Properties	1.01	
Flow Distribution Calculational Uncertainty (Calibration)	1.085	

(o) Nuclear Uncertainty Factors are given on Table VII-B

NOTE: Same values of subfactors apply to both plant T&H and expected operating conditions except when two values are given; in this case, the parenthesized values apply to plant expected operating conditions while the non-parenthesized values apply to THDV conditions.

TABLE VII-B

CRBR FUEL ASSEMBLIES PLENUM PRESSURE NUCLEAR UNCERTAINTY FACTORS
WITH AND WITHOUT CONTROL ASSEMBLY INFLUENCE

	PLENUM TEMPERATURE	BURNUP
DIRECT(o)		
Physics Modeling	1.02(1)	1.02(1)
Control Rod Banking	1.02(2)	1.02(2)
ZPPR-7 Flux Tilt	1.0(4)	1.0(4)
STATISTICAL (3σ)(o)		
Nuclear Data	1.07	1.07
Criticality	1.01(3)	1.01(3)
Fissile Fuel Maldistribution	1.03	1.03

If assembly is influenced by adjacent control rod, replace with:

		BOL	EOL
1) Physics Modeling	Adjacent	1.04	1.02
	Far Side	1.01	1.02
2) Control Rod Banking	Adjacent	1.04	1.02
	Far Side	1.02	1.02
3) Criticality	Adjacent	1.04	1.04
	Far Side	1.01	1.01

4) ZPPR-7 Flux Tilt - Assemblies 9, 10, 13, 14, 15, 16, 17, 23, 25, 37, 38, 41, 42, 43, 44, 45, 51, 53 (0.97 @ BOL, 1.0 @ EOL). Assemblies 8, 11, 19, 36, 39, 47, 65, 68, 101, 104 (0.99 @ BOL, 1.0 @ EOL). Assemblies 62, 98 (0.99 @ BOL, 1.0 @ EOL).

(o) Engineering Uncertainty Factors are given on Table VII-A.

TABLE VIII-A

CRBR INNER/RADIAL BLANKET ASSEMBLIES ROD TEMPERATURES ENGINEERING UNCERTAINTY FACTORS

	COOLANT	FILM	CLADDING	GAP	FUEL	HEAT FLUX
DIRECT(o)						
Power Level Measurement and Control System Dead Band	1.03(1.0)					1.03
Inlet Flow Maldistribution	1.07					
Flow Distribution Calculational Uncertainty (Simulation Bias)	1.03	1.03				
Cladding Circumferential Temperature Variation		1.0(†) 2.2(*)	1.0(†)			
STATISTICAL (3σ)(o)						
Reactor ΔT Variation	1.0(1.144)					
Wire Wrap Orientation	1.01					
Subchannel Flow Area	1.035	1.0				
Film Heat Transfer Coefficient		1.21				
Pellet-Cladding Eccentricity		1.15	1.15			
Cladding Thickness and Conductivity			1.12			
Gap Conductance				1.48(φ)		
Fuel Conductivity					1.10	
Coolant Properties	1.01					
Flow Distribution Calculational Uncertainty (Calibration)	1.199/1.1(+)	1.056				

(*) For cladding midwall temperature calculations. Applies to the nominal temperature drop between cladding midwall and bulk coolant.
(†) For fuel temperature calculations.
(φ) Applies to BOL conditions.
(o) Nuclear Uncertainty Factors are given on Table VIII-B.
(+) Inner/radial blanket.

NOTE: Same values of subfactors apply to both Plant T&H and Expected Operating conditions except when two values are given; in this case, the parenthesized values apply to Plant Expected Operating conditions while the non-parenthesized values apply to THDV conditions.

TABLE VIII-B

CRBR INNER/RADIAL BLANKET ASSEMBLIES ROD TEMPERATURE NUCLEAR UNCERTAINTY FACTORS

	INNER BLANKET		RADIAL BLANKET			
			Row 1		Row 2	
	COOLANT	HEAT FLUX	COOLANT	HEAT FLUX	COOLANT	HEAT FLUX
DIRECT (BOL)(o)						
Physics Modeling	1.06	(*)1.07(1.11)	1.07	(*)1.07(1.02)	1.03	(*)1.07(0.99)
Control Rod Banking	1.02	1.02	1.02	1.02	1.02	1.02
Nuclear Data	1.12	(*)1.10(1.17)	1.13	(*)1.11(1.18)	1.27	(*)1.24(1.32)
Criticality	1.02	1.02	----	----	----	----
Heavy Metal	1.01	1.01	1.01	1.01	1.01	1.01
U-235	1.01	1.01	1.01	1.01	1.01	1.01
DIRECT (EOL)(o)						
Physics Modeling	1.02	(*)1.04(1.12)	1.01	(*)1.07(1.05)	1.01	(*)1.07(1.02)
Control Rod Banking	1.02	1.02	1.02	1.02	1.02	1.02
Nuclear Data	1.03	(*)1.00(1.07)	1.05	(*)1.03(1.10)	1.15	(*)1.13(1.21)
Criticality	1.01	1.01	----	----	----	----
Heavy Metal	1.01	1.01	1.01	1.01	1.01	1.01
U-235	1.0	----	----	----	----	----

(*) Non-parenthesized values apply at the peak power position (i.e., near core midplance). Parenthesized values apply at core upper/lower axial extension interface.

(o) Engineering Uncertainty Factors are given on Table VIII-A.

TABLE IX-A

CRBR INNER/RADIAL BLANKET ASSEMBLIES MIXED MEAN EXIT TEMPERATURE
ENGINEERING UNCERTAINTY FACTORS

	ASSEMBLY EXIT
DIRECT(o)	
Power Level Measurement and Control System Dead Band	1.03(1.0)
Inlet Flow Maldistribution	1.07
STATISTICAL(3σ)(o)	
Reactor ΔT Variation	1.0(1.144)
Coolant Properties	1.01

(o) Nuclear Uncertainty Factors are given on Table IX-B.

NOTE: Same values of subfactors apply to both plant T&H and expected operating conditions except when two values are given; in this case, the parenthesized values apply to plant expected operating conditions while the non-parenthesized values apply to THDV conditions.

TABLE IX-B

CRBR INNER/RADIAL BLANKET ASSEMBLIES MIXED MEAN
EXIT TEMPERATURE NUCLEAR UNCERTAINTY FACTORS

	INNER BLANKET	RADIAL BLANKET	
		Row 1	Row 2
DIRECT (BOL)(o)			
Physics Modeling	1.01	1.02	1.02
Control Rod Banking	1.02	1.02	1.02
Nuclear Data	1.12	1.13	1.27
Criticality	1.02	----	----
Heavy Metal	1.01	1.01	1.01
U-235	1.01	1.01	1.01
DIRECT (EOL)(o)			
Physics Modeling	1.01	1.02	1.02
Control Rod Banking	1.02	1.02	1.02
Nuclear Data	1.03	1.05	1.15
Criticality	1.01	----	----
Heavy Metal	1.01	1.01	1.01
U-235	----	----	----

(o) Engineering uncertainty factors are given on Table IX-A.

TABLE X-A

CRBR INNER/RADIAL BLANKET ASSEMBLIES PLENUM PRESSURE
ENGINEERING UNCERTAINTY FACTORS

	PLENUM TEMPERATURE	BURNUP
DIRECT(o)		
Power Level Measurement and Control System Dead Band	1.03(1.0)	1.02
Inlet Flow Maldistribution	1.07	
Flow Distribution Calculational Uncertainty (Simulation Bias)	1.03	
STATISTICAL (3σ)(o)		
Reactor ΔT Variation	1.0(1.144)	
Wire Wrap Orientation	1.01	
Coolant Properties	1.01	
Flow Distribution Calculational Uncertainty (Calibration)	1.299/1.1(+)	

(o) Nuclear Uncertainty Factors are given on Table X-B

(+) Inner/radial blanket

NOTE: Same values of subfactors apply to both plant T&H and expected operating conditions except when two values are given; in this case, the parenthesized values apply to plant expected operating conditions while the non-parenthesized values apply to THDV conditions.

6001A-661A

TABLE X-B

CRBR INNER/RADIAL BLANKET ASSEMBLIES PLENUM PRESSURE NUCLEAR UNCERTAINTY FACTORS

	INNER BLANKET		RADIAL BLANKET			
			Row 1		Row 2	
	PLENUM TEMPERATURE	BURNUP	PLENUM TEMPERATURE	BURNUP	PLENUM TEMPERATURE	BURNUP
DIRECT (BOL)(o)						
Physics Modeling	1.06	1.06	1.03	1.03	1.03	1.03
Control Rod Banking	1.02	1.02	1.02	1.02	1.02	1.02
Nuclear Data	1.12	1.12	1.13	1.13	1.27	1.27
Criticality	1.02	1.02	----	----	----	----
Heavy Metal	1.01	1.01	1.01	1.01	1.01	1.01
U-235	1.01	1.01	1.01	1.01	1.01	1.01
DIRECT (EOL)(o)						
Physics Modeling	1.02	1.02	1.01	1.01	1.01	1.01
Control Rod Banking	1.02	1.02	1.02	1.02	1.02	1.02
Nuclear Data	1.03	1.03	1.05	1.05	1.15	1.15
Criticality	1.01	1.01	----	----	----	----
Heavy Metal	1.01	1.01	1.01	1.01	1.01	1.01
U-235	----	----	----	----	----	----

(o) Engineering uncertainty factors are given on Table X-A.

TABLE XI

FUEL ASSEMBLIES UNCERTAINTY FACTORS FOR DUCT TEMPERATURE CALCULATIONS

Direct	Heat Generation	Assembly Flow	ΔH	Film	Duct	Interstitial Gap
Power Level Measurement and Control System Dead Band	1.03(1.03)					
Inlet Flow Maldistribution		1.05(0.95)		(1)		
Flow Distribution Calculational Uncertainty (Simulation Bias)			1.03(1.03)	(1)		
Nuclear	See Table XII					
Statistical (3σ)						
Reactor ΔT Variation			1.0/1.144(2) (1.0/1.144)			
Nuclear	See Table XII					
Wire Wrap Orientation			1.01(0.99)			
Subchannel Flow Area			1.071(0.9)			
Flow Distribution Calculational Uncertainty (Calibration)			1.08(0.92)(3)			
Geometrical Deviations					(4)	(4)
Duct Conductivity					1.1(1.1)	
Film Heat Transfer Coefficient				(1)		1.0
Coolant Properties			1.017(1.017)			1.017(1.017)

NOTES

Numbers outside parentheses are positive uncertainties, in parentheses are negative uncertainties.

(1) Bracketed by: $K_{Na}/\delta(\infty)$ - see Section 3.2.2.4 for explanation.

(2) Plant thermal-hydraulic design value/expected operating conditions.

(3) Negative value to be used against a different type of assembly, e.g., fuel adjacent to blanket, not fuel to fuel, unless uniformly applied to all assemblies of the same type. See Section 3.2.2.3 for further explanation.

(4) Variations of dimensions due to tolerances, etc., are explicitly considered in TRITØN by changing value of inter-assemblies pitch and ducts thickness.

6001A-661A

TABLE XII

FUEL ASSEMBLIES HEAT GENERATION NUCLEAR UNCERTAINTIES

Group I - Assemblies #10, 14, 15, 37, 43, 44

	POSITIVE		NEGATIVE	
Direct	BOL	EOL	BOL	EOL
Physics Modeling	1.02	1.01	0.98	0.99
Control Rod Banking	1.03	1.02	1.03	1.02
ZPPR-7 Flux Tilt	0.97	1.0	0.97	1.0
Statistical (3σ)				
Experimental	1.07	1.07	0.93	0.93
Criticality	1.02	1.02	1.02	1.02
Fissile Maldistribution	1.03	1.03	0.97	0.97
Total				
0σ	1.019	1.030	0.979	1.010
2σ	1.073	1.084	0.931	0.961
3σ	1.10	1.111	0.908	0.936

Group II - Assemblies #62, 98

Direct				
Physics Modeling	1.02	1.01	0.98	0.99
Control Rod Banking	1.03	1.02	1.03	1.02
ZPPR-7 Flux Tilt	0.99	1.0	0.99	1.0
Statistical				
Same as Group I				
Total				
0σ	1.040	1.030	0.999	1.010
2σ	1.095	1.084	0.95C	0.961
3σ	1.122	1.111	0.926	0.936

TABLE XII (CONT'D)

Group III - Assemblies #9, 13, 16, 17, 23, 25, 38, 41, 42, 45, 51, 53

	POSITIVE		NEGATIVE	
Direct	BOL	EOL	BOL	EOL
Physics Modeling	1.01	1.01	0.99	0.99
Control Rod Banking	1.02	1.02	1.02	1.02
ZPPR-7 Flux Tilt	0.97	1.0	0.97	1.0
Statistical (3σ)				
Experimental	1.07	1.07	0.93	0.93
Criticality	1.01	1.01	1.01	1.01
Fissile Maldistribution	1.03	1.03	0.97	0.97
Total				
0σ	0.999	1.030	0.980	1.010
2σ	1.050	1.083	0.931	0.959
3σ	1.076	1.109	0.907	0.934

Group IV - Assemblies #8, 11, 19, 36, 39, 47, 65, 68, 101, 104

Direct				
Physics Modeling	1.01	1.01	0.99	0.99
Control Rod Banking	1.02	1.02	1.02	1.02
ZPPR-7 Flux Tilt	0.99	1.0	0.99	1.0
Statistical				
Same as Group III				
Total				
0σ	1.020	1.030	1.0	1.010
2σ	1.072	1.083	0.95	0.959
3σ	1.099	1.109	0.925	0.934

TABLE XII (CONT'D)

Group V - Assemblies #2, 3, 26, 27, 28, 29, 30, 33, 34, 48, 49, 50

Direct	POSITIVE BOL & EOL	NEGATIVE BOL & EOL
Physics Modeling	1.01	0.99
Control Rod Banking	1.02	1.02
Statistical		
Same as Group III		
Total		
0σ	1.030	1.010
2σ	1.083	0.959
3σ	1.109	0.934

TABLE XIII

BLANKET ASSEMBLIES UNCERTAINTY FACTORS FOR DUCT TEMPERATURE CALCULATIONS

Direct	Heat Generation	Assembly Flow	ΔH	Film	Duct	Interstitial Gap
Power Level Measurement and Control System Dead Band	1.03(1.03)					
Inlet Flow Maldistribution		1.07(0.93)		(1)		
Flow Distribution Calculational Uncertainty (Simulation Bias)			1.03(1.03)	(1)		
Nuclear	See Table XIV					
Statistical (3σ)						
Reactor ΔT Variation			1.0/1.144(2) (1.0/1.144)			
Wire Wrap Orientation			1.0			
Subchannel Flow Area			1.15(0.75)			
Flow Distribution Calculational Uncertainty (Calibration)			1.2(0.8)(3)			
Geometrical Deviations					(4)	(4)
Duct Conductivity					1.1(1.1)	
Film Heat Transfer Coefficient				(1)		1.0
Coolant Properties			1.017(1.017)			1.017(1.017)

NOTES:

Numbers outside parentheses are positive uncertainties, in parentheses are negative uncertainties.

(1) Bracketed by: $K_{Na}/\delta(\infty)$ - see Section 3.2.2.4 for explanation.

(2) Plant thermal-hydraulic design value/expected operating conditions.

(3) Negative value to be used against a different type of assembly, e.g., fuel adjacent to blanket, not fuel to fuel, unless uniformly applied to all assemblies of the same type. See Section 3.2.2.3 for further explanation.

(4) Variations of dimensions due to tolerances, etc., are explicitly considered in TRITØN by changing value of inter-assemblies pitch and ducts thickness.

TABLE XIV

INNER AND RADIAL BLANKET ASSEMBLIES HEAT GENERATION NUCLEAR UNCERTAINTIES

Factor (all factors are direct)	Inner Blanket				Radial Blanket First Row				Radial Blanket Second Row			
	Positive		Negative		Positive		Negative		Positive		Negative	
	BOL	EOL	BOL	EOL	BOL	EOL	BOL	EOL	BOL	EOL	BOL	EOL
Experimental	1.12	1.03	0.92	0.93	1.13	1.05	0.95	0.91	1.27	1.15	0.99	0.99
Heavy Metal Content	1.01	1.01	0.99	0.99	1.01	1.01	0.99	0.99	1.01	1.01	0.99	0.99
U-235 Content	1.01	1.0	0.99	1.0	1.01	1.0	0.99	1.0	1.01	1.0	0.99	1.0
Modeling	1.06	1.02	0.94	0.98	1.07	1.01	0.97	0.95	1.03	1.01	0.93	0.95
Criticality	1.02	1.01	1.02	1.01	1.0	1.0	1.0	1.0	1.0	1.0	1.0	1.0
Control Rod Banking	1.02	1.02	1.02	1.02	1.02	1.02	1.02	1.02	1.02	1.02	1.02	1.02
TOTAL	1.26	1.09	0.88	0.93	1.26	1.09	0.92	0.87	1.36	1.20	0.92	0.95

TABLE XV

PRIMARY CONTROL ASSEMBLIES UNCERTAINTY FACTORS FOR DUCT TEMPERATURE CALCULATIONS

Direct	Heat Generation	Assembly Flow	Flow Split	ΔH_{bundle}	ΔH_{bypass}	Film	Duct	Interstitial Gap
Power Level Measurement and Control System Dead Band	1.03(1.03)							
Inlet Flow Maldistribution		1.08(0.92)				(1)		
Flow Distribution Calculation Uncertainty				1.08(0.92)(3)		(1)		
Bundle/Bypass Flow Split			1.1(1.0)			(1)		
Nuclear	1.15(0.85)							
Statistical (3σ)								
Reactor ΔT Variation				1.0/1.144(2) (1.0/1.144)	1.0/1.144(2) (1.0/1.144)			
Absorber Maldistribution	1.03(0.97)							
Wire Wrap Orientation				1.0				
Subchannel Flow Area				1.16(0.87)	1.23(0.89)			
Geometrical Deviations							(4)	(4)
Duct Conductivity							1.1(1.1)	
Film Heat Transfer Coefficient						(1)		1.0
Coolant Properties				1.017(1.017)	1.017(1.017)			1.017(1.017)

NOTES:

Numbers outside parentheses are positive uncertainties, in parentheses are negative uncertainties.

(1) Bracketed by: $K_{Na}/\delta(\infty)$ - see Section 3.2.2.4 for explanation.

(2) Plant thermal-hydraulic design value/expected operating conditions.

(3) Negative value to be used against a different type of assembly, e.g., fuel adjacent to blanket, not fuel to fuel, unless uniformly applied to all assemblies of the same type. See Section 3.2.2.3 for further explanation.

(4) Variations of dimensions due to tolerances, etc., are explicitly considered in TRITØN by changing value of inter-assemblies pitch and ducts thickness.

6001A-661A

TABLE XVI

CRBR EXPECTED OPERATING CONDITIONS DURING PLANT LIFETIME

Parameter	Clean & Unplugged Heat Exchangers (New Plant)				Estimated (2 Year Fouling)				Fouled & Plugged Heat Exchangers (30 Year Fouling)			
	Nominal	Mean	σ	$T_{97.7}$	Nominal	Mean	σ	$T_{97.7}$	Nominal	Mean	σ	$T_{97.7}$
Primary Hot Leg Temperature (^{o}F)	943	946	13	968	950	954	13	976	960	964	13	987
Primary Cold Leg Temperature (^{o}F)	698	697	13	722	705	704	11	725	714	714	12	736
Primary ΔT (^{o}F)	245	249	12	273	245	250	12	274	246	250	12	275
Power (MWt)	975	975		1004	975	975		1004	975	975		1004

NOTE: Design and control uncertainties are included.

TABLE XVII

PLANT EXPECTED CONDITIONS AND ASSOCIATED UNCERTAINTIES
CONSIDERED ON CRBRP CORE THERMOFLUIDS ANALYSES

	First Core	Second Core
Nominal Inlet Temperature (^{o}F)	704	711
Nominal Reactor ΔT (^{o}F)	250	250
Reactor ΔT Uncertainty Factor (3σ)(*)	1.144	1.144
Inlet Temperature Uncertainty (3σ) (^{o}F)	33	36
Loop-to-Loop Imbalance (3σ) (^{o}F)	4.6	4.6
Combined Uncertainty on Inlet Temperature (2σ) (^{o}F) - (Additive to Nominal)	22.2	24.6

(*) To be combined with other uncertainties on $F_{\Delta H}$

NOTE: Power Level Measurement/Control Dead Band Uncertainty is already included in above uncertainties.

TABLE XVIII

GEOMETRIES AND OPERATING CONDITIONS (0σ LEVEL) CHARACTERIZING FUEL PINS USED IN POWER-TO-MELT UNCERTAINTY ANALYSIS

PARAMETER	F/A 101 (X/L = 0.409)	F/A 14 (X/L = 0.318)
Cladding Length, in.	77.19	77.19
Fuel Length, in.	36.24	36.24
Cladding Inner Radius, in.	0.100	0.100
Cladding Thickness, in.	0.015	0.015
Fuel-Cladding Radial Gap, mils	3.25	3.25
Reactor Inlet Temperature, ^{o}F	735	735
Initial Gas Pressure, atm.	1.0	1.0
Initial Xenon Fraction	0.094	0.094
Fuel Density, % T.D.	91.3	91.3
Initial PuO_2, w/o	32.9	32.9
BOC1 Power, kw/ft	13.23	12.77
BOC1 Flux (E > 0.1) (x 10^{15})	3.18	3.29
BOC1 Cladding OD Temp., ^{o}F	960	875
BOC1 Plenum Temp., ^{o}F	1171	1082

TABLE XIX

POWER-TO-MELT RESULTS

ASSEMBLY (PEAK PIN)	MAXIMUM LINEAR POWER RATING, 0σ (kw/ft)	HISTORY	Q_{MELT} (kw/ft)	OVERPOWER (% NFP)
F/A 101	13.23	8 hrs. to 0.7 NFP(*)	14.70	11.1
	13.23	above + 50 hrs. to 0.9 NFP	17.41	31.5
	13.23	above + 50 hrs. to NFP	18.39	39.0
F/A 14	12.77	8 hrs. to 0.7 NFP	14.97	17.2
	12.77	above + 50 hrs. to 0.9 NFP	17.24	35.0
	12.77	above + 50 hrs. to NFP	18.42	44.2

(*) Nominal Full Power

TABLE XX

CENTER TEMPERATURES AND POWERS-TO-MELT OF INCIPIENT MELT SECTIONS AS COMPUTED BY LIFE-3

Pin No.	Calculated T_{max} °F	(°C)	Calculated Power-to-Melt kW/ft	(kw/m)	Observed Power-to-Melt kW/ft	(kw/m)
P19-35	5009	(2765)	16.62	(54.5)	16.69	(54.6)
P19-02	4978	(2748)	16.04	(52.6)	15.89	(52.1)
P19-24R	5024	(2773)	15.44	(50.6)	15.59	(51.1)
P19-27R	4990	(2754)	19.23	(63.1)	19.16	(62.8)
P19-28	4966	(2741)	19.02	(62.4)	18.82	(61.8)
P19-30	5070	(2799)	17.22	(56.5)	17.79	(58.3)
P19-08	5006	(2763)	15.36	(50.4)	15.40	(50.5)
P20-07	5004	(2762)	15.72	(51.7)	15.75	(51.7)
P20-30	4985	(2752)	16.82	(55.2)	16.70	(54.8)
P20-33	4982	(2750)	19.07	(62.5)	18.98	(62.2)

Average T = 5001 $\pm$ 28°F
(2761 $\pm$ 16°C)

r.m.s. error
= 0.21 kw/ft (.69 kw/m)

std. dev.*
= 0.24 kw/ft (.77 kw/m)

*Two degrees of freedom lost in calibrating LIFE-3 parameters.

TABLE XXI

SPATIAL DEPENDENCE OF POWER UNCERTAINTY CALCULATED FROM COMPARISON OF MEASURED AND CALCULATED CONTROL ROD WORTHS

Control Rod Number	Calculated Minus Measured Power (%)
1	-0.67
2	-1.75
3	-1.8
4	-2.35
5	0.
6	1.85
7	2.25
8	1.5
900	0.45
10	1.2
11	0.7
12	2.25

Average Δ Power = 0.3%

Standard Deviation = 1.7%

TABLE XXII

ADOPTED VALUES FOR EBR-II UNCERTAINTIES

	%
σ_{time}	2.2
σ_{sys}	3.0
σ_{space}	1.8
σ_{fab}	0.8
σ_{PIE}	0.9
σ_{tot}	4.3
σ_{mean}	4.1

TABLE XXIII

CRBRP FUEL ROD TOLERANCES AND UNCERTAINTIES

	Nominal	$\sqrt{3}\sigma_i$
Fuel Pellet Diameter	0.1935 in.	± 0.0015 in.
Cladding Inside Diameter	0.200 in.	± 0.0005 in.
Fuel Pellet Density	91.3% TD	± 1.6% TD
Reactor Power*		± 5.07%
Cladding O.D. Temperature Near Midplane**		± 15.6°F

* Statistical combination of nuclear data, criticality, and fissile fuel maldistribution uncertainties. Value reported was calculated on the basis of preliminary nuclear uncertainties. A recalculation was not deemed necessary at this time since updated nuclear uncertainties are not too dissimilar, considerable margin-to-melting exists and programmed startup parameters are not yet optimized.

** Due to thermal-hydraulic engineering uncertainties (not including uncertainties already accounted for in reactor power).

TABLE XXIV

SENSITIVITY OF POWER-TO-MELT TO DESIGN UNCERTAINTIES

			CHANGE IN POWER-TO-MELT FOR ONE PERCENT CHANGE IN DESIGN UNCERTAINTY $\partial\overline{REPOW}_M/\partial(\%X_i)$				
TIME, t. hrs.	REPOW	X_i:	ρ_{pel}	D^*_{pel}	D_{clad}	Power	T_{clad}
8	0.7		-.0040	.112	-.098	-.0107	-.00092
58	0.9		-.0017	.043	-.062	-.0027	-.00069
108	1.0		-.0051	-.051	.060	-.0093	-.00081
158	1.0		-.0051	-.050	.060	-.010	-.00081

* Derivative taken from Figure 76.

TABLE XXV

STATISTICAL COMBINATION OF POWER-TO-MELT
UNCERTAINTIES DUE TO DESIGN UNCERTAINTIES

TIME, t hrs.	REPOW	ONE SIGMA POWER UNCERTAINTY RESULTING FROM DESIGN UNCERTAINTY $\sigma_i \partial \overline{REPOW}_M / \partial X_i$					STATISTICAL COMBINATION
		ρ_{pel}	D_{pel}	D_{clad}	Power	T_{clad}	$\sigma_{\overline{R}}$
8	0.7	-.0041	.050	-.014	-.0337	-.0036	.062
58	0.9	-.0017	.019	-.0089	-.0085	-.0027	.023
108	1.0	-.0052	-.023	.0087	-.0294	-.0032	.039
158	1.0	-.0052	-.022	.0087	-.0315	-.0032	.040

TABLE XXVI

EFFECT OF MELTING POINT UNCERTAINTY OF
σ_{TM} = 5.8°F ON UNCERTAINTY OF POWER-TO-MELT

t(hrs)	$\partial\bar{Q}_M/\partial T_M$ kw/ft/°F	σ_{extrap} (kw/ft)	(REPOW Units)
8	.0095	.055	.0043
58	.0069	.040	.0031
108	.0061	.035	.0027
158	.0058	.034	.0026

TABLE XXII

TOTAL UNCERTAINTY ON CRBRP REACTOR POWER-TO-MELT
IN REACTOR POWER UNITS WHERE NOMINAL FULL POWER IS 1.0

t (hrs)	REPOW	$\sigma_{\overline{R}}$	σ_{mean}	σ_{extrap}	TOTAL σ_{REPOW_M}	$\overline{REPOW_M}$ (nominal, t)	$\overline{REPOW} - 3\sigma_{REPOW_M}$ -1.15/1.03 REPOW
8	0.7	.062	.047	.0043	.078	1.152	.136
58	0.9	.023	.055	.0031	.060	1.335	.150
108	1.0	.039	.058	.0027	.070	1.415	.088
158	1.0	.040	.059	.0026	.071	1.437	.107

TABLE XXVIII

COMPARISON OF 3-σ MINIMUM POWER-TO-MELT TO POWER AT 15% OVERPOWER

ASSEMBLY	Q_1 = Power at Start of Jump / NFP*	$\frac{1.15\ Q_1}{1.03}$	Q_2 = Q_{melt} / NFP*	Q_3 = $3\sigma_{REPOW_M}$ (Table XXVII)	Q_4 = $Q_2 - Q_3$	Margin = $Q_4 - \frac{1.15\ Q_1}{1.03}$
F/A 101	0.70	0.782	1.111	0.234	0.877	0.095
F/A 101	0.90	1.005	1.315	0.180	1.135	0.130
F/A 101	1.00	1.117	1.390	0.210	1.180	0.063
F/A 14	0.70	0.782	1.172	0.234	0.938	0.156
F/A 14	0.90	1.005	1.350	0.180	1.170	0.165
F/A 14	1.00	1.117	1.442	0.210	1.232	0.115

*NFP = Nominal Full Power

TABLE XXIX

SUMMARY OF LIFE-3 RUNS FOR INNER BLANKET POWER-TO-MELT ANALYSES

RUN #	PIN (IB/A 99)	ELEVATIONS, IN. (WORST ELEV. UNDERLINED) (Midplane = 32 in.)	CLADDING TEMP. HCF	CLADDING SWELLING	POWER HCF AT WORST ELEVATION	NEUTRON FLUX HCF AT WORST ELEVATION	POWER LEVEL (1.03) HCF	POWER-TO-MEL * (NFP = 1.0)
1	Hot	18, 24, <u>32</u>, 40, 46	0σ	Nominal	Midplane Value	Same as Power	Yes	1.360
2	Hot	18, 24, <u>32</u>, 40, 46	3σ	Nominal	Midplane Value	Same as Power	Yes	1.301
3	Hot	18, 24, <u>32</u>, 40, 46	0σ	Maximum	Midplane Value	Same as Power	Yes	1.333
4	Peak	23, 30, <u>32</u>	0σ	Nominal	Midpane Value	Same as Power	Yes	1.366
5	Peak	23, 30, <u>32</u>	3_σ	Nominal	Midplane Value	Same as Power	Yes	1.280
6	Peak	28, 30, <u>32</u>	0_σ	Nominal	Midplane Value	Same as Power	No	1.398
7	Peak	28, 30, <u>32</u>	0_σ	Maximum	Midplane Value	Same as Power	No	1.359
8	Peak	30, 32, <u>34</u>, 36, 38	0_σ	Nominal	Chopped Cosine	1.15	Yes	1.338

(*)NFP = Nominal Full Power

TABLE XXX

MARGIN-TO-MELT ANALYSIS
(REACTOR POWER UNITS - 0σ POWER = 1.0)

	PEAK PIN				HOT PIN
	WORST ELEVATION		MIDPLANE		MIDPLANE
	CASE 1	CASE 2	CASE 1	CASE 2	CASE 1
A. Reduction in power-to-melt because of uncertainties in cladding swelling parameters (3σ)			0.039		0.027
B. Overall extrapolation uncertainty, σ_{extrap} (Item A combined with remaining uncertainties)			0.0377		0.0365
C. Reduction in power-to-melt because of uncertainties in cladding temperature (3σ)			0.086		0.059
D. Overall design uncertainty, $\sigma_{\bar{R}}$ (Item C combined with remaining uncertainties)			0.0289		0.0200
E. Power-to-melt for base case, $\overline{REPOW}_M$	1.338		1.366	1.398	1.360
F. EBR-II experimental uncertainties, $\sigma_{mean} = 0.041 * \overline{REPOW}_M$	0.0549		0.0560	0.0573	0.056
G. Total σ_{REPOW_M} = $(\sigma_{mean}^2 + \sigma_{extrap}^2)^{1/2}$	0.0726		0.0734	0.0744	0.070
H. Margin-to-melt = $\overline{REPOW}_M - 3\sigma_{REPOW_M} - C_1$*REPOW; where $C_1 = 1.15/1.03$, Case 1 $C_1 = 1.15$, Case 2	0.004	0.000	0.029	0.025	0.033

6001A-661A

TABLE XXXI

FUEL ASSEMBLY COMPONENT PRESSURE DROP DATA LINEAR RECRESSION ANALYSIS

COMPONENT	LINEAR REGRESSION FUNCTION	NO. OF DATA POINTS	MEAN OF ln(Re)	STANDARD DEVIATION ABOUT MEAN OF ln(Re)	MEAN OF ln(D)	STANDARD DEVIATION ABOUT MEAN OF ln(D)	STANDARD ERROR OF EST'MATE
Inlet Nozzle	ln(K)=0.9177-.05289 ln(Re)	222	13.64	0.3560			0.0841
Inlet Nozzle-Orifice Shield:							
-- 1 Plate	ln(K)=2.352-.09211ln(Re)-1.452ln(D)	41	13.95	0.3763	-.1845	0.1256	0.0170
-- 2 Plates	ln(K)=1.708-.05022ln(Re)-3.293ln(D)	73	13.73	0.3684	-.3528	0.1057	0.0472
-- 3 Plates	ln(K)=2.240-.08226ln(Re)-3.891ln(D)	60	13.61	0.3560	-.4064	0.1165	0.0207
-- 4 Plates	ln(K)=2.293-.07141ln(Re)-4.032ln(D)	43	13.52	0.2982	-.4454	0.1040	0.0136
-- 5 Plates	ln(K)=2.225-.03072ln(Re)-3.651ln(D)	42	13.45	0.2589	-.4484	0.0997	0.0165
Shield	ln(K)=0.3988-.03879ln(Re)	17	13.82	0.3768			0.0966
Rod Bundle:							
-- Inlet	K = 0.370	--					0.2(*)
-- Rod Friction	see Table XXXII	161	entire range				0.0524
		46	full flow				+0.0312,-0.0262
-- Outlet	K = 0.178	--					0.2(*)
Outlet Nozzle	ln(K)=.00495-.04902ln(Re)	16	13.67	0.7483			0.0450

(*) A 20% uncertainty was selected as a bounding value (not standard error), since no data are available.

TABLE XXXII

FUEL ASSEMBLY COMPONENT HYDRAULIC CORRELATIONS

COMPONENT	CORRELATION	REFERENCE AREA (IN^2)	REFERENCE HYDRAULIC DIAMETER (IN)	REFERENCES
Inlet Nozzle	$K=2.504\ Re^{-0.0529}$	3.976	2.250	29
Inlet Nozzle-Orifice-Shield:				
-- 1 Plate	$K=10.50\ Re^{-0.0921}\ D^{-1.452}$	3.976	2.250	29
-- 2 Plates	$=5.519\ Re^{-0.0502}\ D^{-3.293}$			
-- 3 Plates	$K=9.396\ Re^{-0.0823}\ D^{-3.891}$			
-- 4 Plates	$K=9.909\ Re^{-0.0714}\ D^{-4.032}$			
-- 5 Plates	$K=9.253\ Re^{-0.0307}\ D^{-3.651}$			
Shield	$K=1.490\ Re^{-0.0388}$	3.976	2.250	29
Rod Bundle:				
-- Inlet	$K=0.370$	6.724	0.1281	33
-- Rod Friction	$f=84/Re$ for $Re \leq 1000$	6.724	0.1281	26-28
	$f=(1.080+0.0927\ (1000/Re)^2+0.1694*(1000/Re)^4)\ f_c$			
	where $f_c^{(*)}=4Log_{10}(2.51/(Re\sqrt{f_c}))$			
-- Outlet	$K=0.178$	6.724	0.1281	33
Outlet Nozzle	$K=1.005\ Re^{-0.0490}$	5.899	2.116	29

(*) f_c is the Colebrook friction factor correlation[34] for a smooth tube.

TABLE XXXIII

INNER BLANKET ASSEMBLY COMPONENT HYDRAULIC CORRELATIONS

COMPONENT	CORRELATION	REFERENCE AREA (IN^2)	REFERENCE HYDRAULIC DIAMETER (IN)	REFERENCES
Inlet Nozzle	$K=2.504\ Re^{-0.0529}$	3.976	2.250	29
Inlet Nozzle Orifice Shield	$K=C\ Re^{-0.05}$	3.976	2.250	29,30
Shield	$K=2.0$	2.405	1.750	33
Rod Bundle:				
-- Inlet	$K=0.427$	3.956	0.1338	33
-- Rod Friction	$f=110/Re$ for $Re \leq 400$	3.956	0.1338	31
	$f=(110/Re)\sqrt{1-\psi} + (0.55/Re^{0.25})\sqrt{\psi}$ where $\psi = (Re-400)/4600$ for $400 < Re < 5000$			
	$f=0.55/Re^{0.25}$ for $Re \geq 5000$			
-- Outlet	$K=0.290$	3.956	0.1338	33
Outlet Nozzle	$K=1.005\ Re^{-0.0490}$	3.976	2.250	29

TABLE XXXIV

RADIAL BLANKET ASSEMBLY COMPONENT HYDRAULIC CORRELATIONS

COMPONENT	CORRELATION	REFERENCE AREA (IN^2)	REFERENCE HYDRAULIC DIAMETER (IN)	REFERENCES
Inlet Nozzle	$K=2.504\ Re^{-0.0529}$	1.767	1.500	29
Inlet Region	$K=C\ Re^{-0.05}$	1.767	1.500	29,30
Shield	$K=2.0$	2.405	1.750	33
Rod Bundle:				
-- Inlet	$K=0.427$	3.956	0.1338	33
-- Rod Friction	$f=110/Re$ for $Re \leq 400$	3.956	0.1338	31
	$f=(110/Re)\sqrt{1-\psi} + (0.55/Re^{0.25})\sqrt{\psi}$ for $400 < Re < 5000$ where $\psi = (Re-400)/4600$			
	$f=0.55/Re^{0.25}$ for $Re \geq 5000$			
-- Outlet	$K=0.290$	3.956	0.1338	33
Outlet Nozzle	$K=1.005\ Re^{-0.0490}$	3.976	2.250	29

TABLE XXXV

DETAILED PRESSURE DROP BREAKDOWN FOR PLANT THDV CONDITIONS (41.446 x 10^6 lb/hr) AND MAXIMUM UNCERTAINTIES

Orificing Zone	1	2	3	4	5	6 F/A	6 IB/A	7	8	9	10C	10P	11	12
Average Zone Flow	187131	174126	164395	151088	147235	177270	69072	87447	76853	61360	47569	47569	34563	25356
Component ΔP (psi)														
Inlet Nozzle	8.7	7.6	6.8	5.8	5.5	7.9	1.3	2.0	1.6	4.9	3.0	3.0	1.6	0.9
Assembly Orifice	40.0	48.6	55.3	63.5	66.9	46.5	69.9	44.9	60.5	69.6	42.2	42.2	22.5	12.2
Shield	6.4	5.5	5.0	4.2	4.0	5.7	5.6	8.9	6.9	4.4	2.6	2.6	1.4	0.7
Rod Bundle Inlet	1.1	1.0	0.9	0.7	0.7	1.0	0.5	0.8	0.6	0.4	0.2	0.2	0.1	0.1
Rod Bundle	51.5	45.3	40.8	35.1	33.6	46.7	35.9	54.3	43.3	29.3	18.7	18.7	10.7	6.2
Rod Bundle Outlet	0.6	0.5	0.4	0.4	0.3	0.5	0.4	0.6	0.4	0.3	0.2	0.2	0.1	0.1
Outlet Nozzle	1.6	1.4	1.3	1.1	1.0	1.5	0.5	0.8	0.6	0.4	0.2	0.2	0.1	0.1
Total Assembly	109.9	109.9	110.5	110.8	112.0	109.8	114.1	112.3	113.9	109.3	67.1	67.1	36.5	20.3
LIM, Upper Portion and Orifice	2.9	2.5	2.3	1.9	1.8	2.6	0.4	0.6	0.5	5.7	47.3	48.8	79.6	95.5
LIM, Lower Portion	5.6	6.0	5.6	5.7	4.6	6.0	4.8	5.5	4.0	3.4	4.0	2.5	2.3	2.6
Inlet Plenum						5.8								
Outlet Plenum						2.2								
Vessel Nozzle-to-Nozzle						126.4								
Primary Loop						37.1								
Pump Head						163.5								

NOTES:

-- All flows for cycle 4, except zone 6 IB/A which is for cycle 2;

-- All flow resistance uncertainties at +3σ or maximum bounding value, whichever appropriate;

-- Minimum pump head curve;

-- Zone 1 through 8 and 10C are fed by central modules, zones 9, 10P, 11 and 12 by peripheral modules.

TABLE XXXVI

DETAILED PRESSURE DROP CORRELATIONS FOR UPDATED
PLANT EXPECTED OPERATING CONDITIONS (46.420×10^6 lb/hr)

Orificing Zone	1	2	3	4	5	6 F/A	6 IB/A	7	8	9	10C	10P	11	12
Average Zone Flow	210118	195515	184588	169646	165320	199045	77613	98189	86292	68897	53317	53715	39909	29518
Component ΔP (psi)														
Inlet Nozzle	10.4	9.1	8.1	6.9	6.5	9.4	1.5	2.4	1.8	5.9	3.6	3.6	2.0	1.1
Assembly Orifice	17.5	27.8	35.4	44.8	48.5	25.2	52.5	24.6	42.1	52.3	31.6	32.1	17.9	9.9
Shield	7.6	6.6	5.9	5.0	4.8	6.8	6.7	10.7	8.3	5.3	3.2	3.2	1.8	1.0
Rod Bundle Inlet	1.2	1.0	0.9	0.8	0.7	1.0	0.5	0.8	0.6	0.4	0.3	0.3	0.1	0.1
Rod Bundle	58.4	52.4	46.4	39.9	38.1	53.1	40.0	60.4	48.2	32.6	20.8	21.1	12.5	7.4
Rod Bundle Outlet	0.6	0.5	0.5	0.4	0.4	0.5	0.4	0.6	0.5	0.3	0.2	0.2	0.1	0.1
Outlet Nozzle	1.8	1.6	1.4	1.2	1.1	1.6	0.6	0.9	0.7	0.4	0.3	0.3	0.1	0.1
Total Assembly	97.5	98.0	98.6	99.0	100.1	97.6	102.2	100.4	102.2	97.2	60.0	60.8	34.5	19.7
LIM, Upper Portion and Orifice	3.1	2.7	2.4	2.0	1.9	2.8	0.4	0.7	0.5	6.0	43.0	43.6	69.9	84.4
LIM, Lower Portion	6.3	6.2	5.9	5.9	4.9	6.5	5.0	5.8	4.2	3.7	3.9	2.5	2.5	2.8
Inlet Plenum						6.0								
Outlet Plenum						2.4								
Vessel Nozzle-to-Nozzle						115.3								
Primary Loop						41.8								
Pump Head						157.1								

NOTES:

-- All flows for cycle 4, except zone 6 IB/A which is for cycle 2;
-- All flow resistances are nominal;
-- Nominal pump head curve;
-- Zone 1 through 8 and 10C are fed by central modules, zones 9, 10P, 11 and 12 by peripheral modules.

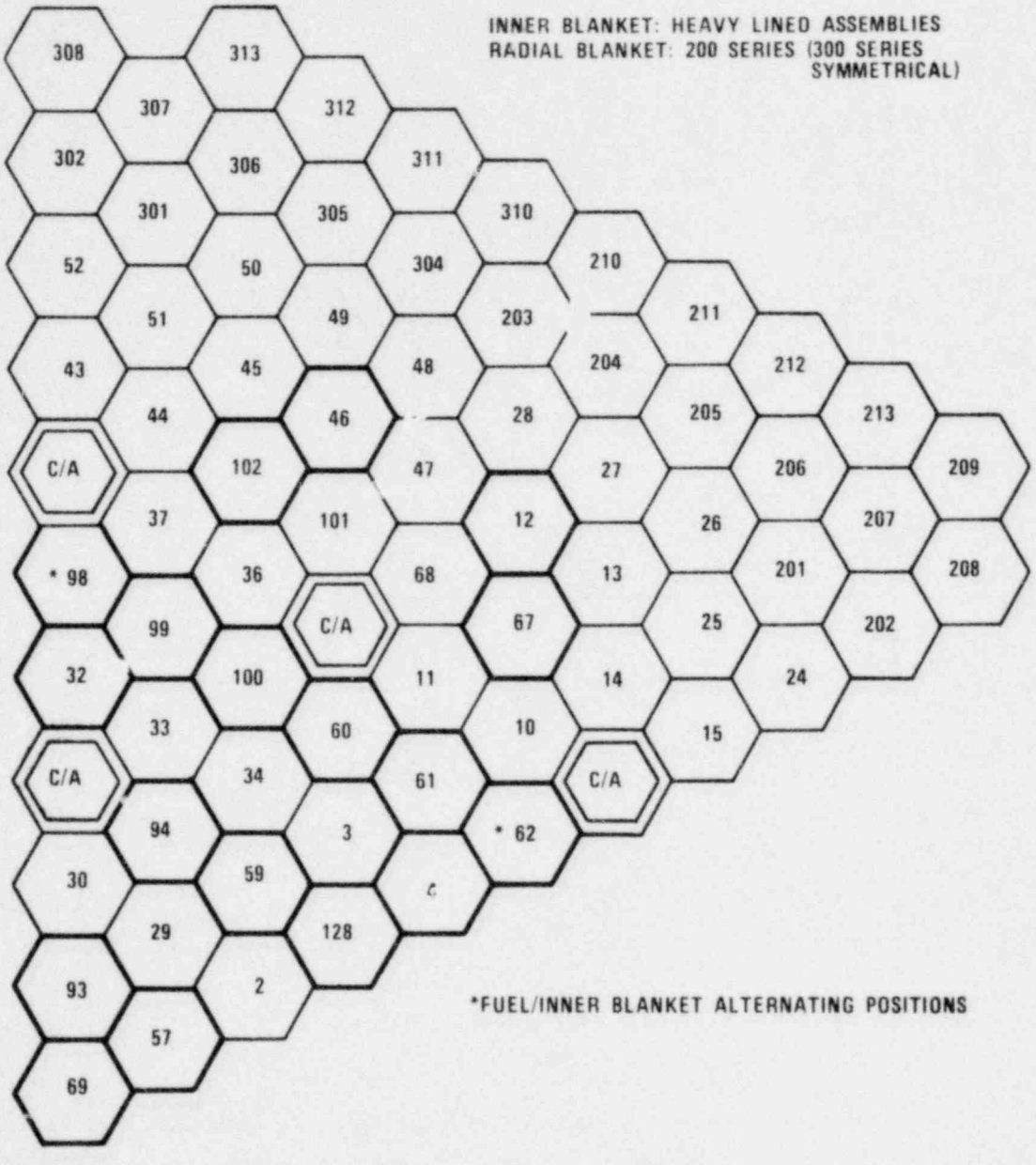

Figure 1 CRBRP Heterogeneous Core (Rev. 4) - 60° Symmetry Sector and Assemblies Numbering Scheme

1668-68

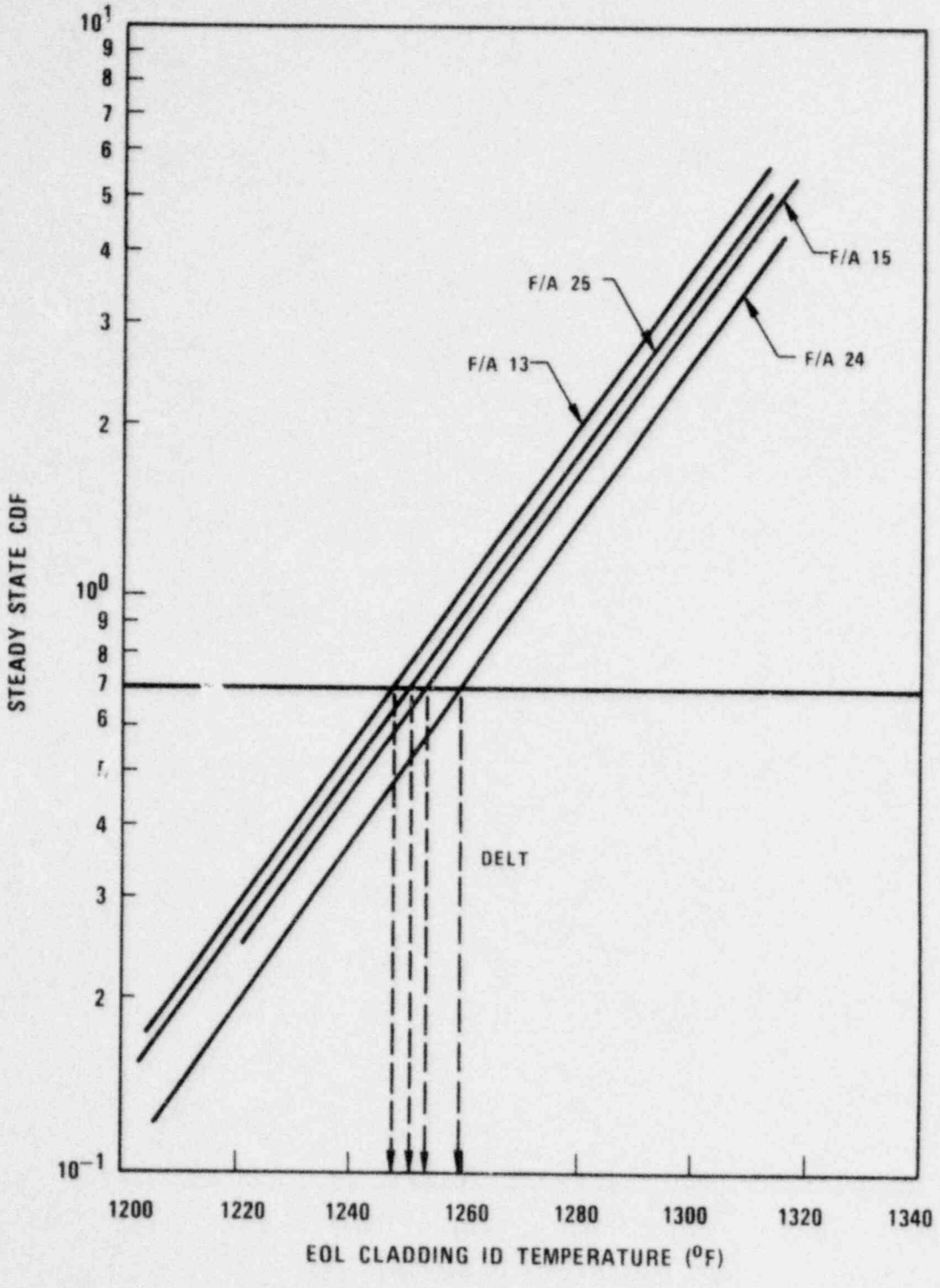

Figure 2 Typical DELT Determination for First Core Fuel Assemblies

1668-67

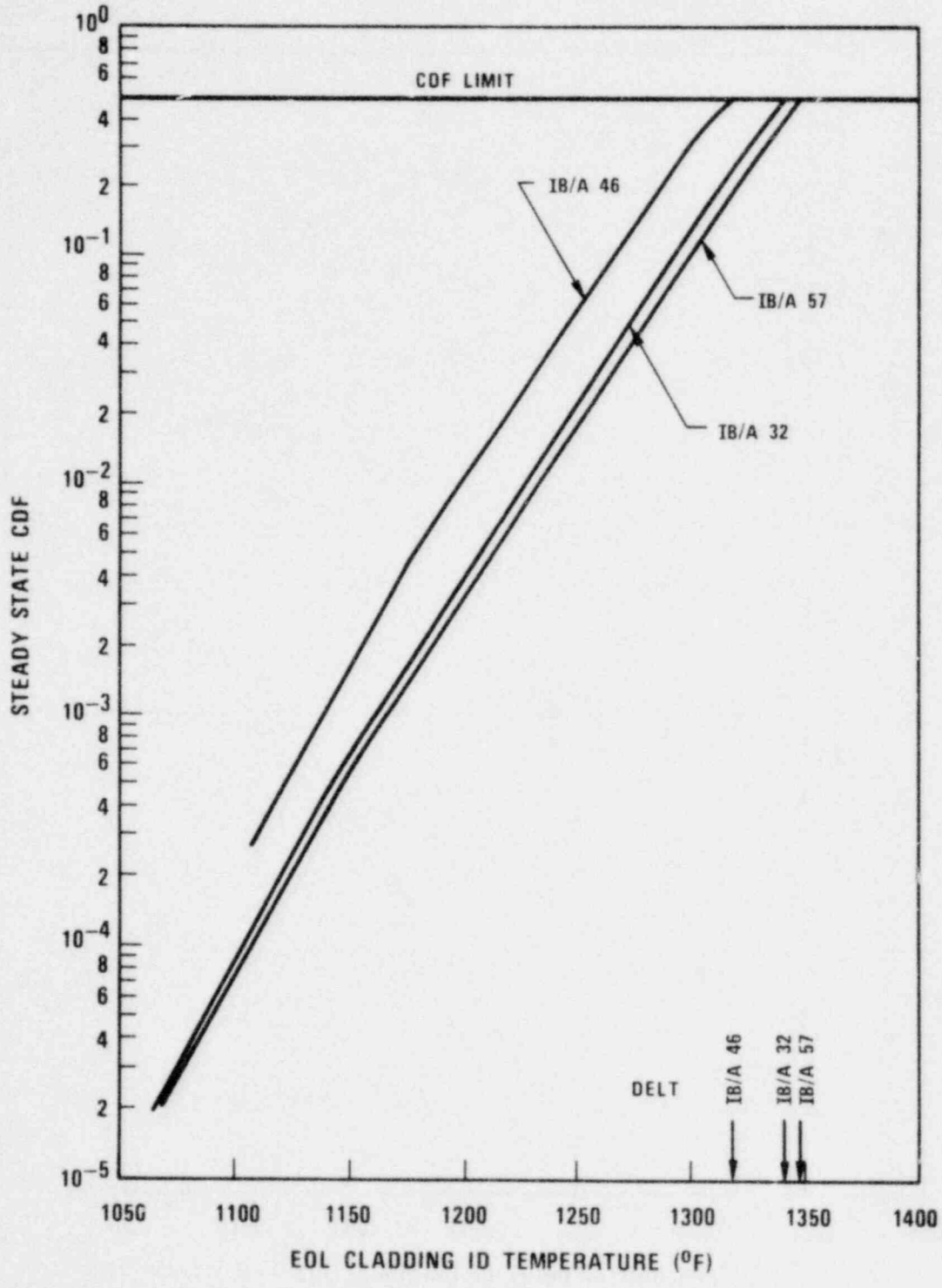

Figure 3 Typical DELT Determination for First Core Inner Blanket Assemblies

1668-66

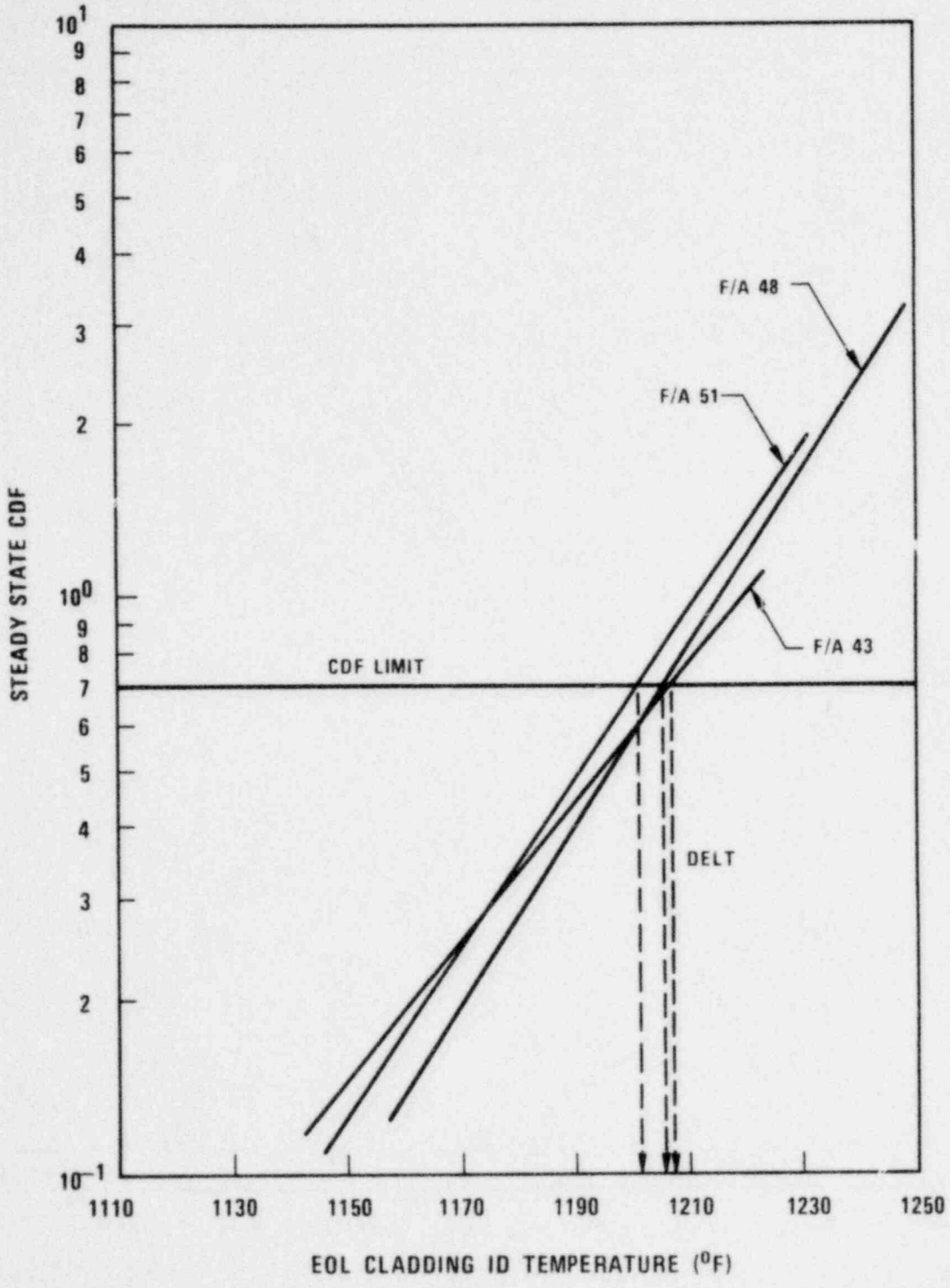

Figure 4 Typical DELT Determination for Second Core Fuel Assemblies

1668-65

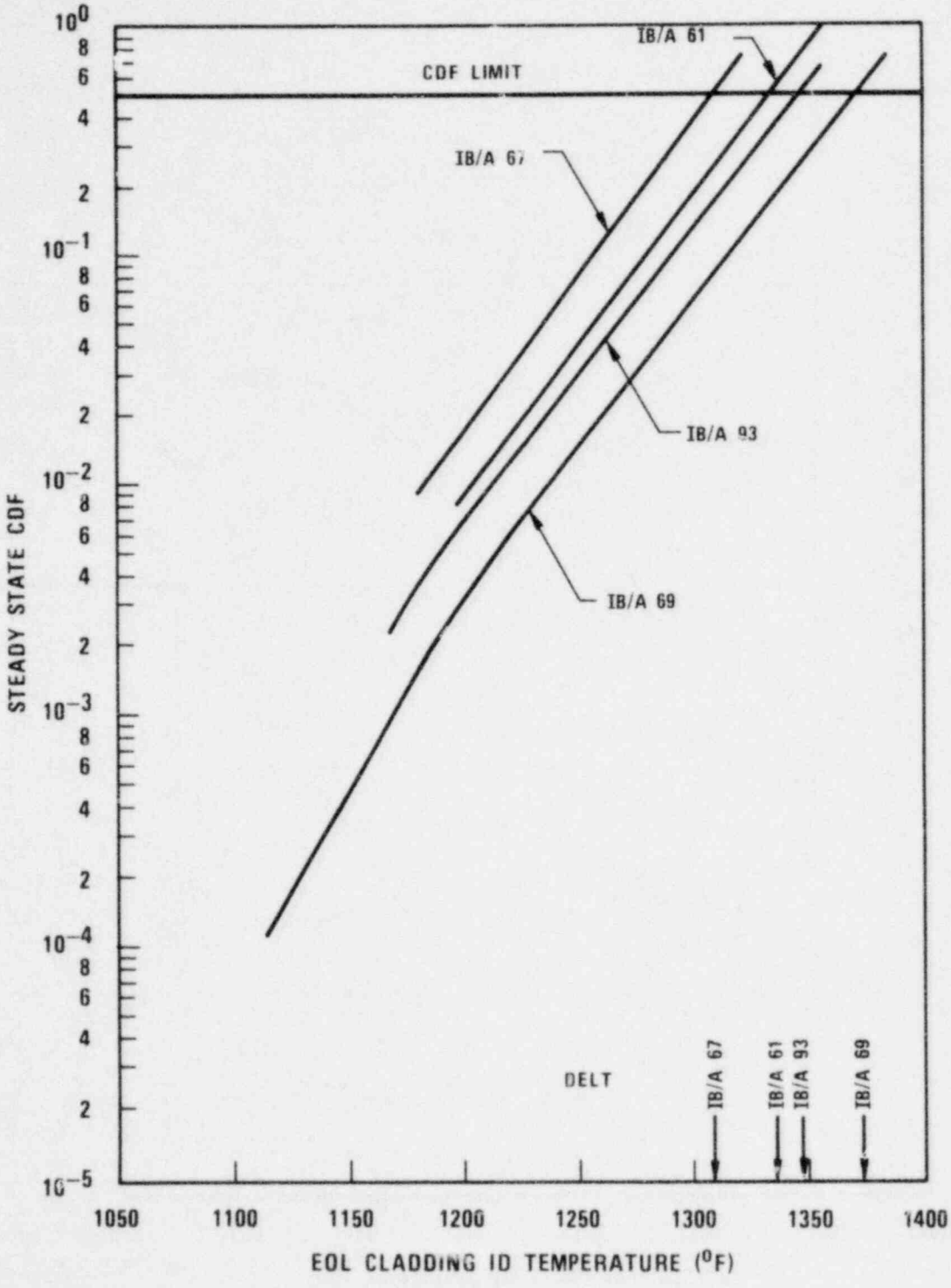

Figure 5 Typical DELT Determination for Second Core Inner Blanket Assemblies

1668-64

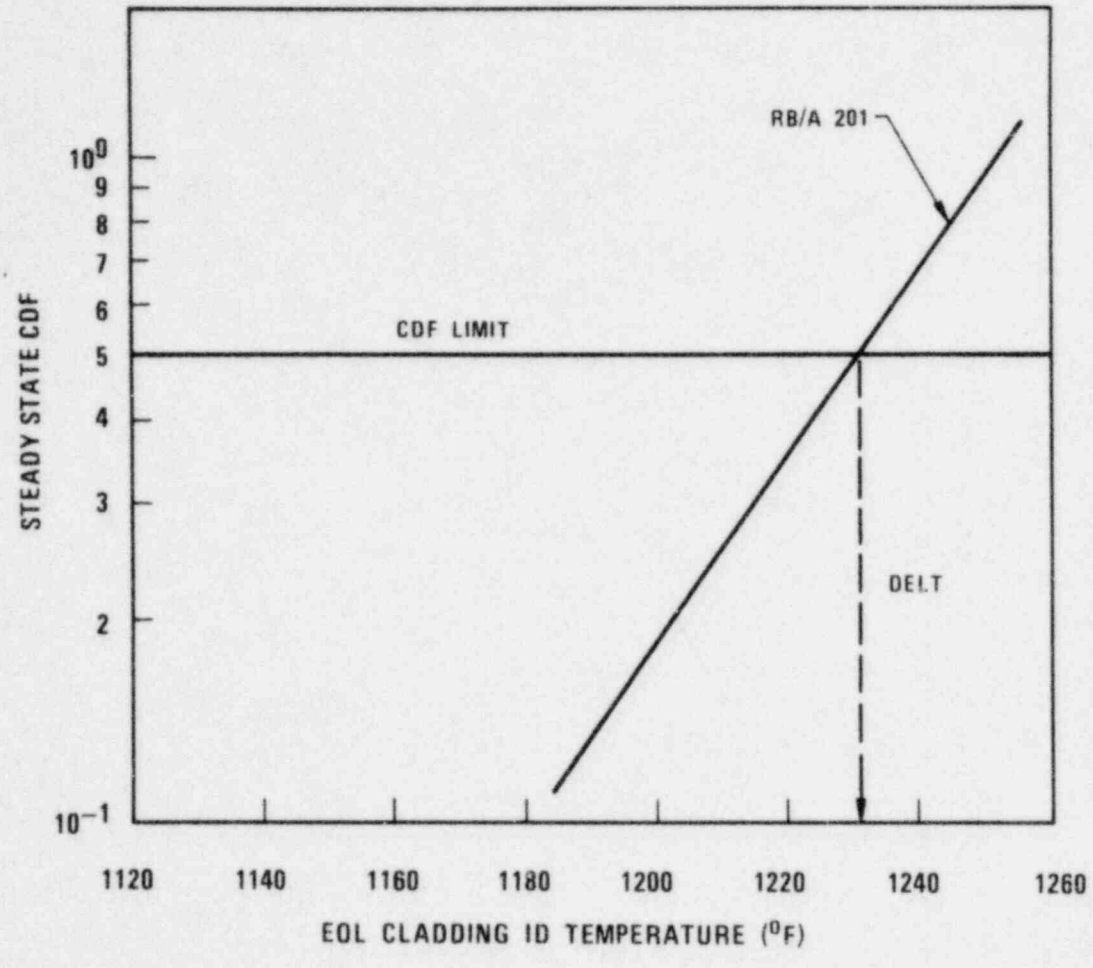

Figure 6 Typical DELT Determination for Radial Blanket Assemblies

1668-63

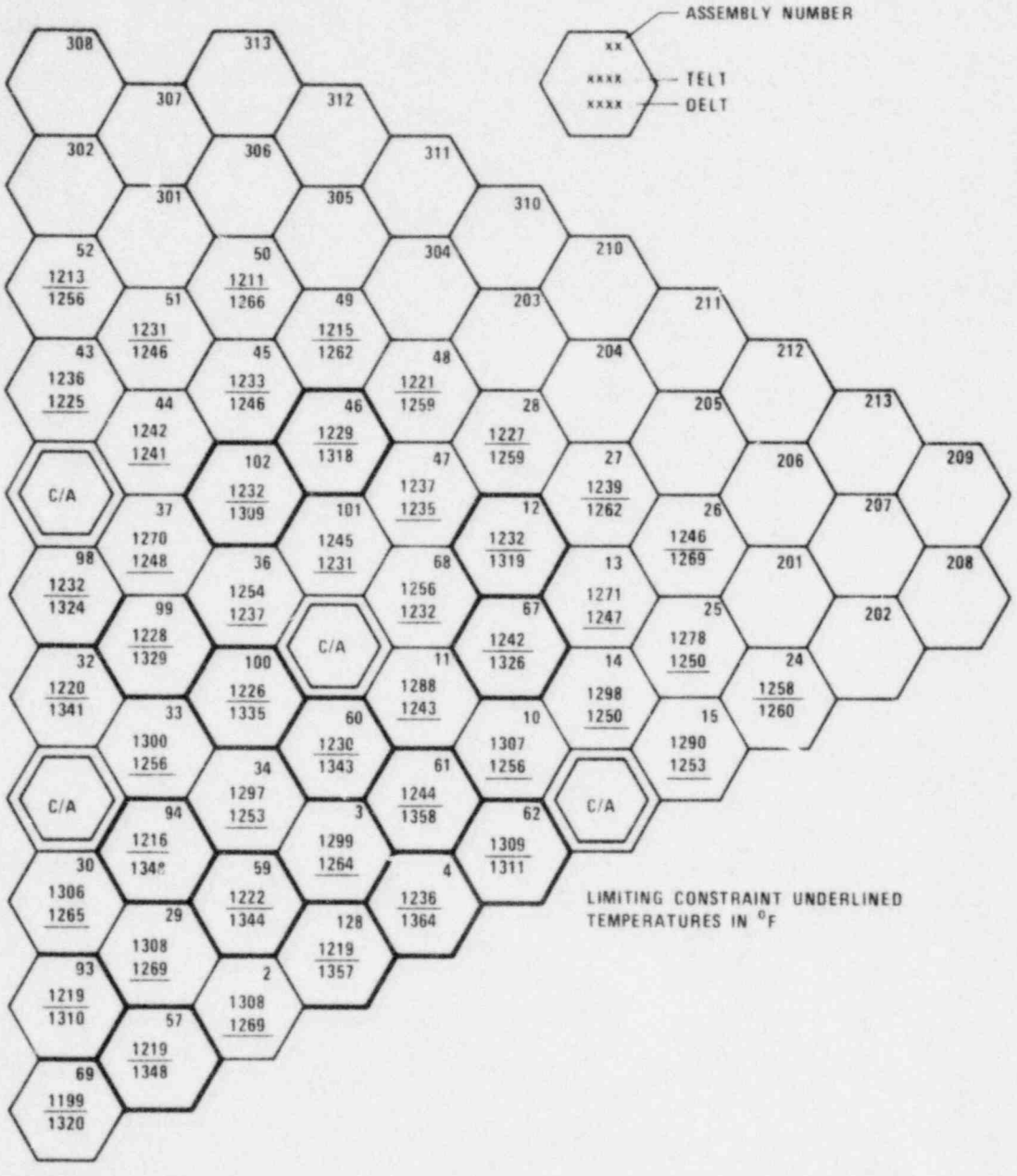

Figure 7 Individual Assemblies Limiting Temperatures at First Core

1668-62

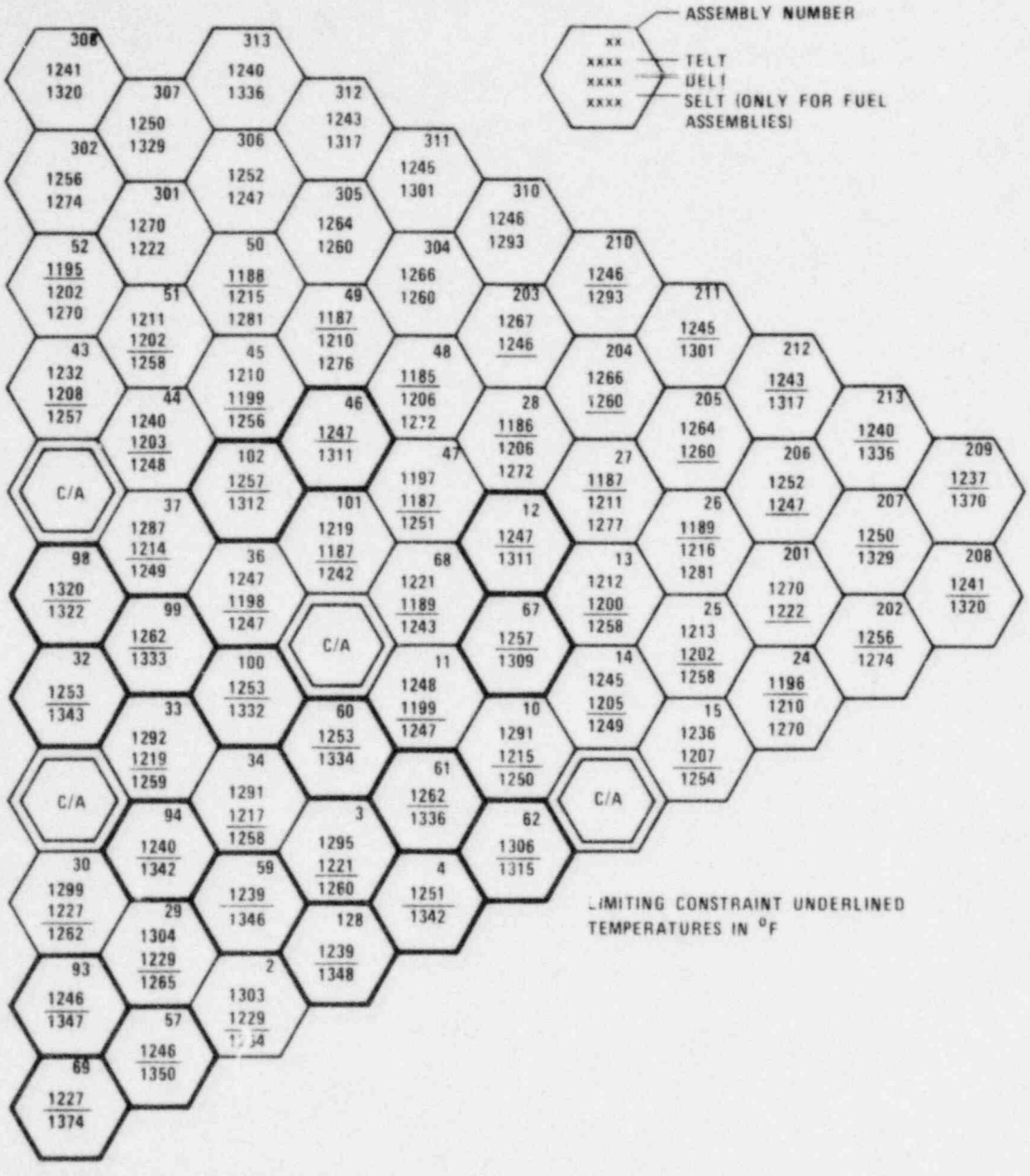

Figure 8 Individual Assemblies Limiting Temperatures at Second Core

1668-59

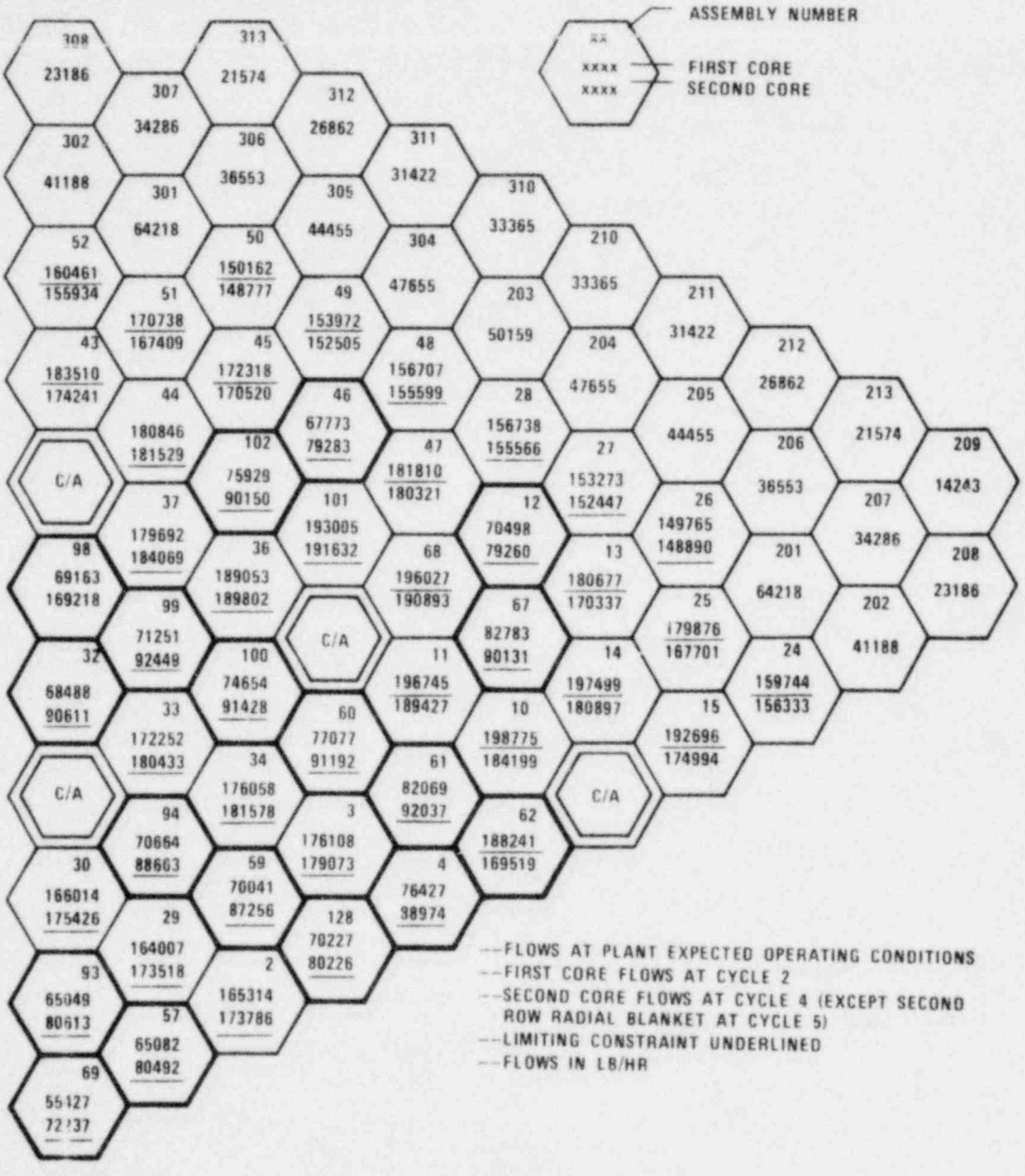

Figure 9 Individual Assemblies Minimum Flow Rates at First and Second Core Necessary to Satisfy the Constraints

1668-60

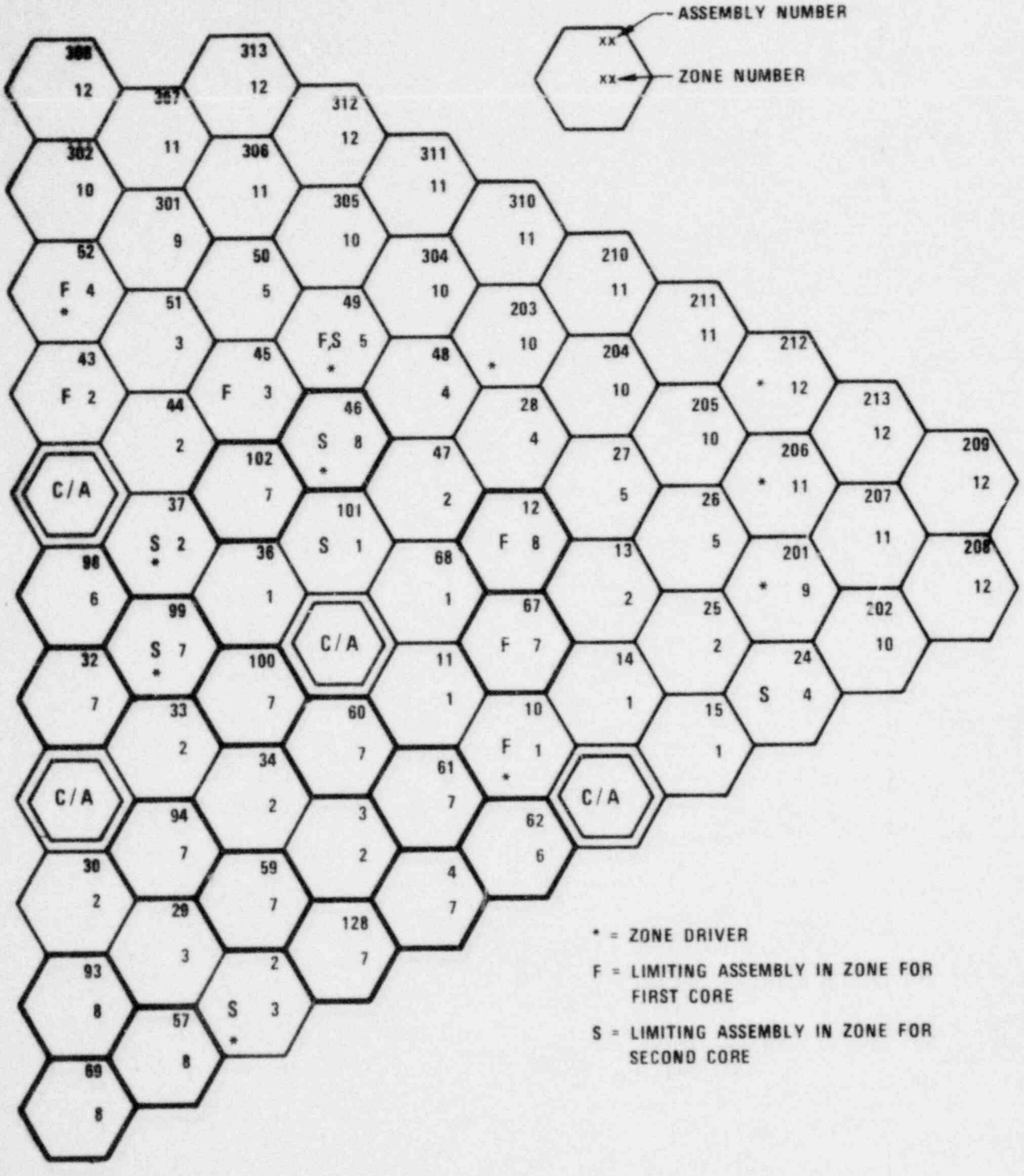

Figure 10 Core Orificing Scheme

1668-61

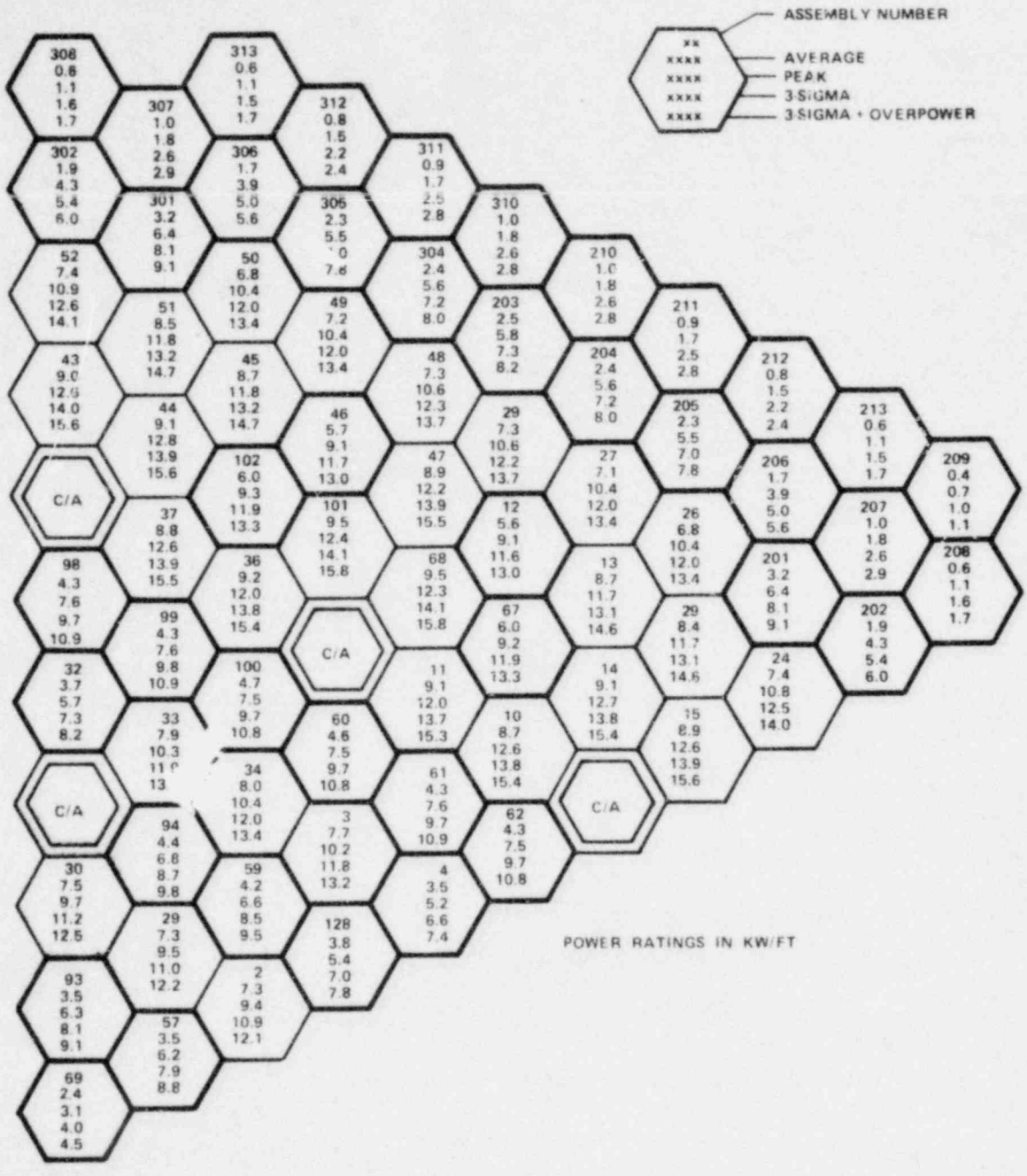

Figure 11 Core Assemblies Linear Power Ratings at BOC1

1668-52

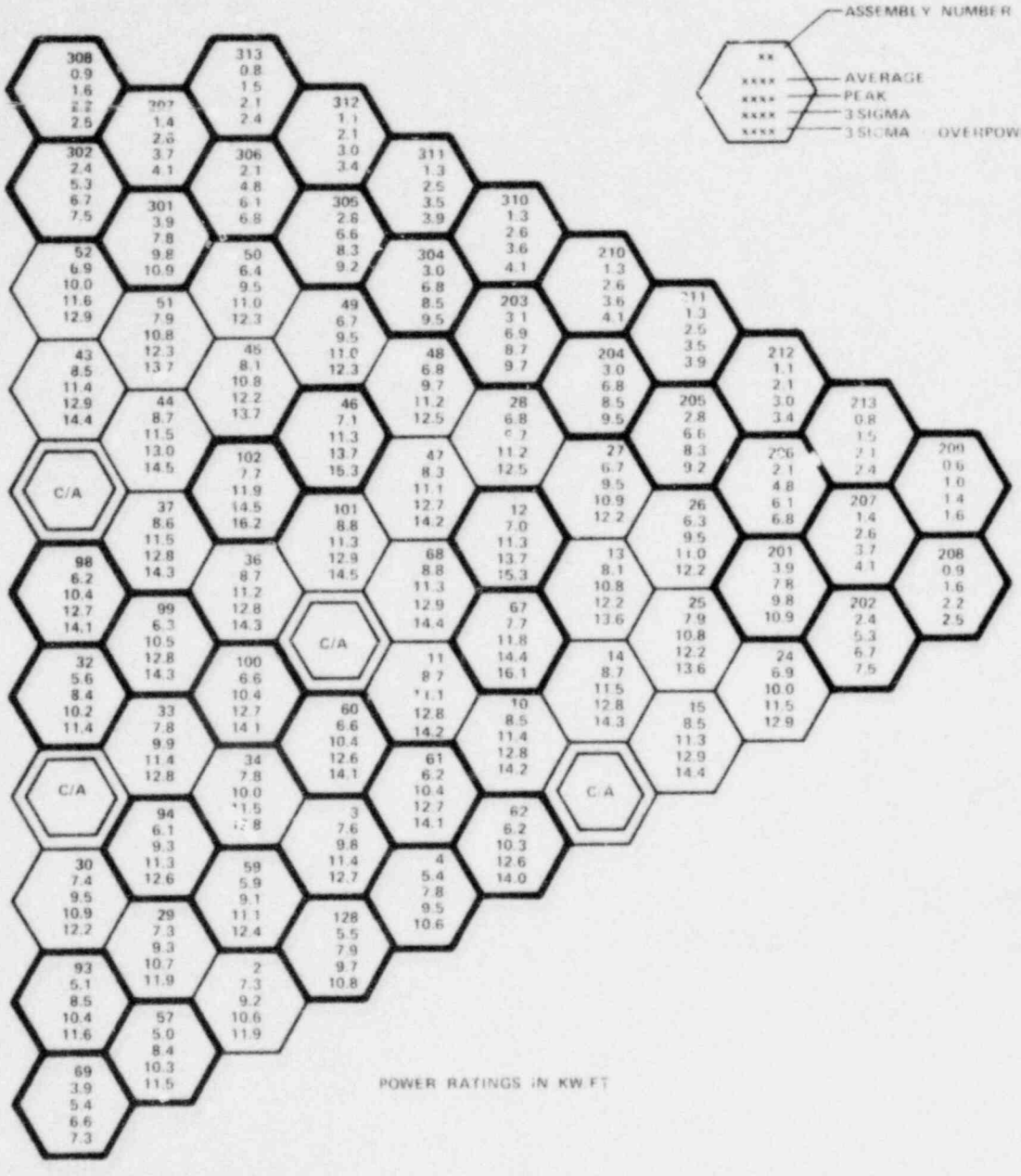

Figure 12 Core Assemblies Linear Power Ratings at EOC1

1681-35

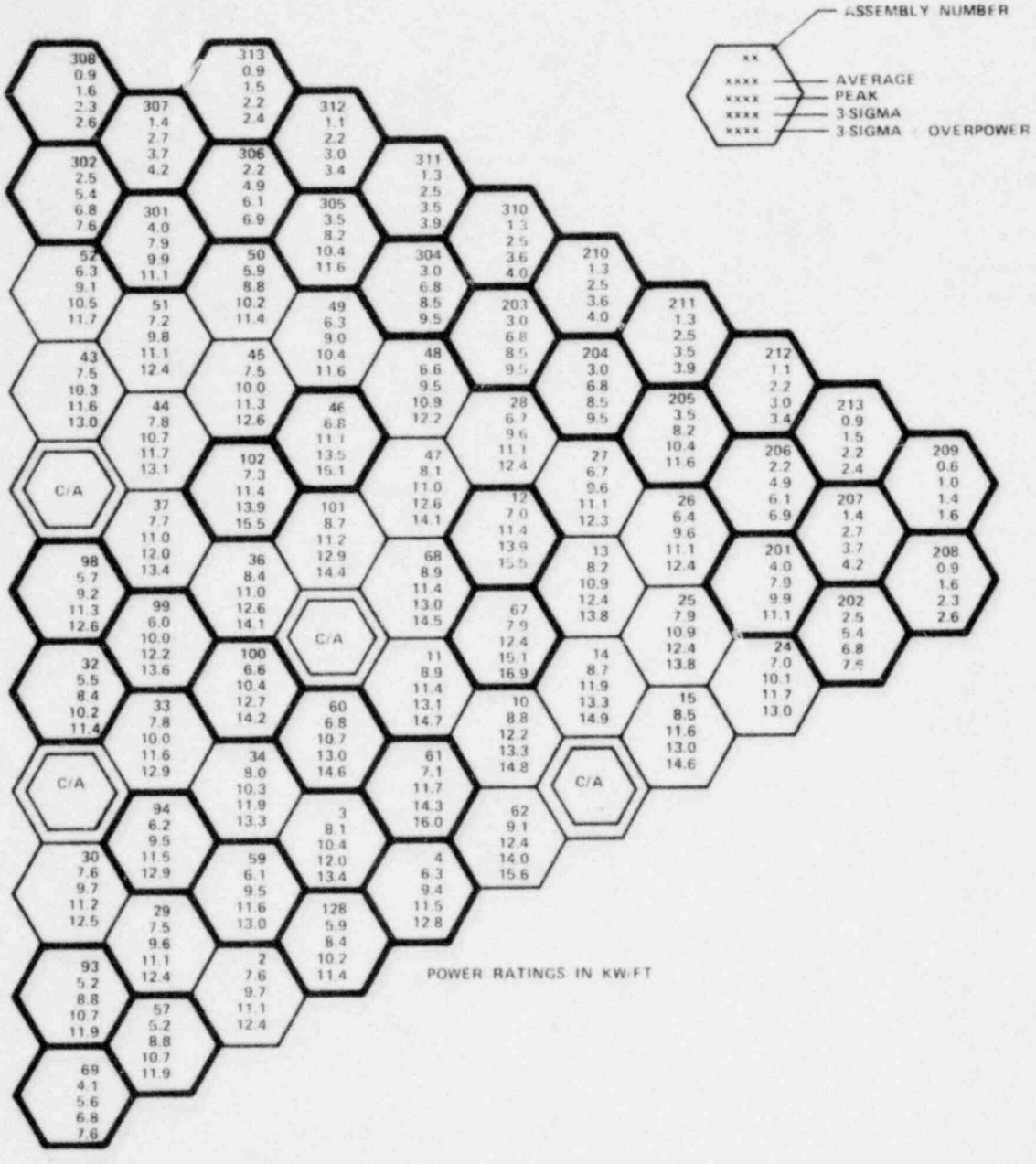

Figure 13 Core Assemblies Linear Power Ratings at BOC2

1681-36

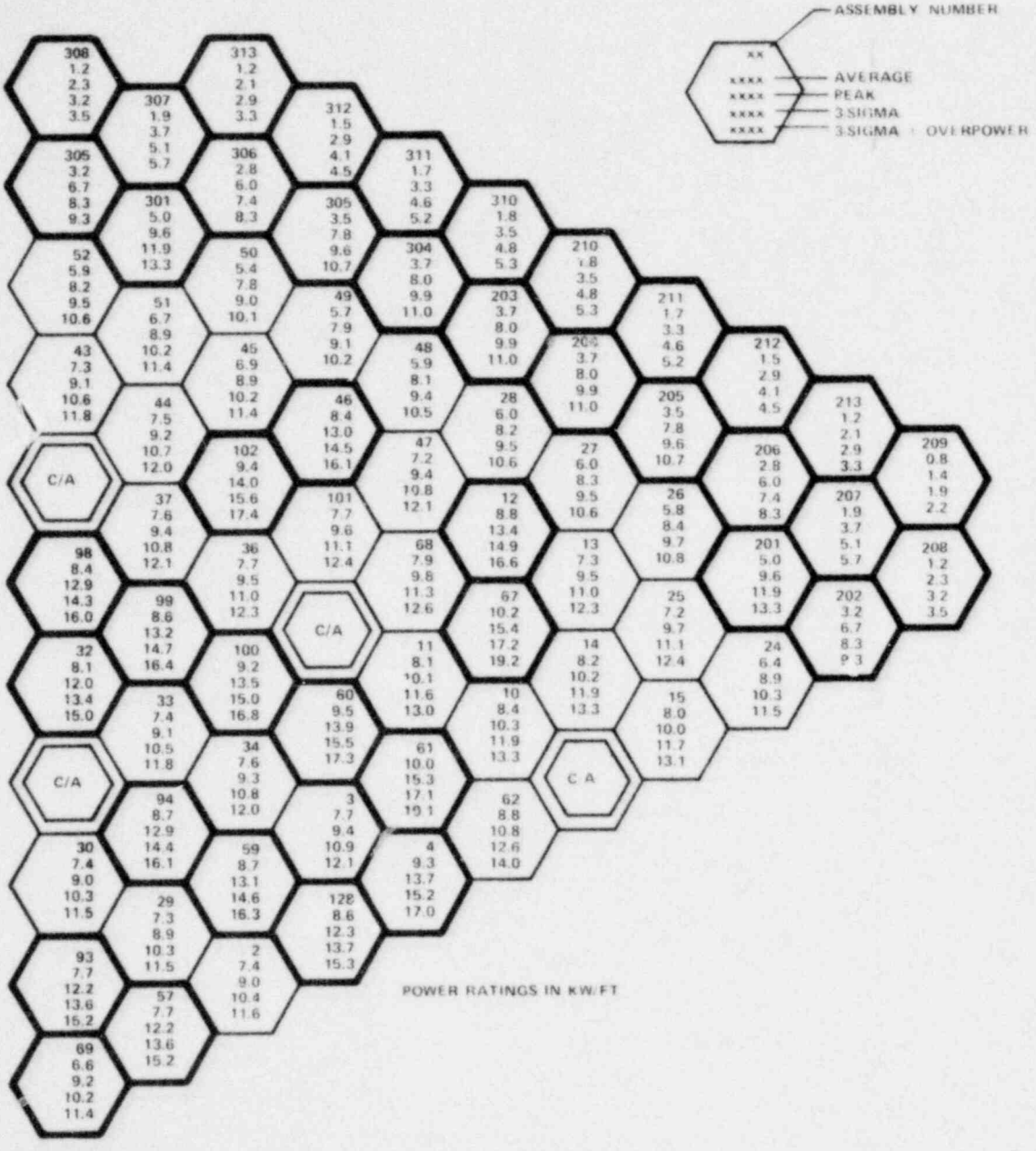

Figure 14 Core Assemblies Linear Power Ratings at EOC2

1681-37

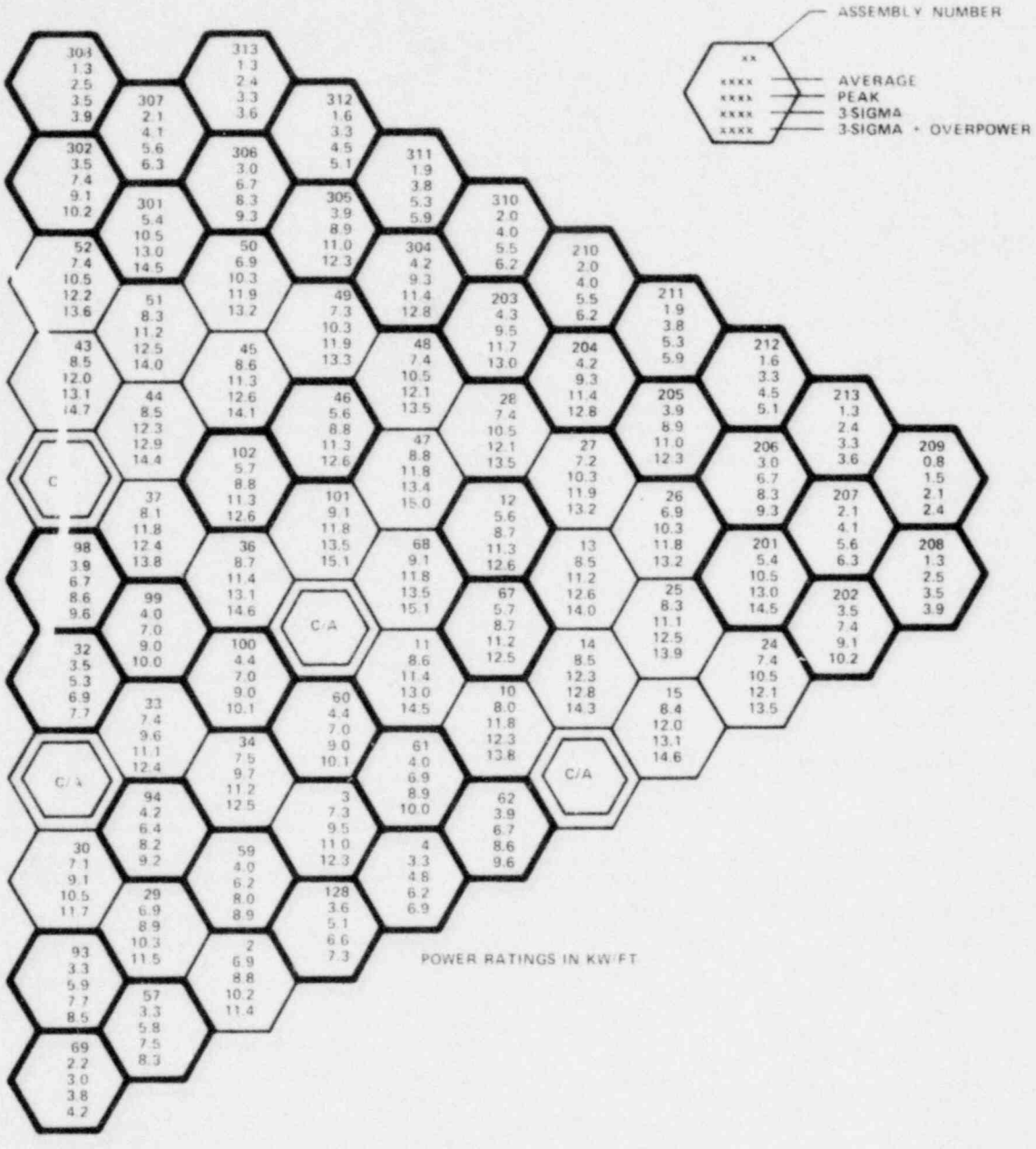

Figure 15. Core Assemblies Linear Power Ratings at BOC3

1681-38

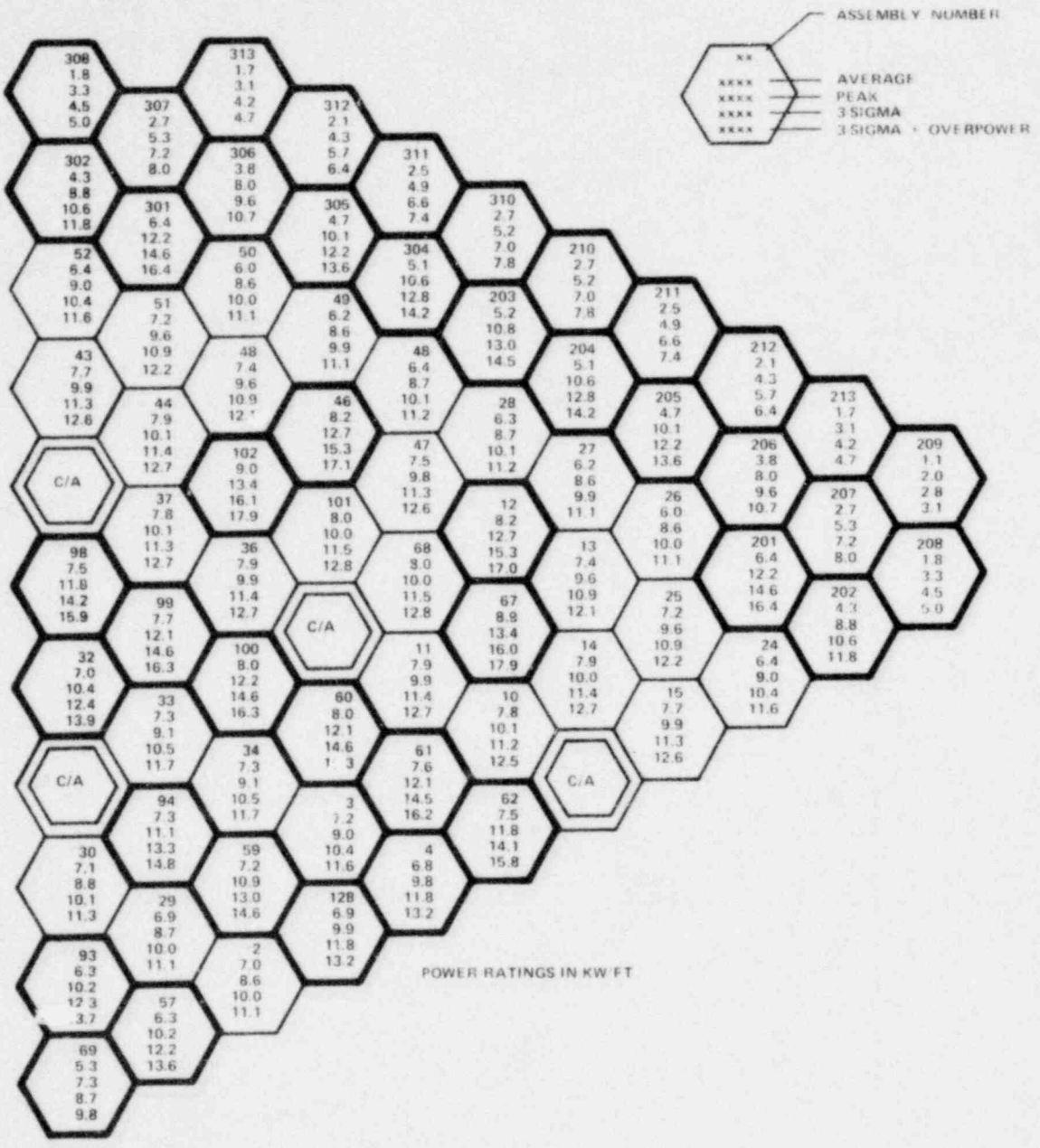

Figure 16 Core Assemblies Linear Power Ratings at EOC3

1681-39

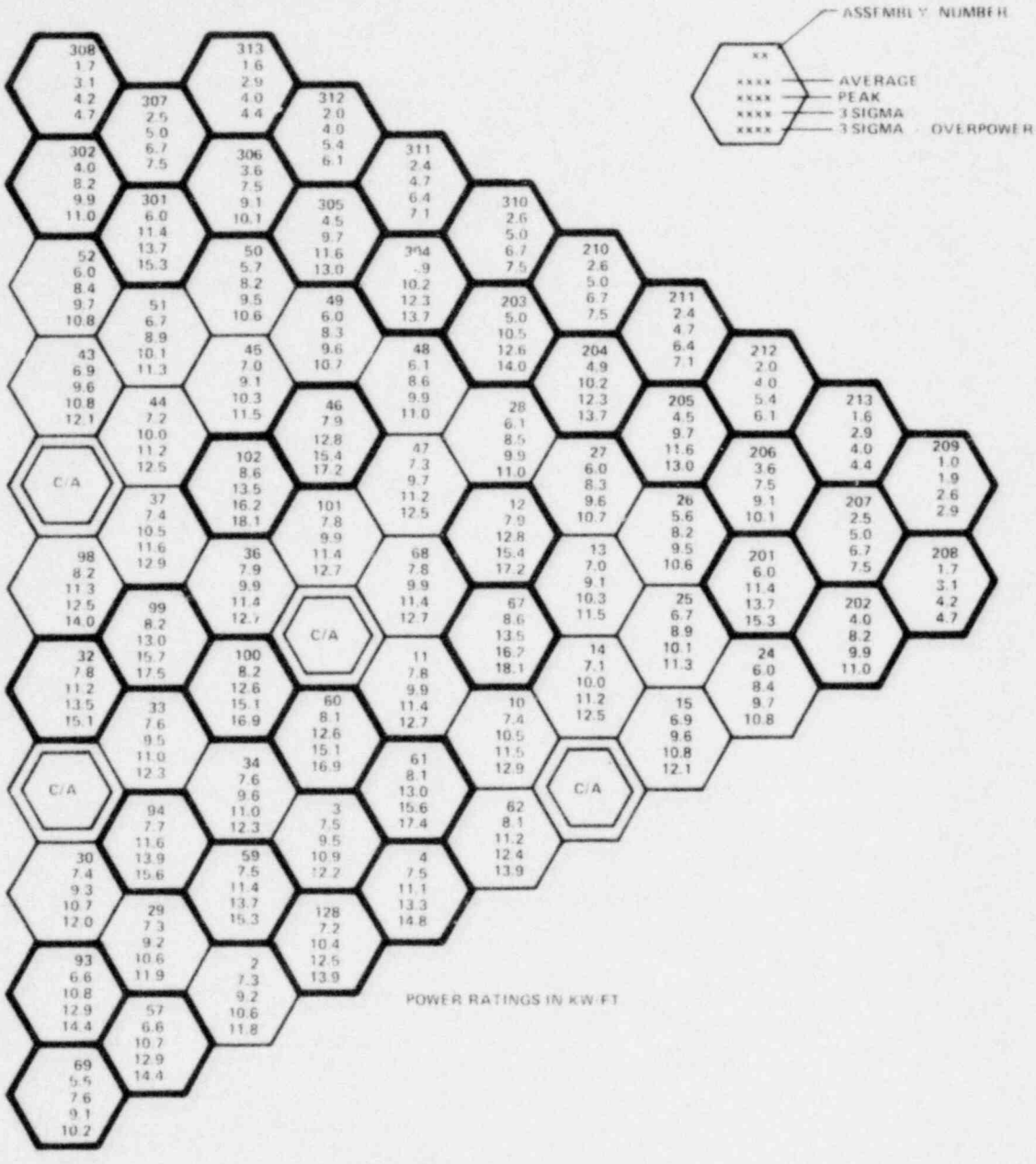

Figure 17 Core Assemblies Linear Power Ratings at BOC4

1681-40

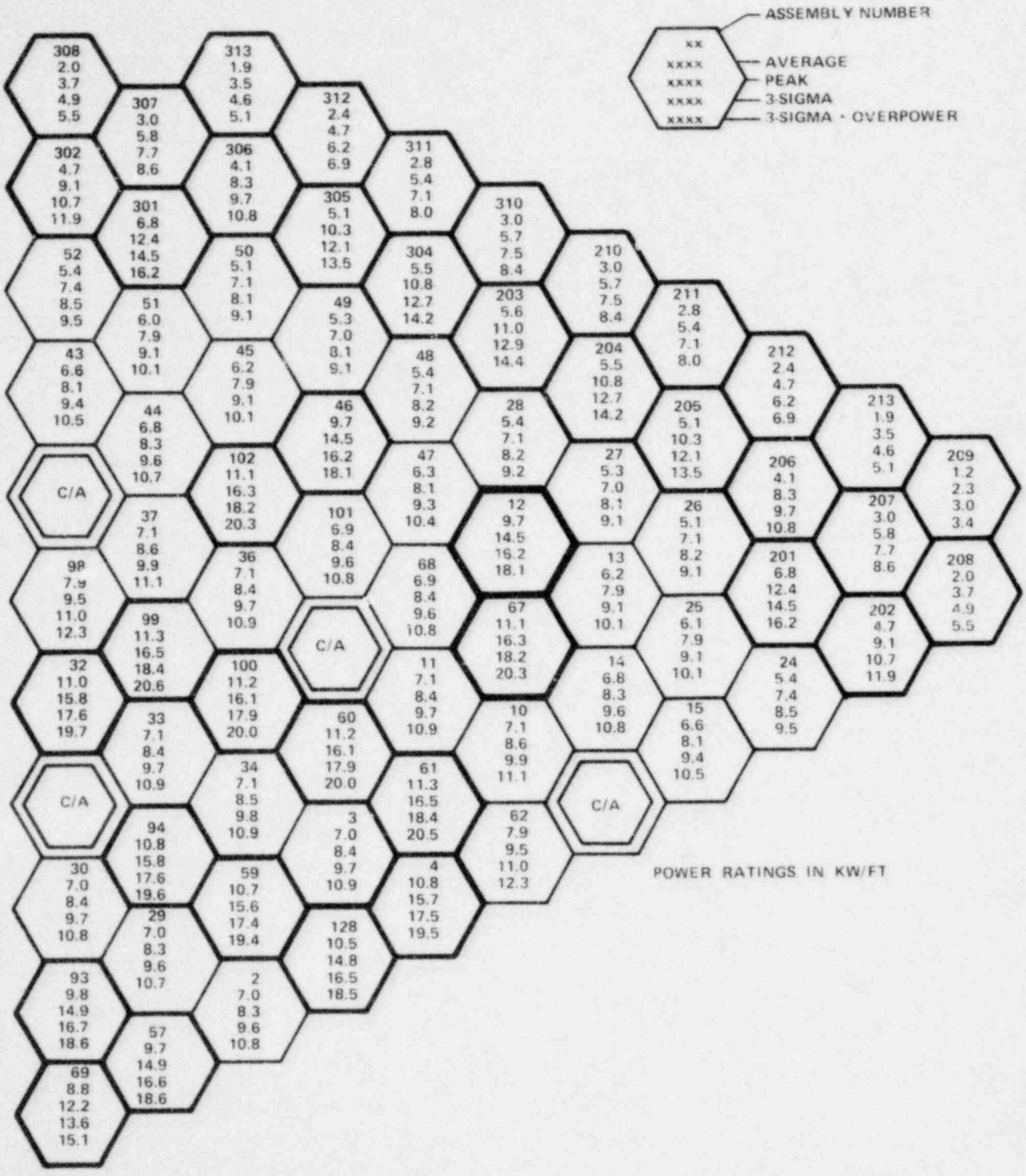

Figure 18 Core Assemblies Linear Power Ratings at EOC4

1668-51

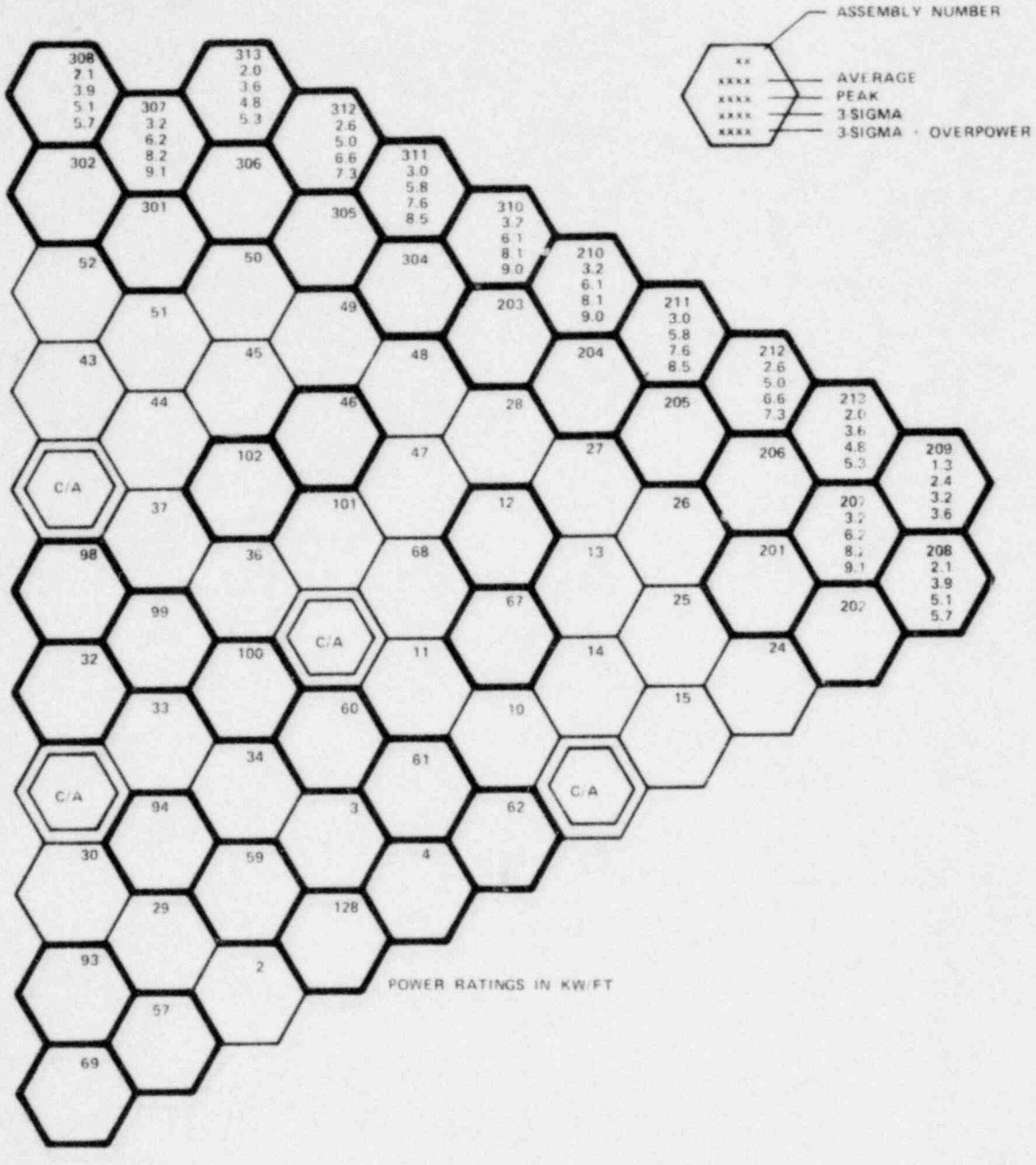

Figure 19 Core Assemblies Linear Power Ratings at BOC5

1681-42

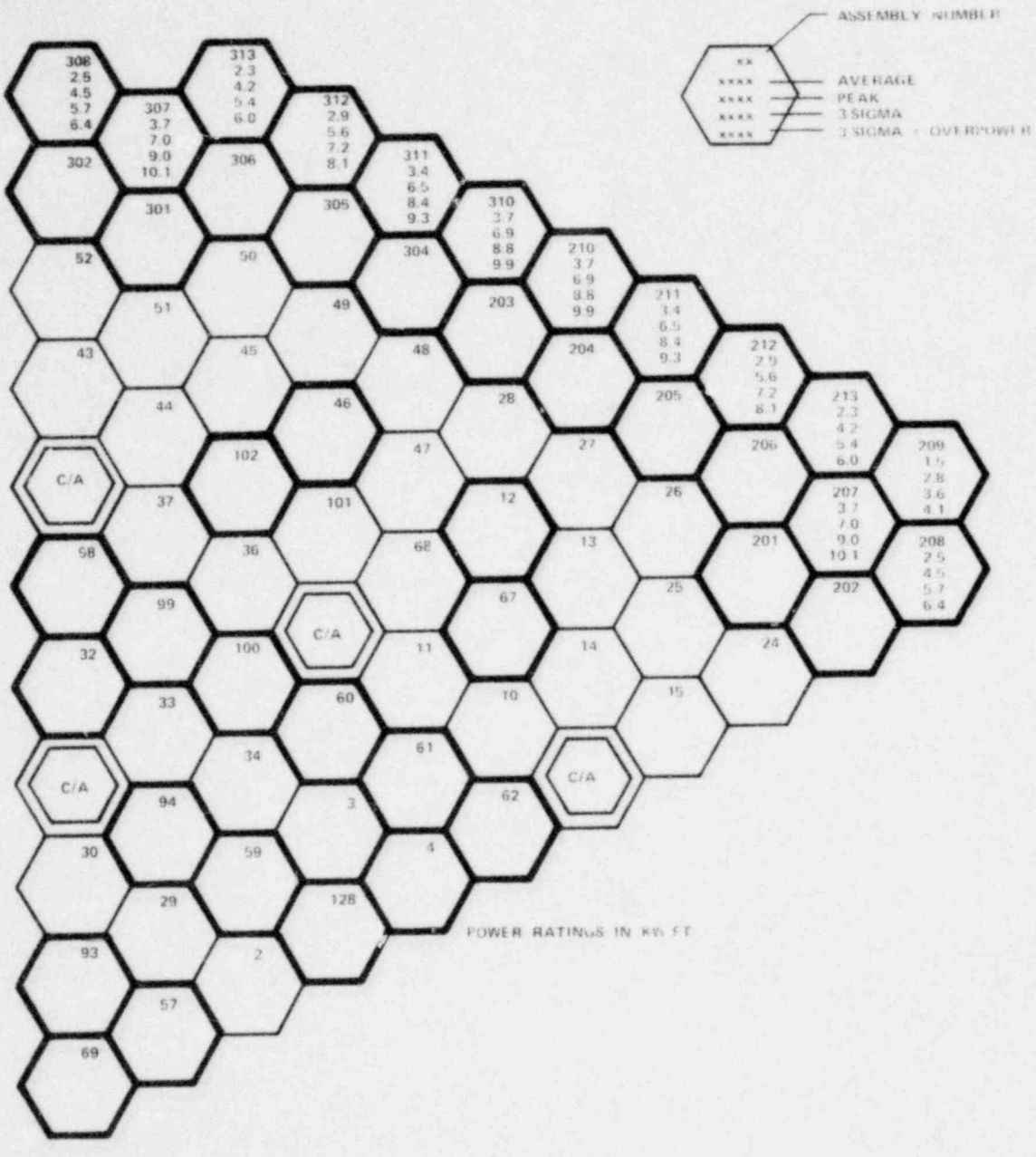

Figure 20 Core Assemblies Linear Power Ratings at EOC5

1681-43

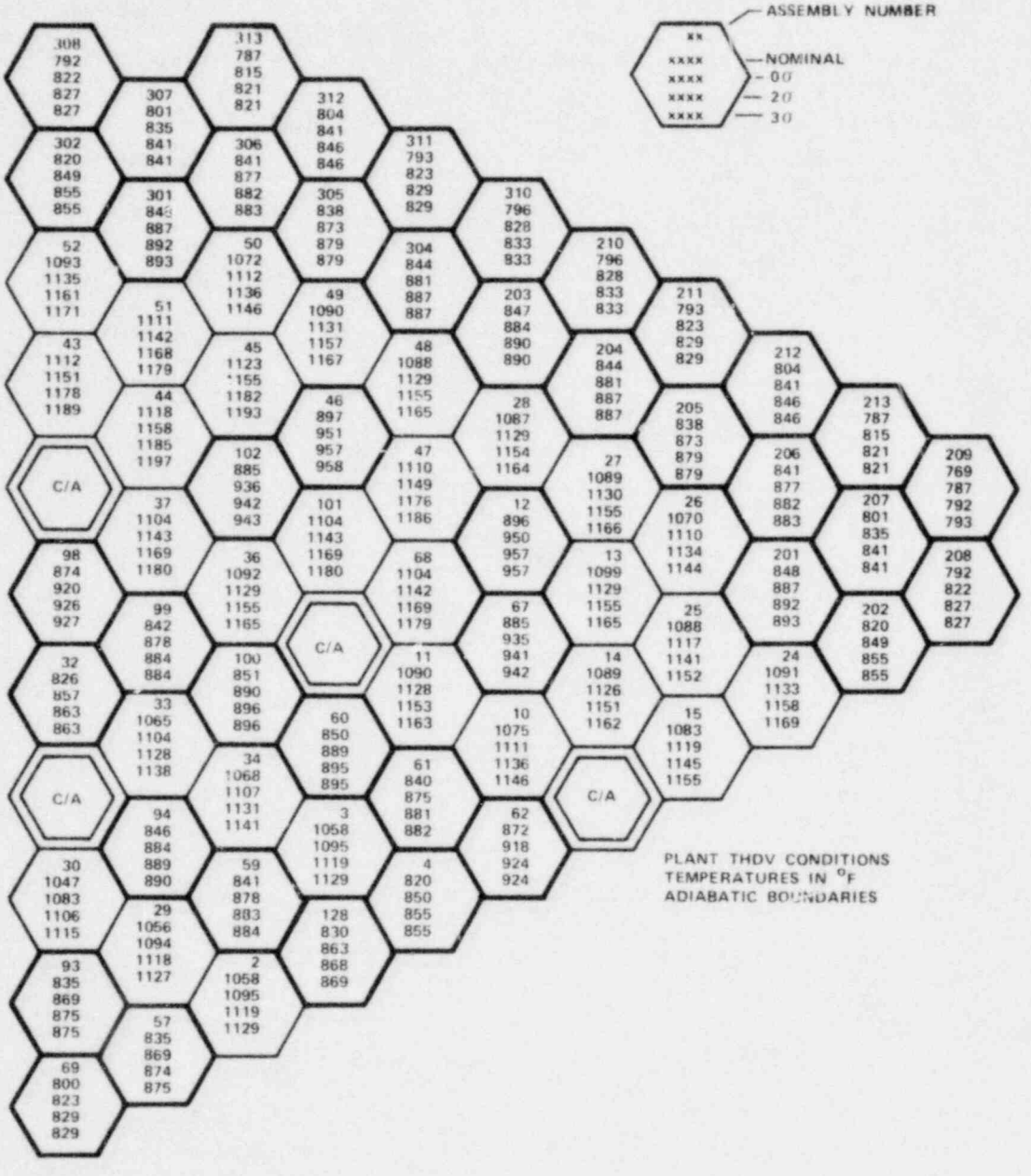

Figure 21 Core Assemblies Mixed Mean Outlet Temperatures at BOC1

1668-50

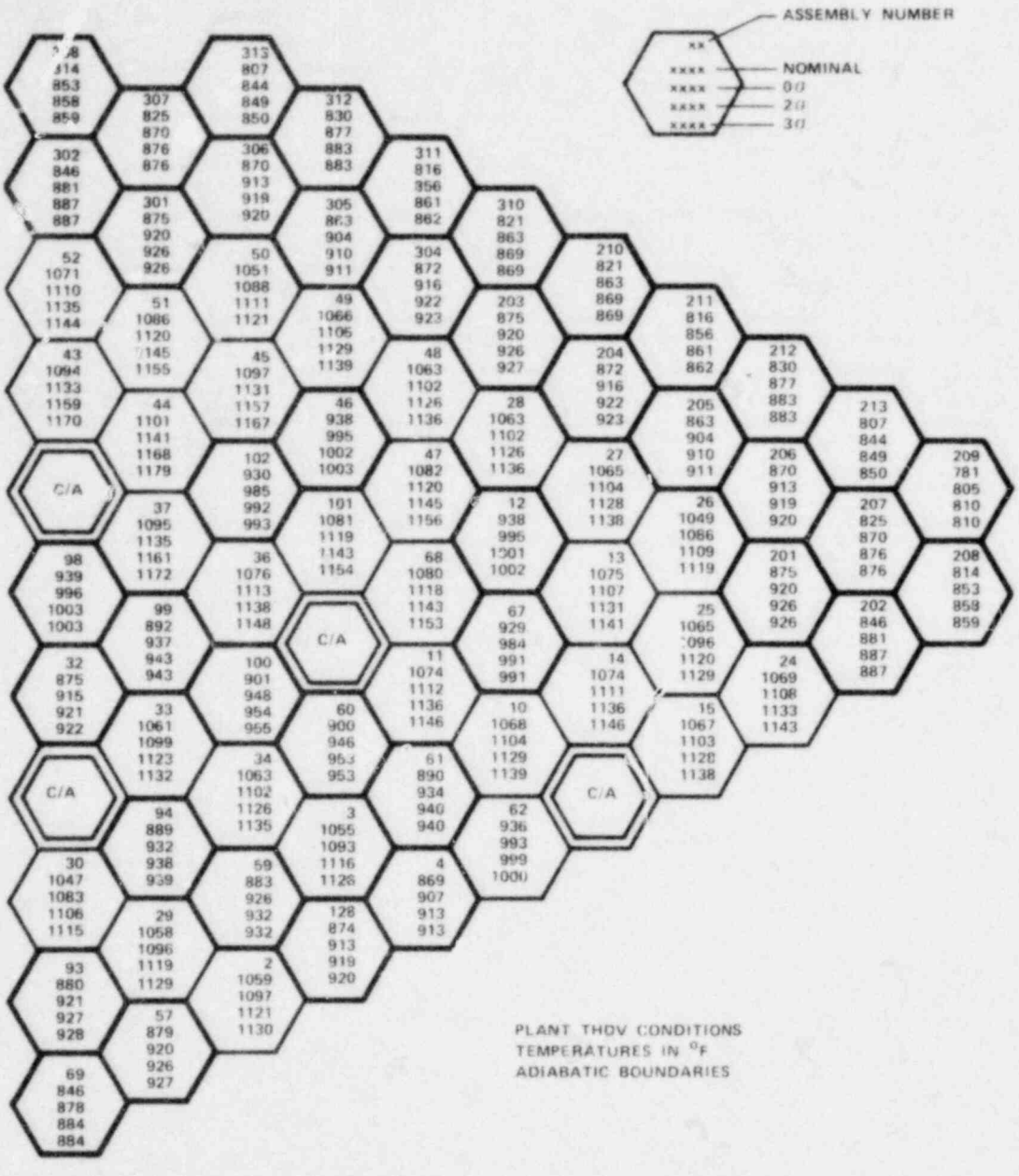

Figure 22 Core Assemblies Mixed Mean Outlet Temperatures at EOC 1

1668-120

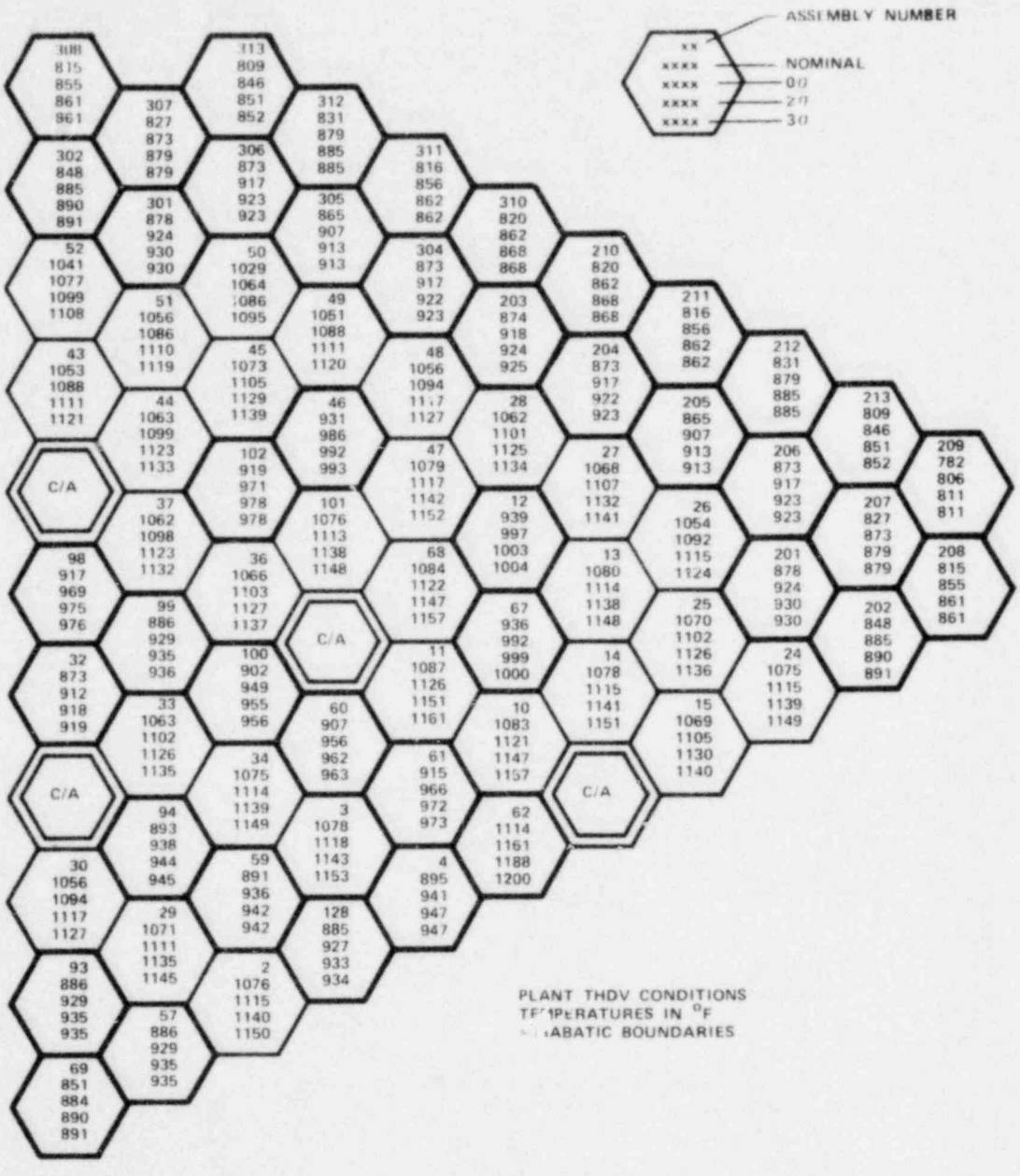

Figure 23 Core Assemblies Mixed Mean Outlet Temperatures at BOC2

1668-121

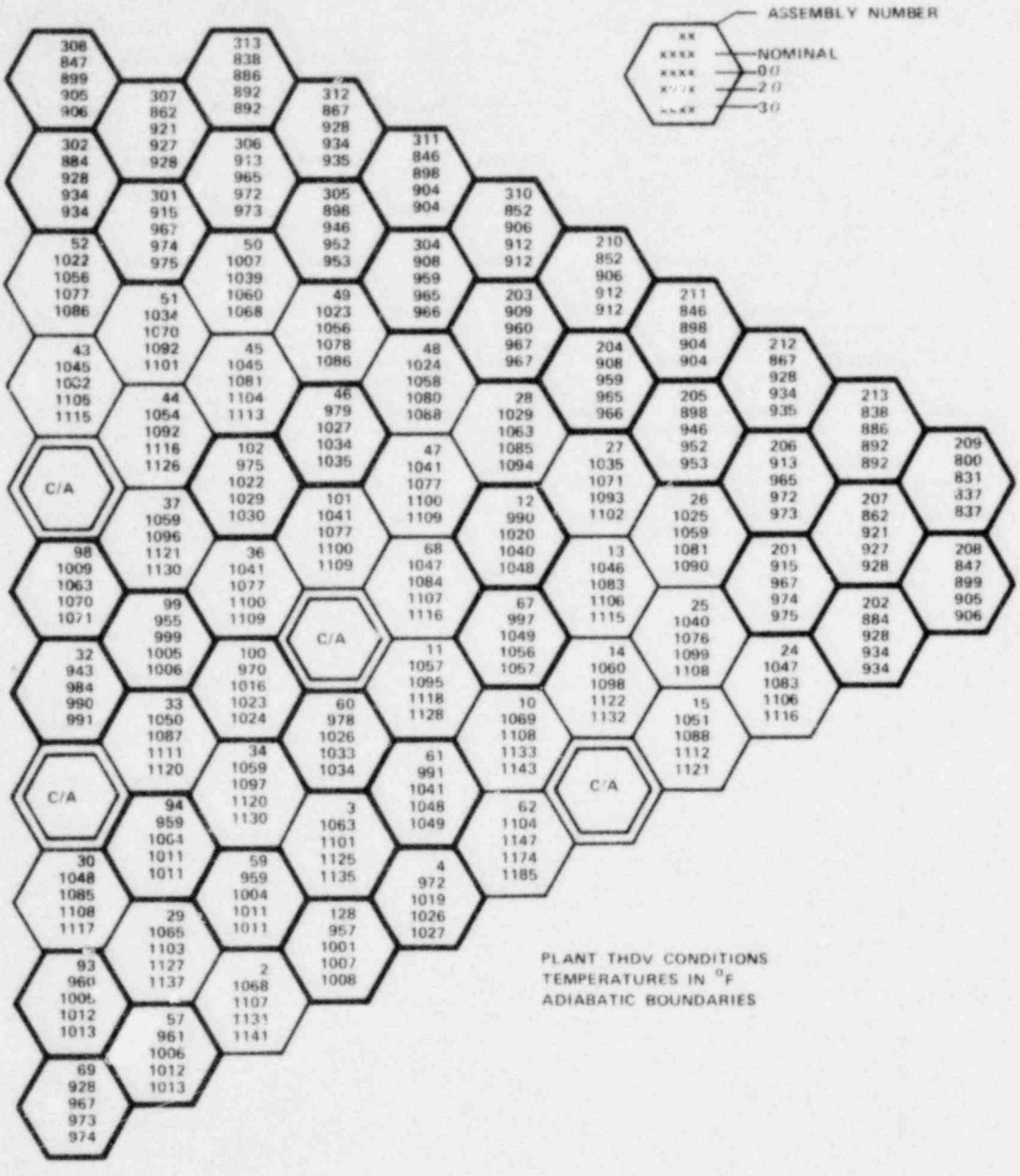

Figure 24 Core Assemblies Mixed Mean Outlet Temperatures at EOC2

1668-114

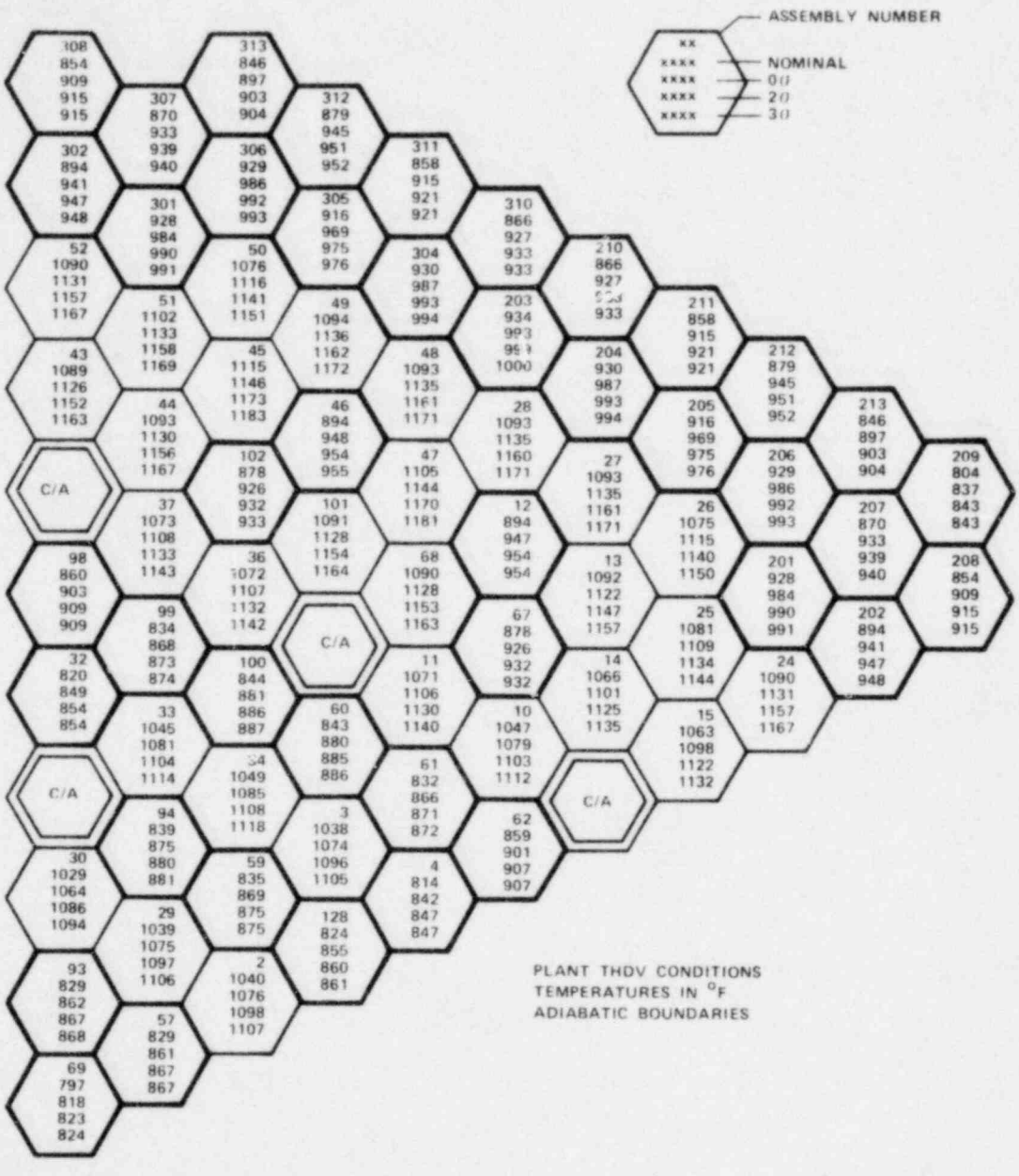

Figure 25 Core Assemblies Mixed Mean Outlet Temperatures at BOC3

1668-115

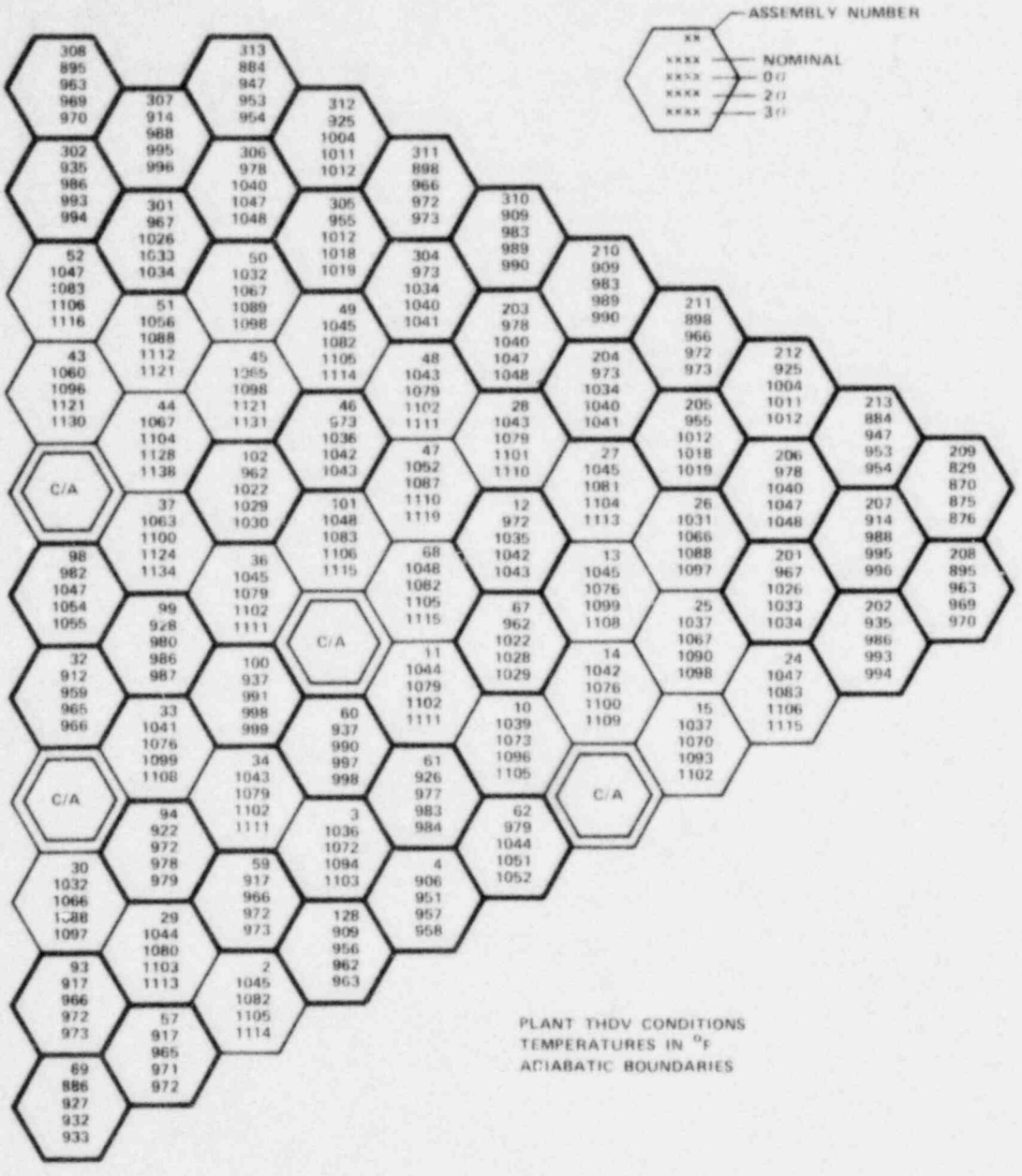

Figure 26 Core Assemblies Mixed Mean Outlet Temperatures at EOC 3

1668-118

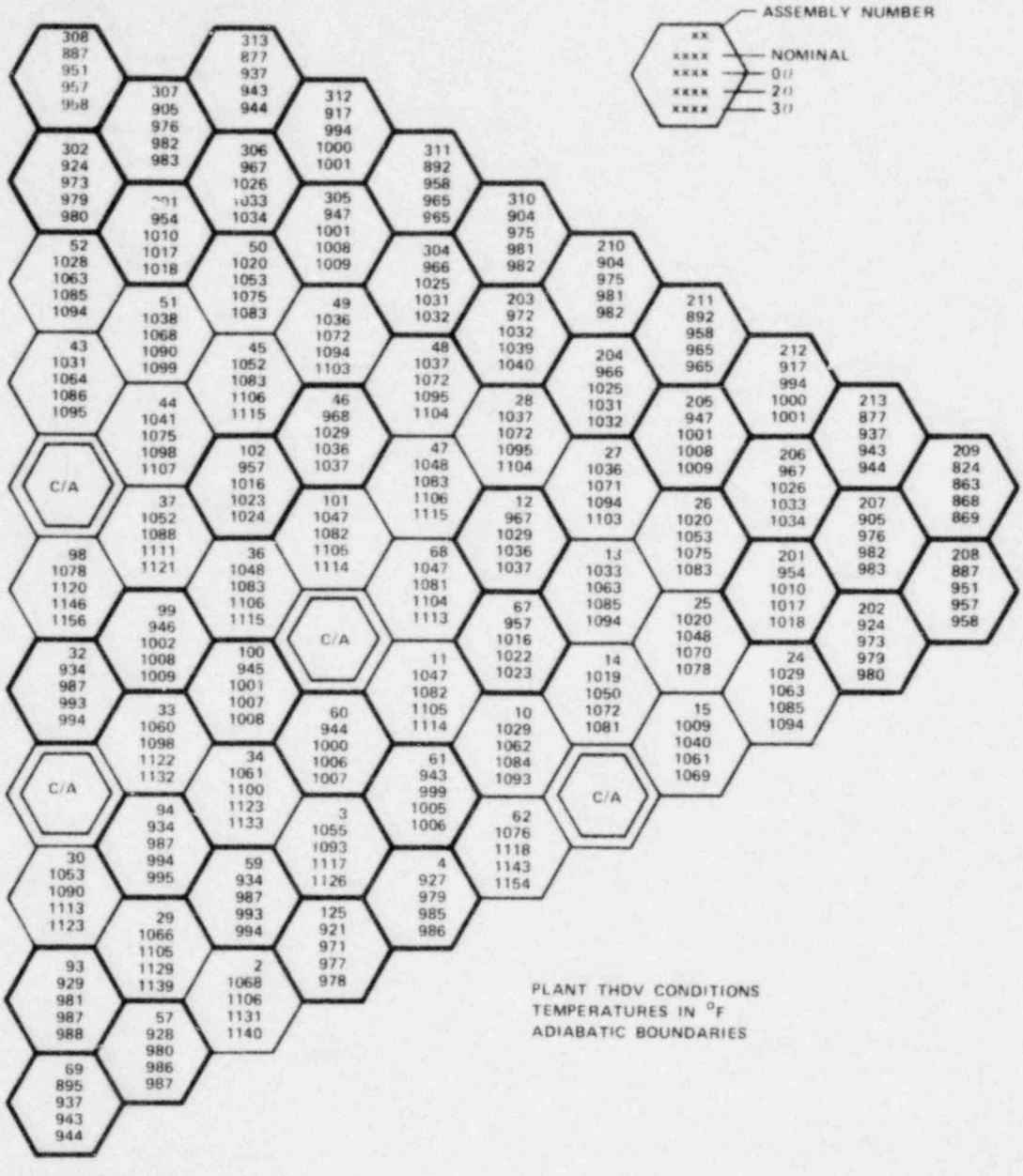

Figure 27 Core Assemblies Mixed Mean Outlet Temperatures at BOC4

1668-119

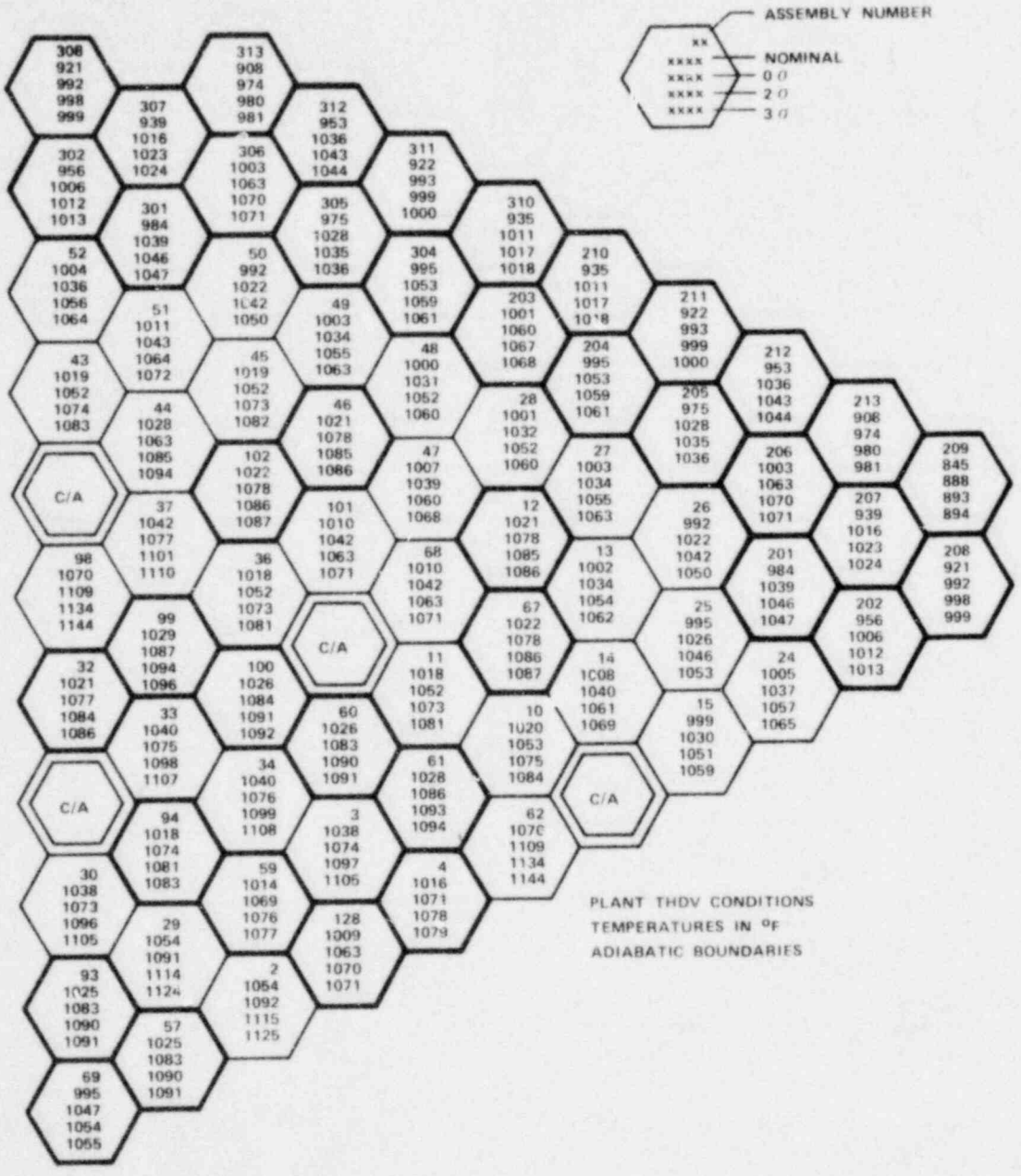

Figure 28 Core Assemblies Mixed Mean Outlet Temperatures at EOC4

1668-49

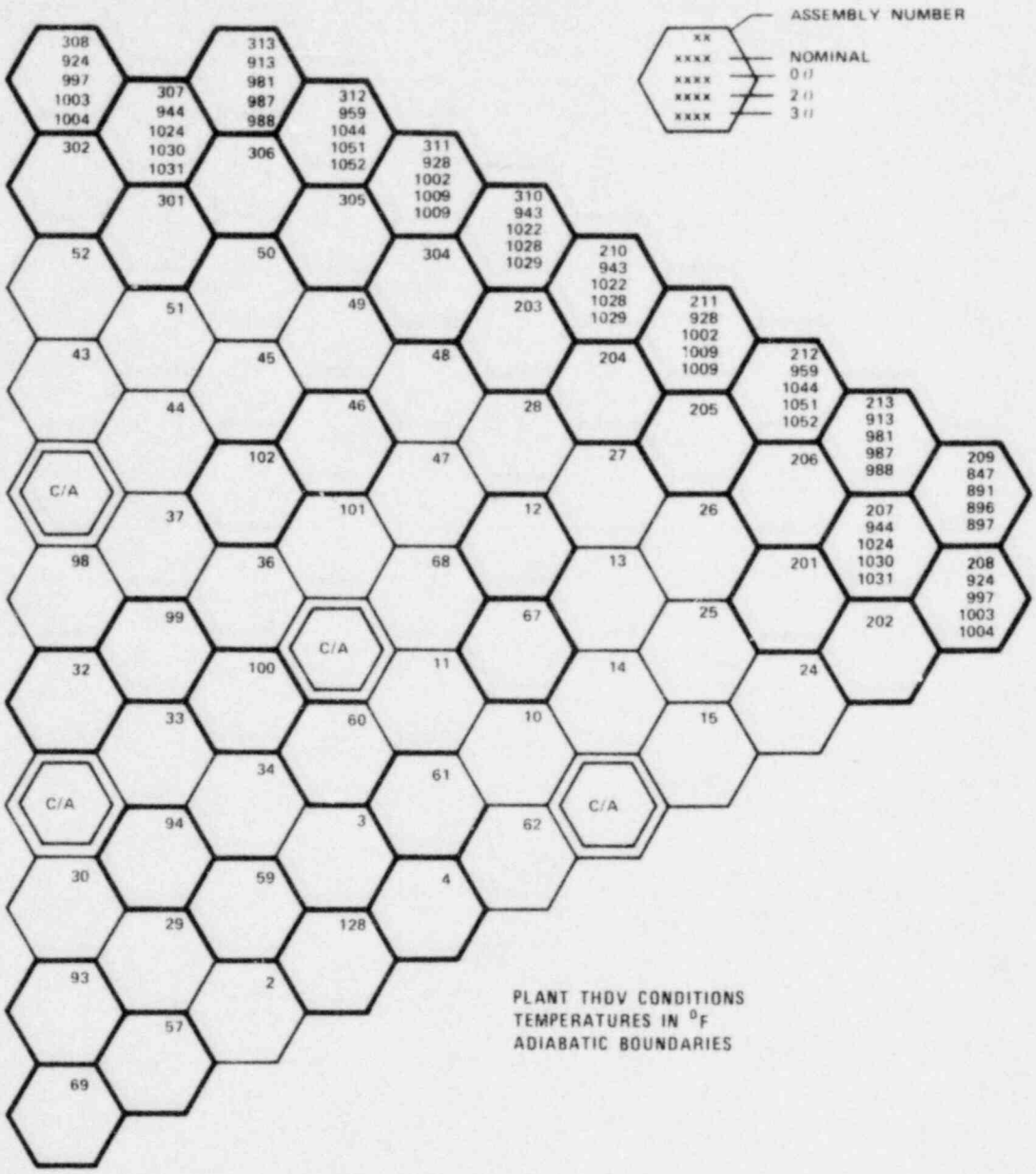

Figure 29 Radial Blanket Second Row Assemblies Mixed Mean Outlet Temperatures at BOC5

1668-112

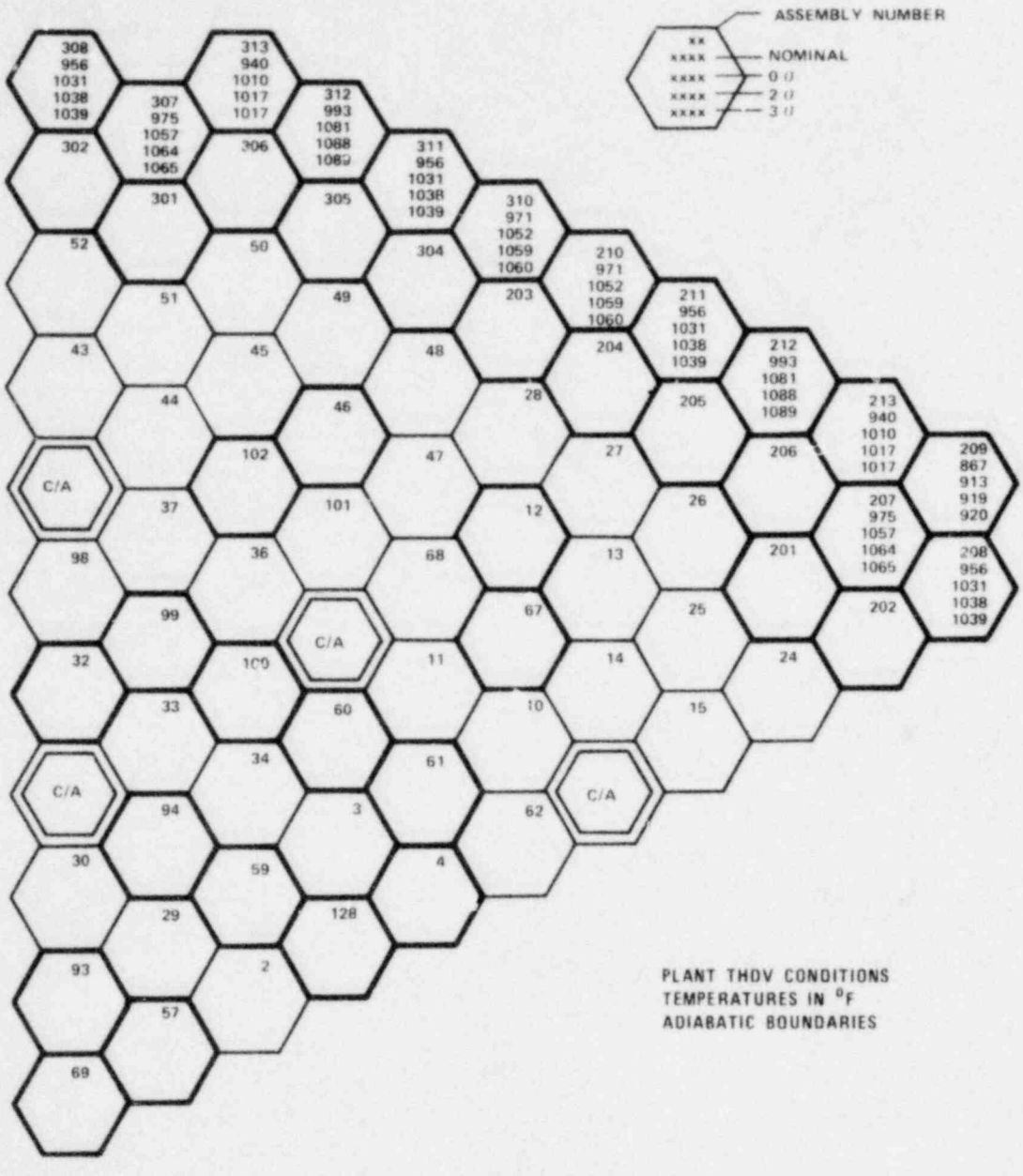

Figure 30 Radial Blanket Second Row Assemblies Mixed Mean Outlet Temperatures at EOC 5

1668-107

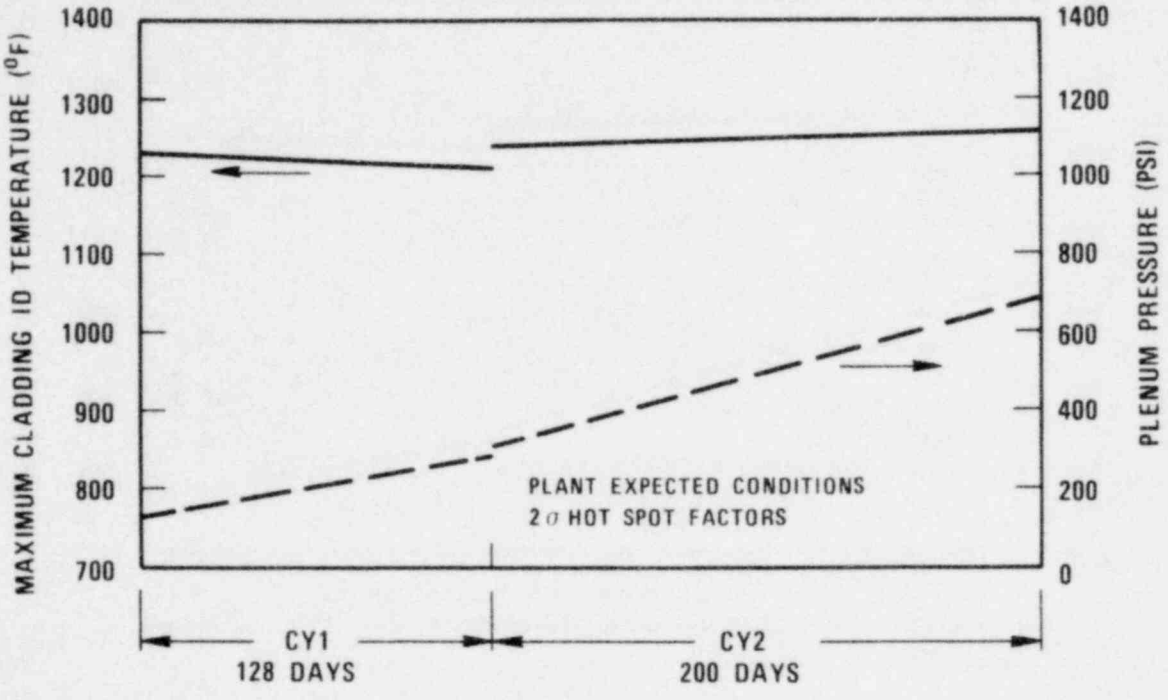

Figure 31 Lifetime Cladding Temperature/Pressure History in Fuel Assembly #[illegible] Core, Orificing Zone 1

1668-32

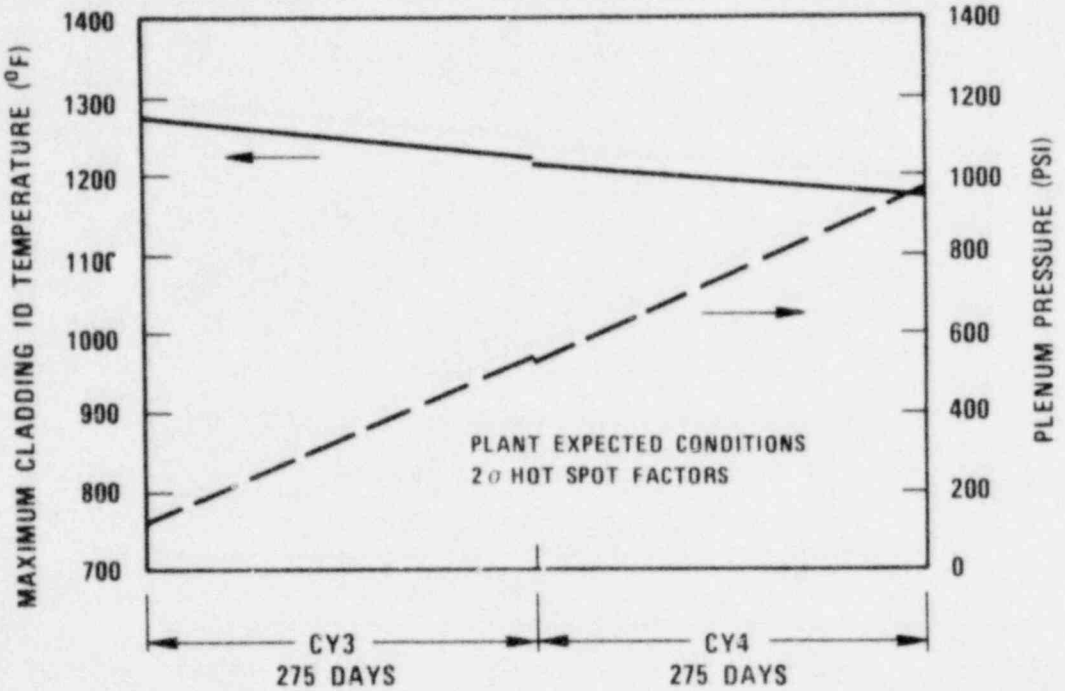

Figure 32 Lifetime Cladding Temperature/Pressure History in Fuel Assembly #101, Second Core, Orificing Zone 1

1668-33

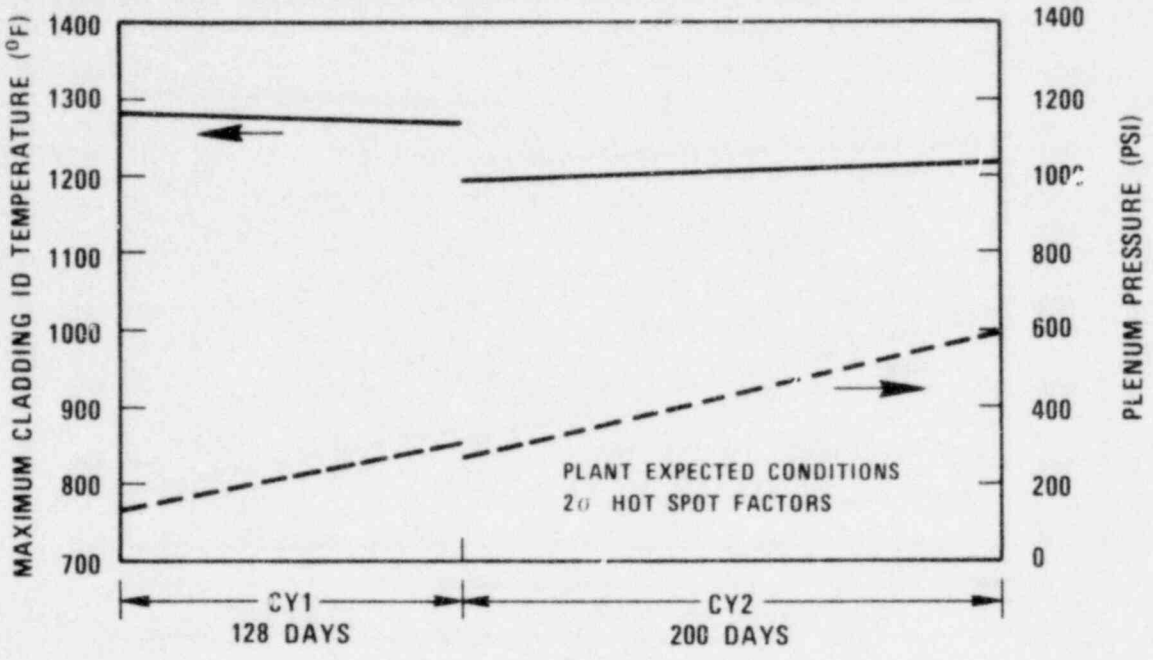

Figure 33 Lifetime Cladding Temperature/Pressure History in Fuel Assembly #43, First Core, Orificing Zone 2

1681-13

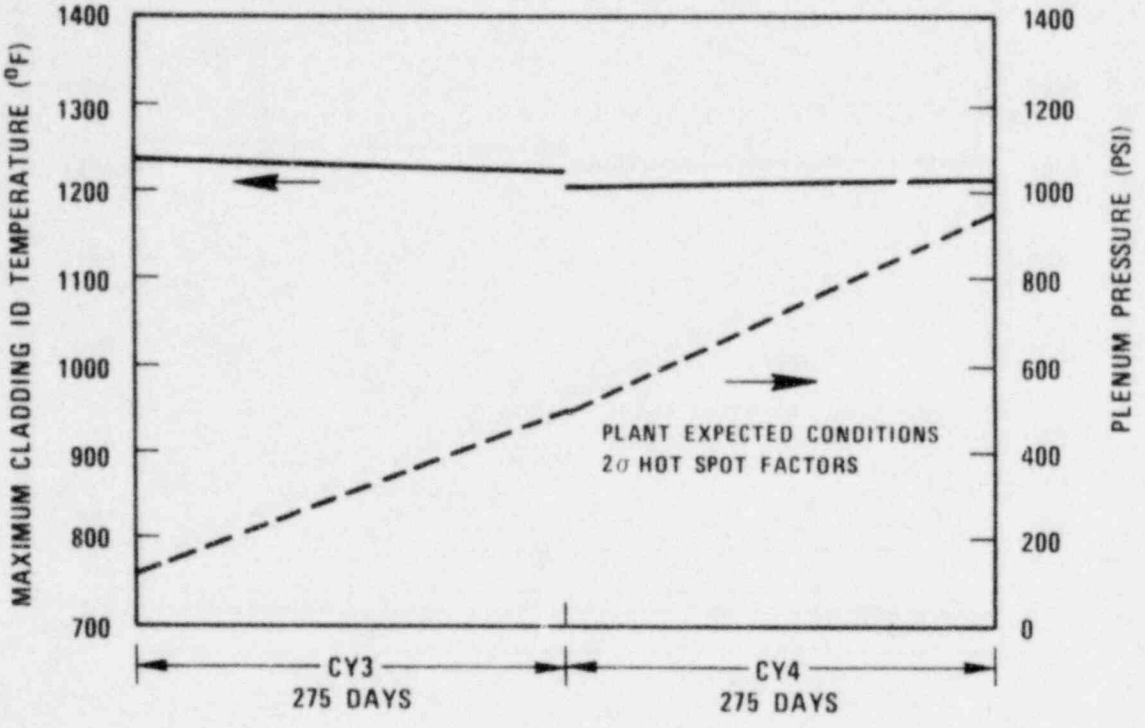

Figure 34 Lifetime Cladding Temperature/Pressure History in Fuel Assembly # 37, Second Core, Orificing Zone 2

1681-14

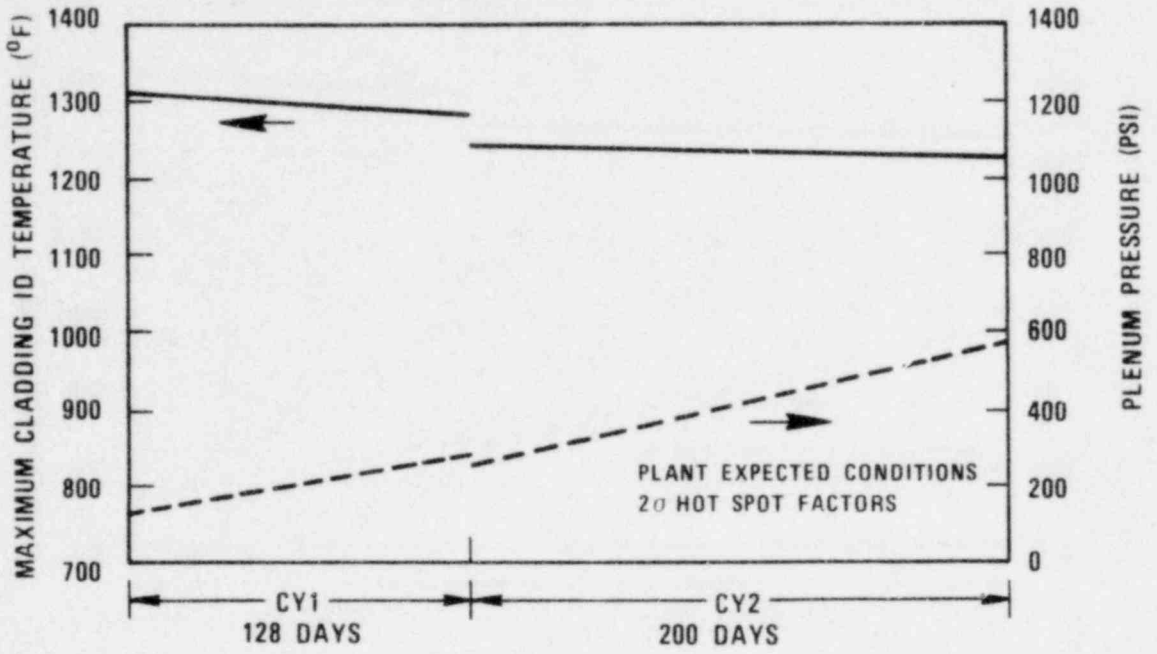

Figure 35 Lifetime Cladding Temperature/Pressure History in Fuel Assembly #45, First Core, Orificing Zone 3

1681-15

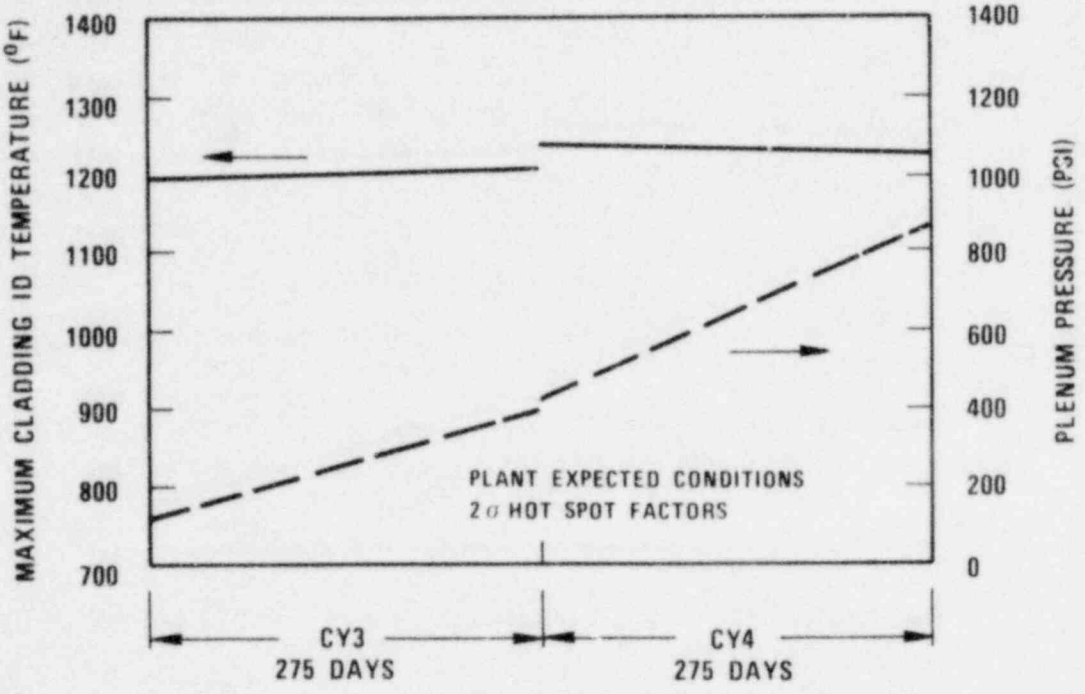

Figure 36 Lifetime Cladding Temperature/Pressure History in Fuel Assembly #2, Second Core, Orificing Zone 3

1668-34

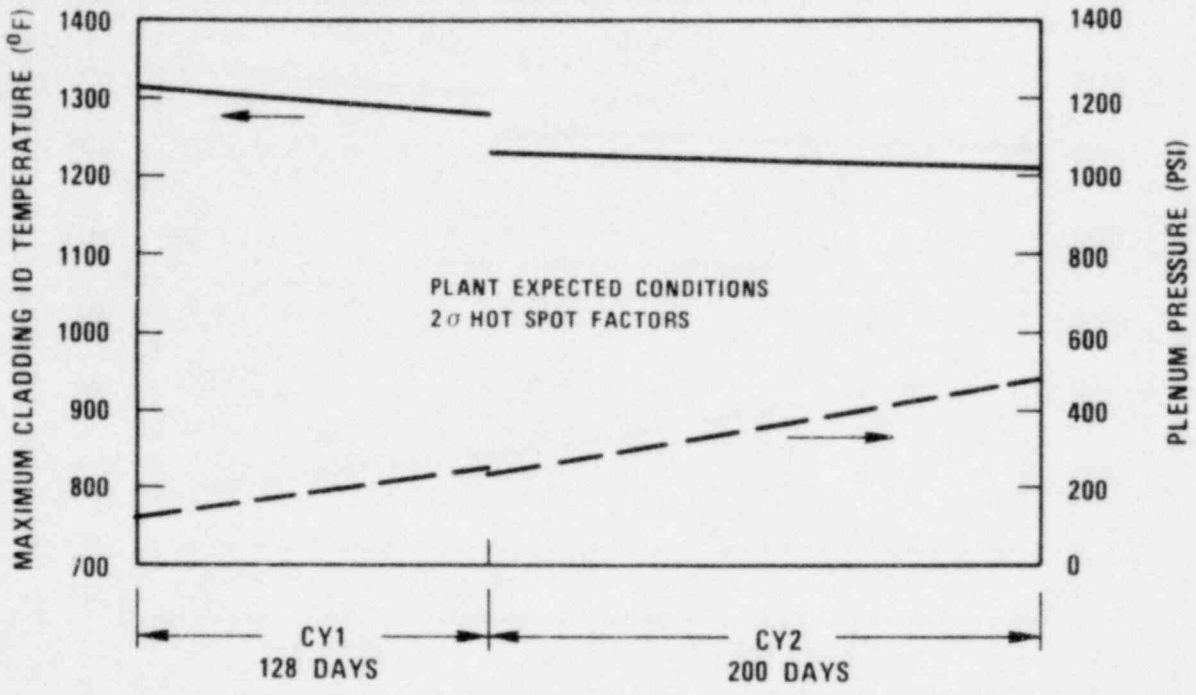

Figure 37 Lifetime Cladding Temperature/Pressure History in Fuel Assembly #52, First Core, Orificing Zone 4

1668-35

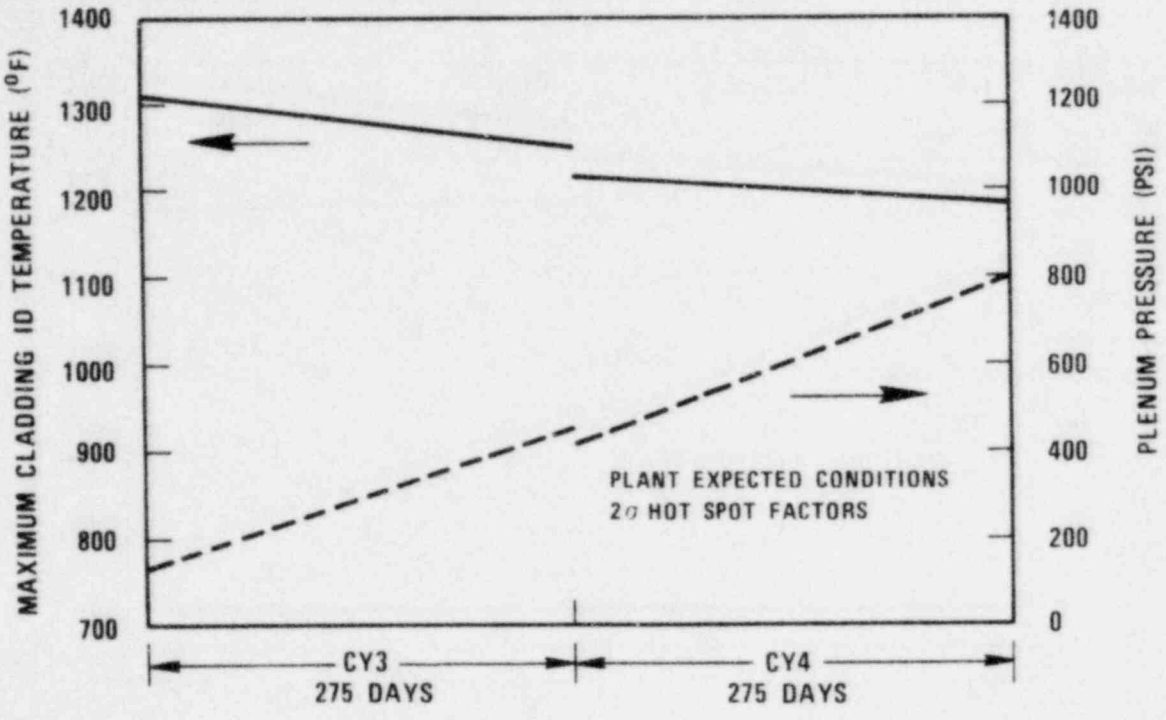

Figure 38 Lifetime Cladding Temperature/Pressure History in Fuel Assembly # 24, Second Core, Orificing Zone 4

1681-18

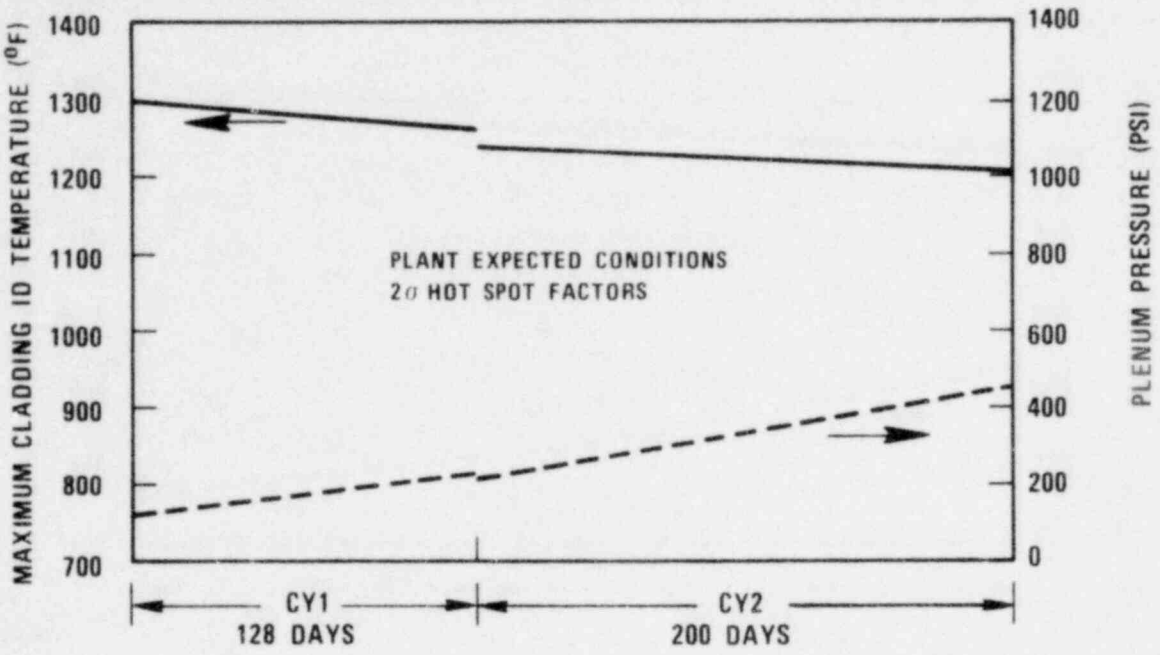

Figure 39 Lifetime Cladding Temperature/Pressure History in Fuel Assembly #49, First Core, Orificing Zone 5

1681-19

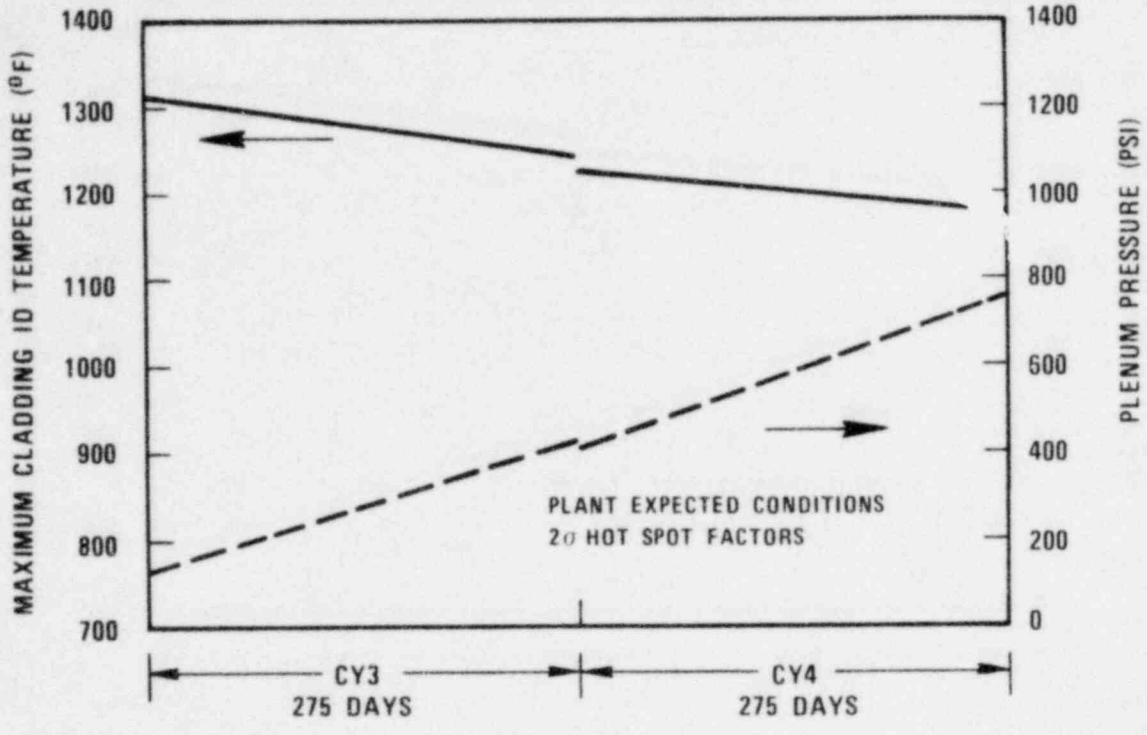

Figure 40 Lifetime Cladding Temperature/Pressure History in Fuel Assembly #49, Second Core, Orificing Zone 5

1681-20

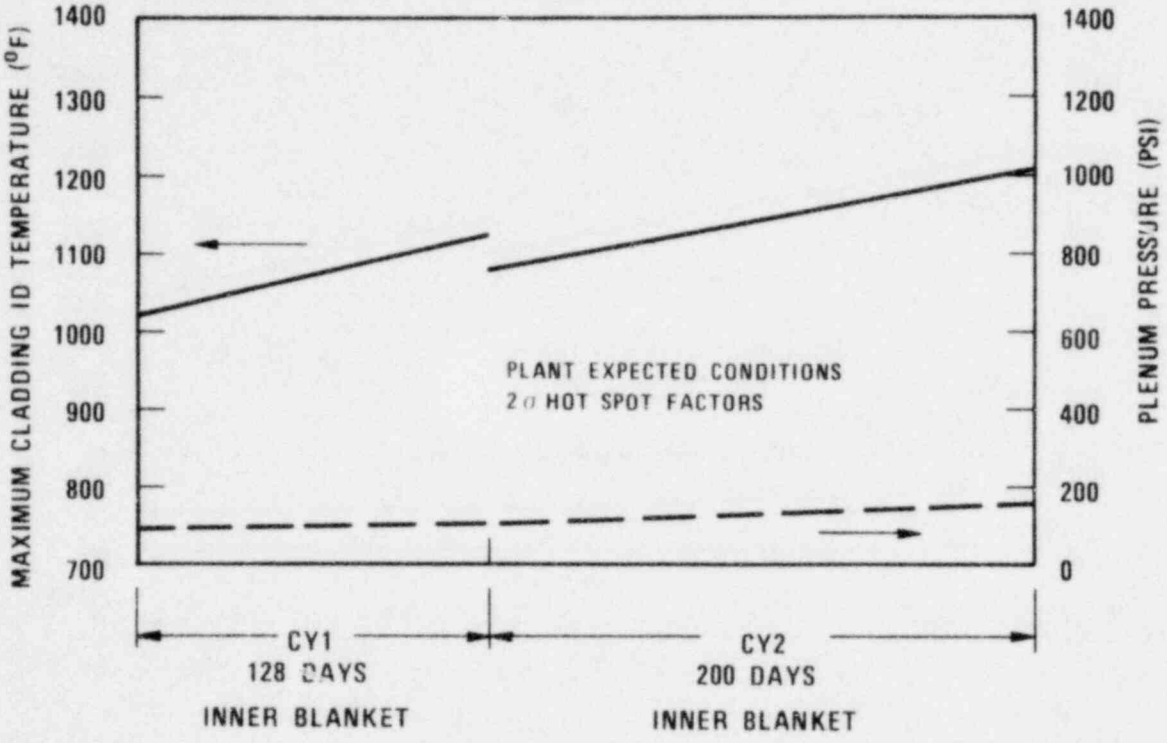

Figure 41 Lifetime Cladding Temperature/Pressure History in Assembly #98, First Core, Orificing Zone 6, Row 6 Alternating Position

1668-36

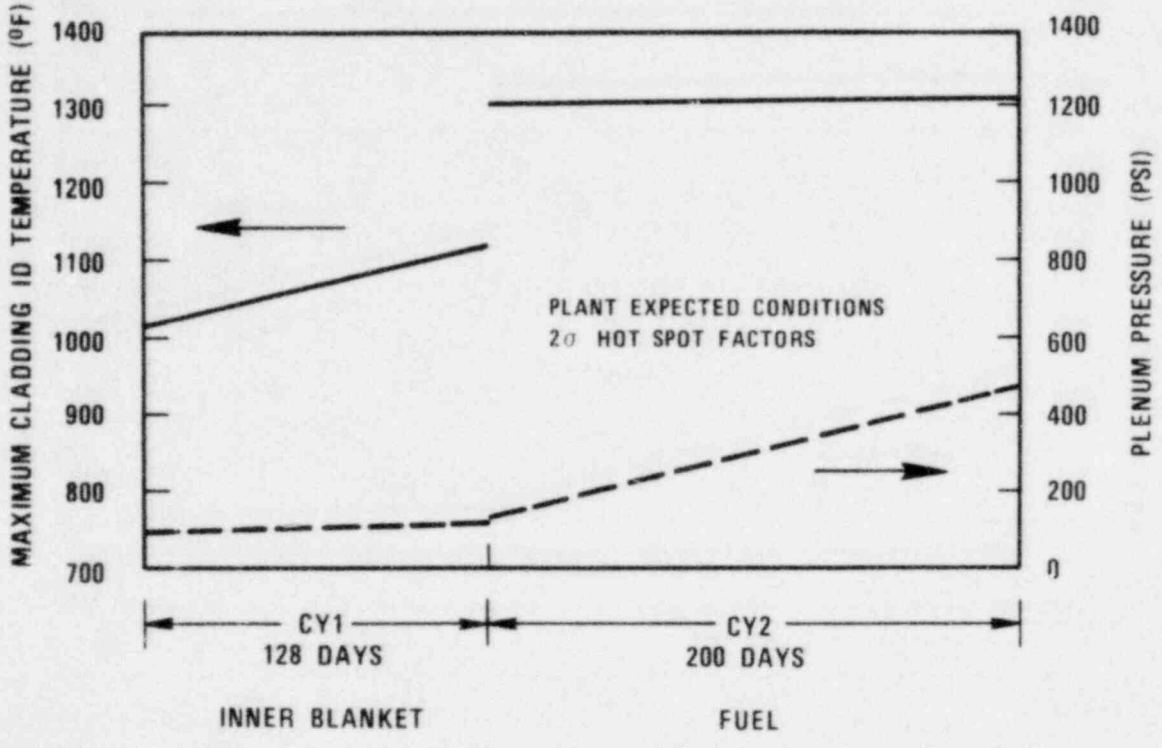

Figure 42 Lifetime Cladding Temperature/Pressure History in Assembly #62, First Core, Orificing Zone 6, Row 6 Alternating Position

1681-22

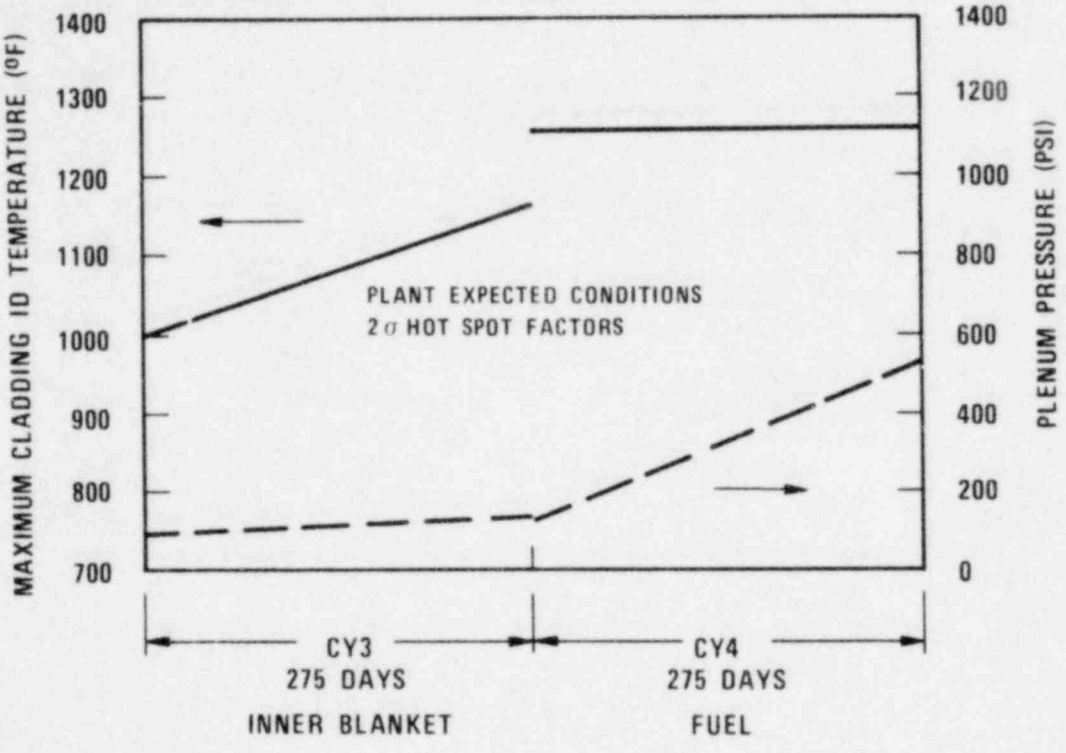

Figure 43 Lifetime Cladding Temperature/Pressure History in Assembly #62, Second Core, Orificing Zone 6, Row 6 Alternating Position

1668-37

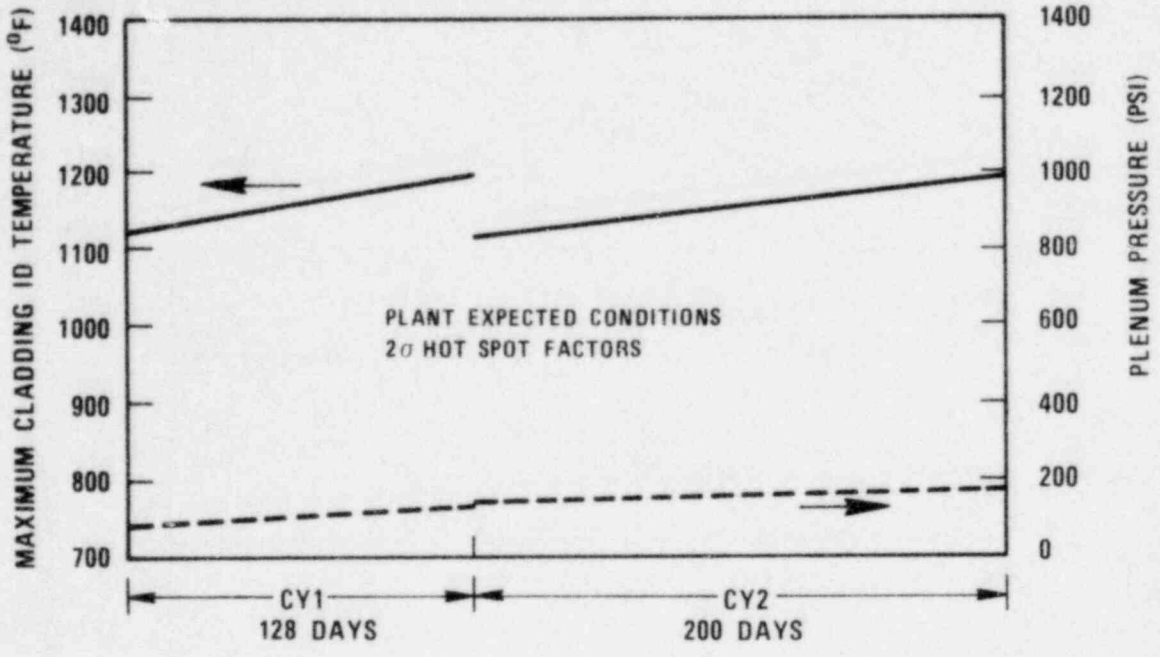

Figure 44 Lifetime Cladding Temperature/Pressure History in Inner Blanket Assembly # 67, First Core, Orificing Zone 7

1681-24

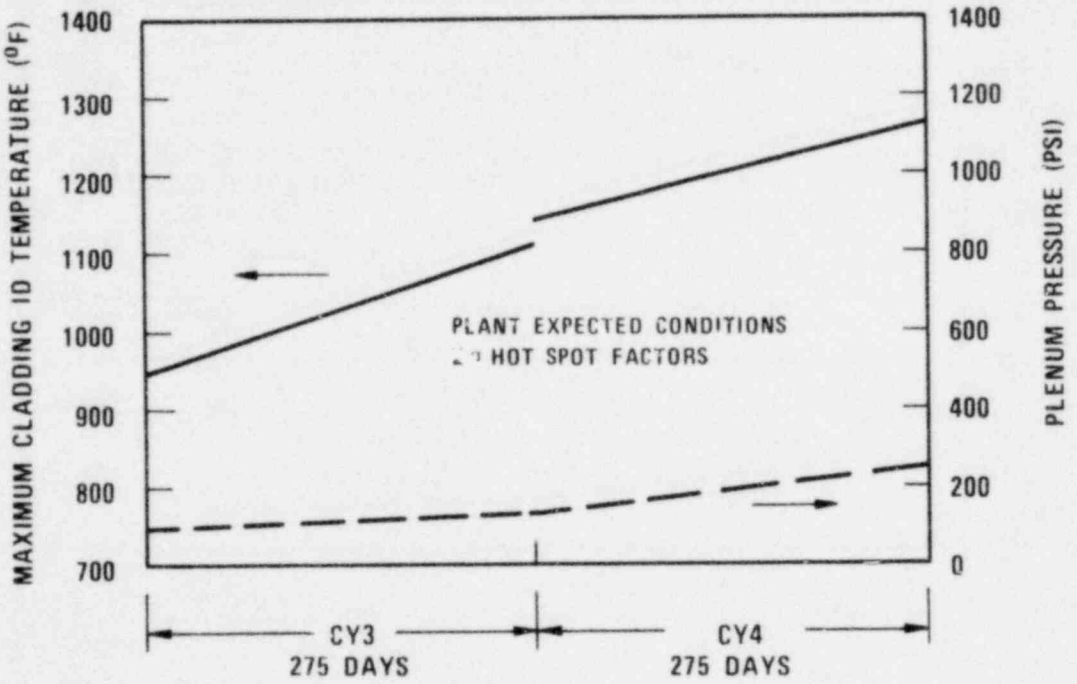

Figure 45 Lifetime Cladding Temperature/Pressure History in Inner Blanket Assembly #99, Second Core, Orificing Zone 7

1668-38

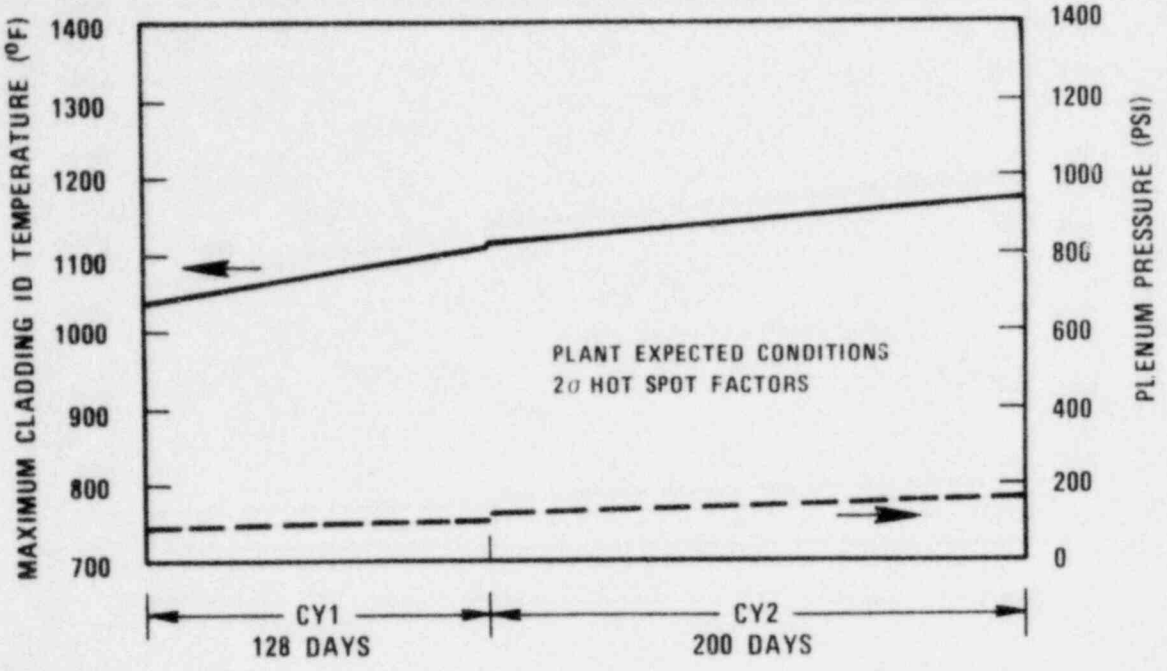

Figure 46 Lifetime Cladding Temperature/Pressure History in Inner Blanket Assembly # 12, First Core, Orificing Zone 8

1681-26

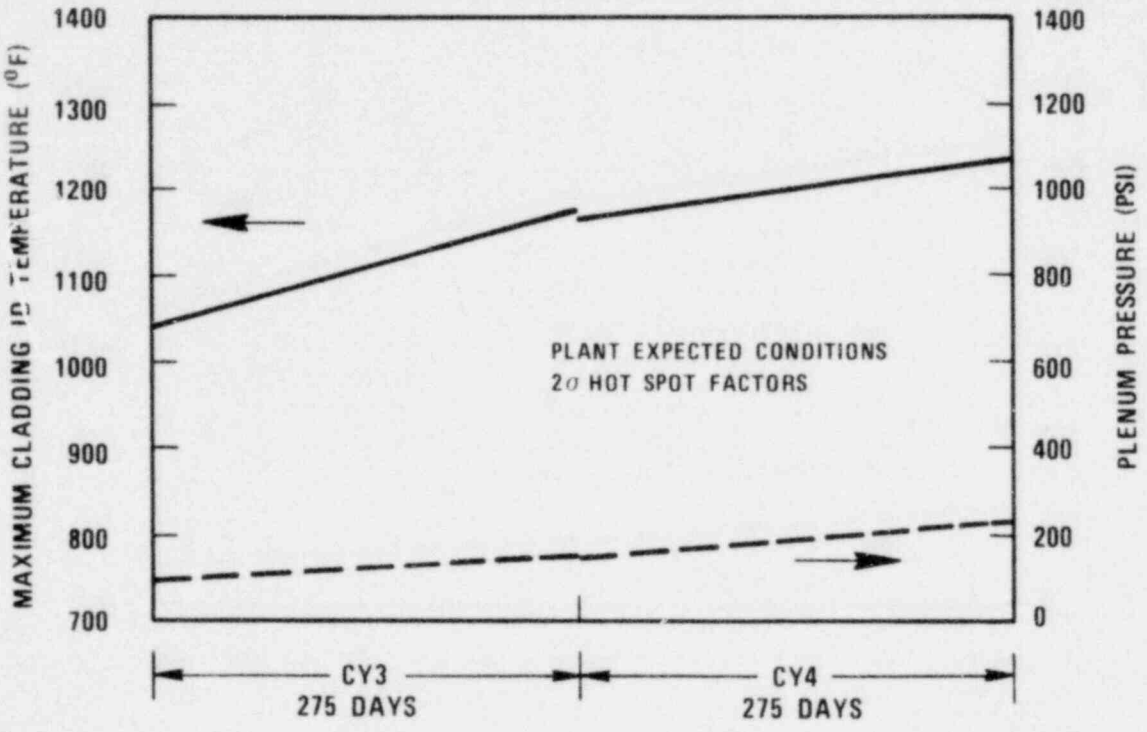

Figure 47 Lifetime Cladding Temperature/Pressure History in Inner Blanket Assembly #46, Second Core, Orificing Zone 8

1681-27

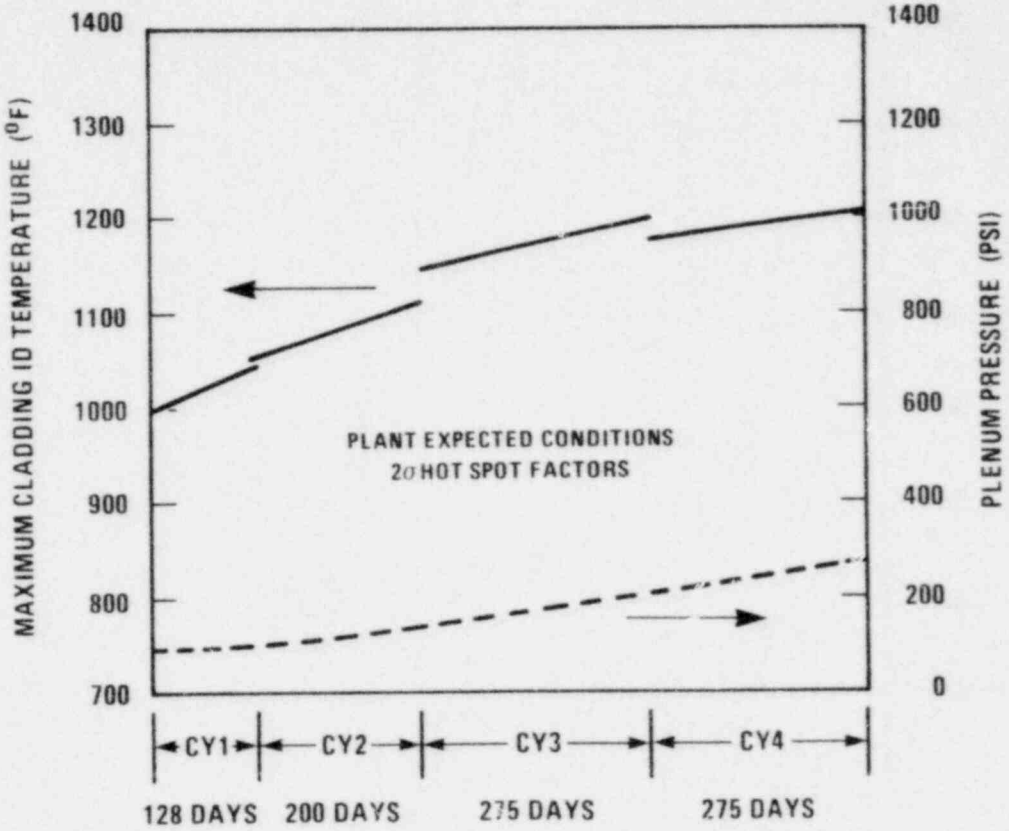

Figure 48. Lifetime Cladding Temperature/Pressure History in Radial Blanket Assembly #201, Orificing Zone 9

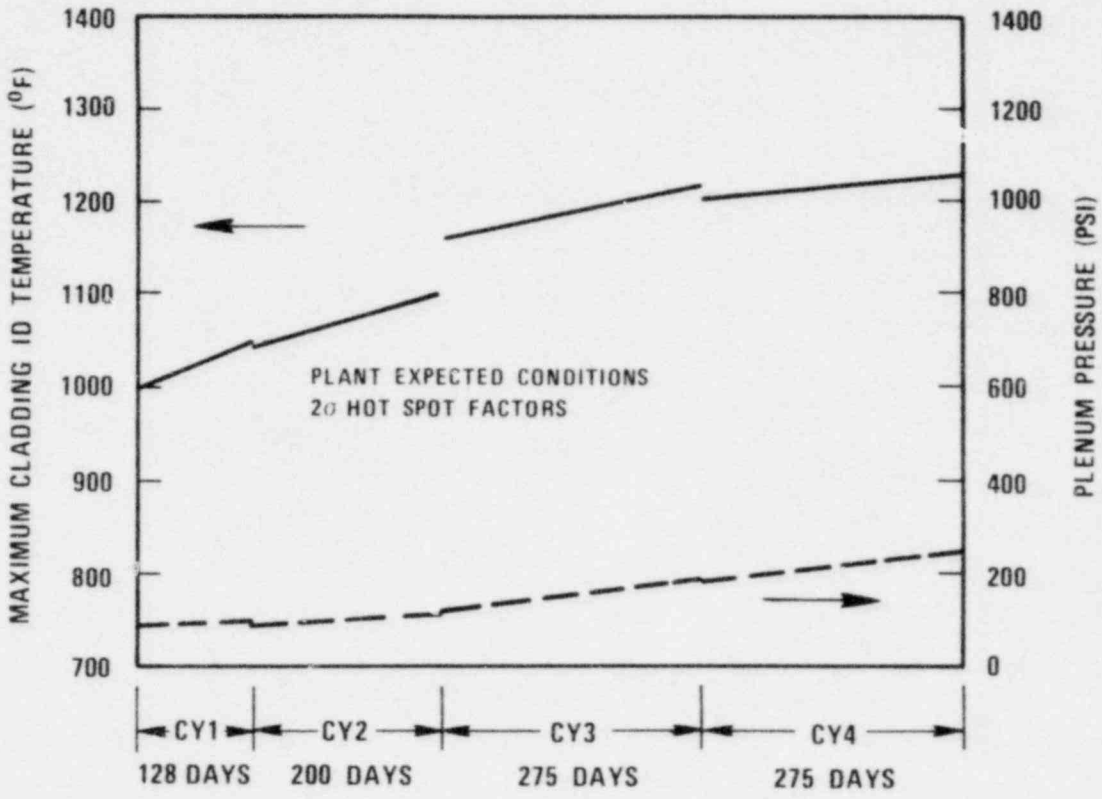

Figure 49 Lifetime Cladding Temperature/Pressure History in Radial Blanket Assembly #203, Orificing Zone 10

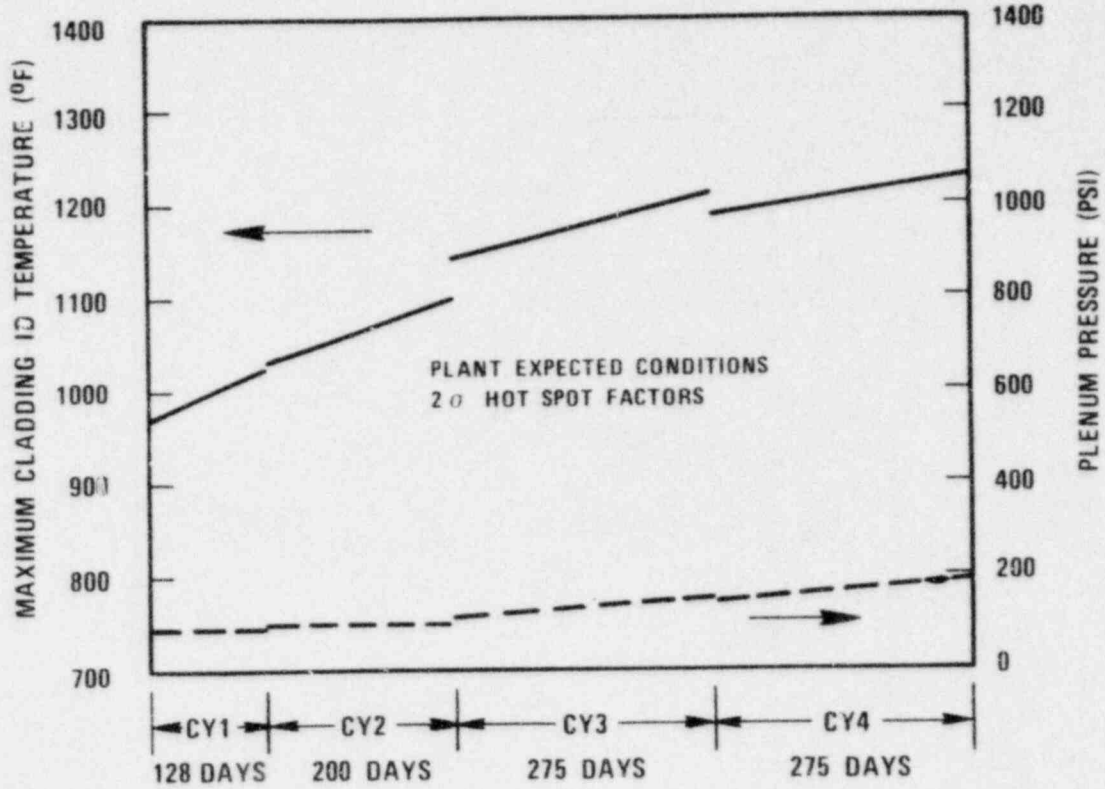

Figure 50 Lifetime Cladding Temperature Pressure History in Radial Blanket Assembly #206, Orificing Zone 11

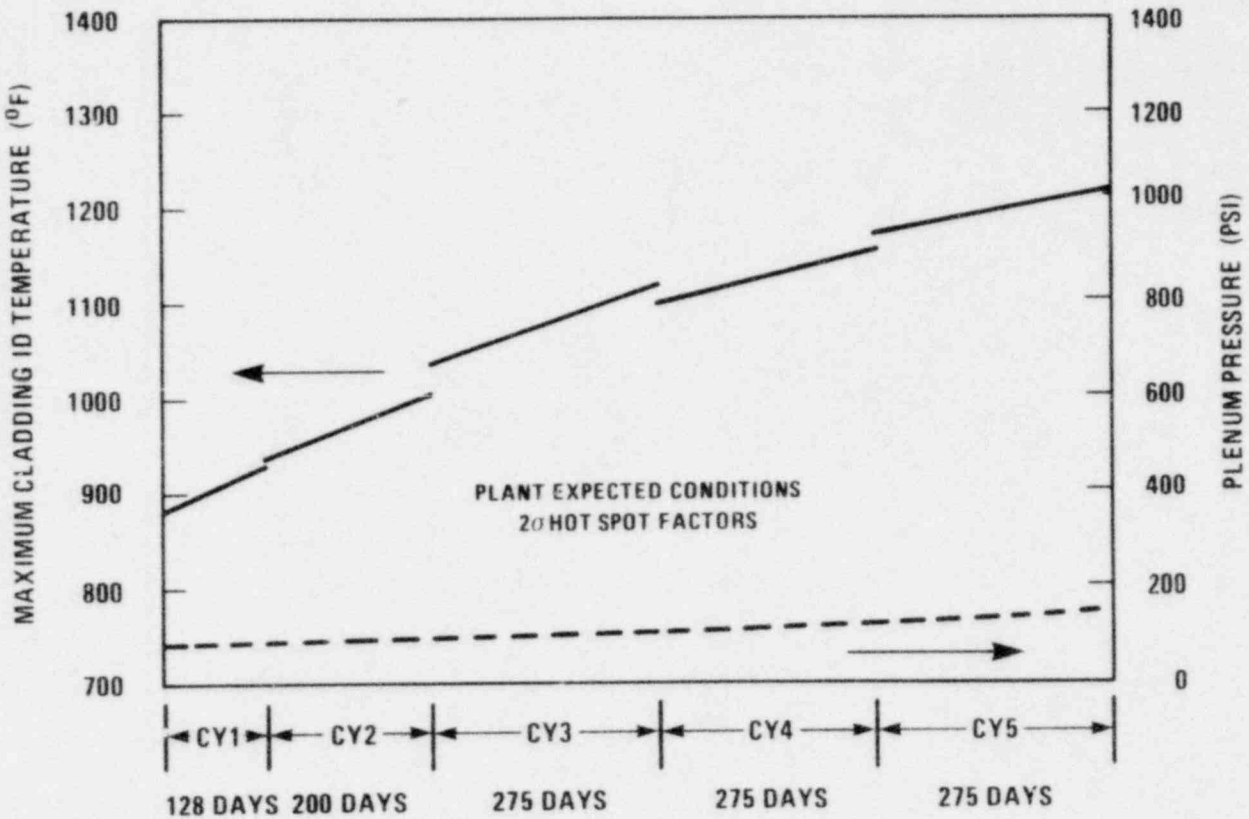

Figure 51 Lifetime Cladding Temperature/Pressure History in Radial Blanket Assembly #212, Orificing Zone 12

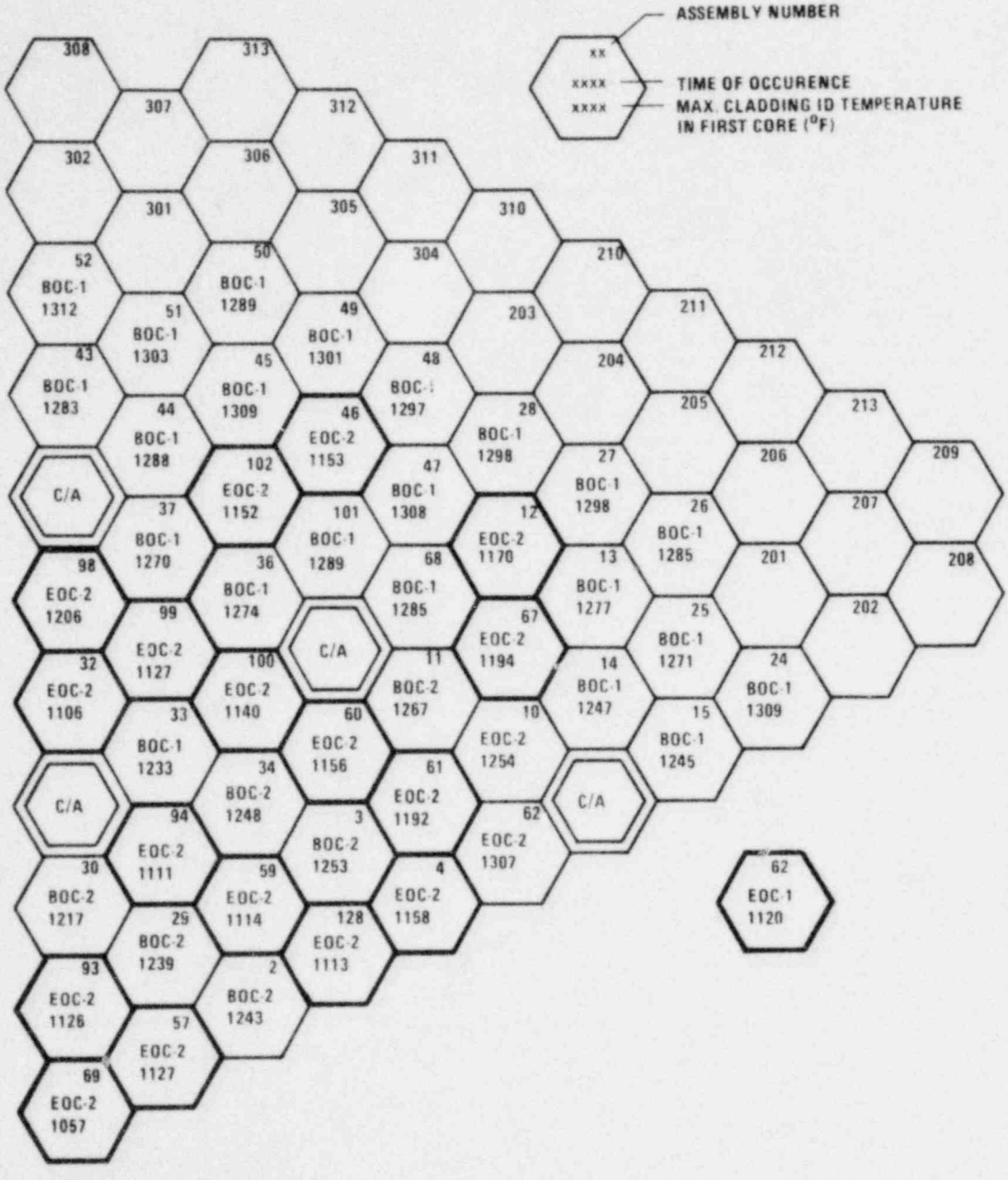

Figure 52 Envelope of Assemblies Maximum Cladding ID Temperature at Plant Expected Conditions During the First Core and Time of Occurence

1668-41

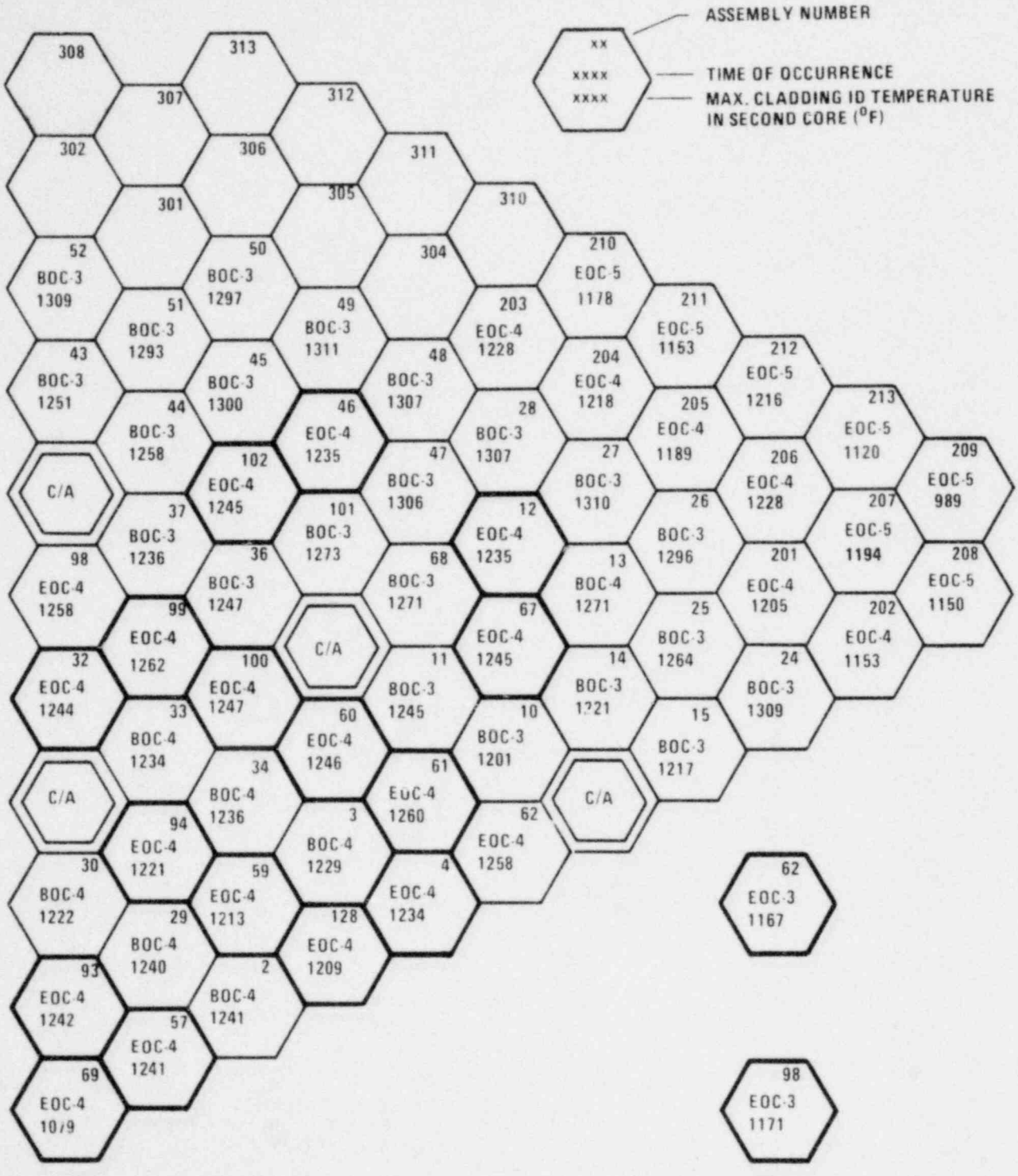

Figure 53 Envelope of Assemblies Maximum Cladding ID Temperature at Plant Expected Conditions During the Second Core and Time of Occurrence

1668-42

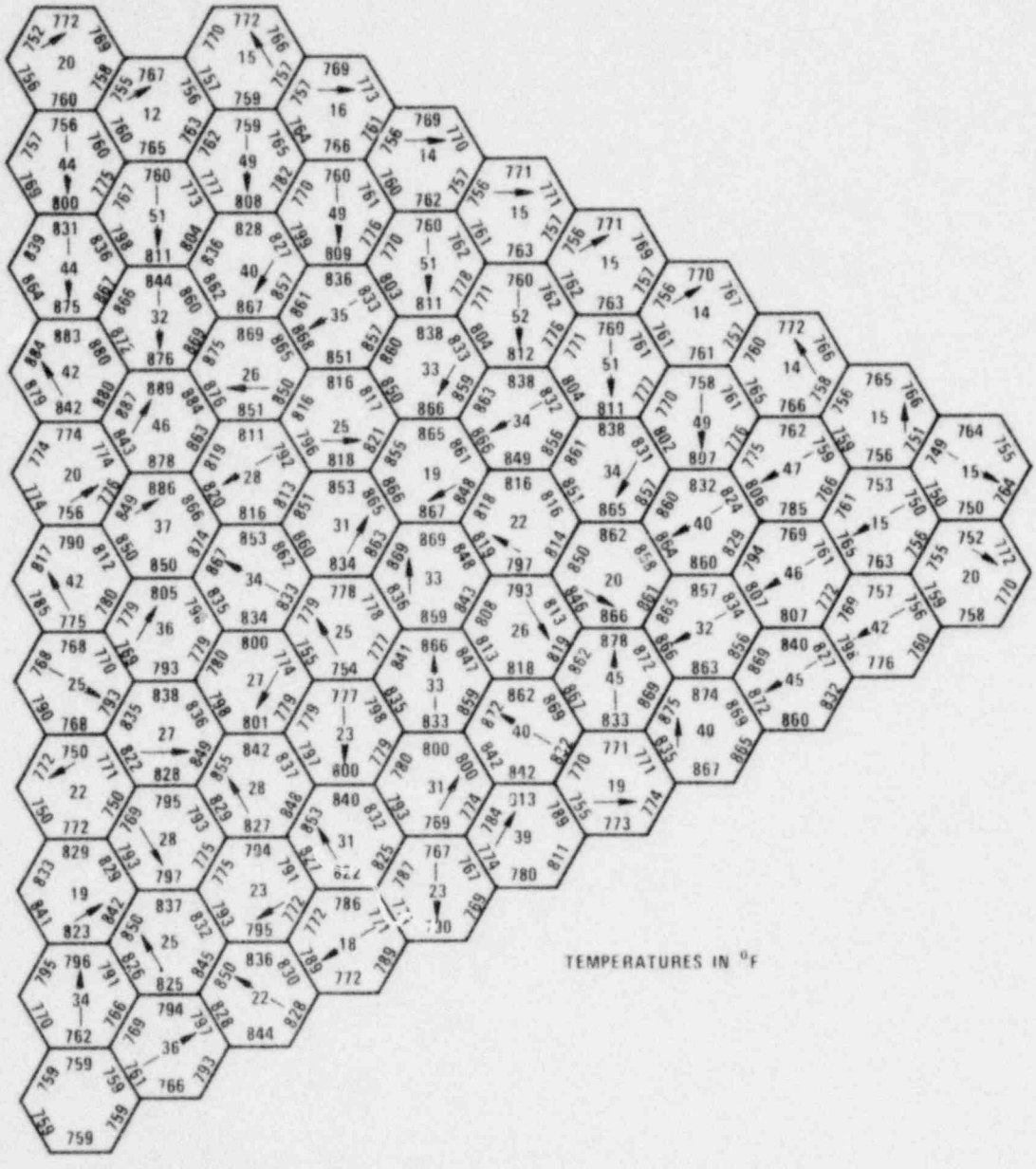

Figure 54 Core Wide Duct Midwall Temperatures at 32" Elevation, BOC1, Under Nominal Conditions

1668-109

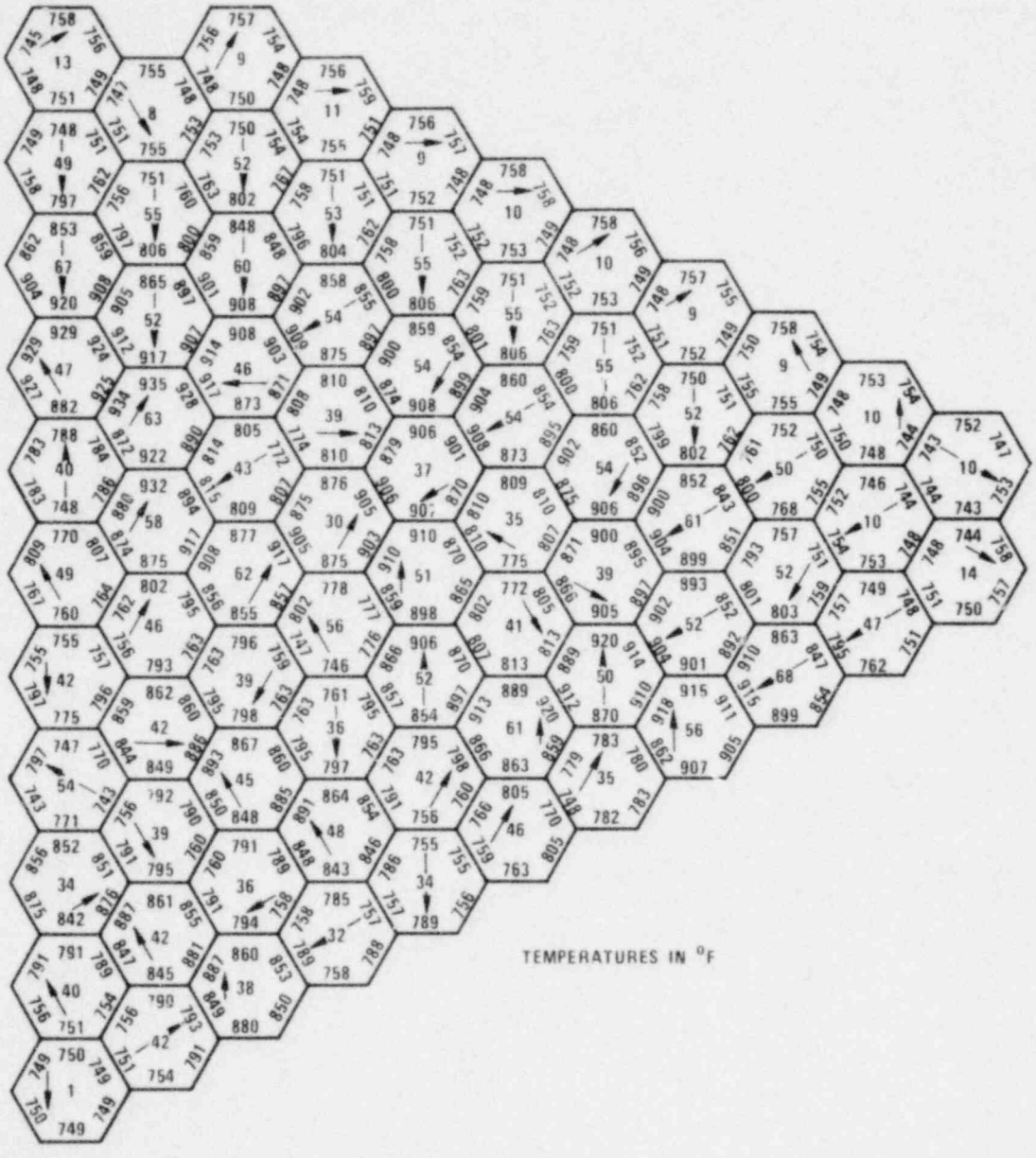

Figure 55 Core Wide Duct Midwall Temperatures at 32" Elevation. BOC1. Accounting for Uncertainties

1668-110

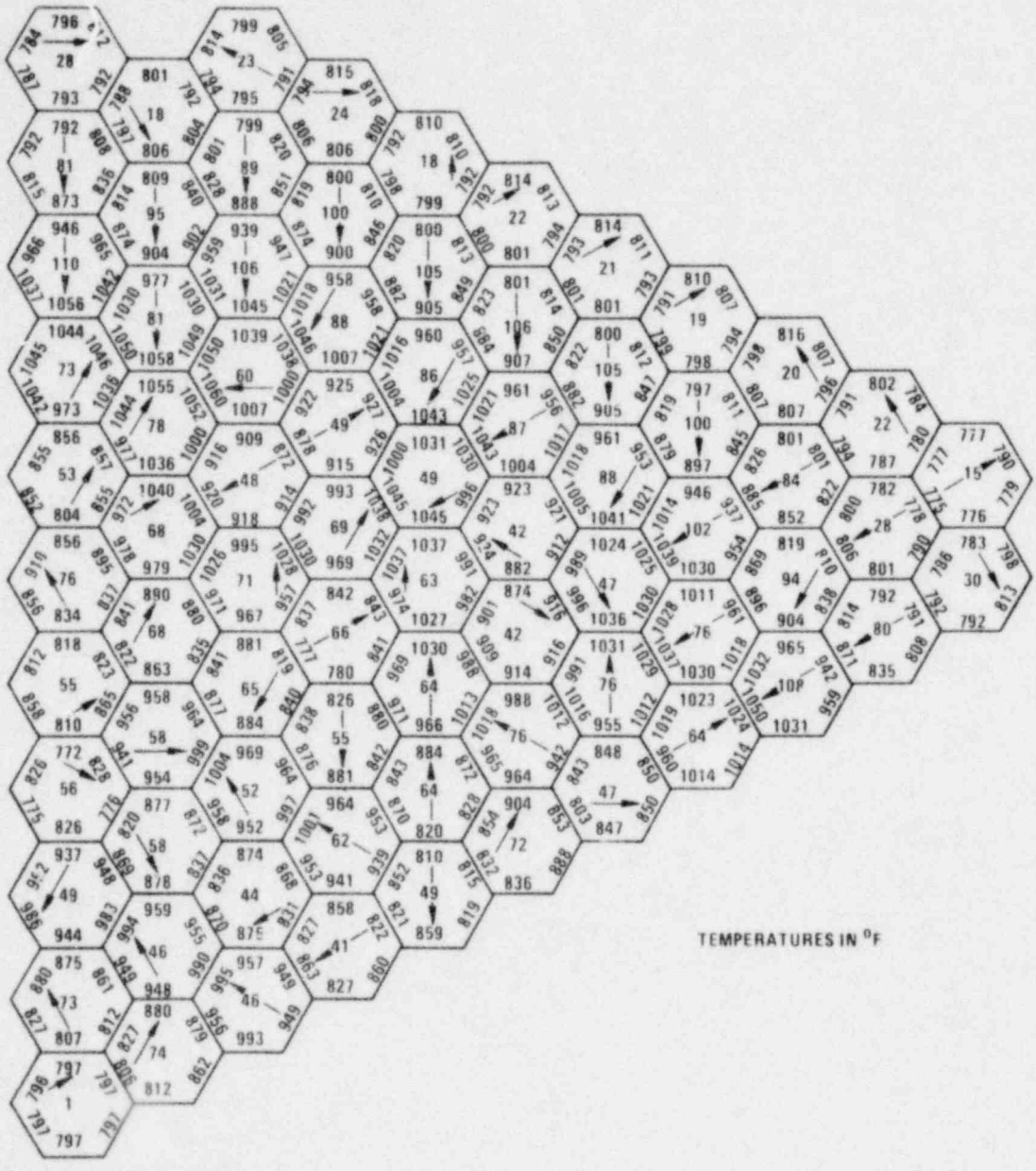

Figure 56. Core Wide Duct Midwall Temperatures at 60" Elevation, BOC1, Under Nominal Conditions

1668-43

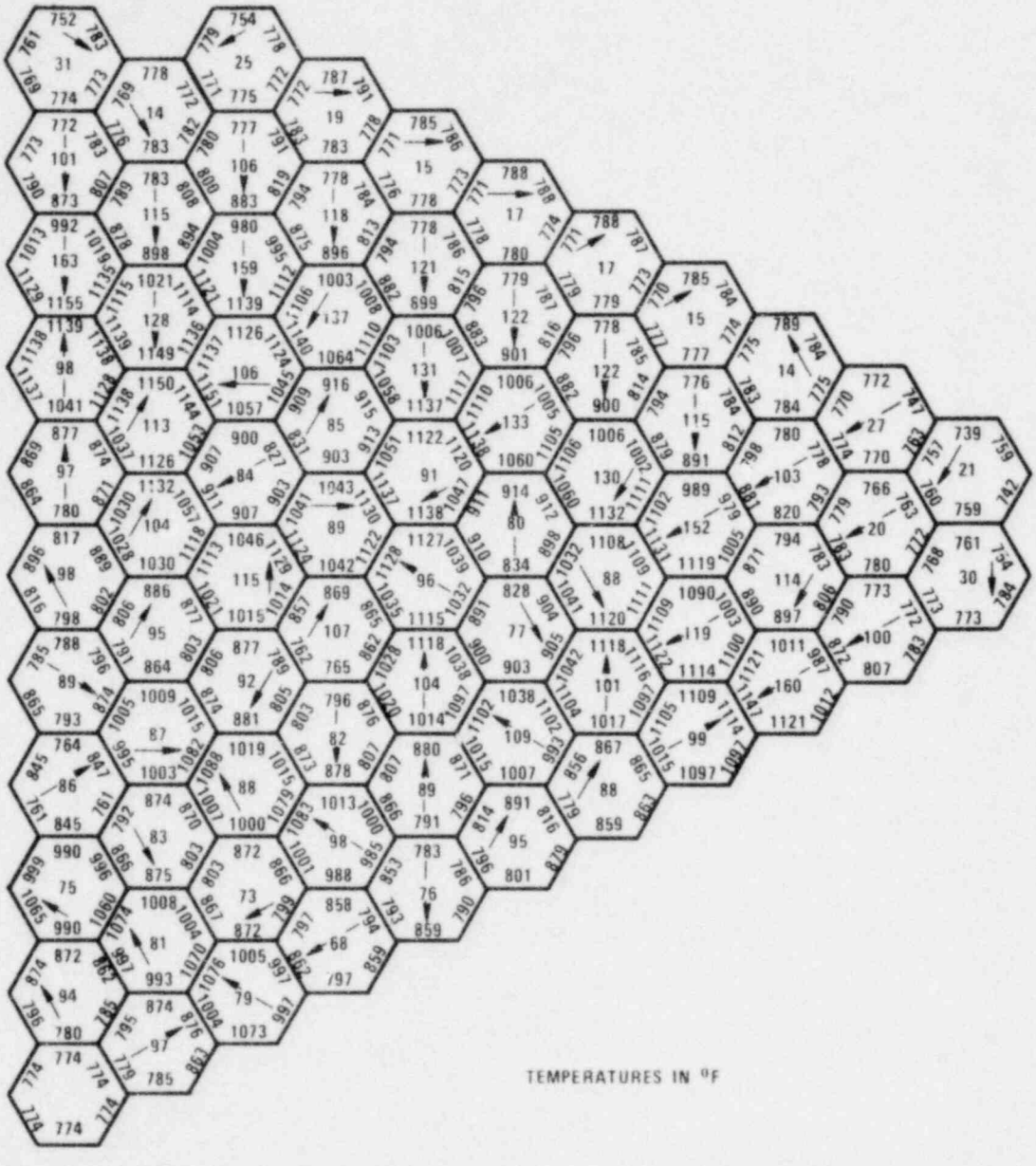

Figure 57 Core Wide Duct Midwall Temperatures at 60" Elevation, BOC1, Accounting for Uncertainties

1668-108

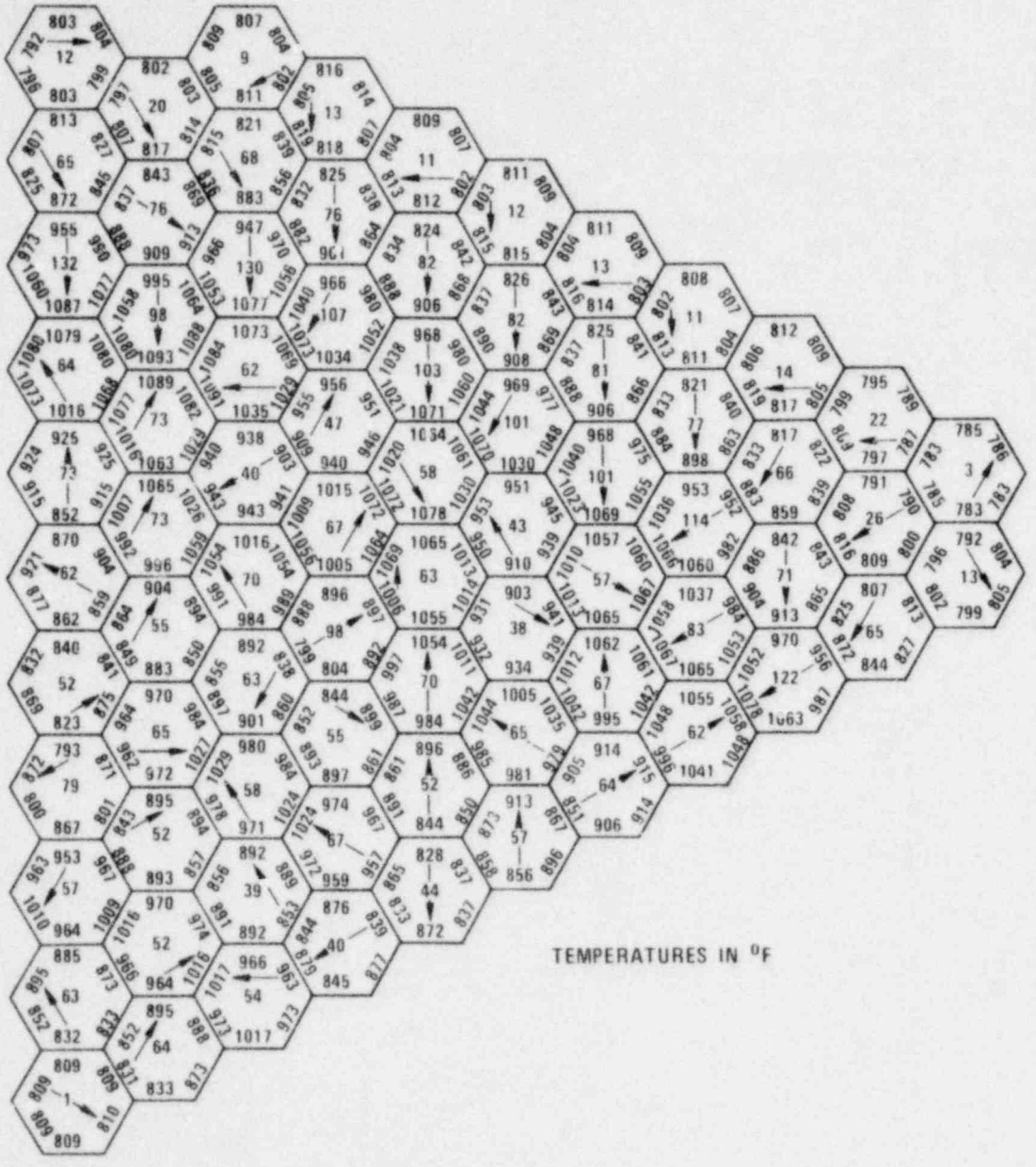

Figure 58 Core Wide Duct Midwall Temperatures at 112" Elevation, BOC1, Under Nominal Conditions

1668-44

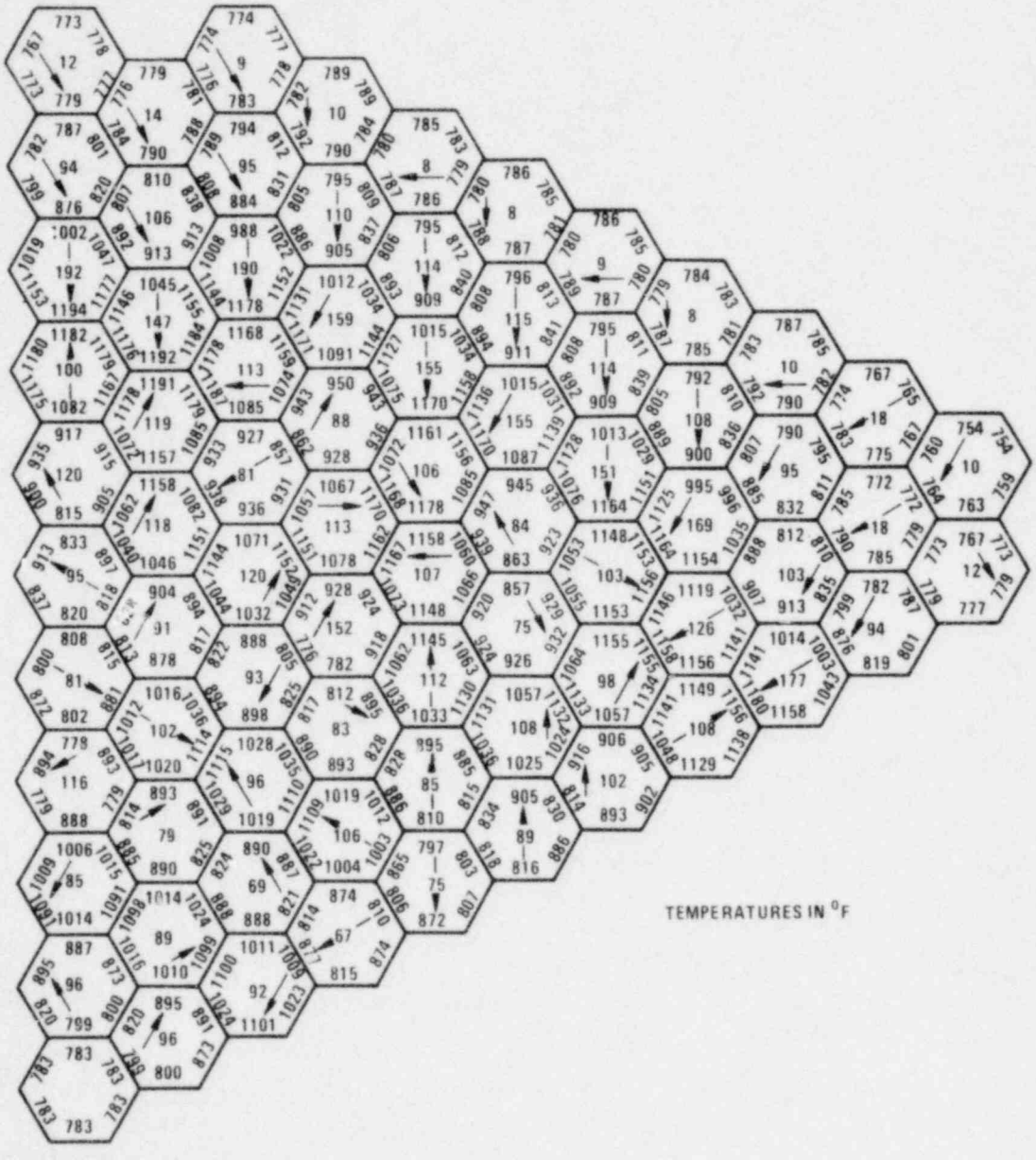

Figure 59 Core Wide Duct Midwall Temperatures at 112" Elevation, BOC1, Accounting for Uncertainties

1668-104

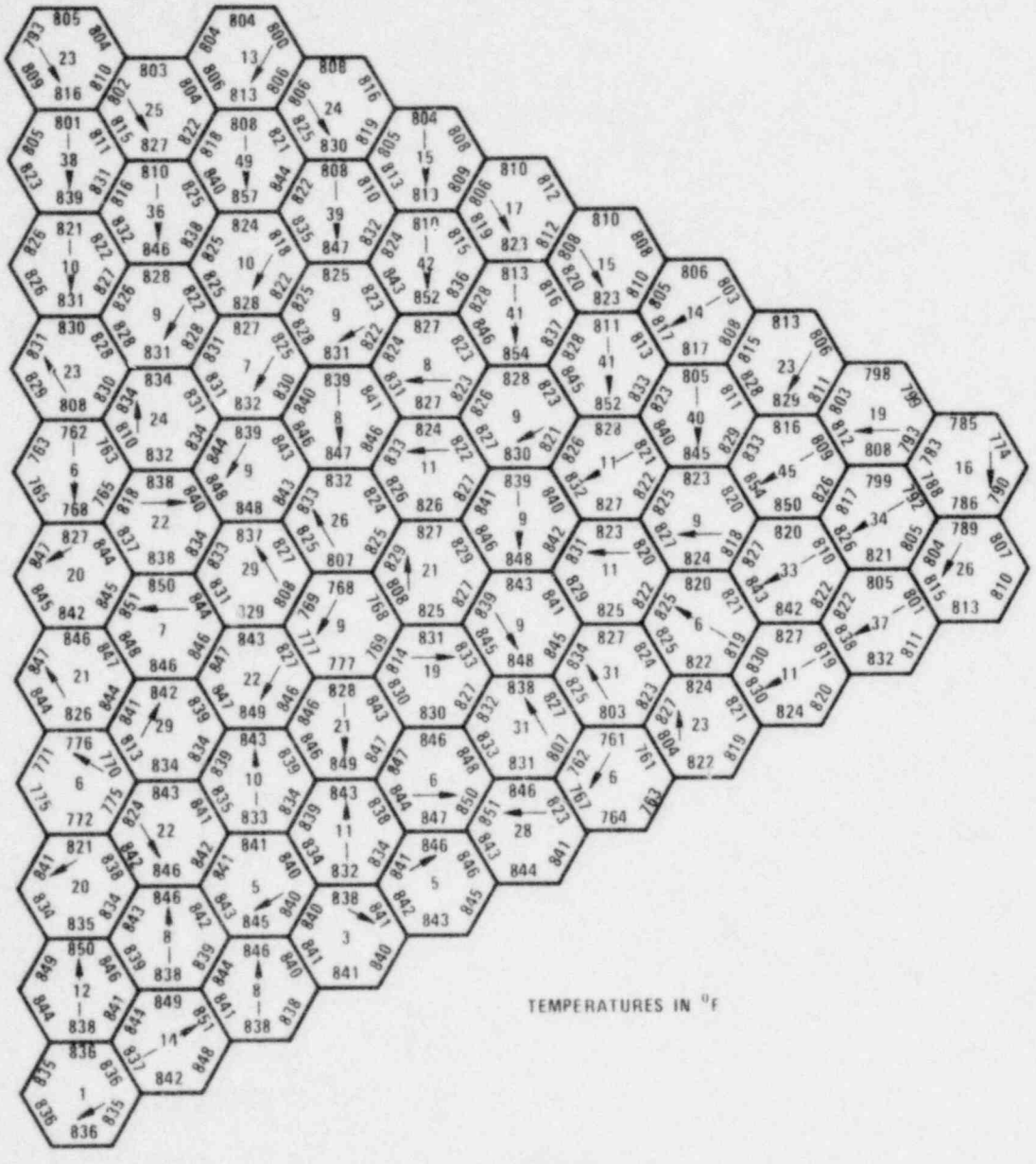

Figure 60 Core Wide Duct Midwall Temperatures at 32" Elevation, EOC4, Under Nominal Conditions

1668-116

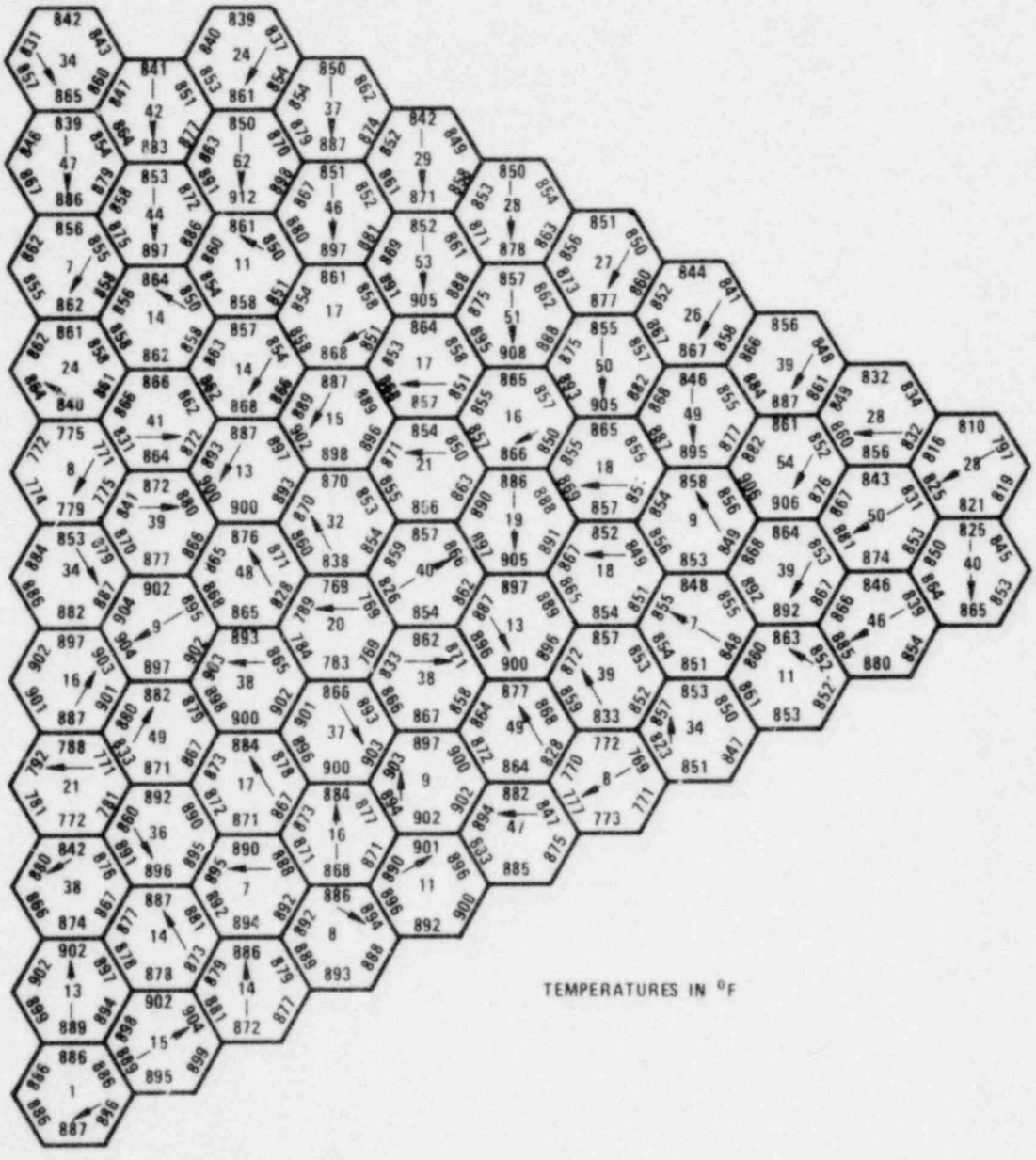

Figure 61 Core Wide Duct Midwall Temperatures at 32" Elevation, EOC4, Accounting for Uncertainties

1668-117

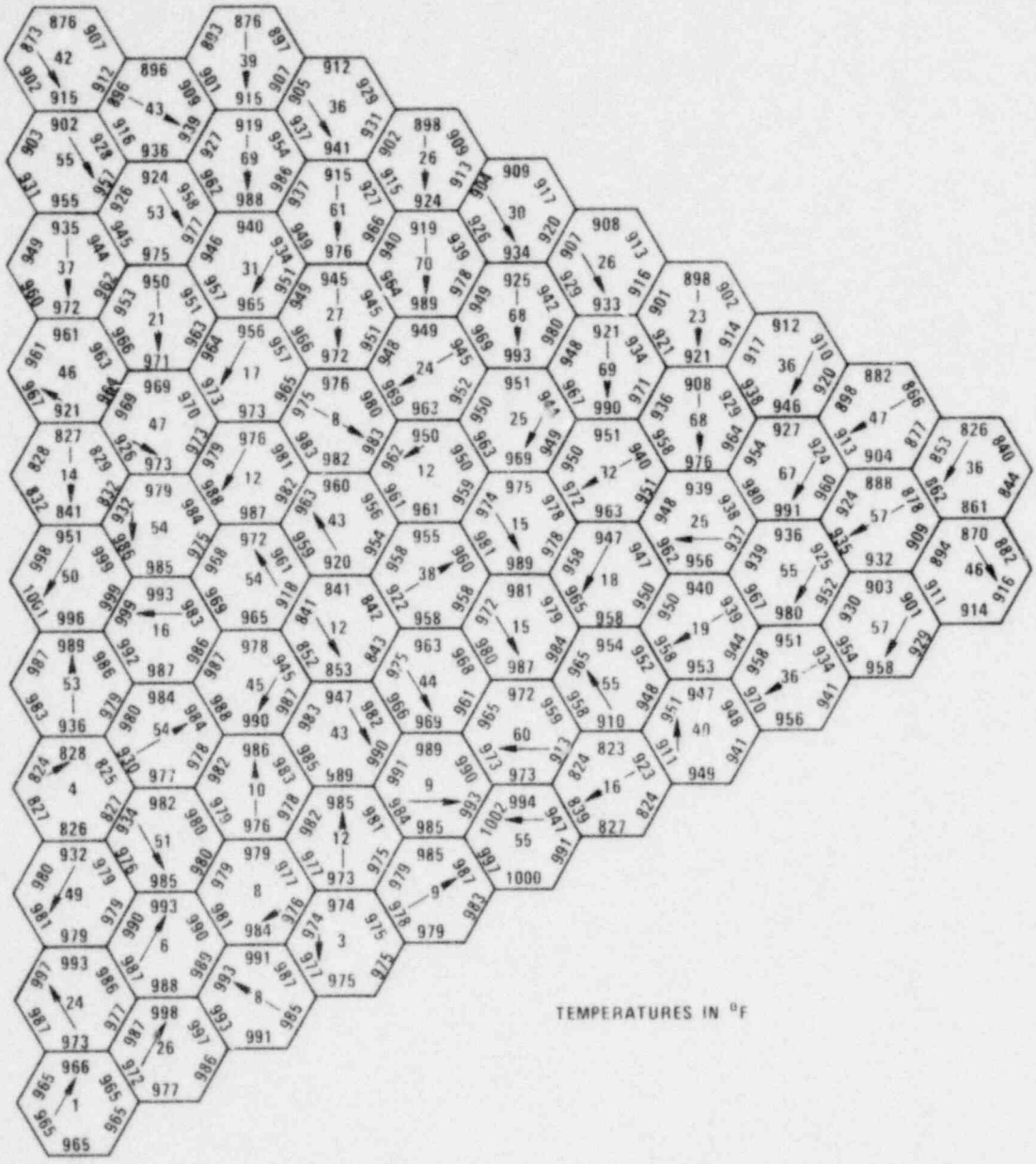

Figure 62 Core Wide Duct Midwall Temperatures at 60" Elevation, EOC4, Under Nominal Conditions

1668-45

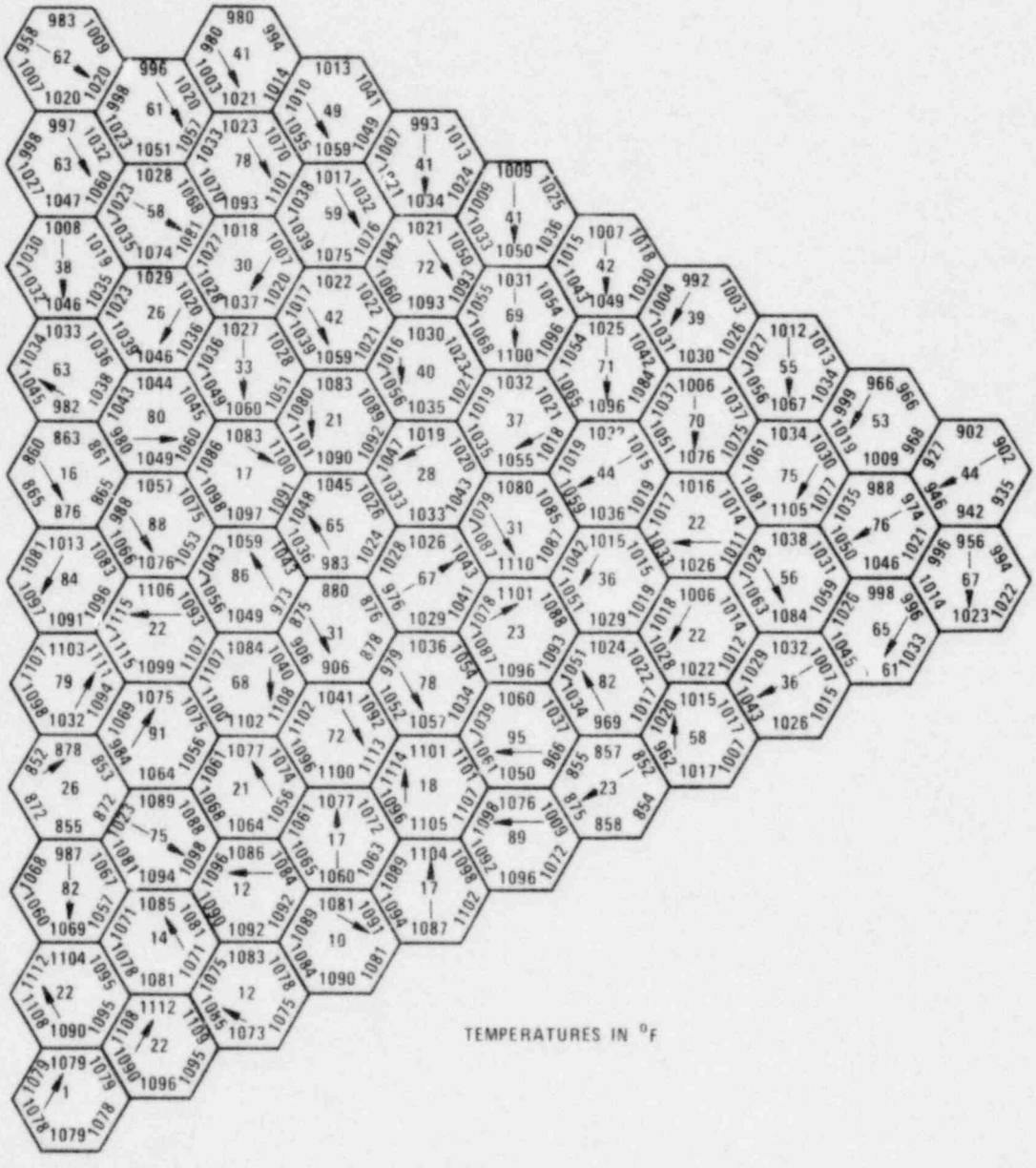

Figure 63. Core Wide Duct Midwall Temperatures at 60" Elevation, EOC 4, Accounting for Uncertainties

1668-113

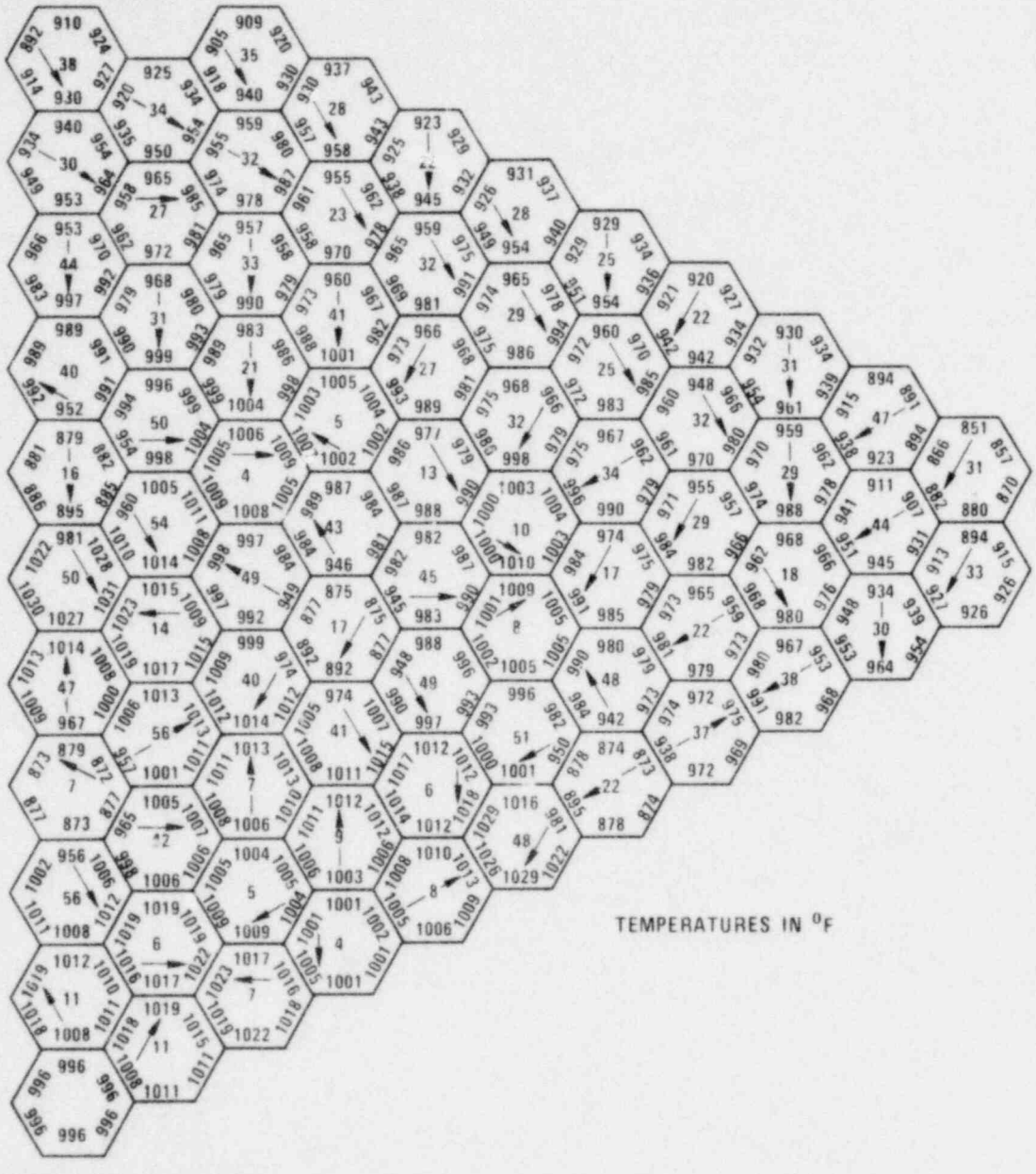

Figure 64 Core Wide Duct Midwall Temperatures at 112" Elevation, EOC4, Under Nominal Conditions

1668-46

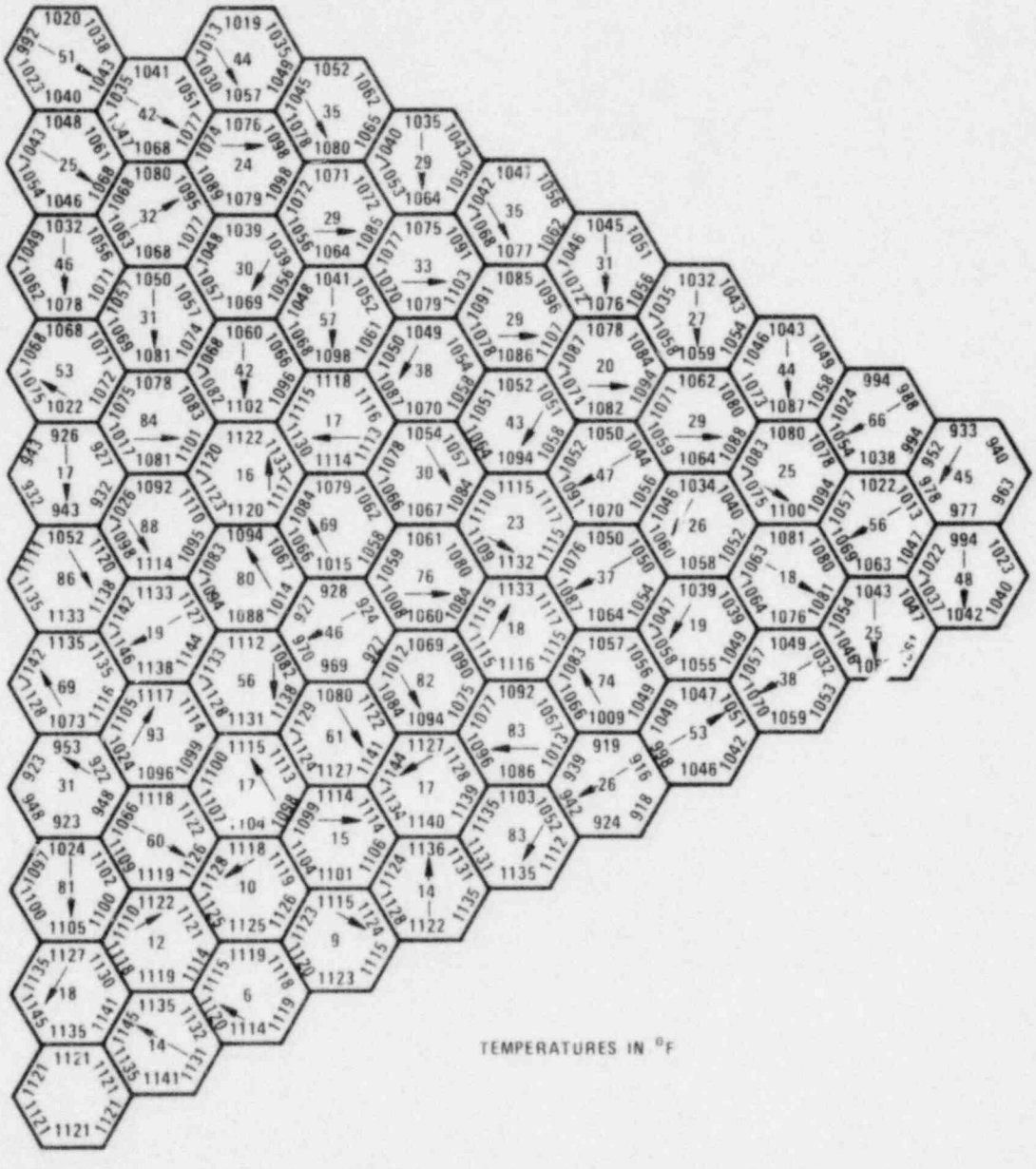

Figure 65 Core Wide Duct Midwall Temperatures at 112" Elevation, EOC4, Accounting for Uncertainties

1668-111

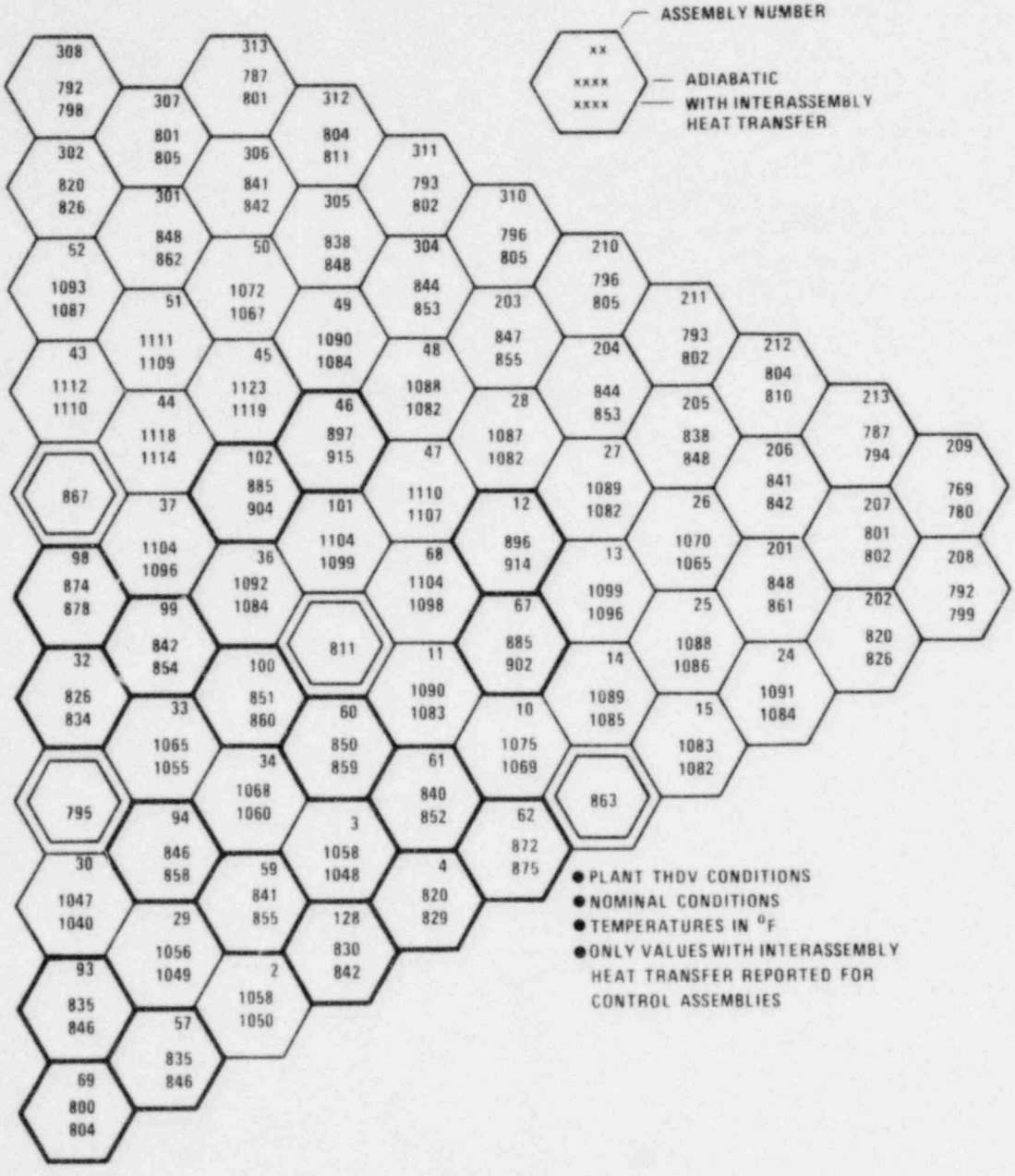

Figure 66 Comparison of Assemblies Mixed Mean Exit Temperatures at BOC1 Under Adiabatic Conditions and Including Inter-Assembly Heat Transfer Effects

1668-47

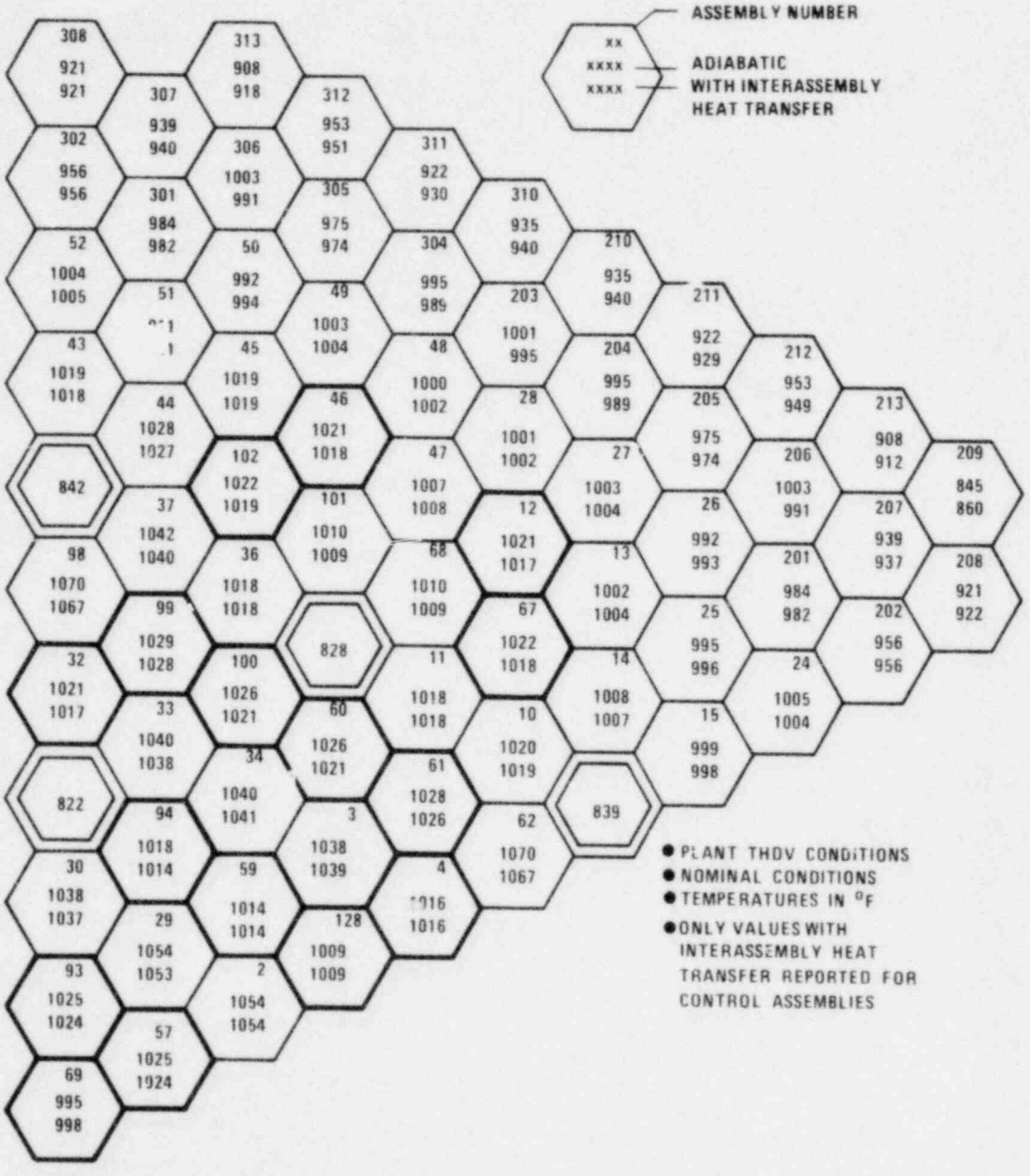

Figure 67 Comparison of Assemblies Mixed Mean Exit Temperatures at EOC4 Under Adiabatic Conditions and Including Inter-Assembly Heat Transfer Effects

1668-48

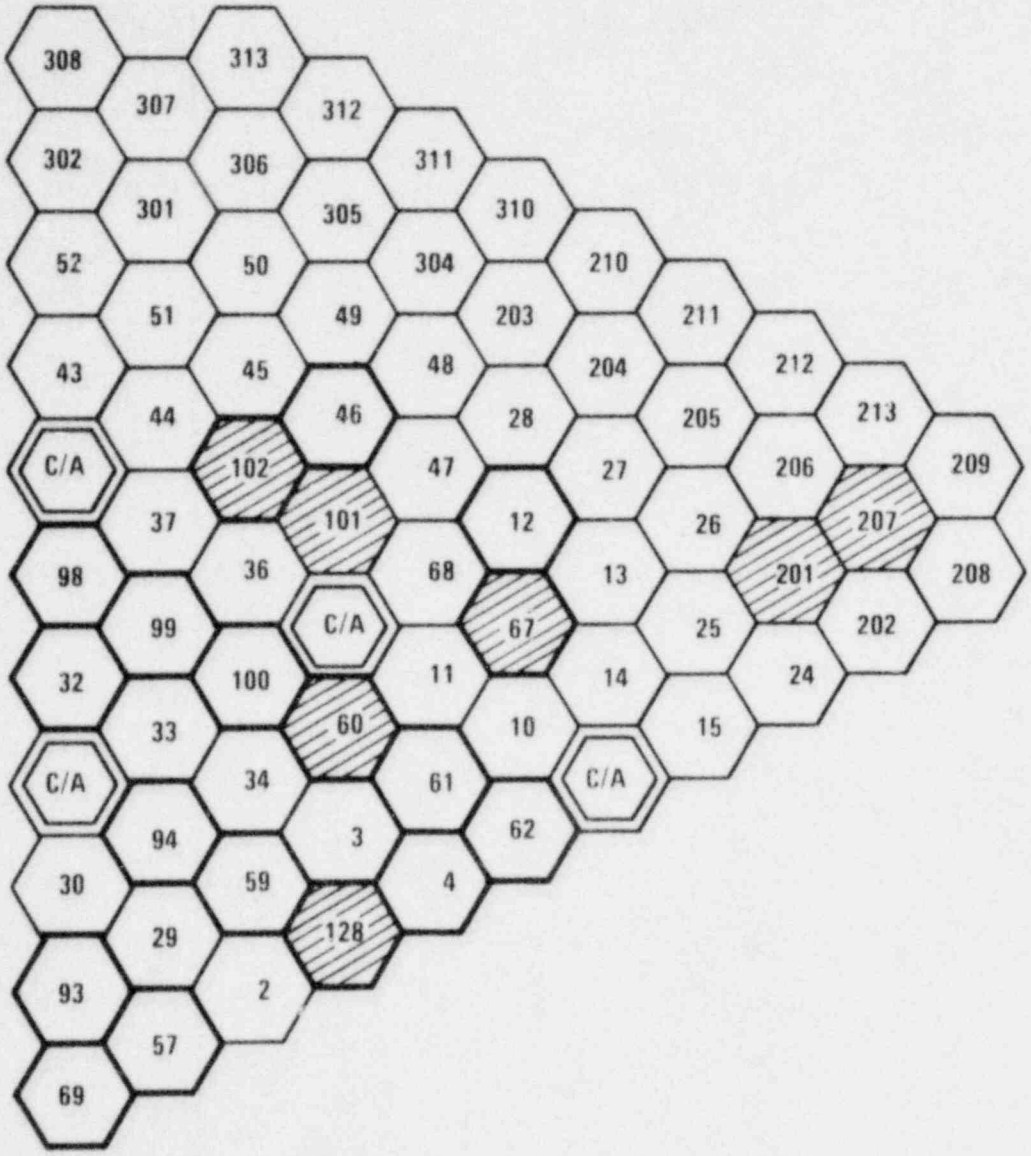

Figure 68 Selected Assemblies Analyzed Throughout Life with TRITON for Duct Dilation and Bundle/Duct Interaction Analyses

1668-103

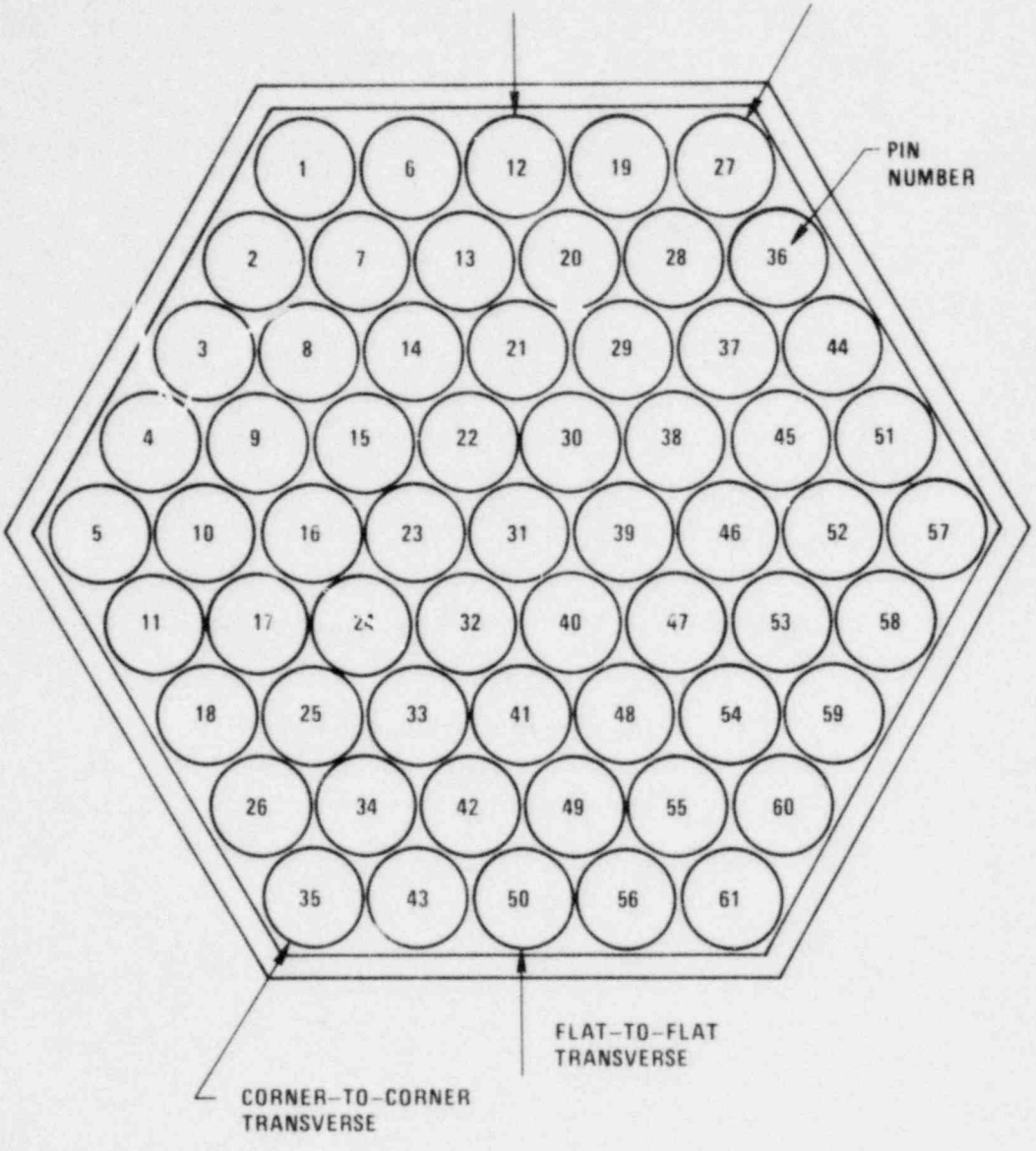

Figure 69 Cross-Assembly Transverses Where Average Rod Cladding Temperatures Have Been Calculated by TRITON

1668-102

INNER BLANKET ASSEMBLY #102 AT BOC3

AXIAL POSITION (IN.)	ASSEMBLY FACE					
	1	2	3	4	5	6
0.50	730	730	730	730	730	730
6.00	731	731	731	731	731	731
12.00	733	733	733	733	734	733
18.00	743	743	745	744	742	744
24.00	760	760	766	766	758	767
30.00	784	784	796	794	778	795
36.00	808	807	825	826	800	827
42.00	830	830	854	852	821	853
48.00	847	846	875	877	837	875
54.00	858	858	888	887	849	888
60.00	863	862	894	897	856	894
66.00	867	866	898	900	862	899
72.00	869	868	902	905	866	902
78.00	872	870	904	906	869	906
84.00	873	872	906	910	873	908
90.00	875	874	907	911	875	911
96.00	877	875	909	914	878	913
102.00	879	877	910	914	880	916
108.00	880	878	912	917	882	917
112.00	881	879	912	917	883	919

TEMPERATURES IN ^{0}F

INNER BLANKET ASSEMBLY #102 AT EOC3

AXIAL POSITION (IN.)	ASSEMBLY FACE					
	1	2	3	4	5	6
0.50	730	730	730	730	730	730
6.00	731	731	731	731	731	731
12.00	735	735	735	735	736	735
18.00	747	748	750	749	748	748
24.00	770	770	776	775	771	775
30.00	800	801	812	809	803	809
36.00	833	834	850	849	837	849
42.00	865	867	888	884	870	883
48.00	888	889	915	913	895	911
54.00	902	904	931	928	910	927
60.00	909	910	938	938	919	935
66.00	913	914	943	942	926	941
72.00	916	917	946	947	930	945
78.00	919	919	948	949	934	949
84.00	921	920	950	952	937	951
90.00	923	922	951	953	939	954
96.00	925	923	953	956	941	957
102.00	926	924	953	956	943	959
108.00	928	926	954	958	945	960
112.00	929	926	955	958	946	962

Figure 70 Typical Average Midwall Duct Temperatures Calculated by TRITON for Duct Dilation and Bundle/Duct Interaction Analyses

1668-100

CORNER–TO–CORNER TRANSVERSE

AXIAL POSITION (IN.)	PIN NUMBER								
	35	34	33	32	31	30	29	28	27
0.50	731	731	731	731	731	731	731	730	730
12.00	745	744	743	742	741	739	738	737	736
16.00	762	759	758	755	753	750	748	745	743
32.00	865	864	862	851	839	826	814	799	790
48.00	923	929	933	921	903	883	861	836	824
56.00	920	928	934	925	907	886	864	840	828
64.00	917	923	929	922	906	886	863	842	833
64.50	917	923	929	922	906	885	863	841	833

RADIAL BLANKET ASSEMBLY #201 AT BOC2
TEMPERATURES IN °F

FLAT–TO–FLAT TRANSVERSE

AXIAL POSITION (IN.)	PIN NUMBER								
	50	42–49	41	32–40	31	22–30	21	13–20	12
0.50	731	731	731	731	731	731	731	731	731
12.00	743	742	742	741	741	740	739	739	738
16.00	757	756	755	754	753	751	750	748	747
32.00	851	852	851	845	839	832	825	814	807
48.00	912	916	919	912	903	891	878	858	846
56.00	914	918	921	916	907	895	880	860	847
64.00	913	916	918	914	906	893	878	858	847
64.50	913	915	918	914	906	893	878	858	847

Figure 71 Typical Average Rod Cladding Midwall Temperatures Calculated by TRITON for Duct Dilation and Bundle/Duct Interaction Analyses

1668-101

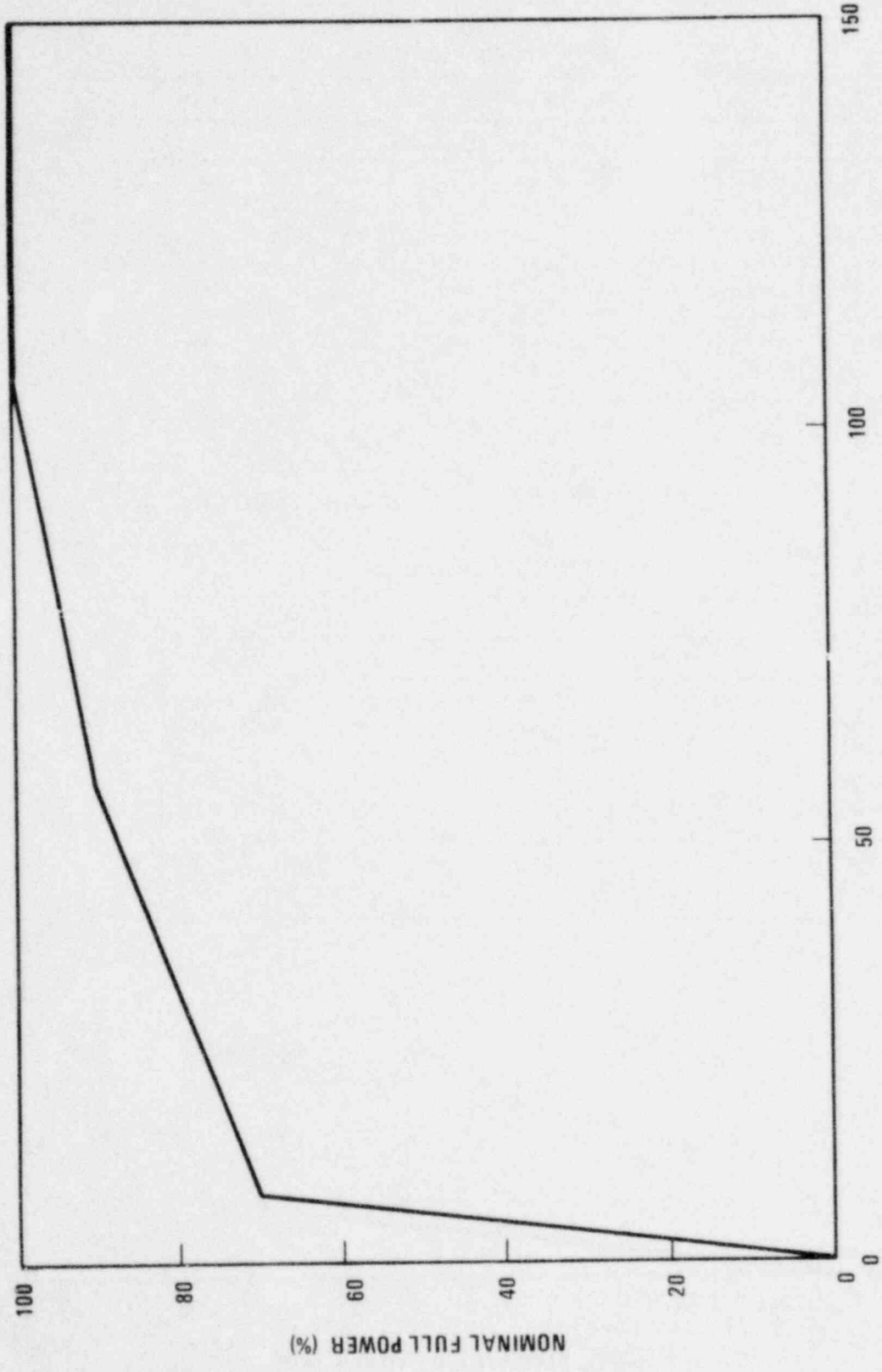

Figure 72 Power History (Programmed Startup) Used in Fuel Assemblies Power-to-Melt Analyses

1668-2

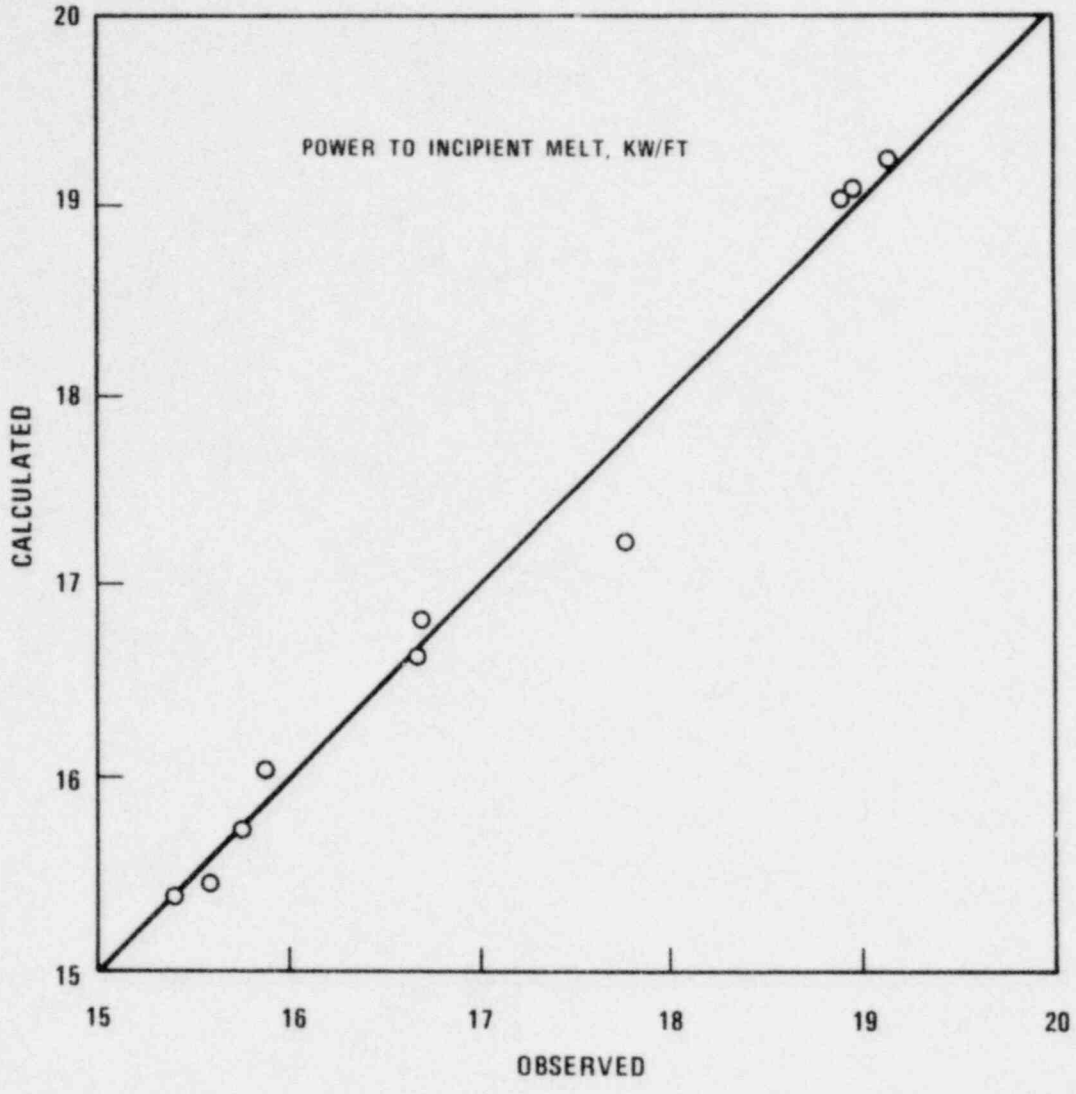

Figure 73 LIFE-3 Thermal Calibration

1681-2

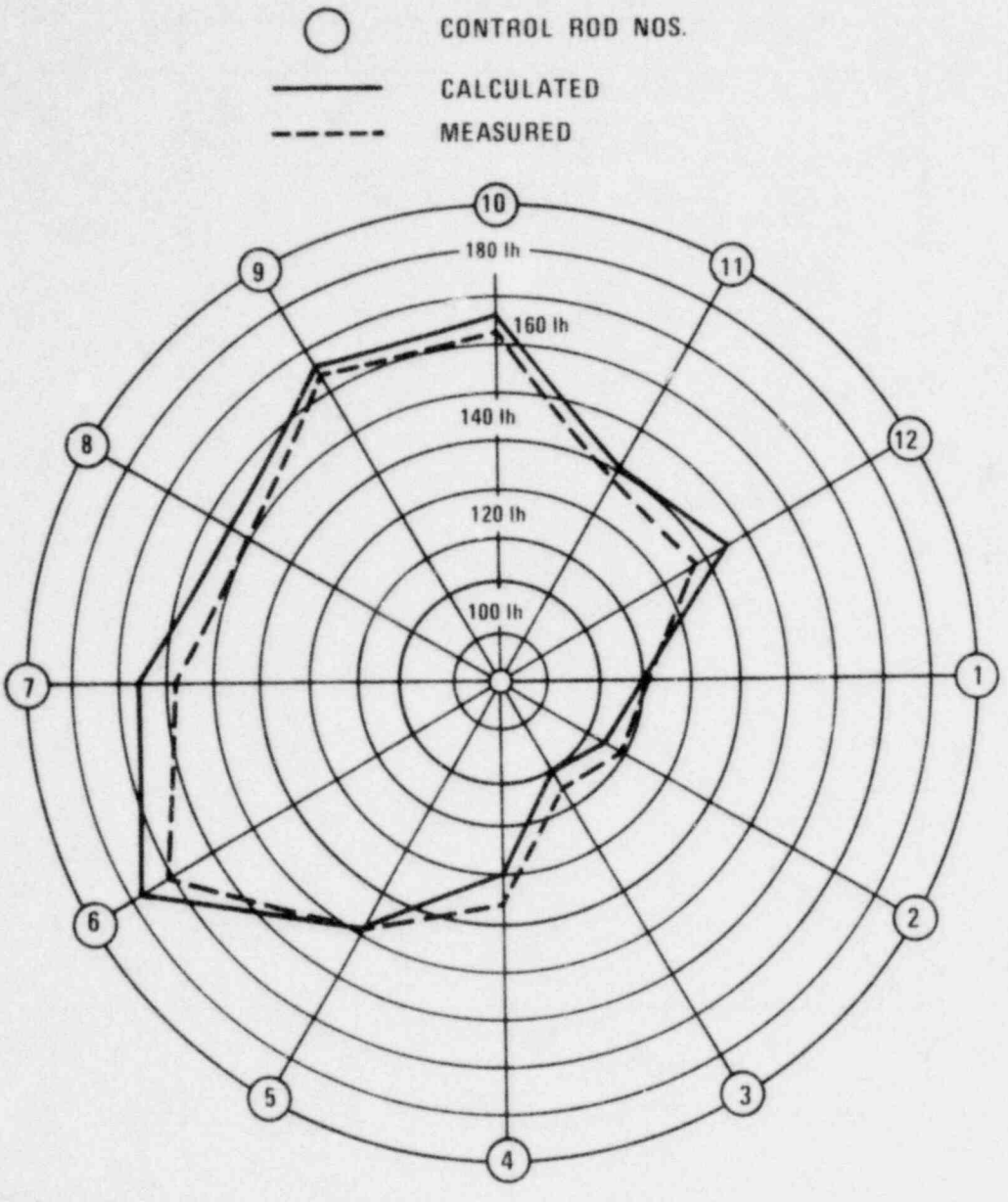

Figure 74 Control-Rod Worths for EBR-II Run 27A

1681-4

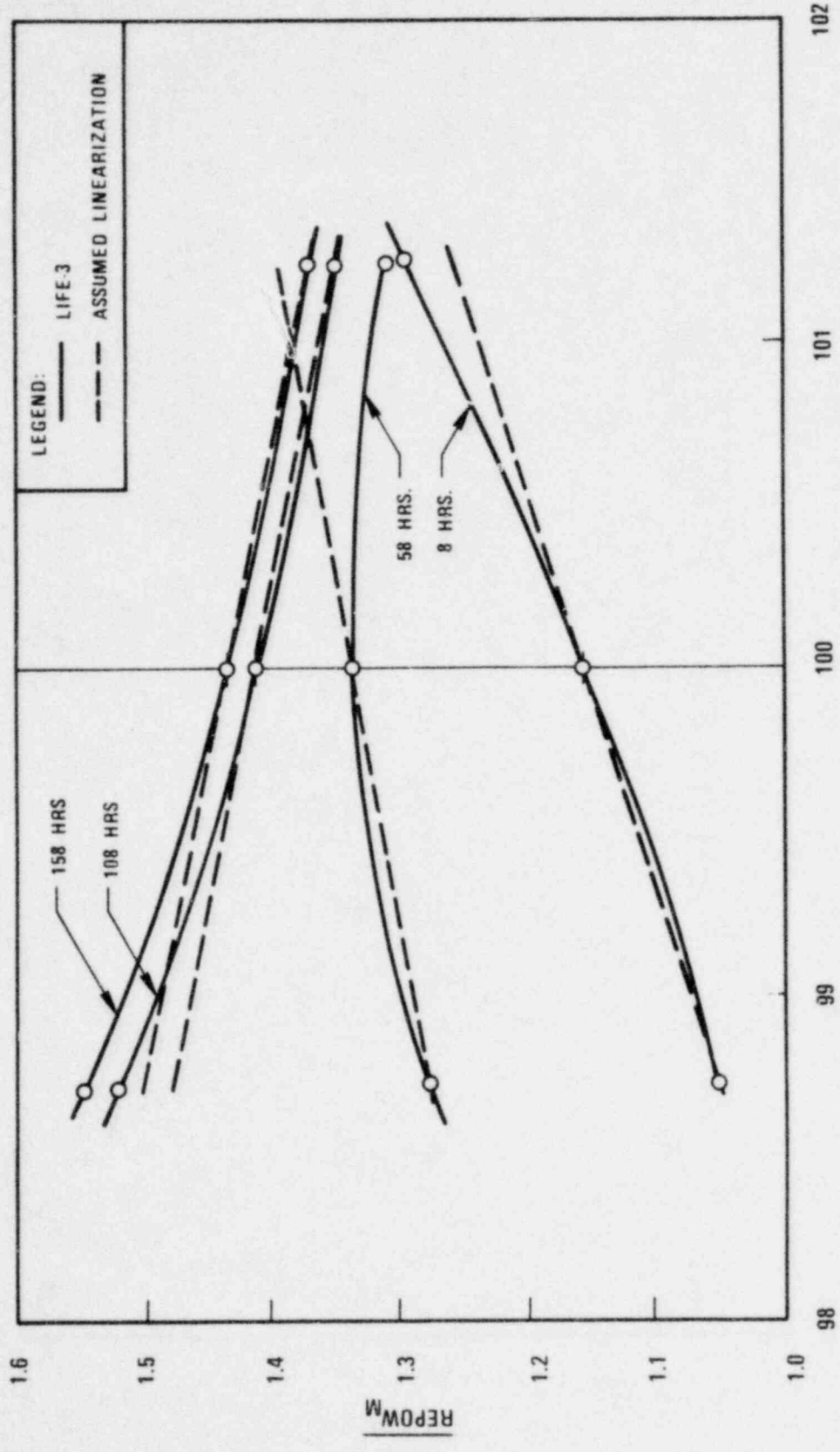

1681-3

Figure 75 Variation of Power-to-Melt with Pellet Diameter

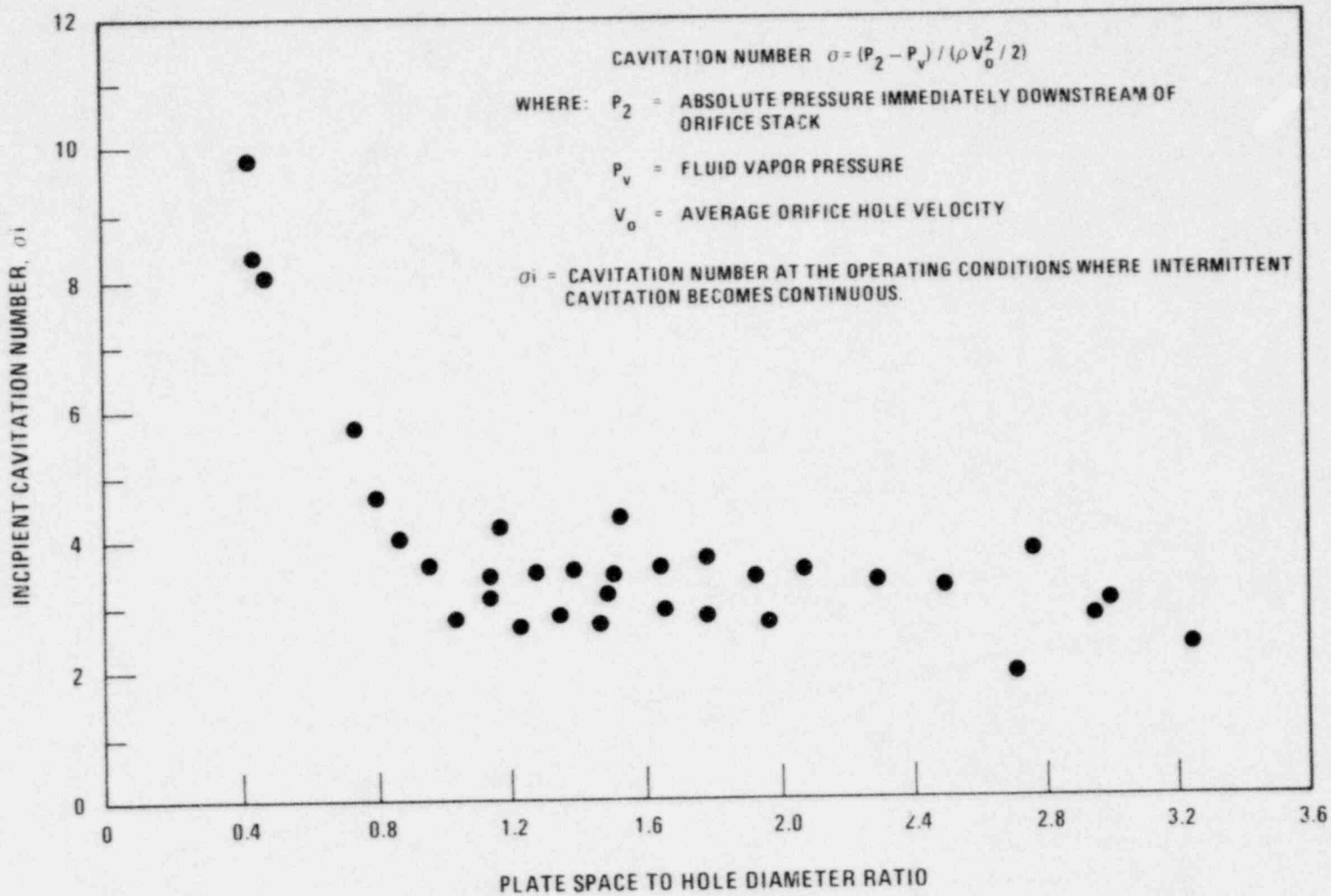

Figure 76 Typical CRBRP Fuel Assembly Orifice Stack Cavitation Data

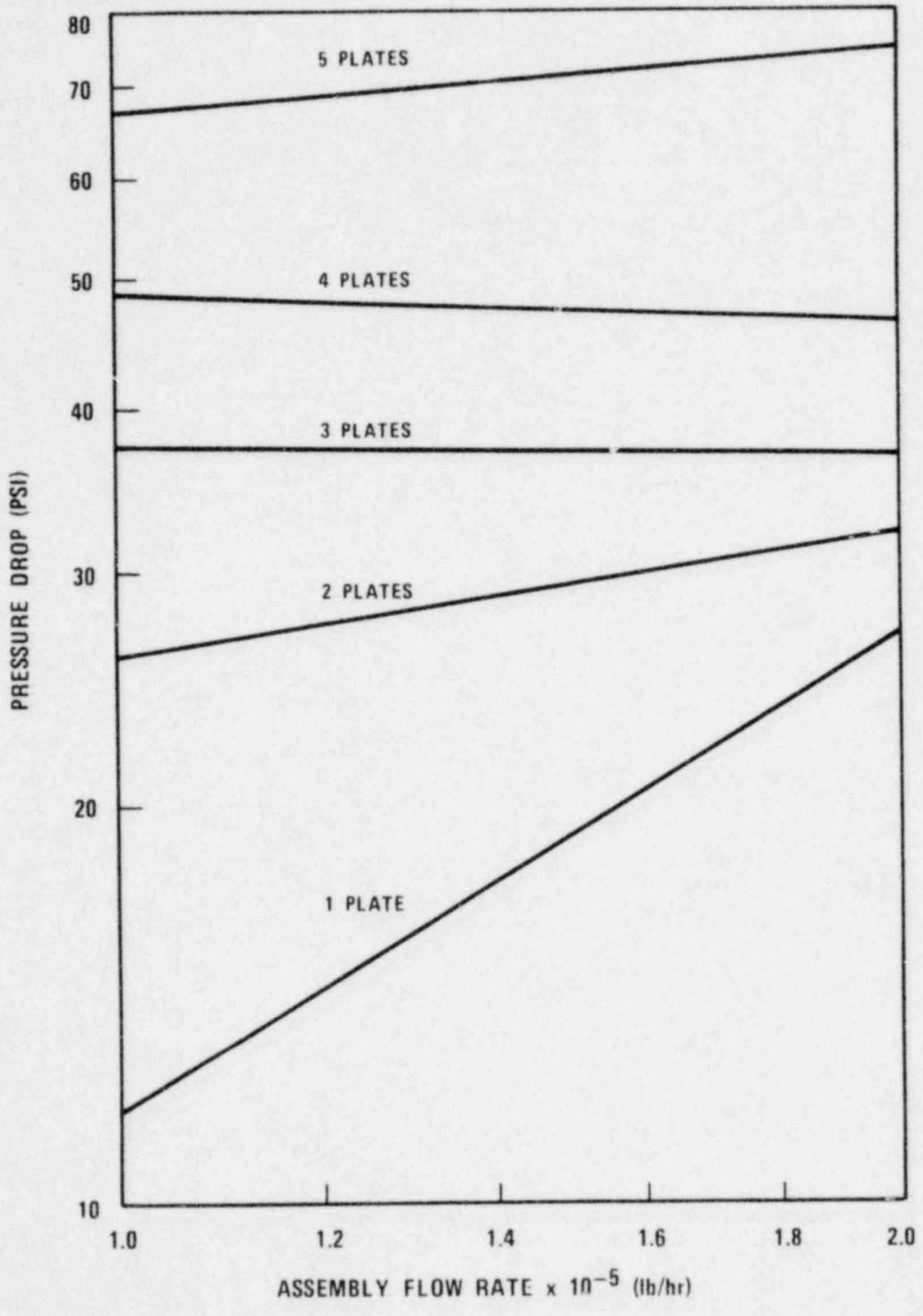

Figure 77 Fuel Assembly Inlet Nozzle-Orifice-Shield Pressure Drop for Orifice Hole Velocity Limit of 40 Ft/Sec

1668-57

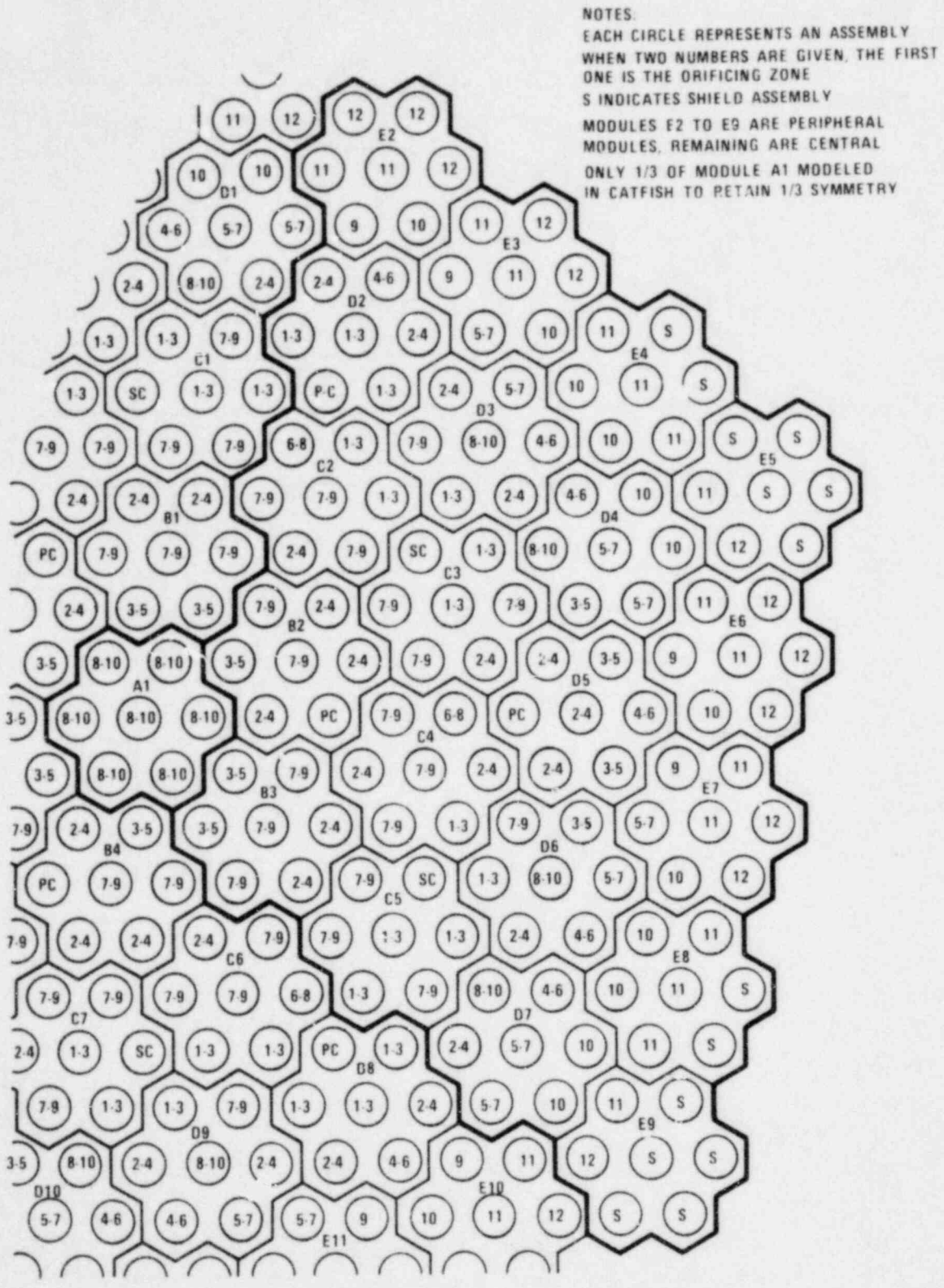

Figure 78. Map of CRBRP Lower Inlet Modules (1/3 Symmetry Sector)

1668-58